Revealing the Hidden

pXRF Multi-Element Analysis of Nok Culture Features (Central Nigeria)

Inauguraldissertation
zur Erlangung des Grades eines Doktors der Philosophie
im Fachbereich Sprach- und Kulturwissenschaften
der Johann-Wolfgang-Goethe-Universität zu Frankfurt am Main

vorgelegt von Annika Schmidt
aus Aalen

2019
(Einreichungsjahr)
2020
(Erscheinungsjahr)

1. Gutachter: Prof. Dr. Peter Breunig
2. Gutachter: Prof. Dr. Hans-Peter Wotzka

Tag der mündlichen Prüfung: 9. Juli 2019

Acknowledgements

First and above all, I want to express my deepest gratitude to my supervisor Prof. Peter Breunig for his continuous support, encouragement and generosity over the last few years. My academic education has largely been influenced by him – he has constantly inspired me to keep an eye on the 'bigger picture' and to focus on the essentials. His passion for Africa and its archaeology is contagious and I will be always extremely grateful for the opportunity to participate in the Nok project. Special thanks go to Prof. Hans-Peter Wotzka, whose opinion I genuinely value, for accepting to be my second supervisor and his useful comments.

This thesis would not have been possible without the financial funding of the Nok project provided by the German Research Foundation. I also wish to thank the Nigerian National Commission for Museums and Monuments for their cooperation and our academic partners at the University of Jos and Ahmadu Bello University Zaria.

I gratefully acknowledge the input of Prof. Katharina Neumann, who always revealed any weak spots. I would like to extend my deepest gratitude to Dr. Gabriele Franke & Dr. Alexa Höhn. Besides proofreading, they contributed to this thesis through sound advice, critical comments and profound discussions. Dr. Amy Styring deserves many thanks for her thoughtful and thorough corrections of my written English, while still preserving my own style. I also thank Kirstin Brauneis-Fröhlich for the appealing layout of this book. Thanks go to graphic designer Gaby Försterling for designing the book cover and improving the layout of my biplot graphics. I am also very grateful to Ute Mangold-Scherer for her motivating words and help in all administrative matters. Thanks also go to the German Embassy in Abuja, in particular to Regine Heß and her husband Colin Davidson, for their support.

I want to acknowledge the feedback given by Dr. Markus Helfert, in particular regarding technological and methodical questions, and the opportunity to use a second pXRF device. My deepest appreciation goes to Prof. em. Vera Pawlowsky-Glahn, who answered my countless questions and proofread the statistics chapter. Thanks to her, this thesis gained a new level of quality. I also thank Dr. Raimon Tolosana-Delgado for his geostatistical remarks. Many thanks go to Prof. Edward Mitchell, who conducted the analysis of soil communities and to Dr. Jens Amendt and Dr. Hayley Mickleburgh, who shared their expert knowledge on forensic approaches.

Many thanks go to all participants of the Nok project and other colleagues: Dr. Nicole Rupp for her idea to excavate at Ido and mentioning the approach of soil communities, Jana Maidhof, who conscientiously assisted with sieving the soil samples, and André Burmann for his thoughts, in particular on rituality. I also appreciate the input from Dr. Christina Beck, Johannes Behringer, Dr. Barbara Eichhorn, Eyub F. Eyub, Manuela Fels, Henrik Junius, Dr. Sonja Magnavita, Tanja Männel, Jennifer Markwirth, Klaus-Peter Nagel and Prof. em. Paul Sinclair, who all contributed in different ways to this thesis. I also gratefully acknowledge the interest and practical suggestions from Prof. Rüdiger Krause and Dr. Astrid Stobbe.

Nigeria and all Nigerians who were involved in the Nok project will always have a special place in my heart and the list is far too long to mention them all. Particularly helpful during fieldwork was the late Anas Ibrahim through his careful sampling, as well

as Amos Obadiah, Haruna Yakubu Husaini and Gideon Zomo Bala, who always found a solution for every problem. Special thanks go to Ali Bature for his help and permission to sample the Fulani village he lives in.

Last but not least, I thank my entire family for their support and encouragement, in particular my parents Heribert and Helga Schmidt, and all members of the families Schmidt, Orlowitsch, Groth, Klimpl and Stahl. I also thank Clarissa Agricola, my friend and fellow sufferer, who has accompanied me through years of both joy and suffering. Second to none, I thank my partner and best friend Rolf Stahl. Besides assisting at the excavation at Ido, he has patiently yet thoughtfully listened to all my hypotheses, problems and ideas, and contributed to this thesis by commenting and proofreading. He has motivated me to keep going, inspired me to surpass myself and constantly encouraged my scientific ambitions. Therefore, this thesis is dedicated to him.

CONTENTS

METHODOLOGY AND APPROACH

OUTCOME AND SYNTHESIS

APPENDICES

List of Figures

List of Tables

List of Appendices

Appendix 3: Pit Features – Balance Settings, Interpolations and Biplots

Appendix 4: Fulani Village – Plan & Biplots

Symbols for Elements

Ag	Silver	**Mn**	Manganese
Al	Aluminium	**Nb**	Niobium
As	Arsenic	**Ni**	Nickel
Ba	Barium	**P**	Phosphorus
Bi	Bismuth	**Pb**	Lead
Ca	Calcium	**Rb**	Rubidium
Cd	Cadmium	**S**	Sulphur
Ce	Caesium	**Se**	Selenium
Cl	Chlorine	**Si**	Silicon
Co	Cobalt	**Sr**	Strontium
Cr	Chromium	**Th**	Thorium
Cu	Copper	**Ti**	Titanium
Fe	Iron	**V**	Vanadium
Hg	Mercury	**Y**	Yttrium
K	Potassium	**Zn**	Zinc
La	Lanthanum	**Zr**	Zirconium
Mg	Magnesium		

1 Introduction

It does not require a crime scene to search for a corpse – finding traces of dead bodies to confirm *c.* 3000-year-old burials is part of the archaeological investigations in this thesis. Buried for millennia in the acidic soil, the bodies have disintegrated completely, leaving no visible human remains behind. However, the soil might have absorbed and preserved traces of the decomposed bodies in the form of enrichments of certain elements, yet to be revealed. Likewise, the living can change the soil composition. The soil as an archive records human impact in the form of elemental signatures and deciphering its entries enables the reconstruction of performed activities. The infills of pits represent an excerpt of this archive and their analysis is another subject of this thesis. This evidence – from both the living and the dead – is entangled in the soil and in order to '*Reveal the Hidden*', multi-element analysis with a portable X-ray fluorescence (pXRF) device is engaged.

The context of the analyses is the Nigerian **Nok Culture**, known for its sophisticated terracotta figurines, which dates from *c.* the 15th century BCE until the end of the 1st century BCE (Breunig 2018; Breunig & Rupp 2016; Breunig 2014; Franke 2017; Fagg 1990). Finds and features attest to human impact, but distinct settlement evidence is absent in the archaeological record and the layout and function of Nok sites are poorly understood (Breunig & Rupp 2016: 247–251); multi-phased activities, as indicated by the obtained ^{14}C data (Franke 2017: 56–57; Breunig & Rupp 2016: 247), complicate their interpretation. Most evidence manifests itself in features of unknown or uncertain function, such as the stone-pot-arrangements and pits, which are the subject of this analysis.

Stone-pot-arrangements are considered to be burial features, indicated by arranged and modified stones associated with complete pots and, in a few cases, a necklace made of stone beads (Rupp 2010: 70; Rupp 2014: 142–144; Breunig & Rupp 2016: 251; Breunig 2018: 399). Depositions of large fragments of terracotta figurines emerge in the vicinity of them and suggest an affiliation to the burials (Breunig 2018; Wotzka 2017). However, the absence of bones or other mortal remains within the stone-pot-arrangements leaves their interpretation as burials unresolved.

Pits or pit-like structures, found in various shapes and sizes, have withheld conclusive interpretation (Breunig & Rupp 2016: 248; Breunig 2018: 394; Höhn *et al.* 2018: 294–295; Schmidt 2014: 112–113). Located adjacent to or between stone-pot-arrangements, they imply a funerary or ritual context. However, mundane finds associated within these pits suggest the disposal of settlement waste rather than performed rituality. Pits also emerge as isolated features and point to settlement evidence, but the recurring ambiguity of both ritual and non-ritual characteristics impedes a conclusive interpretation. The occurrence of pits with unknown or equivocal function, the *phénomène des fosses* (Mbida Mindzie 1995: 41–47), is also known from other sites in West and Central Africa.

pXRF multi-element analysis of stone-pot-arrangements and pits aims to shed light on the layout and formation of **Nok sites**. Confirming stone-pot-arrangements as interments grants insight into mortuary practices and contextualises adjacent finds and features, such as the deposition of terracotta figurines. Identifying the nature of pit infills facilitates the reconstruction of performed activities and the identification of functional areas. This might enable the distinction of ritual and non-ritual areas and the comprehension of the formation and layout of Nok sites.

Studies that have conducted pXRF elemental analysis on soils are rare and particularly scarce in West Africa. Considering the age of and the adverse conditions on Nok sites, such as the soil acidity and erosional processes, the utilisation of this method to provide evidence for decayed bodies and to reconstruct performed activities is **pioneering work**. It requires spadework in the form of a systematic approach in order to avoid failure due to technical or methodical flaws and to successfully reveal elemental signatures entangled in the soil.

The **background and context** chapters comprise an insight into the Nok Culture, its research history and state of the art (chapter 2), the environmental setting of the sites with a focus on soils and their properties (chapter 3), as well as the archaeological research question explained in the context of relevant sites and features of West and Central Africa (chapter 4). The **methodology and approach** section encompasses information on the device, its precision and limits, and sample preparation (chapter 5), as well as a literature review of elemental signatures known from archaeological and forensic studies, analysis of a modern Fulani village and details on elements and their behaviour (chapter 6). It is followed by a description of Nok sites selected to conduct pXRF analysis (chapter 7), as well as the fundamentals of the statistical approach (chapter 8). The **outcome and synthesis** of this thesis comprise the results obtained from the pXRF analyses, soil pH and forensic approaches (chapter 9), the interpretation and discussion of the results (chapter 10), as well as concluding thoughts and an outlook for the future (chapter 11).

BACKGROUND AND CONTEXT

2 The Nok Culture

Research on the Nok Culture began in the first half of the 20th century. The Nok Culture owes its name to Bernard Fagg, the first archaeologist to explore the background of its terracotta figurines. His daughter Angela Rackham (née Fagg), Joseph Jemkur and Robert Soper continued with a few excavations during the second half of the last century. Since the terracotta figurines have become famous on the art market, looting is severely affecting the preservation of Nok sites and illicit digging holes are scattered throughout the landscape. With the beginning of the new millennium research on the Nok Culture has been pursued by the Goethe University Frankfurt and the National Commission for Museums and Monuments (NCMM) in Nigeria, together with the University of Jos and Ahmadu Bello University Zaria as project partners. The long-term research project funded by the German Research Foundation (DFG) has enabled numerous excavations and allowed a new insight into the Nok Culture.

2.1 First Exploration and Excavations

Bernard Fagg, an archaeologist and administrative officer of the British colonial power in Nigeria, was the first to describe the terracotta figurines in the first half of the 20th century. During his employment in Jos he and his wife Catherine catalogued the finds, among them heads of terracotta figurines, in the local museum. The first recorded find of a terracotta head dates back to 1928, when workers of a tin mine accidentally dug out the 'monkey head'. The co-owner of the mine, Colonel J. Dent Young, gave the head to the museum in Jos, where it was later examined by Bernard Fagg (Fagg 1990: 11–12). After the discovery of another terracotta part, the 'Jemaa head', Fagg recognized the stylistic similarities of both pieces and assumed them to have the same cultural background. The village in which he first found a terracotta head is the eponym of the **Nok Culture** (Fagg 1956: 1083). Together with Young, he raised awareness of the terracotta figurines among the tin workers and started surveys in order to find more pieces (Fagg 1990: 11–19). As all pieces until that point in time came from alluvial contexts, in situ finds of terracotta figurines and associated material became crucial.

The discovery and excavation of non-alluvial Nok sites began in the 1960s at *Taruga*, *Katsina Ala* and *Samun Dukiya* (Fagg Rackham 2014: 85–89). The results from *Taruga* were ground-breaking. Bernard Fagg excavated the site in three campaigns between 1965 and 1969, after a trial excavation yielded promising finds in 1961 (Fagg 1968: 27). Site prospection with a magnetometer revealed more than 60 anomalies and a total of ten iron furnaces and almost two dozen iron slag heaps were identified during that time (Fagg 1968: 28). Due to the absence of any polished stone axes and the abundance of iron slag and furnaces – as well as distinctive terracotta pieces and pottery – Fagg attributed the Nok Culture to the Iron Age (Fagg 1968: 29; Fagg 1969: 49). According to ^{14}C and thermoluminescence dates[1] he assumed that the Nok Culture dated from the second half of the first millennium BC to the beginning of the first millennium AD (Fagg 1990: 19–20). A detailed publication on *Taruga* with information on the site and materials was published

[1] All mentioned ^{14}C dates obtained by the Goethe University Frankfurt Nok project are calibrated in OxCal 4.2 using the IntCal13 calibration curve (Bronk Ramsey 2009; Reimer et al. 2013) and lie within the 2-sigma (95.4%) probability range (see Franke 2017: 38). All other dates not obtained by the project are cited as originally published.

in 2017 (Fagg Rackham *et al.* 2017). The excavation at *Katsina Ala* was carried out by Robert Soper in 1963 on behalf of the Nigerian Department of Antiquities. Apart from a brief overview (Fagg Rackham 2014: 87–88), details of the excavation were never published (Jemkur 1992: 3). Results of the excavation at *Samun Dukiya*, excavated by Angela Rackham in the winter of 1969/70, were published in 1972 (Fagg Rackham 1972) and re-evaluated with new dates in 2017 (Fagg Rackham 2017). Angela Rackham worked in Nigeria until 1977 together with the Nigerian archaeologist Joseph Jemkur, who then continued the research by excavating the sites of *Chado*, *Old Zankan* and *Rafin Masoyi* (Jemkur 1992). Apart from a stylistic analysis of the terracotta figurines published by Claire Boullier in her doctoral thesis on the Nok terracottas (Boullier 2001), no further notable research on the Nok Culture took place until the beginning of the new millennium[2].

[2] For a detailed description of the research history of Nok see Fagg Rackham 2014 and Jemkur 2014.

2.2 Long-Term Project at the Goethe University Frankfurt

The Project

The attention of the researchers at the Goethe University Frankfurt was drawn to the Nok Culture in 2005 due to their fieldwork in northeast Nigeria. Archaeological discoveries in the Nigerian Chad Basin led to the DFG Research Unit 510 dealing with *Ecological and cultural change in West and Central Africa* between 1000 BC and 500 AD. Evidence of significant cultural change in the middle of the first millennium BC pointed to emerging social complexity (Breunig 2009a; Magnavita C. & Magnavita S. 2001; Magnavita C. *et al.* 2006; Breunig & Rupp 2016: 238–240). In search of similar developments of early complexity, finds from the Nok Culture received attention. The assumption was that the manufacture of the sophisticated Nok terracotta figurines and the iron metallurgy required structures associated with a complex society (Breunig & Rupp 2016: 241–242; Breunig 2018: 391). After initial research on Nok sites in 2005 and 2006, excavations with promising results followed in 2007 and 2008, together with the prospection of more than 30 new sites (Breunig & Rupp 2016: 241). This led to an application and in 2009 the granting of a long-term research project to the African Archaeology and Archaeobotany research

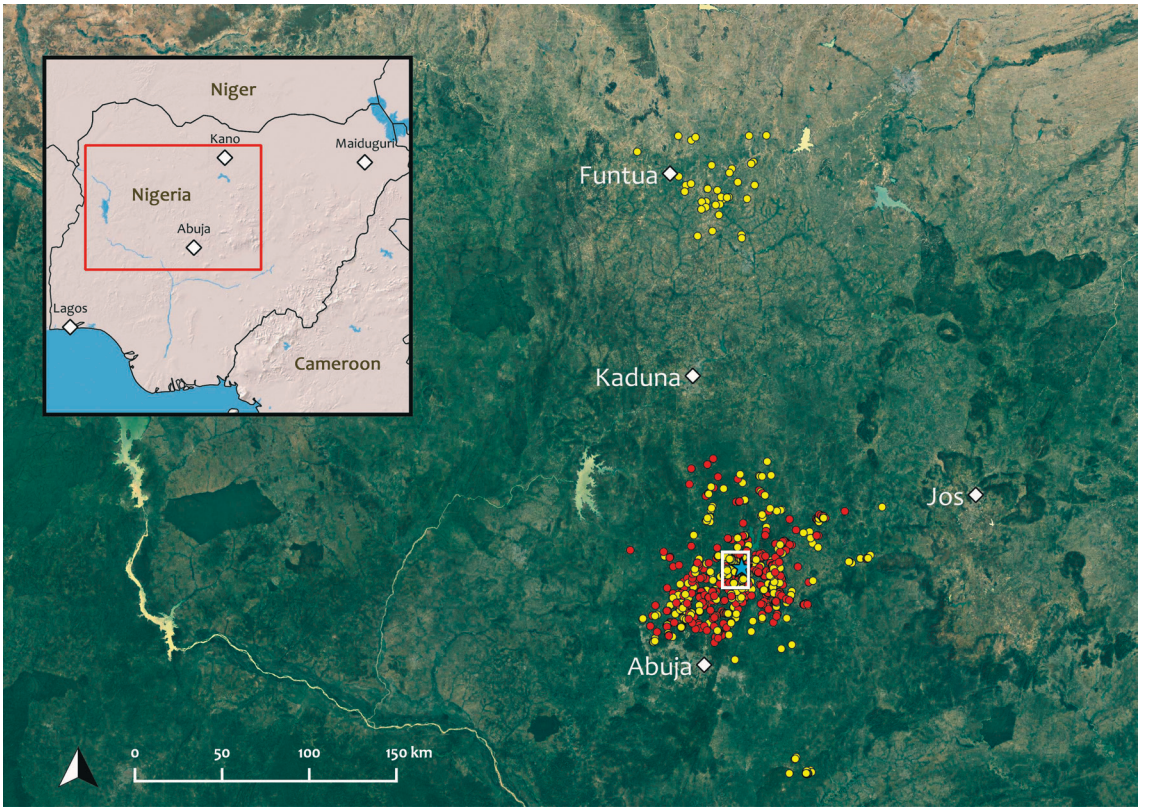

Fig. 2-1: Distribution of sites assigned to Nok (red dots, n = 441) and probably Nok or further investigations necessary (yellow, n = 416). The blue star represents the location of the research station in Janjala within the key study area (white box). Base map from Google Satellite and ESRI Shaded Relief provided by QuickMapsServices (QGIS plugin), for land borders see http://thematicmapping.org/.

group of the Goethe University on the *Development of complex societies in sub-Saharan Africa: The Nigerian Nok Culture* (Breunig 2009b; Breunig & Rupp 2010). The project cooperates with the Nigerian National Commission for Museums and Monuments (NCMM), the University of Jos and Ahmadu Bello University Zaria.

Comprehensive research during the project's 12-year duration (2009-2020) addresses the chronology, site structure and regional variety of the Nok Culture. The political situation in Nigeria, however, has grown worse over the years, impeding both extensive excavations and regional surveys. The outcome of more than ten years of research has granted a holistic view; the most recent state of research was published by Breunig & Rupp (2016). Within the scope of several theses the pottery and its chronology (Franke 2017), the material character and context of the terracotta figurines (Beck 2017; Burmann 2016), iron production (Junius 2016b), and structural analysis on a site (Schmidt 2014) were examined. The scientific results were shared with the wider public through the exhibition *Nok – Origin of African Sculpture* in 2013/2014 at the *Liebieghaus Skulpturensammlung* Frankfurt, now displayed at the Kaduna museum in Nigeria, together with accompanying exhibition catalogues (Breunig 2013; Breunig 2014).

Research Area

The overall distribution of the Nok Culture is based on the finds of terracotta fragments made during the last century, stretching from the northwest at Kagara, beyond the Kaduna river, to the southeast at Katsina Ala, beyond the Benue river and along the Katsina Ala river (Fagg 1959; Breunig & Rupp 2016: Fig. 1). However, this distribution arises from a few isolated pieces with insecure authenticity. Based on the results of the project's survey, we instead assume that the Nok Culture occupied the region between Abuja and Jos (Breunig 2018: 392; Franke 2016: 260).

With the beginning of the Nok project in 2009 investigations initially concentrated on a 20 x 15 km *key study area* (see Fig. 2-1, white box), chosen to a particularly high abundance of sites in this area (Breunig & Rupp 2016: 242). In the course of time, both excavations and survey expanded beyond the key study area. Surveys in the proximity of Abuja and towards Kaduna and Jos furnished further Nok Culture sites. An additional survey around Funtua at the border between the states of Katsina and Kaduna, towards the *Katsina and Sokoto* tradition (Boullier 2008: 189), yielded more terracotta figurines. However, no excavations took place and further investigations are necessary to prove an affiliation to the Nok Culture.

A total of more than 900 recorded sites were documented by the Nok project, among them almost 450 Nok Culture sites and *c.* 180 sites classified as probably Nok. In *c.* 230 cases further investigations are necessary to prove any affiliation to Nok. The remaining sites cannot be attributed to Nok. Of the almost 80 excavated sites, two thirds contained Nok material. Most excavations cover a few square meters, being primarily dug for the collection of potsherds and datable material (Breunig & Rupp 2016: 242). The two large-scale excavations, at *Pangwari* and *Ifana*, are exceptional cases with an excavated area of more than 2600 m² and 1000 m², respectively. The objective at *Pangwari* was to reveal the settlement layout, at *Ifana* to prove a link between terracotta depositions and stone-pot-arrangements.

2.3 State of the Art

Chronology

By test pitting, in order to collect potsherds and their associated organic material for ^{14}C dating, knowledge of the Nok chronology has grown continually. The outcome of the analysis has culminated in a chronology separated into three phases: **Early**, **Middle** and **Late Nok** (Franke 2017).

A total of 257 ^{14}C dates and 27 luminescence dates (as of January 2019) were obtained by the project[3]. According to the ^{14}C data the Nok Culture dates from 1500 BCE to the end of the 1st century BCE (Franke & Breunig 2014; Franke 2016; Franke 2017). The first ^{14}C dates in the middle of the 2nd millennium BCE are assigned to the Early Nok phase (1500-900 BCE). There is no evidence for the production of terracotta figurines during that phase. The heyday of the Nok Culture is during the Middle Nok phase (900-400 BCE), supported by the peak in ^{14}C dates around 800 BCE (Franke 2017: 56). During that time terracotta figurines emerge and somewhat later iron production begins. The subsequent Late Nok phase (400-1 BCE) lasts from the 4th century BCE and ends, after a sharp decline in the number of sites and associated finds, at the end of the 1st century BCE (Franke 2017: 55–57).

Seven pottery groups can be distinguished (Franke 2017), which enable a more precise chronology: The earliest pottery is designated as the *Puntun Dutse* group and occurs during the Early Nok phase (Franke 2017: 220). Further analysis on the Early Nok pottery is impeded by the fact that most of the sites are multi-phased and Early Nok material is often mixed up with younger layers (Breunig & Rupp 2016: 244). The dating of the following Middle Nok phase is hampered by the plateau of the calibration curve between *c*. 800 to 400 BCE. However, with the help of ^{14}C data and pottery groups, the calibrated dates can be separated into two stages **before** and **during** the plateau (Schmidt 2014: 108; Franke 2016). The features dating from the 10th to 9th century BCE comprise finds of the pottery groups *Ido* and *Ifana*, followed by the pottery groups *Pangwari* and *Tsaunim Gurara* during the 8th to 5th century BCE (Franke 2017: 220). At the site of *Pangwari*, the ^{14}C dates associated with *Ifana* and *Pangwari* potsherds point to a contemporaneity or short time interval between both groups (Franke 2017: 195; Höhn *et al.* 2018: 21). The *Pandauke* and *Ungwar Kura* groups emerge during the calibration plateau, but contrary to the other groups they extend into the 1st century BCE (Franke 2017: 223). They are designated as Late Nok pottery, although potsherds of the *Ungwar Kura* group may represent a local tradition (Franke 2017: 198).

The interpretation of the established ^{14}C and pottery chronology allows a new insight into the development of the Nok Culture. The Early Nok phase is characterised by the absence of evidence for terracotta figurines and iron processing (Franke 2017: 219–221). An affiliation to the Nok Culture is proven by the continuity of site occupation, the development of pottery design and the chemistry of the clay from which the pottery is made (Franke & Beck 2017: 272). During Middle Nok the appearance of terracotta figurines and iron production is recorded. However, the established pottery chronology revealed

[3] For a detailed list of all ^{14}C and luminescence dates collected until 2014 see Franke 2016 and Franke 2017: 35–49.

that the terracottas and the emergence of iron were not contemporaneous (Franke 2016: 273). The figurines occur mainly in the context of the early Middle Nok pottery groups *Ido*, *Ifana* and *Pangwari* (Schmidt 2014: 114; Schmidt 2016: 66–67; Höhn *et al.* 2018), and coincide with the ^{14}C dates, thus placing the beginning of terracotta use to the 9th century BCE (Franke 2016: 273; Franke 2017: 56). Pottery from furnaces belong to the *Tsaunim Gurara* and *Pandauke* groups, pointing to an emergence of iron production not before the 7th century BCE, and thus later than the height of terracotta use (Franke 2016: 273). In Late Nok, the number of sites declines significantly and only a few finds attest to occupation during that time. Evidence of the Nok Culture disappears at the end of the 1st century BCE. Finds and features associated with younger dates clearly differ from Nok. The main characteristic is the absence of terracotta figurines and the change in pottery manufacture. The use of carved wooden and fibre roulettes for decoration (Franke 2017: 191) and a different fingerprint chemistry of the pottery (Beck 2017: 102) prove the dissociation to Nok (Franke & Beck 2017). The lack of characteristic Nok attributes thus attests that the period after the end of the 1st century BCE is not linked to the Nok Culture.

Archaeological Features

The search for undisturbed Nok sites is challenging as most sites are discovered through illicit diggings or farming activities. Although we found a high number of sites, almost all were in some way affected by lootings, which in turn is the main reason for the discovery of new sites (Breunig & Rupp 2016: 244). Not much attention is given by the looters to cultural remains *without* any terracotta fragments. Thus, the knowledge of Nok sites mainly comes from areas where terracotta fragments have been found.

The overall appearance of Nok sites is similar, mainly consisting of shallow cultural layers or find concentrations indicating brief occupation episodes (Breunig & Rupp 2016: 245). No distinct features reflecting occupation evidence such as house structures, ditches or hearths dating to the Nok Culture have yet been found[4] (Breunig 2018: 394); no stone structures were found and instead we suppose the use of huts made from organic material (Breunig & Rupp 2016: 247). In general, features are scarce and analysing the structure of Nok sites remains difficult (Breunig & Rupp 2016: 241). Based on our knowledge, we assume scattered farmsteads or dispersed settlements (Breunig & Rupp 2016: 245; Breunig 2018: 394–395). The multi-phased occupation of Nok sites (Schmidt 2014; Höhn *et al.* 2018) hampers an estimation of their former extent and level of exploitation (Breunig & Rupp 2016: 247).

Features like pits, stone-pot-arrangements, terracotta depositions, and iron furnaces are recorded (Rupp 2014c; Schmidt 2014; Junius 2016a; Höhn *et al.* 2018) and reflect site types such as settlements, burial and ritual sites, or iron producing sites (Breunig & Rupp 2016: 248). However, their spatial, temporal and contextual relationship is still unsolved. Recurring finds, both inside and outside of features, are terracotta figurines or fragments (Männel & Breunig 2016; Burmann 2016), potsherds (Franke 2017), stone artefacts (Rupp 2014b), charcoal, burnt clay, and few iron objects (Eggert 2014; Junius 2016b). The feature types will be presented briefly; the pits and stone-pot-arrangements are the key elements of this thesis and discussed in detail in chapter 4.1.

[4] The only exception is a stone circle at the site of *Puntun Dutse* (Breunig & Rupp 2016: 247).

Pits are the most common features. They are present on almost every site in various shapes and contain material dated to different phases, although the majority belongs to Middle Nok. They mostly measure 1-2 m in diameter with depths of 50 cm, in some cases up to 2 m (Breunig & Rupp 2016: 248). Their use and hence the basis for interpretation of sites is yet unsolved as the pits appear in different contexts and their find inventory is ambiguous (Schmidt 2014: 112–113; Breunig & Rupp 2016: 248; Höhn *et al.* 2018). **Stone-pot-arrangements** are features interpreted as burials, despite their absence of bones (Rupp 2010: 70; Nagel 2014; Schmidt 2014; Schmidt 2016). This feature comprises one or two complete pots next to a stone accumulation, among them grinders, within an area void of finds. Two of these feature types contained finds of stone beads arranged as if on a string, both in *Ido* and *Ifana* (Rupp 2010: 70; Schmidt 2016: 65, 70). In addition, a discoloration with distinct outlines at *Kurmin Uwa* indicated the remains of a burial pit. **Terracotta depositions,** accumulations of large, well preserved fragments of terracotta figurines, are rare and occur only at a few sites, e.g. at *Pangwari* and *Ifana* (Männel & Breunig 2016; Breunig 2018) or with a similar appearance at *Utak Kamuan Garaje Kagoro* (Rupp 2014a). **Iron furnaces** have a homogenous appearance (Junius 2016b: 192) with an average diameter of approximately one metre and with an adjacent pit filled with charcoal, slag and tuyère fragments. Usually two or three furnaces are found close to each other (Junius 2016b: 107–108).

Archaeobotanical Evidence

The overall lack of undisturbed features identified as Early Nok limits the knowledge of subsistence and environment during that time. However, evidence of pearl millet (*Pennisetum glaucum*), which was ^{14}C dated to the Early Nok phase, attests to its use during that time. Pearl millet is indigenous to the Sahel and was domesticated there, thus it can provide evidence that the Nok people migrated from the North (Höhn & Neumann 2016: 332; Breunig & Rupp 2016: 241–242). The use of African canarium (*Canarium schweinfurthii*) in Early Nok is attested as well.

During Middle Nok the environment appears stable (Höhn & Neumann 2016: 332). Fruit and seed remains of domesticated pearl millet and cow pea (*Vigna unguiculata*) as well as wild fruits, African canarium and *Vitex* sp., contributed significantly to the subsistence (Kahlheber 2009: 7; Höhn & Neumann 2014: 179–180). Although there is no evidence of farmland, the charcoal assemblages indicate 'a shifting cultivation system with long fallow periods' (Höhn & Neumann 2016: 332). The acidic soil impedes any evidence of animal bones (Höhn & Neumann 2014: 183), although the depiction of hunting weapons on the terracotta figurines suggests hunting of game.

The conservative cultivation methods with limited crop diversity during Middle Nok in combination with climatic changes seem to be responsible for the decline of sites during Late Nok. Climatic changes around 400 BCE, attested by the pollen diagram from Nyabessan in the rainforest of southern Cameroon, led to high evapotranspiration during the short summer dry season and a prolonged winter dry season. The assumed high impact of the Middle Nok people on the environment, e.g. caused by gaining material for iron-smelting, resulted in an open landscape. The combination of short and heavy rainy seasons due to climatic change together with opened woodland led to intensive erosion of the topsoil. The resulting harvest shortfall together with a lack of flexibility of

cultivation methods is considered to be the most likely explanation for the decline of sites starting around 400 BCE (Höhn & Neumann 2016: 348–350).

The end of the Nok Culture and its contrast to the period after the end of the first century BCE is also reflected by the use of new plants, namely fonio (*Digitaria exilis* Stapf) and oil palm (*Elaeis guineensis* Jacq.). This is proven for the site *Janruwa C*, dating to the first centuries CE (Höhn & Neumann 2016: 351).

From Social to Ritual Complexity

As indicated by the initial project's title *Development of complex societies in sub-Saharan Africa: The Nigerian Nok Culture*, the working hypothesis was that the assumed high settlement density and the terracotta figurines in combination with emerging iron production reflect signs of complex societies (Breunig 2009b).

In the course of time, however, no evidence for social complexity was found in the archaeological record, as discussed in Beck (2017). According to McIntosh (1999: 4), social complexity is traditionally reflected by a list of characteristics such as surplus production and specialisation, population growth, political centralization, and vertical hierarchies of wealth, power, and status. On Nok sites these attributes are absent. There is no evidence for hierarchically organised structures, which manifest in settlement or burial stratification, or any other signs for social complexity such as long-distance trade, agricultural intensification or architectural remains, which require communal effort (Beck 2017: 135–139; Breunig & Rupp 2016: 251–253; Breunig 2018: 391–392, 397). To the contrary, it turned out that the emergence of iron processing and the production of terracotta figurines are subsequent rather than joint developments. Furthermore, no centralised production sites for the terracotta figurines were found, as formerly suggested (Beck 2017: 119, 135).

Instead of discovering evidence for centralised terracotta production, another hypothesis for the manufacture of the figurines arose. Material analysis suggests the use of the same clay source for all figurines, taken from a special deposit of river sediments (Beck 2017: 119), whereas pottery was produced from different, local clay deposits (Beck 2017: 102). Beck assumes that complexity is expressed in other ways, without centralisation but with an organisation, where **rituality** plays an important role (Beck 2017: 137–138). This correlates with McIntosh (1999), who states that the definition of social complexity, with the above mentioned attributes, does, in general, not apply for sub-Saharan Africa.

Thus, Beck deduces that in the case of Nok

> *'the findings would support the model of a horizontally organised society with central authority resting in the ritual sphere and relying on ritual power, in which the terracotta figures link the people living in dispersed settlements as a symbol of identity.'*
>
> (Beck 2017: 135)

The Nok terracottas, formerly interpreted as an indication of social complexity, now turn out to be a key element for the interpretation of **ritual complexity**, expressed by their production. Beside the use of specific clay sources, the terracottas are characterised by recurring features (Männel & Breunig 2016: 327) indicating a stylistic 'ritualisation' of the figurines.

The context of the terracotta figurines also supports the concept of ritual complexity. Apart from the dumped fragments found in pits, probably being waste, the figurines seem to have been carefully placed depositions (Burmann 2016; Breunig & Rupp 2016: 249). These terracotta depositions were found, e.g. at *Pangwari* or *Ido*, in the context of stone-pot-arrangements and deep pits (Schmidt 2014; Schmidt 2016; Höhn *et al.* 2018). Due to their spatial proximity, a mutual context between those feature types was suggested but not evident. The results of the excavation at *Ifana* in 2016, however, represent a breakthrough – the link between terracotta depositions and stone-pot-arrangements was proven (Breunig 2018: 399–400). The stone-pot-arrangements, being tentatively interpreted as burials, would then imply not only a ritual but a mortuary context for the terracotta figurines (Breunig 2018: 400).

2.4 Summary

Based on the research of the 20th century, the terracotta figurines became renowned, both in scientific circles and the illegal art market. Apart from the awareness of the Nok Culture through their sophisticated terracotta figurines, knowledge of the complex was limited. As the terracotta fragments were found associated with stone artefacts and iron objects, or within the context of iron production, the Nok Culture was initially dated by Bernard Fagg to the transition from Stone to Iron Age, ranging from 500 BC to 200 AD.

The chronology established by the Nok project at the Goethe University Frankfurt shows an earlier onset in the middle of the 2nd millennium BCE and an earlier ending at the end of the 1st century BCE. The previous assumption of a contemporaneity of the terracotta figurines with the production of iron has not been confirmed. The affiliation of Early Nok to the Nok complex despite the absence of terracotta figurines demonstrates that the Nok Culture is not exclusively defined by its figural tradition. With the onset of a new pottery development after the beginning of the 1st millennium CE, the end of the Nok Culture was earlier than assumed by Fagg.

After the hypothesis that the Nok Culture represents a complex society has been dismissed, crucial issues of dating the emergence of iron smelting, the use of the terracotta figurines and the perception of mortuary practices came to the fore. As already discussed, new chronological evidence has proven that iron smelting furnaces occur later than the terracotta figurines, which are found in the context of stone-pot-arrangements and deep pits. The spatial and temporal connection between terracotta depositions, stone-pot-arrangements and pits emphasises the relevance of identifying their former use (see chapter 4.1), as the function of the associated terracotta figurines may also be solved.

3 Environment and Soils

3.1 Environment

Reconstruction of the environmental conditions in Central Nigeria over the last two millennia BCE, relevant to the Nok Culture, is limited to site-specific analysis, e.g. at the sites of *Janruwa C* or *Pangwari* (Höhn *et al.* 2018; Höhn & Neumann 2016; see also chapter 2.3). Comprehensive reconstruction is impeded by the lack of adequate reference material such as pollen diagrams, and most information available relates to regions far from the Nok Culture area, such as from Nyabessan in southern Cameroon (Ngomanda *et al.* 2009; Höhn & Neumann 2016: 349). Therefore, the description of the environmental setting refers to modern conditions.

The area of research is located in the tropical climate zone with summer rainfall (Schultz 2005: 193), which is characterized by two seasons and relatively high and constant temperatures. Rainfall occurs during summer when the intertropical convergence zone (ITCZ) shifts northwards and the solar altitude is at its maximum (Eitel 2001: 175). The rainy season lasts from April to mid-October and has its peak in August (Abaje *et al.* 2010: 90).

The mean annual rainfall in Kaduna, of which the southern part is the centre of our research area, ranges between *c.* 1030 mm in the North (Zaria) and *c.* 1730 mm in the South (Kafanchan) (Abaje *et al.* 2016: 98). The average temperature ranges from 22.9 °C in December to 28.9 °C in April with a mean relative humidity of 70-90% during the rainy and 25-30% during the dry season, when the most evaporation occurs (Abaje *et al.* 2016: 99).

According to White (1983: 176), the area is part of the *Guinea-Congolia/Sudania regional transition zone* with its characteristic flora and vegetation. The formerly widespread forests, of various types, were destroyed by human impact and replaced with secondary grassland and secondary wooded grassland.

Within the Kaduna Plains much of the landscape is almost level or undulating with an elevation between 600 and 800 m. Rocky hills and inselbergs tower 50 to 200 m above the surrounding landscape (Bennett *et al.* 1979: 12–13). The research area lies on the *Basement Complex*, the oldest geological formation in Nigeria with an age older than 600 million years (Obaje 2009: 9). It comprises igneous and metamorphic rocks with granites, gneisses, migmatites, schists, and quartzites (Bennett *et al.* 1979: 13). Cappings of laterite, since renamed as (petro)plinthite (Jones *et al.* 2013: 26), can be found on all rock types (Bennett *et al.* 1979: 13).

3.2 Soils

3.2.1 Soils of the Tropics with Summer Rainfall

Depending on geology, topography and especially the age of the land surface, a broad variety of soils occurs in the tropics with summer rainfall (Scheffer *et al.* 2010: 373) forming a patchwork of so-called *soil landscapes* (Scheffer *et al.* 2010: 365). These soil landscapes are classified by their dominant soil type (Scheffer *et al.* 2010: 365, 367). Dominant soils in the tropics with summer rainfall are **Acrisols, Lixisols, Plinthosols, Nitisols, and Vertisols** – in contrast to the wet tropics southwards or the Sahel northwards (Scheffer *et al.* 2010: 364 Fig. 8.2-1; Schultz 2005: 27 Table 4.2).

Such a broad classification, however, diverges from the actual distribution and diversity in the tropics (Eitel 2001: 207). The common allocation of Acrisols, Lixisols and Vertisols to the semi-humid savannas, in contrast to the allocation of Ferralsols and Plinthisols to the wet tropics, distorts the actual distribution. A more precise distinction is that Ferralsols and Plinthosols are old and strongly weathered soils on geomorphodynamic stable reliefs. Lixisols and Acrisols are younger soils with a more brownish colour, found on erodible areas like slopes (Eitel 2001: 192). This emphasises that the distribution of soils in the landscape is much more differentiated and affirms the concept of soil landscapes. Thus follows an overview of the featured **properties of the soils** in the tropics with summer rainfall rather than individual soil types. The dominant soil types with their associated soils on Nok sites are explained in detail in chapter 3.2.3. The knowledge of the soil properties helps not only to understand the soil itself, but is crucial for this thesis as they affect the occurrence and behaviour of chemical elements (see also chapter 6.5).

The main characteristic property of soils in the tropics with summer rainfall is the strong influence of intensive chemical weathering, mainly through hydrolysis (Eitel 2001: 179, 208). Chemical weathering dissolves minerals and leads to leaching of dissolved products, namely through *decationisation* and *acidification* (Scheffer *et al.* 2010: 282). Other determining soil-forming processes in semi-humid savannas are depletion, transformation, translocation, and turbation (Scheffer *et al.* 2010: 371 Tab. 8.4-1). Intensive moisture penetration and water seepage lead to drainage of carbonates, resulting in soil *decalcification*, which, in turn, causes *acidification* of the soil (Eitel 2001: 24). *Acidification* can, especially towards the equator, induce *desilication*, the destruction of silicate minerals and conversion of (primary) silicates to two-layered silicates, namely Kaolinite (Eitel 2001: 28, 179). Both *acidification* and *desilication* rely on the disintegration of lithogenic Fe(II)-minerals. Newly formed oxides and hydroxides initiate processes of transformation, e.g. goethite causes *brunification* and hematite causes *rubification*. As a consequence of mineral weathering, *loamification* can also occur (Eitel 2001: 24, 179). The main translocation process is *lixivation*, where clay disperses and relocates downwards (Eitel 2001: 179, 181). Characteristic for these soils is also weak humus accumulation, very heavy eluviation and also very heavy *hydro-* and *bioturbation* (Scheffer *et al.* 2010: 371 Fig. 8.4-1). The profile horizons often appear blurred with sparse organic matter and the soil texture mostly consists of sand and clay (Jones *et al.* 2013: 31).

In such strongly weathered soils both the cation exchange capacity (CEC) and pH values are low. The *cation-exchange capacity* (CEC) is defined by the capacity of clays to retain and supply nutrients such as calcium, magnesium, potassium, and ammonium (Jones *et*

al. 2013: 27). The sum of these exchangeable base cations determines the base saturation (FAO 2014: 2). Strongly weathered clays have a low CEC (low activity clays) with less than 24 cmol(+)/kg and supply phosphate, sulphate and nitrate rather than base cations. Less weathered clays with a CEC higher than 24 cmol(+)/kg are considered high activity clays, such as Alisols (Jones *et al.* 2013: 27, 52). In general, pH values of soils range between pH 4 and pH 11, with pH 7 being neutral. Higher values are alkaline and values below pH 7 are considered as acidic (Jones *et al.* 2013: 11). The pH values of soils within the research area range from alkaline (lithic Leptosols) to acidic (haplic Lixisols) and very acidic (haplic Alisols) (Jones *et al.* 2013: 134).

3.2.2 Soil Base Map

The required information for this thesis was obtained from the up-to-date, reliable and comprehensive compilation: the **Soil Atlas of Africa** (Jones *et al.* 2013), a collaborative initiative of the European Union, the African Union and the Food and Agriculture Organisation of the United Nations (FAO). The data for this map is derived from the Soil Geographical Database of Eurasia, FAO Soil Map of the World and the Harmonized World Soil Database (HWSD). The **HWSD** (Version 1.2) was used to obtain detailed information on the soils within the research area, e.g. the pH values (FAO/IIASA/ISRIC/ISS-CAS/JRC 2012).

The soil designations used in the Soil Atlas of Africa refer to the FAO world reference base for soils, an international soil classification system (FAO-UNESCO 1974; FAO-UNESCO 1997; FAO 2014), agreed as official terminology by the 16th Congress of the International Union of Soil Science (Jones *et al.* 2013: 47). In this system, areas are classified into Reference Soil Groups (RSG). The definition of the RSG is based on diagnostic horizons, diagnostic properties and diagnostic materials (FAO 2014: 9). The information obtained from the HWSD, however, refers to the old nomenclature of the FAO[5]; to use a consistent nomenclature, the soil types were listed according to the revised legend from 1997 (FAO-UNESCO 1997).

Other soil maps exist, such as those published by the Survey Department of Lagos in 1952, another two by the FAO, the Soil Map of Africa (1964) and the FAO-UNESCO Soil Map of the World (1974). Later maps were made by the Federal Department of Agricultural Land Resources in 1990 (Odeh *et al.* 2012: 454). These data, however, were either not suitable for this thesis or using old classification systems. Numerous soil surveys have been conducted in Nigeria, but unfortunately the data were neither adequately customized nor summarized due to problems of georeferencing, methodology and other discrepancies (Odeh *et al.* 2012: 453–454).

3.2.3 Soils on Nok Sites

According to the Soil Atlas of Africa, most of the Nok sites are located on **haplic Lixisols** and **lithic Leptosols**, and a few on **haplic Alisols** (Fig. 3-1). However, the map shows only the dominant soil types (Jones *et al.* 2013: 69) and associated soils are stated in the soil

[5] For example, Alisols were formerly a subgroup of Acrisols and now form a separate group (FAO-UNESCO 1997: 6).

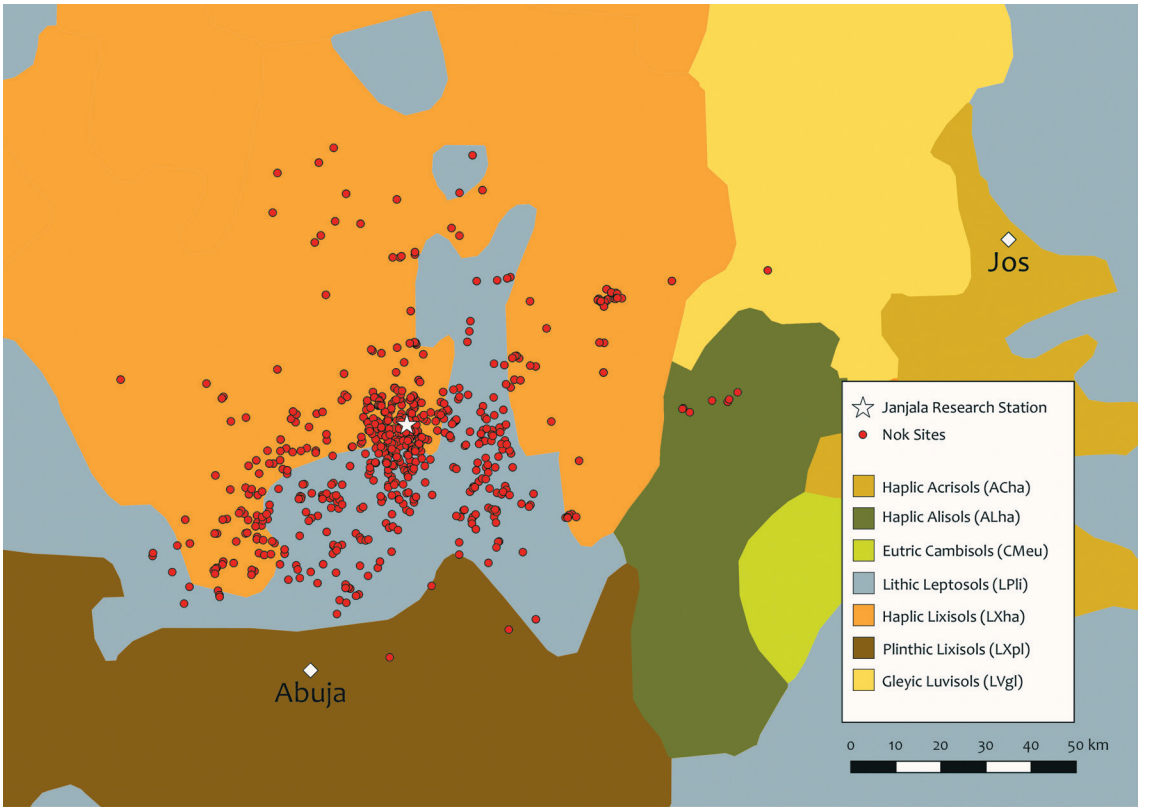

Fig. 3-1: Distribution of Nok sites (n = 441) on different soils. The map shows the dominant soil types based on the data obtained from the **Soil Atlas of Africa** (Jones *et al.* 2013). Base map see Dewitte *et al.* 2013 and Spaargaren *et al.* 2010.

description. Another soil type, **Cambisols**, was found on Nok sites during a field survey and will be discussed as well.

Haplic Lixisols

Haplic: 'Having no applicable other qualifier' (Jones *et al.* 2013: 51).
Lixisols: 'Slightly acid soils with a clay-enriched subsoil and low nutrient-holding capacity (from Latin *lixivia*, washed-out substances)' (Jones *et al.* 2013: 55).
pH: Slightly acidic, *c.* pH 6-6.3 (FAO/IIASA/ISRIC/ISS-CAS/JRC 2012; Scheffer *et al.* 2010: 152 Tab. 5.6-1).

Lixisols represent a typical soil on metamorphic rocks in semi-humid savannas. They are soils with kaolinitic horizons affected by lixivation. Kaolinite is the dominant clay mineral beside small amounts of three-layer silicates (Eitel 2001: 181). Lixisols are characterized by low-activity clays with high base saturation (FAO 2014: 7–8). They comprise an argic subsoil, i.e. the horizon has a distinctly higher clay content than the overlying horizon. Between the surface and the subsoil is a bleached eluviation horizon caused by loss of iron oxides and clay minerals (FAO 2014: 155). These soils are slightly acidic. The loose soil structure with low aggregate stability suffers from erosional processes and is not

able to hold much organic matter and macronutrients (Jones et al. 2013: 55; Hartmann 2013: 34). Associated soils in this area are Plinthic Lixisols[6] and Leptosols[7] (FAO/IIASA/ISRIC/ISS-CAS/JRC 2012).

Lithic Leptosols

Lithic: 'Having continuous rock within 10 cm depth' (Jones *et al.* 2013: 51).
Leptosols: 'Shallow soil over hard rock or gravelly material (from Greek *leptos*, thin)' (Jones *et al.* 2013: 51).
pH: Slightly alkaline, *c.* pH 7.6 (FAO/IIASA/ISRIC/ISS-CAS/JRC 2012; Scheffer *et al.* 2010: 152 Tab. 5-6.1).

Leptosols are thin soils or soils with many coarse fragments with less than 20% fine earth over continuous rock, mainly found in the mountainous areas (FAO 2014: 154; Jones *et al.* 2013: 50). Therefore Leptosols have a loose soil structure (Jones *et al.* 2013: 55). Associated soils in this area are Lixisols[8] (FAO/IIASA/ISRIC/ISS-CAS/JRC 2012).

Haplic Alisols

Haplic: 'Having no applicable other qualifier' (Jones *et al.* 2013: 51).
Alisols: 'Very acid soils with a clay-enriched subsoil and high nutrient-holding capacity (from Latin *alumen*, alum)' (Jones *et al.* 2013: 52).
pH: Very to moderately acidic, *c.* pH 5.2-5.5[9] (FAO/IIASA/ISRIC/ISS-CAS/JRC 2012; Scheffer *et al.* 2010: 152 Tab. 5-6.1).

Unlike Lixisols, Alisols have *high-activity clays* and a *low base saturation* (FAO 2014: 8). Like Lixisols, they embed an *argic* subsoil horizon (FAO 2014: 136). A bleached eluviation horizon can appear between the *argic* subsoil and the surface horizon, caused by a loss of iron oxides and clay minerals (FAO 2014: 137). The acidity is high and responsible for the weathered minerals releasing large amounts of aluminium (Jones *et al.* 2013: 52). Alisols can be found in hilly or undulating relief (FAO 2014: 136). Associated soils in this area are Leptosols[10] (FAO/IIASA/ISRIC/ISS-CAS/JRC 2012).

Cambisols

Cambisols: 'Soil that is only moderately developed on account of limited age' (from Latin *cambiare*, to change)' (Jones *et al.* 2013: 53).
pH: n/a for this region in the HWSD.

[6] Defined as Plinthic Luvisols in the HWSD (FAO-UNESCO 1997: 6).
[7] Defined as Lithosols in the HWSD (FAO-UNESCO 1997: 6).
[8] Defined as Ferric Luvisols in the HWSD (FAO-UNESCO 1997: 6).
[9] This information refers to Acrisols, of which Alisols were a subgroup in the old definition; Alisols now form a separate group (FAO-UNESCO 1997: 6).
[10] Defined as Lithosols in the HWSD (FAO-UNESCO 1997: 6).

Cambisols are not present on the map, but are mentioned by Eitel (Eitel 2001: 192) and were found within the research area during a field study in 2011[11]. Cambisols are young soils with moderately developed and indistinct horizons; their occurrence in the tropics is rare (Jones *et al.* 2013: 53, 60). Weathering processes strongly influence the depletion of nutrients (Jones *et al.* 2013: 60; FAO 2014: 143), although within the tropics their nutrient content is richer than Acrisols and the CEC is greater (FAO 2014: 144). An absence of illuviated clay, organic matter and Al and Fe compounds are characteristic (FAO 2014: 143).

3.3 Summary

The research area of the Nok project is located in the tropical climate zone with summer rainfall, which is characterised by two seasons and relatively high and constant temperatures. Located on the Basement Complex, its geology comprises mainly igneous and metamorphic rocks. The present-day soils are strongly influenced by chemical weathering and have low pH values. Most soils on Nok sites are haplic Lixisols, lithic Leptosols, haplic Alisols or Cambisols.

[11] Internal report of soil types on Nok sites conducted by Jürgen Wunderlich, Institute of Physical Geography, Goethe University Frankfurt.

4 Research Question and Archaeological Context

4.1 Research Question

The aim of this thesis is to identify and interpret Nok Culture features by employing pXRF multi-element analysis. This enables understanding of the function of features and grants insight into the structure of Nok sites by locating functional areas. Based on the archaeological evidence, **stone-pot-arrangements** are interpreted as burials, although the absence of preserved bone material questions this assumption. Employing pXRF analysis on soils can reveal the former presence of a body by finding traces of a decomposed body on an atomic level, i.e. primarily through enrichment of phosphorus. **Pits**, the most common yet least understood features, evade any conclusive interpretation regarding their former use. Soil analysis using pXRF helps to trace back former activities by revealing specific elemental signatures, i.e. both enrichments and depletions of several elements, and to interpret these signatures by utilising literature knowledge and data obtained from a modern Fulani village (chapter 6.3).

4.1.1 Stone-Pot-Arrangements

The affirmation of the hypothesis that stone-pot-arrangements were burial features is, besides the analysis of pit features (chapter 4.1.2), the main objective of this thesis. Confirming stone-pot-arrangements as burials makes it possible to draw conclusions about mortuary practices and to understand the former function and layout of sites.

The archaeological evidence suggests that stone-pot-arrangements can be interpreted as burials; the presence of necklaces within some of the features is the strongest indication (Rupp 2010: 70; Nagel 2014; Schmidt 2014: 101–102; Schmidt 2016). However, neither bones nor other human remains considered as hard evidence were found, since the acidic soil dissolves all remnants. In spite of the disappearance of visible evidence, forensic and archaeological studies have identified residues of a decayed body in the associated soil, after the process of decomposition has taken place (see chapter 6.2 and 6.4). These residues occur in the form of retained elements, which can be revealed by pXRF analysis. Elements associated with grave soils, besides phosphorus as the main indicator, are calcium, potassium, copper, manganese, and some rare earth elements (e.g. Bethell & Carver 1987; Keeley *et al.* 1977; Cook *et al.* 2006: 638; Carter *et al.* 2007). The pXRF analysis was applied at several sites and features (see chapter 7.1 for a complete list).

Stone-pot-arrangements are recurring features at Nok sites (Rupp 2010: 70; Breunig & Rupp 2016: 251; Breunig 2018: 399; Rupp 2014c: 142–144) consisting of a placement of stones next to one or two complete ceramic vessels (see Fig. 4-1). The situated stones comprise both natural and modified stones, among them grinding stones, and some stones are erected vertically (Fig. 4-1 c). Alongside the stones lie one or two decorated vessels. All pots found in stone-pot-arrangements are, according to their form and decoration, designated to the Middle Nok phase. Their position in the feature varies from being adjacent to each other to being several tens of centimetres apart, and in some cases they were placed on different heights. Stone beads, arranged as if on a string (Fig. 4-1 a, b) were found at the sites *Ido 2009* (Rupp 2010: 70 Fig. 4), *Janruwa A* (Rupp 2014c: 166, Fig. 15.16) and *Ifana 3*. However, these finds are exceptional and single beads are found

only occasionally. Beads characteristic of the Nok Culture are made from siliceous rocks such as quartz, chalcedony, jasper or carnelian (Rupp 2014b: 162–164) and their form is mostly cylindrical (Fig. 4-2).

At *Ido* and *Pangwari*, arrangements of stone artefacts or stones that were artificially arranged without adjacent pots or stone beads have been found. Due to their resemblance to the stone-pot-arrangements these 'stone-arrangements' might be considered as a specific subtype with a similar function.

Fig. 4-1: Stone-pot-arrangements from *Ido 2009* (a), *Ifana 3* (b), *Pangwari* (c), and *Kurmin Uwa 2B* (d). The white arrow in (a) indicates the position of the necklace. The pot and stone bead necklace from *Ifana 3* (b) represent only a part of the complete feature, which yielded a second pot and had a characteristic stone arrangement.

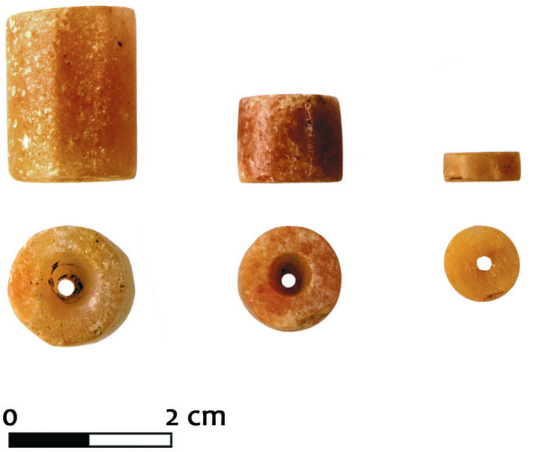

Fig. 4-2: Stone beads from the necklace found at *Ifana 3* (feature 18).

Fig. 4-3: Stone-pot-arrangement at *Kurmin Uwa 2D* with a clear outline of the fill indicating a grave pit.

Apart from the aforementioned finds, stone-pot-arrangements are void of any finds, including datable material such as charred plant material[12]. The outlines of the features are not visible since any discolouration is absent and any identification or distinction of

[12] One charcoal piece was found at *Pangwari I* (feature 18) and ^{14}C dated to 780-541 BCE.

layers is not possible[13]. One exception is a feature at *Kurmin Uwa 2D*, where a pit feature enclosing the stone-pot-arrangement has been found (Fig. 4-3). This represents the only burial feature with a clearly visible pit fill.

4.1.2 Pit Features

Pits or pit-like structures represent the most common yet least understood features of the Nok Culture (Breunig 2018: 394; Breunig & Rupp 2016: 248; Schmidt 2014: 112–113) and the partly ambiguous archaeological evidence points to both a ritual and non-ritual use (Höhn *et al.* 2018: 294–295). Employing pXRF analysis enables the identification of their former function, which, in turn, can expose their former context. The basis for this approach is that every event or infill of the pit, e.g. the exposure to fire or accumulation of faecal material, imprints a specific elemental signature in the soil. By revealing the elemental signatures of the Nok pits by employing pXRF analysis, the process of events can be reconstructed. Combining the knowledge of the activities that took place with the archaeological evidence facilitates an interpretation of the pits with regards to their former use and, in consequence, an association to a ritual or non-ritual context. Ideally, the elemental signatures allow the identification of pit categories concordant with recurring parameters such as size or find inventory. Information about the origin and formation of specific signatures imprinted in the soil were obtained by reviewing the literature and analysing a modern Fulani village (see chapter 6.3). A complete list of analysed Nok sites and pits is provided in chapter 7.1.

No uniform definition exists for the Nok pit features; a standardised definition is precluded by the large diversity of the pits. Furthermore, pits yield ^{14}C dates from all phases of the Nok Culture (see chapter 2.3), although the majority of data concentrate in the Middle Nok phase. This resembles the overall picture of the Nok Culture, since the majority of obtained ^{14}C data cluster in the Middle Nok phase (Franke 2017: 56). The pits (see Fig. 4-4) are either circular or irregular shaped and vary between 20 cm and 2 m, in both diameter and depth (Schmidt 2014; Breunig & Rupp 2016: 245, 248; Höhn *et al.* 2018). Some features appear as shallow depressions rather than real pits (Breunig & Rupp 2016: 248). Most pits are convex, i.e. their size decreases towards the bottom. Some pits are rather large and tub-shaped, some are small with steep profile walls. Their visibility ranges between strong discolorations with clear outlines to fills almost impossible to distinguish from the surrounding soil (Breunig & Rupp 2016: 248; Schmidt 2014). Their find inventory includes complete but broken vessels, potsherds, stone artefacts such as hatchets or grinding stones, terracotta pieces, charcoal or other charred plant material as well as burnt clay (see e.g. Breunig & Rupp 2016: 248–249; Rupp 2014b; Schmidt 2014). In general, iron objects on Nok sites are extremely rare. Apart from iron production sites, finds related to iron production such as slag or tuyère are usually absent in pits. Exceptions are e.g. slag fragments, which are often interpreted as being younger and mixed up with older layers (Breunig & Rupp 2016: 241, 249; Eggert 2014; Franke 2017: 196–197).

The state of find preservation ranges from complete objects to small shattered pieces and from strongly weathered to well preserved, with remains of slip on some terracotta pieces (Männel & Breunig 2016: 320, 323). Regarding the stratigraphy, a distinction of

[13] Some of the Nigerian labourers reported that the soil inside the stone-pot-arrangements at *Pangwari* had a softer texture compared to the surroundings, which might indicate a pit fill.

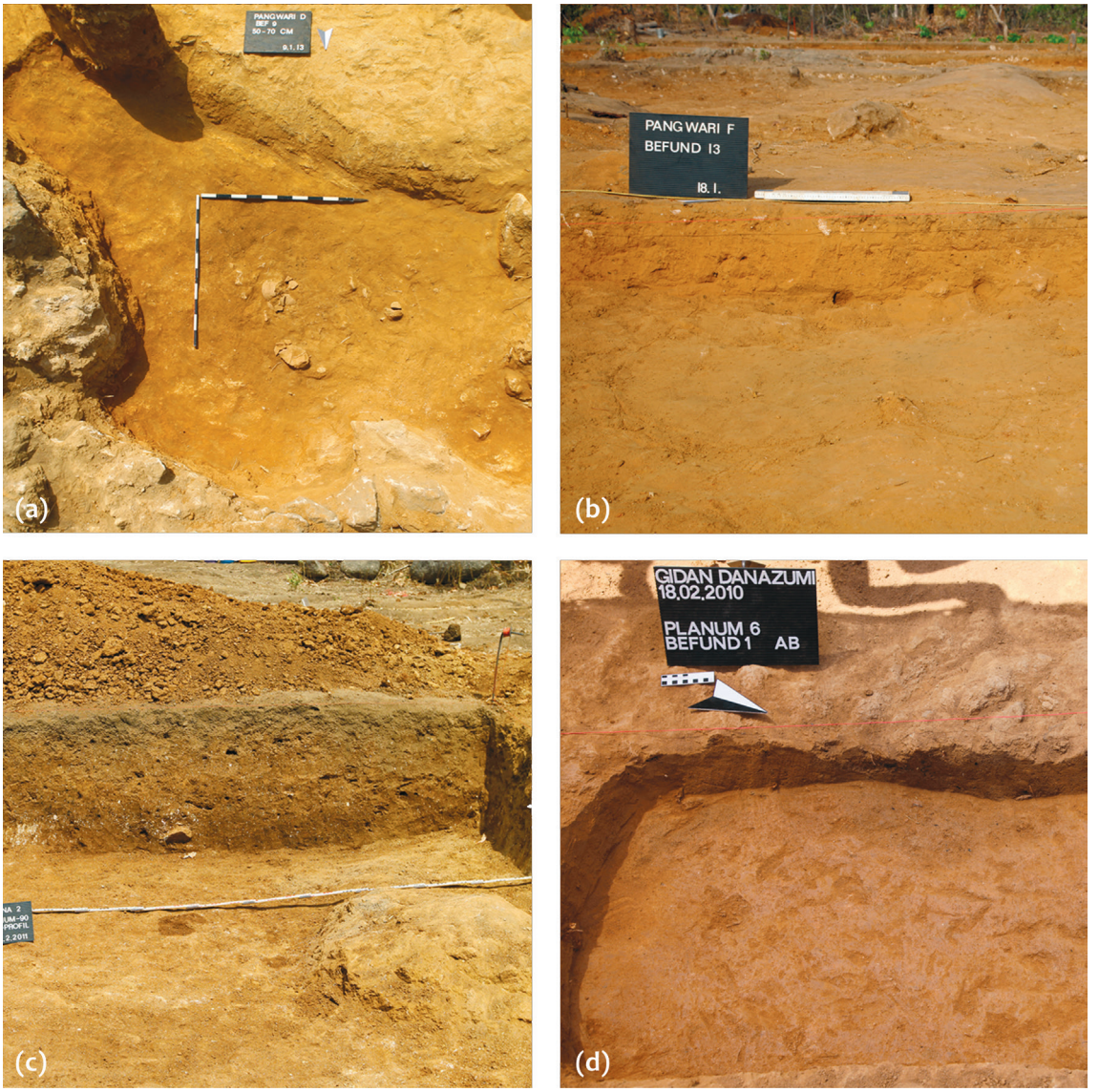

Fig. 4-4: Pit features from *Pangwari* (a, b), *Ifana 2* (c) and *Gidan Danazumi* (d). Form and size vary as much as the visibility in the soil, from strong discolorations (c) to very slight changes of the soil colour (b), which are almost invisible to the eye.

layers or different pit fills by soil colour is, apart from the greyish top-soil, rarely possible (Breunig & Rupp 2016: 245). One successful approach to distinguish layers is the three-dimensional visualisation of finds and dated material with respect to their position in the feature by utilising spatial information obtained during excavation (Schmidt 2014; Höhn *et al.* 2018). However, the sites and features can be multi-phased, which complicates the interpretation (Höhn *et al.* 2018; Breunig & Rupp 2016: 244–246; Schmidt 2014: 114–115). The location of pits within sites is variable and depends on the size of the excavated area, e.g. can pits occur next to stone-pot-arrangements and terracotta depositions (*Pangwari* and *Ido 2016*) or in the context of other pit features (*Kusuma 1* and *Ifana 2*).

A pit at *Pangwari* (feature 11) is representative of the problems relating to the interpretation of these features. The pit is located between a terracotta deposition and stone-pot-arrangements, is very large and has an irregular shape measuring 1.5 to 2.5 m with large protrusions (Fig. 4-5); the fill of the pit is in situ up to 1 m in depth (Schmidt 2014: 79–83; Höhn *et al.* 2018: 286–289). The find inventory comprises numerous small and partly weathered pieces of potsherds and terracotta fragments, stone artefacts, charcoal and other charred plant material such as pearl millet and burnt clay, all pointing to settlement waste (Schmidt 2014: 79–83; Höhn *et al.* 2018: 286–289). Atypical for settlement waste is the presence of a 'placement' consisting of a terracotta head, a complete but broken vessel, together with a grinding stone (Höhn *et al.* 2018: 294; Schmidt 2014: 79–83).

This 'placement', together with the spatial and temporal proximity to stone-pot-arrangements and the terracotta depositions, point to a ritual context rather than that of a settlement. Furthermore, the large size of the pit contradicts its interpretation as a simple waste pit. The abundance of typical settlement waste, however, remains unexplained (Höhn *et al.* 2018: 294–295). In general, another (unsolved) peculiarity is the appearance of terracotta fragments in two contradictory contexts: as large pieces within terracotta depositions and as smaller pieces together with typical settlement waste (Breunig 2012: 91; Burmann 2016: 123–124; Männel & Breunig 2016: 327–328; Breunig & Rupp 2016: 249; Rupp 2014a).

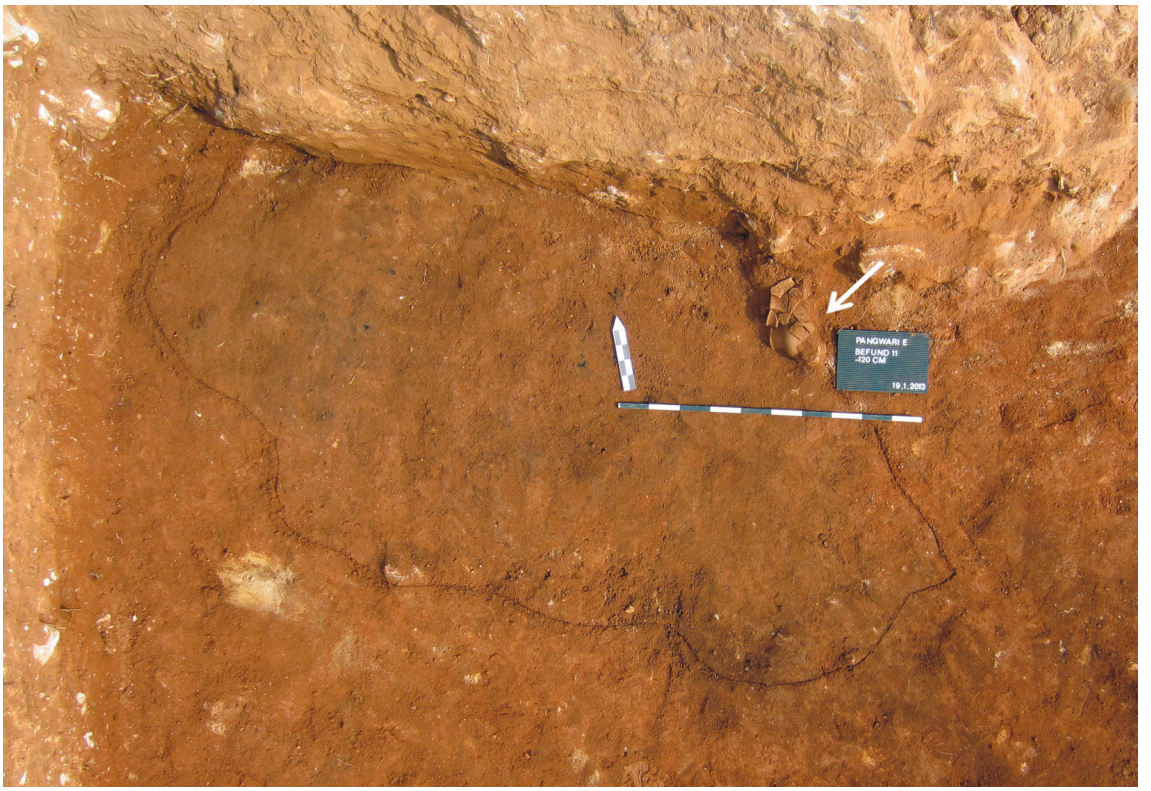

Fig. 4-5: Top-view of pit feature 11 at *Pangwari* showing its extremely large size. The feature is located in trench *E* between a terracotta deposition to the east and stone-pot-arrangements to the west. The remains of a complete but broken vessel is indicated by the white arrow.

4.2 West and Central African Context

Problems of identifying burials are not restricted to the Nok Culture – in West and Central Africa, where acidic soil predominates, bone preservation is frequently poor. Pits with an inconclusive function occur in several West and Central African contexts, summarised as *pit phenomenon* (Mbida Mindzie 1995: 41–47).

This chapter aims to contextualise the Nok features rather than compile all of the burials and pit features in West and Central Africa. The selection of the West and Central African examples is based on parallels with the Nok features either in their appearance or the underlying research question. This can help to reveal whether their interpretation as burials is likely to be correct and provide new ideas for how they could alternatively be interpreted.

The presented examples originate from manifold different chronological and regional contexts. The majority are from Central Africa, mainly southern Cameroon and DR Congo, as the Iron Age burials and pit features here were considered to be most relevant to the Nok context. The features from the southern part of Cameroon are especially of interest, as elemental analysis of the features has been conducted (see chapter 6.2). The age of the selected examples ranges from the end of the 3rd millennium BCE to the beginning of the 2nd millennium CE[14]. The closest sites[15] are located in the Nigerian Chad Basin (at *Zilum*) and southern Cameroon (Yaoundé) at a distance of *c.* 700-800 km; the most distant sites scatter along the Lulonga, a tributary of the Congo River, at a distance of more than 1,500 km.

In terms of comparable material that is contemporaneous and in close proximity to the Nok Culture, there is a general paucity[16]. The Nok Culture lacks any known predecessors; the people of Early Nok probably migrated from the North as indicated by their use of pearl millet, which was domesticated in the Sahel (Höhn & Neumann 2016: 332; Breunig & Rupp 2016: 241–242). After the end of the 1st century BCE the evidence for the Nok Culture vanishes; the following centuries are devoid of terracotta figurines, comprise a newly developed pottery tradition (Franke 2017: 191; Beck 2017: 102) and prove the use of new plants (Höhn & Neumann 2016: 351). The archaeological evidence found in the first centuries CE, after the end of the Nok Culture, mainly consists of a few large pits with unknown functions (see e.g. Höhn & Neumann 2016) and was not studied in detail by the Nok project.

4.2.1 Burial Features

The presented examples comprise features interpreted as burials, both with and without bone remains. Examples from Burkina Faso and the Nigerian Chad basin are, due to bone remains, verified as burials and show similarities to the Nok stone-pot-arrangements. The examples from the southern part of Cameroon are – except for one case – devoid of bone material, but display strong indications of being burials due to their appearance. The latter are of special interest because elemental analysis has been conducted on these features (see chapter 6.2).

---

[14] All dates extracted from the literature were originally given as calibrated ^{14}C data, unless specified otherwise. To provide uniformity, all dates are expressed as BCE/CE.

[15] Measured from the research station in Janjala at the centre of the key study area (see chapter 2, Fig. 2-1).

[16] For a comparison with respect to the pottery tradition see Franke 2017: 201–213.

Bead Collars and Stone Slabs from Kissi

The Iron Age site of *Kissi* near the Mare de Kissi in the northeast of Burkina Faso resembles the Nok features through the presence of **stone beads and collars** as grave goods, artificially arranged **stone slabs** and the occurrence of **burial pits**. In contrast to the Nok features, however, bones were preserved within the burials. The settlement at *Kissi* is divided into three occupation phases, beginning with the early phase from the 1st to 4th century CE, middle phase from 4th to 8th/9th century CE and the last phase from 9th to 12th century CE. Burials from all phases occur at the cemetery, although the majority of and the richest burials date to the middle phase (Magnavita S. 2009: 83). During the Iron Age, inhumations in pits predominate at *Kissi*, aside from one jar burial, probably dating to the late occupation phase. The inhumations are embedded in elongated pits and were marked by stone slabs on the surface, both vertically and horizontally placed (Magnavita S. 2009: 83–84; Magnavita S. 2015: 25, 175). It remains uncertain, however, whether these markers are contemporaneous or were added later (Magnavita S. 2015: 175–176). The most common grave goods were jewellery, especially beads or bead collars, besides weaponry, of which arrows were preferred. A total of almost 5,000 beads were found, most of them made from siliceous stones and with cylindrical forms. Bead collars are arranged on the dead in the same fashion as if they were wearing them (Magnavita S. 2009: 85; Magnavita S. 2003: 129, 175). Pots are absent as grave goods (Magnavita S. 2015: 175). What is remarkable is the difference in the quantity of grave goods, ranging from none to high amounts (Magnavita S. 2009: 85), indicating a hierarchical or stratified society (Magnavita S. *et al.* 2002).

Single Bead Finds from the Nigerian Chad Basin

In general, there is little evidence for grave goods in the northeast of Nigeria until 800 CE (Magnavita S. *et al.* 2002: 34). Exceptions are the occurrences of **single beads** made from different materials associated with Stone Age burials such as those at the sites of *Kursakata*, *Borno 38* and *Daima I*, all located on the 'firki', the clay plains south of Lake Chad (Connah 1976: 324).

At *Borno 38*, dated mainly between the 2nd millennium BCE and the first half of the 1st millennium BCE, the remains of four individuals, all inhumations without grave goods, were found (Connah 1981: 85, 87). One exception was the grave of one adult containing eight clay beads (Connah 1981: 95).

At *Kursakata*, where occupation started around the beginning of the 1st millennium BCE, ten burials were found in the lower part of the mound. All of these were void of any grave goods with the exception of one burial, which was associated with eight stone beads (Connah 1976: 328).

At *Daima*, a site with different occupation phases dating from around 600 BCE until 1100 CE, 70 inhumations were found in total, differing between older (Later Stone Age) burials without, and younger (early and developed Iron Age) burials with, grave goods (Connah 1976: 372, 342). One exception among the older burials from the Later Stone Age is a cylindrical bone bead found at the neck of an adult skeleton from the lower layers in the stratigraphy (*Daima I*), dating after 600 BCE; the upper burials dating from the end of the early Iron Age and developed Iron Age contain beads made from different materials and other objects (Connah 1976: 343, Fig. 10, 346; Connah 1981: 116).

Burials without Bones: South Cameroon

These Iron Age features are – like the Nok stone-pot-arrangements – void of any bone remains but interpreted as burials. The feature type is characterised by a rectangular shape and contains finds interpreted as offerings. Their interpretation as a burial is based on the singular discovery of bone remains in such a feature at the site of *Akonétye*. Of special interest are the elemental analyses of features at *Campo*, which resemble this specific feature category (see chapter 6.2).

At the site of *Akonétye* in southern Cameroon, two quadrangular burial features (AKO 05/02 and AKO 05/06), dating to 20-420 CE, contained complete vessels located above numerous iron objects (Meister & Eggert 2008: 190–192; Meister 2010: 243). A few bone residues were discovered during the restoration of iron bracelets originating from a feature (Meister & Eggert 2008: 190). The discovery of those bone remains at *Akonétye* indicating a burial were crucial in interpreting the function of this particular feature type occurring in southern Cameroon during the 1st millennium BCE and beginning of the 1st millennium CE. These features were elongated and shallow pits, *c.* 2 m long with a maximum depth of 1 m, together with iron artefacts beneath pots, which can occur intact or as sherds, inverted or vertically piled, in the form of pottery packages or fragmented. Besides the exceptional finds at the site of *Akonétye*, these features were all void of bone remains (Meister 2010: 243, 246–247; Eggert & Seidensticker 2016: 59).

Similar features, dating to the first half of the 1st millennium CE (Eggert & Seidensticker 2016: 61), were identified at *Campo* (for additional examples from Cameroon see Meister 2010). Two rectangular features comprised a kind of sherd pavement above corroded iron objects (Eggert & Seidensticker 2016: 25–30). At *Campo Church*, several features with a similar appearance were found with inverted pots or pot piles located above iron artefacts (Meister 2010: 243–244; Eggert & Seidensticker 2016: 25–30, 34–53). The interpretation that these were the same feature type, i.e. burials, is due to the similarities to the features at *Akonétye* (Eggert & Seidensticker 2016: 59).

At *Mpoengu* near Kribi (Cameroon), an inverted pot placed above iron objects was also observed. In this case, the excavators suggest that these should be interpreted as 'cult sites' and 'depots' of iron objects and ceramic vessels, which were 'probably part of some rituals' (Meister & Eggert 2008: 197 refer to a conference presentation by Gouem Gouem & Lavachery in 2006). Outside Cameroon, another example comparable to the sites of southern Cameroon was found at *Nandá* on Corisco Island between Equatorial Guinea and Gabon. Some of the revealed features, dating to between the late 1st century BCE and the 5th century CE, were also rectangular and resembled those at *Akonétye* (González-Ruibal *et al.* 2013: 116–117, 119, 121). The relevance of the burials at *Nandá* becomes clear as, apart from the aforementioned rectangular grave features, pits indicating a mortuary use were also found in the same context (see *Interpretation of Pits in a Ritual Context* in chapter 4.2.2).

4.2.2 'Pit Phenomenon'

The comparison of pits illustrates the diversity of this *pit phenomenon* and presents the range of possible interpretations for these features. Although these pits can be multi-phased and multi-functional, the different possibilities for interpretation are artificially

divided into two main categories of a ritual and non-ritual context, in order to get a better overview of the existing interpretations.

Interpretation of Pits in a Non-Ritual Context

Examples of pits interpreted as being within a non-ritual context are known from some Stone Age and Iron Age sites within the Lake Chad area in the northeast of Nigeria. At sites of the *Gajiganna* Culture, several pits of unknown function were recorded (Wendt 2007: 16–27). At one of these sites (NA 90-5C), however, a feature interpreted as a **storage pit** was discovered (Wendt 2007: 20–22; Gronenborn 1997). It is a 1.7 m deep and bell-shaped pit, 1.3 m diameter at the bottom, and it yielded a date between 1500 and 1120 BCE. Its appearance resembles storage pits in this area, which are still used today (Gronenborn 1997: 432–434). Similar features in this area occurred at *Zilum*, dating to between the 8th and 4th century BCE. Among them are round pits measuring up to 2 m in diameter with a maximum depth of 1.8 m. Their use as storage pits (e.g. of sorghum) is likely, and some of them might have initially been used as borrow pits, i.e. for the extraction of materials such as clay, and then reused as a storage facility (Magnavita C. 2008: 114, 118; Magnavita C. & Magnavita S. 2001: 48). Features from *Daima II* and *III*, all dating after the beginning of the Common Era, also appear to have been used as storage pits (Connah 1981: 147, 168). Connah compares those features to storage pits found in the Yobe valley, at *Dufuna*, which are 2-3 m deep with a rhomboid opening from the base (Garba 1999: 51). Besides those storage pits and small pits with unknown function, further large pits were discovered. These were interpreted as **borrow-pits** due to their resemblance to borrow-pits in West African villages, which can also be reused as refuse pits (Connah 1981: 147, 168).

Mbida Mindzie (1995) provides further suggestions for the functions of pits in Cameroon dating between the 1st millennium BCE and the middle of the 1st millennium CE (Mbida Mindzie 1995: 641–642). His assumptions relating to pit use derive from examples of sub-Saharan pits with known functions comprising use as **wells** for water supply, for **mineral prospection** of e.g. iron ores, to **extract rocks** for stone tools, to **collect** material for constructing houses or clay for pottery manufacture or as **silos** to store products (Mbida Mindzie 1995: 45), of which the latter possibility is exhaustively discussed by Atangana (1988: 280–300). Furthermore, Mbida Mindzie suggests the use of pits as **traps**, **cesspits** or for **tanning** and **dyeing** of animal skins (Mbida Mindzie 1995: 46). Pedological and chemical evidence from some pits indicate **standing water** (Mbida Mindzie 1995: 149) and the **processing of organic products** (Mbida Mindzie 1995: 398; Mbida Mindzie *et al.* 2000: 152). The use of pits as a **latrine** is also considered due to finds of fish bones associated with concretions rich in calcium and phosphate, which point to evidence of human or animal excrement (Mbida Mindzie *et al.* 2000: 159). Like Connah (1981: 147) Mbida Mindzie discusses the secondary use of pits as refuse pits – assuming that once the primary functions of a pit are fulfilled it will be reused a as **refuse pit** and filled with local soil, broken ceramics and stone tools, iron slag, charcoal and faunal remains (Mbida Mindzie 1995: 46; Mbida Mindzie *et al.* 2000: 152–153, 170). The interpretation of such pits as ritual pits or graves is also mentioned by him (Mbida Mindzie 1995: 44; Mbida Mindzie 2002: 170). Also known from southern Cameroon is the use of refuse pits in the context of **smithing** activities at the site of *Minyin* (first centuries CE), where some pits up to 3 m deep were found containing pots, iron objects, tuyère fragments and slag (Meister 2008: 53; Meister & Eggert 2008: 197 Tab. 1).

Further suggestions are provided within the context of pits dating from the Stone to the Iron Age in Gabon and comprise, among others, the function as **bowl fireplaces**, **post holes** or for the **extraction of palm oil** (Clist 2005: 138–139).

In the context of the *Kintampo* tradition in Ghana, dating from 2100 to 1400 BCE (Watson 2010: 141), similar features are known. A large number of pits were found at *Birimi* and *Ntesero*, whose functions cannot be explained as storage facilities (Casey 2000: 121). At *Ntesero*, large pits are interpreted instead as **water holes** for collecting drainage and storing water (Davies 1980: 206) and small pits as **latrines** or **rubbish pits** (Davies 1980: 207).

Interpretation of Pits in a Ritual Context

The interpretation of pits in a ritual context will be discussed using examples of Iron Age pits from Central Africa. Besides rectangular pits interpreted as burials (see chapter 4.2.1), another feature category occurred at the aforementioned sites of *Akonétye*, *Campo* and *Nandá*, as well as on several other sites: deep pits with different indications of a ritual purpose. At *Nandá*, a third feature type comprising shallow pits was observed.

At the Iron Age site of *Akonétye* (southern Cameroon), dating to the first half of the 1st millennium CE, deep pits containing pottery and iron objects, which indicate a non-domestic use, were found (Meister 2008: 51, 53; Meister & Eggert 2008: 189, Tab. 1). Some pits appear to have been used as rubbish pits based on finds of daub or potsherds (Meister & Eggert 2008: 197). However, there are severe pieces of evidence contradicting their use as simple waste pits, such as the occurrence of recyclable iron objects, the enormous pit sizes with a depth of up to 3.9 m (!), and other peculiarities such as a layer of ceramics comprising several broken pots, which appeared to have been intentionally arranged (Meister & Eggert 2008: 197–198; Meister 2008: 53; Eggert & Seidensticker 2016: 59). The pits seem to have been refilled over a short time period as the dates and pottery are homogeneous (Meister & Eggert 2008: 189).

Iron artefacts associated with pottery within two pits contemporaneous to *Akonétye* were found at the site of *Campo* (southern Cameroon). The occurrence of iron objects and an entire ceramic vessel, as well as pottery concentrations, are consistent with the pits at *Akonétye* (Seidensticker 2016: 154; Seidensticker 2010: 55, 107–108). However, there is no definitive evidence that these pits performed a ritual function (Eggert & Seidensticker 2016: 60).

At *Bwambé-Sommet*, dating to the second half of the last millennium BCE (Meister & Eggert 2008: 197), some pits contained ambiguous find inventories. Large accumulations of potsherds and charred plant material, suggesting their use as refuse pits, were associated with evidence for intentional arrangements of pottery: in one feature the edges of the pit were paved with a 'lining' of potsherds and small stones; another pit contained intentionally shattered pots associated with stones, which were probably used for crushing the pots; and another contained half a pot at its base (Meister 2008: 48; Eggert 2006: 280–281). A pavement of large pot fragments at the bottom of a pit was also observed at the other Cameroonian sites of *Bissiang* (Gouem Gouem 2011: 454, cited in Nlend Nlend 2013: 270) and *Nkang* (Mbida Mindzie 1995: 394; Nlend Nlend 2013: 270).

A similar example originates from *Nandá* on Corisco Island between Equatorial Guinea and Gabon, dating to the first phase at this site, between the late 1st century BCE and the

5th century CE (González-Ruibal *et al.* 2013: 118). Besides the aforementioned rectangular features (chapter 4.2.1), a 1.2 m deep pit contained a broken but almost complete pot placed beneath a stone; this arrangement indicates a possible ritual use (González-Ruibal *et al.* 2013: 132–133). At *Nandá*, a third feature type was identified: shallow, circular holes containing metal offerings (with a few pots or potsherds). The crucial discovery within those pit features, however, were human bone remains stuck to iron objects (González-Ruibal *et al.* 2013: 119, 121–122). These features were thus interpreted as 'secondary interments in which bundles of bones and mostly iron artefacts were placed together in small pits dug directly into the sand' (González-Ruibal *et al.* 2013: 140).

In the context of the *Kintampo* tradition, dating to 2100-1400 BCE (Watson 2010: 141), a feature at *Birimi* could also be interpreted as a burial despite the absence of bones: a circular pit with a complete vessel and a 'perfect projectile point' (Sawatzky 1998, cited in Casey 2000: 120). The sedimentation rate and thermoluminescence age of the pits suggest that these pits at *Birimi* were created and backfilled very quickly (Quickert *et al.* 2003: 1297), which could confirm this interpretation.

Interpreting Pits as Burials?

The paper of Wotzka (1993), highly relevant in this context, deals with the phenomenon of pits with specific attributes, such as intentionally placed pottery, which occur in Central Africa along the Congo River between the 4th century BCE and the 14th century CE. He attempts to explain these phenomena by utilising ethnoarchaeological analogies, which mainly entail funerary rites and practices of the ancestor cult.

These pits are circular, dark discolorations with a diameter of 50-90 cm and depths from a few centimetres up to 180 cm and comprise an inventory of intentionally deposited pottery together with charcoal, burnt clay and some pieces of laterite (Wotzka 1993: 256). One example is from *Boso Njafo*, where a pit consisting of three distinct fills and with a total depth of 1.5 m was discovered. Thirty more or less complete pots were found piled up in this pit, associated with small potsherds, charcoal and burnt clay; the pottery belongs to the earliest pottery in this region, the *Imbonga* group, and dates, together with ^{14}C dates, the feature to the second half of the 1st millennium BCE (Wotzka 1993: 257–259; Kahlheber *et al.* 2014: 483–486). The arrangement and preservation of the finds of all three fills indicate an intentionally deposited ensemble laid down in one event (Wotzka 1993: 259). In order to draw conclusions about the ancient pits, he employed ethnographic analogies from sub-Saharan Africa of attributes characteristic for the pits[17]. Most analogies referred to burial traditions, death cult or ancestor worship (Wotzka 1993: 264–266), of which a main characteristic in sub-Saharan Africa is the intentional destruction and inversion of material goods, especially of pots (Wotzka 1993: 269). One analogy originates from the *Fali* in northern Cameroon, whose graves are conical pits up to 2.5 m deep, covered with an inverted pot and cocooned with a small mound, which was encircled with stones (Wotzka 1993: 266–267, Fig. 7). Those graves can be found without the remains of a body, either due to poor preservation or due to the removal of the body during a secondary rite (Wotzka 1993: 272). Further pits with a similar appearance and unknown function dating from the

[17] Intentionally destroyed pottery, deposition of a complete vessel or several vessels inverted or stacked, more than one pit fill, remains of coating of coal-like organic particles, and many others (Wotzka 1993: 261–264).

4th century BCE onwards (Livingstone Smith *et al.* 2017: 111, 115, Fig. 23) were discovered during expeditions in the 2010s along the Congo river, at the north-eastern Congo bend. Some pits comprised pottery, among them complete and stacked vessels; some pits also intersected with a second pit fill (Livingstone Smith *et al.* 2017: 98–102, Tab. 1).

Numerous authors (see e.g. Meister & Eggert 2008: 198 or Mbida Mindzie 1995: 44, 444) refer to the paper of Wotzka (1993) when considering possible interpretations of pits. Apart from different non-ritual interpretations, Mbida Mindzie discusses the use of pits in southern Cameroon in a ritual context or as graves (Mbida Mindzie 1995: 44; Mbida Mindzie 2002: 170). He refers to an ethnographic analogy describing an old practice of burying the dishes of a dead woman in a pit behind her kitchen (Mbida Mindzie 1995: 394). The tradition of burying pots in the context of certain initiatory rites is also known from the *Bassa* of Cameroon (Gouem Gouem 2011: 454, cited in Nlend Nlend 2013: 271).

4.3 Summary

The research question of this thesis deals with pXRF multi-element analysis to identify and interpret Nok features. Interpreting elemental signatures can make it possible to identify stone-pot-arrangements as burials and expose the former use of pits, which, in turn, grants an insight into the layout and function of Nok sites. Stone-pot-arrangements are, based on the archaeological evidence, tentatively interpreted as burials. As the acidic soil presumably dissolved any bone remains, pXRF analysis can be employed to reveal traces of a decomposed body on an atomic level. Another objective deals with the unknown function of pit features, which frequently occur on Nok sites. Analysis with pXRF reveals the elemental signatures of the pits, which can provide information about the way in which they were used and thus help to assign the pits to a ritual or non-ritual context.

The absence of bones within presumed burials and the unsolved *pit phenomenon* are recurring features on West and Central African sites. Comparisons of verified burial features at *Kissi* and sites in the Chad Basin revealed parallels with the Nok stone-pot-arrangements, such as the use of stones as markers and finds of bead necklaces or single beads. The presumed burial features such as the rectangular features from Cameroon enable insight into other feature types lacking bones, and provide information on elemental analysis conducted on these suspected grave features at *Campo*. The review of pit features uncovered in West and Central Africa has shown that the *pit phenomenon* is not limited to the Nok Culture. Manifold possible interpretations exist, both in a ritual and non-ritual context. The spectrum of everyday uses of pits comprises storage, material extraction, traps, latrines, and, above all, refuse pits. The use of pits to dispose of waste is often referred to as secondary use, which is assumed for most of the pits. Deep pits comprising 'special finds' such as complete vessels, pottery linings or other peculiarities are inconsistent with an everyday use and raise questions about their true function. The discovery of bone fragments within pits at *Nandá* implies a mortuary context, which was already proposed by Wotzka (1993) for pits from the Congo Basin through ethnographic analogies.

METHODOLOGY AND APPROACH

5 pXRF Measurements

5.1 X-ray Fluorescence Analysis

5.1.1 Basic Principles

X-ray fluorescence spectroscopy (XRF) is a method to both identify and quantify the elemental composition of a sample. This approach utilises a specific section of the electromagnetic spectrum, the X-rays. Techniques such as inductively coupled plasma mass spectrometry (ICP-MS) make use of less energetic regions of the (near) visible spectrum whereas extremely energetic photons, gamma rays, are utilized in e.g. neutron activation analysis (Pollard & Heron 2008: 19–20).

Based on the particle-wave duality of electromagnetic radiation two instrumental approaches exist: energy-dispersive XRF (ED-XRF) and wavelength-dispersive XRF (WD-XRF). ED-XRF systems record information of all elements simultaneously by measuring the particles, i.e. counting the number of photons with known energies. WD-XRF systems measure the electromagnetic waves and identify and quantify elements by the characteristic wavelengths of each atom. The measurements can be performed simultaneously for a quick analysis of several elements or sequentially for each element (Pollard & Heron 2008: 41–43). WD based analyses, in contrast to ED-XRF, have a lower limit of detection (LOD) and a higher precision, although 'the ED-XRF determinations were statistically indistinguishable from the data produced by a number of laboratories routinely employing WD-XRF'. The main advantage of ED-XRF is that it is less time consuming and less expensive (Pollard & Heron 2008: 44–45). Especially when employing a *portable* ED-XRF device the advantages are significant: it provides quick analysis of more than 20 elements, with sufficient precision for most elements, can be used for in situ analysis and it is both affordable and user-friendly (Goodale *et al.* 2012: 882). For this thesis, such a portable energy-dispersive XRF device (p-ED-XRF or pXRF) was used[18].

The principle of pXRF analysis is based on the fundamentals of the atomic structure according to the Bohr model. The nucleus in the centre of an atom consists of neutrons, electrically neutral particles, and protons, positively charged particles. Electrons, negatively charged particles, surround the nucleus on circular orbits and cause electrical neutrality through having an equivalent number to the protons. The normal configuration is ground state, meaning that the electrons circle in the inner orbitals with the lowest possible energy (Pollard & Heron 2008: 413–414; Pollard & Heron 2008: 20–21). The pXRF device initiates the analysis by emitting electrons from an X-ray tube towards an anode. The incident electrons collide with the sample and remove the sample's inner electrons, leading to an ionisation of the atom. The resulting vacancy on the inner orbit is filled immediately with an electron from another orbit; the resulting radiation is measured (Beckhoff 2006: 36–37). As each element has a different orbital electron configuration, the quanta of emitted electromagnetic radiation are fixed and provide a unique line in the X-ray spectrum for each element (Pollard & Heron 2008: 20–21; Beckhoff 2006: 37).

---

[18] With thanks to the William Buller Fagg Charitable Trust, which donated the pXRF device to the Nok project.

5.1.2 Device Performance and Settings[19]

Device Type

The instrument used for the analysis was a *Niton XL3t 900S He+*, a portable energy-dispersive X-ray fluorescence analyser with an Ag anode (maxima: 0.1 mA, 50 kVp, 2 watts). The second device used for comparison measurements (see chapter 5.2.3) was a *Niton XL3t 900S He GOLDD* and is property of the research unit for pottery ('Forschungsstelle Keramik') of the Institute of Archaeological Sciences at the Goethe University Frankfurt. Both devices feature a silicon-drift-detector (SDD), which enables the measurement of the light elements Mg, Al, Si, P, and S without helium flush. The use of a helium flush is optional for both devices and can help to increase the measurements' precision and limit of detection of the lighter elements.

Measurement Mode

All measurements were executed in the mode for minerals *Mining Cu/Zn* with factory calibration (FC). The device offers different measurement modes and filter settings, depending on the measured material and sample matrix, e.g. alloys, rocks or liquids. The mode *Mining Cu/Zn* measures light elements starting with Mg and is suitable for soil or other bulk samples with a SiO_2 matrix. The factory calibration of this mode is based on the fundamental parameter algorithm and can be empirically (fine) calibrated by using linear corrections (see chapter 5.2).

During the measurements, the device cycles through a predefined set of filters. The filters *main*, *low*, *high*, and *light* with their different ranges were utilised. As light elements are more difficult to detect, the light filter was activated for twice as long to increase the measurement precision. All measurements persisted for **300 seconds with each filter lasting 60/60/60/120** seconds (main/low/high/light range). Exceptions were made at *Ifana 3* (feature 8), measured for 120 seconds (30/0/0/90), and at *Ifana 2*, measured for 180 seconds (40/40/40/60).

The samples relevant for the calibration and sample preparation (see chapter 5.2 and 5.3) were measured **four times** to calculate the total variance (see chapter 8.3.3). Based on the outcome of chapter 5.3.1, however, it turned out to be sufficient to measure the samples from Nok sites and features **once**.

Measured Elements and Detection Limits

An overview of the elements measured by the pXRF device and their limit of detection (LOD) is given in Table 5-1. All listed elements were considered in this thesis, with the exception of the non-detected elements as well as the elements S, As and Hg, which were above the LOD only in exceptional cases. Non-detected elements in samples from Nok sites were Mg, Co, Se, Ag, Cd, Bi, and Th, which were *all* below the limit of detection. The elements P, Ni and Cu were partly analysed as the values were, depending on the

[19] All technical information provided by *analyticon instruments* (analyticon.eu) and the *User's Guide for NITON XL3t 900 Analyzer with GOLDD Technology Version 6.5*. See also Beck 2017: 51–53 and Helfert *et al.* 2011: 6–7.

Symbol	Element	Filter	Detected by device	Detection limit in ppm
Mg	Magnesium	Light	-	3500
Al	Aluminium	Light	✓	
Si	Silicon	Light	✓	
P	Phosphorus	Light	(✓)	250
S	Sulphur	Light	(✓)	70
Cl	Chlorine	Light	✓	
K	Potassium	Low	✓	
Ca	Calcium	Low	✓	
Ti	Titanium	Low/Main	✓	
V	Vanadium	Low/Main	✓	
Cr	Chromium	Low/Main	✓	
Mn	Manganese	Main	✓	
Fe	Iron	Main	✓	
Co	Cobalt	Main	-	20
Ni	Nickel	Main	(✓)	25
Cu	Copper	Main	(✓)	12
Zn	Zinc	Main	✓	
As	Arsenic	Main	(✓)	3
Se	Selenium	Main	-	3
Rb	Rubidium	Main	✓	
Sr	Strontium	Main	✓	
Y	Yttrium	Main	✓	
Zr	Zirconium	Main	✓	
Nb	Niobium	Main	✓	
Ag	Silver	Main/High	-	*
Cd	Cadmium	Main/High	-	8
Ba	Barium	High	✓	
La	Lanthanum	High	✓	
Ce	Caesium	High	✓	
Hg	Mercury	Main	(✓)	*
Pb	Lead	Main	✓	
Bi	Bismuth	Main	-	3
Th	Thorium	Main	-	*
(Bal)	(Balance)	Main	✓	

Tab. 5-1: Filter settings for measured elements and their detection limits. Limits of detection are calculated as three standard deviations (99.7% confidence interval) for each element, using 60-second analysis times per filter; all LODs without use of helium flush. Information on detection limits provided by *analyticon instruments.*

✓ measured, (✓) partly below LOD, - all below LOD, *no information or application-specific. Balance sums up all elements not identified by the device.

analysed site or feature, often below the LOD. All given detection limits are stated for ideal measurement conditions and fluctuate due to many different factors.

Most measured elements are covered by the main filter. Additional elements and subsequent high sensitivity analysis of K, Ca, Ti, V, Cr are conducted with the low filter. The high filter records the elements Ag, Cd, Ba, La, and Ce and the light filter the elements Mg, Al, Si, P, S, and Cl, respectively. The use of the light filter without helium flush is possible for devices with integrated SDD detector. Elements not identified by the device are estimated through scattered radiation and summed up as 'balance'. This allows an accurate quantification of all measured elements.

The device measures chemical elements, but not chemical compounds. Thus, the use of e.g. 'phosphorus' instead of 'phosphates' is preferred, in spite of the actual occurrence within the sample. All values provided by the device are given in parts per million (ppm).

Error

The error value for each element provided by the pXRF device reflects the 2-sigma deviation of the measurements, based on the square root of the counted X-ray quanta. With help of the coefficients obtained by the fundamental parameter calibration, the deviations are adjusted in consideration of all elements (see Helfert *et al.* 2011: 7). However, since this algorithm is unpublished and its calculation cannot be reconstructed, the error values were not discussed in this thesis[20]. Furthermore, the treatment of data through linear corrections (see chapter 5.2) distorts the relationship between the obtained value and estimated error, which refers to the raw data. The calculation of the total variance (see chapter 8.3.3) was considered to be more useful for estimating the measurement reliability.

[20] One exception is the error provided for the pXRF results with factory calibration used for the estimation of linear corrections (App. 1-2, see chapter 5.2).

5.2 Empirical Calibration with Linear Corrections

The calibration of a pXRF device is necessary to translate the measured X-ray counts into element concentrations (see chapter 5.1.1). This can be carried out by inverse prediction, i.e. measuring samples with known element composition to determine the best equation between counts and concentration (Johnson 2014: 565). The device provides various calibration sets for different sample matrices. For this thesis, the factory calibration of the mode Mining Cu/Zn was used (see chapter 5.1.2). Empirical calibration serves as an optional enhancement for the factory calibration. In contrast to the factory calibration, which translates X-ray counts to element concentrations, the empirical calibration utilises linear corrections to align the element concentrations to the expected outcome.

For empirical calibration, it is common to employ reference standards, samples with a precisely known composition. After adjusting the device to these standards by linear corrections, the composition of unknown samples can be analysed reliably. The standards should be as similar as possible to the sampled material. To provide an optimal empirical calibration, Nok standards made from archaeological soils within the research area were prepared. Unlike conventional reference standards with known element composition, the composition of each individual Nok standard had to be determined by a laboratory. Material for the standards were sent to *ActLabs* in Canada and analysed by Fusion-ICP and ICP-MS. After the laboratory results had been received, the Nok standards were measured with the pXRF analyser in order to align the results with the outcome of the laboratory. Besides their use for the empirical calibration, the Nok standards served as control samples. They are being measured periodically in order to check whether the device is operating within the established parameters.

5.2.1 Nok Standards

To provide a successful empirical calibration, standards as similar as possible to the Nok samples were prepared by using soil from Nok sites. Standards for calibration should fulfil certain conditions such as being homogenous and properties like surface texture, grain size and packing density should be as similar as possible to the unknown samples (Hahn-Weinheimer *et al.* 1995: 106). Thus, the samples for preparing the Nok standards were sieved through a 2 mm mesh and ground in a ball mill to a size < 125 µm to achieve a homogenous soil matrix with a smooth surface texture. If the grain size is too large, there is a risk of measuring cavities or single quartz grains. Furthermore, the laboratory requires a fine grain size for analysis. Each sample was homogenised and split into two sub-samples: material for the laboratory (see Tab. 5-2), which will be destroyed after measurement, and material for the Nok standards. Both sub-samples originate from the same sample, which allows the alignment of the results obtained from the Nok standards with the results obtained from the laboratory. Eight samples were sent to the laboratory, taken from the sites *Ifana 1* (IFA 1), *Kurmin Uwa 1* (KU 1) and *Kusuma 1* (KM 1). Three additional samples (sample no. 2, 5, 11) were sent to the laboratory for a pre-study on the effect of sample preparation (see chapter 5.2.5).

Sample no.	Site and XRF no.	Feature
1	KM 1 XRF #14	Feature 2
2*	KM 1 XRF #14	Feature 2
3	KU 1 XRF #79	On-site, non-feature
4	KM 1 XRF #162	Feature 3
5*	KM 1 XRF #162	Feature 3
6	IFA 1 XRF #333	Feature 5
7	KM 1 XRF #53	Feature 5
8	KU 1 XRF #160	On-site, non-feature
9	KU 1 XRF #44	Feature 3
10	IFA 1 XRF #70	On-site, non-feature
11*	KU 1 XRF #160	On-site, non-feature

Tab. 5-2: Samples sent to the laboratory. *Samples 2, 5 and 11 were used only for the pre-study on the effect of sample preparation, thus there exist no corresponding Nok standards.

The samples were analysed by *ActLabs* in Canada with *Lithium Metaborate/Tetraborate Fusion-ICP and ICP/MS*[21]. The original data (see App. 1-1) from the laboratory are given both in ppm (trace elements) and weight percent oxides (major elements). The alignment of the pXRF results with the laboratory results, however, requires a common unit. To standardize the units, the major elements given in weight percent oxides were converted in ppm on the basis of the known molar masses.

The Nok standards were measured by two portable XRF analysers of the Goethe University in Frankfurt (see chapter 5.1.2). With the main device (device 1) each sample was measured four times and the median[22] calculated (see App. 1-2). The second device (device 2) was used for comparison and each sample measured once. Values below the limit of detection were excluded.

5.2.2 Alignment of Results by Linear Corrections

The alignment of the obtained pXRF results with the results from the laboratory requires linear correction equations. Utilising Excel (instead of the pXRF device) for calculating the equations and applying these to the raw data offers several advantages:

- the calibration equations can be changed afterwards for selected elements without repeated measurements of the samples,
- a negative incline cannot be configured using the settings of the device,
- a direct comparison of raw data and calibrated data is possible.

[21] See http://www.actlabs.com/page.aspx?page=516&app=226&cat1=549&tp=12&lk=no&menu=64, last visit on September 2017.

[22] The median was used as a robust alternative to the mean (Filzmoser *et al.* 2018: 91).

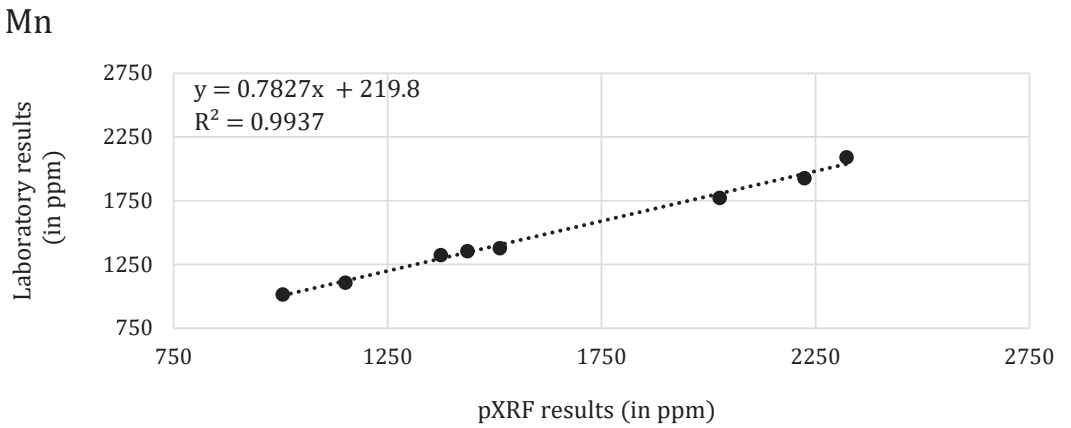

Fig. 5-1: Scatter graph for the empirical calibration of manganese. The black dots represent the values of the Nok standards (see Tab. 5-2) estimated by the laboratory (y-axis) and the pXRF device before applying the empirical calibration (x-axis). The line of best fit is indicated by the dotted line with its calculated equation in the upper left corner.

To calculate the equations, the results of the pXRF measurements were plotted against the laboratory results (see Fig. 5-1). For each element the equation of the line of best fit was calculated (in Excel) together with the coefficient of determination (R^2), which classifies the accuracy of the model with values between 0 (no values on the line of best fit) and 1 (all values on the line of best fit). If R^2 was below 0.9, the equation was adjusted by omitting outliers and re-calculated. If R^2 was above 0.9, but obvious outliers were visible, they were omitted as well to achieve a higher precision. Table 5-3 shows the calculated and applied alignment equations.

5.2.3 Success of Calibration

The outcome of the calibration, i.e. the empirical calibration with linear corrections, was examined by comparing the laboratory results with the results of the pXRF device **before** and **after** applied calibration (see App. 1-3). The comparisons have shown that for most elements the factory calibration (FC) would have been sufficient as the deviation was in most cases proportional.

In order to examine the outcome and to provide comparability, the data were plotted in a diagram with points and interpolated curve progressions. A high congruity of curves indicates a successful calibration. Calcium, for example, shows a proportional shift along the y-axis with consistent curve progression (Fig. 5-2). When analysing soil samples, the difference between the samples, i.e. the progression of the curve, is of interest, rather than a precise determination of single values along the y-axis. For comparison reasons, the results of the second pXRF device are shown as well.

The elements K, Ca, Ti, Mn, Fe, Zn, Rb, Sr, and Y were considered to have been successfully calibrated due to the high congruence of the laboratory results and calibrated data (see App. 1-3). The results for the elements Al, Si, P, V, Zr, Nb, Ba, La, and Pb, were also satisfactory although a few samples showed small deviations or samples had to be omitted. The calibrations of Ni and Cu were less satisfying, as most pXRF results were

Element symbol	Equation with all standards		Equation with omitted standards		
	Equation	R^2	Equation	R^2	Standards omitted
Al	y = 2.2261x – 17,168	0.7277	**y = 2.1702x – 14,620**	**0.9956**	3, 4 and 6
Si	y = 1.6358x – 54,941	0.9178	**y = 1.6048x – 53,058**	**0.9938**	6 and 10
P	y = 0.3931x + 419.1	0.9784	**y = 0.4203x + 331.77**	**0.9746**	6 and 7 (< LOD)
Cl	*Not measured by the laboratory*				
K	**y = 0.834x + 687.91**	**0.9877**			
Ca	**y = 1.4897x + 231.35**	**0.9982**			
Ti	**y = 2.0805x – 8,551.7**	**0.8877**	*No clear outliers can be identified*		
V	y = 0.6002x – 142.57	0.7797	**y = 0.6014x – 129,52**	**0.9786**	6, 7 and 10
Cr[1)]	*Results from the laboratory are imprecise, no equation calculated*				
Mn	**y = 0.7827x + 219.8**	**0.9937**			
Fe	**y = 0.929x – 165.79**	**0.9871**			
Ni[1)]	*Results from the laboratory are imprecise, no equation calculated*				
Cu[1)]	*Results from the laboratory are imprecise, no equation calculated*				
Zn	**y = 1.1324x + 30.749**	**0.9673**			
Rb	**y = 2.5685x + 2.485**	**0.9923**			
Sr	**y = 0.1839x – 0.5043**	**0.9891**			
Y	**y = 1.0784x – 0.6057**	**0.9919**			
Zr	**y = 1.308x + 132.01**	**0.9627**			
Nb	y = 1.0777x + 7.8068	0.8769	**y = 1.4381x – 2.9153**	**0.9666**	4
Ba	y = 1.3702x – 228.37	0.781	**y = 1.2433x – 164.37**	**0.9183**	10
La[2)]	y = -0.2149x + 108.12	0.4999	**y = -0.2435x + 111.5**	**0.8328**	1 and 3
Ce[2)]	y = 1.4631x – 310.73	0.7837	*No clear outliers can be identified*		
Pb	**y = 1.4326x + 9.9154**	**0.9206**			

Tab. 5-3: Calibration equations (linear corrections) for the empirical calibration of all elements, sorted by atomic number.

[1)] The laboratory results of Cr, Ni and Cu were provided as rounded values and were not used to calculate a calibration equation. A simple comparison of the values (App. 1-3) has shown that in the case of Cr the results of both pXRF devices appeared more reliable compared with the results from the laboratory; in the case of Ni and Cu only three standards were above the LOD. As the Ni values were close to the results from the laboratory, no calibration equation was used; as the Cu values were half of the results from the laboratory, a simplified equation stating y = x*2 was used.

[2)] High dispersions impeded a useful empirical calibration.

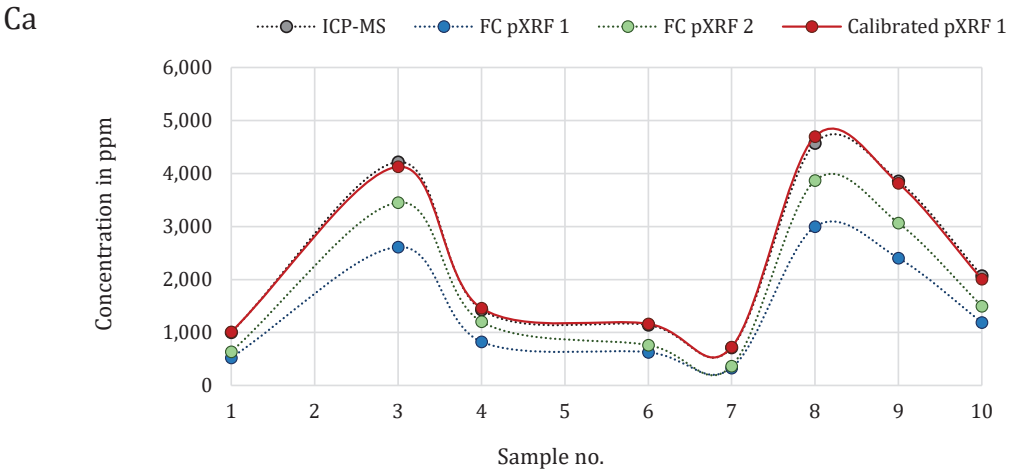

Fig. 5-2: Example for the empirical calibration of calcium. Laboratory results (grey) are shown in comparison to the pXRF results *before* (blue) and *after* (red) applied calibration by linear corrections. The comparison with the second device (green) affirms the obtained measurement results.

below the limit of detection and the laboratory results were rounded up. The calibration of the elements Cl, Cr and Ce was unacceptable or the results were below the limit of detection.

Although applying an empirical calibration of the device can be effective in some cases, the use of the factory calibration would have been sufficient for both pXRF devices as the trends of the curve progressions were identical to the laboratory for most elements. The Nok standards, however, are useful for regular control measurements.

5.2.4 Control Measurements

Besides the use of standards for calibration, periodical measurements of standards help to assure that the device works within the established parameters. Before, after and during the measurements, Nok standards were measured and the results compared with the expected values.

Regular measurements have proven useful as some of the obtained results were disturbed by instrumental errors that would have affected whole measurement series (restarting the

Standard	1	3	4	6	7	8	9	10
Total Variance	0.1057	0.0433	0.0381	0.0381	0.0313	0.0396	0.0312	0.0289
n	62	12	45	19	19	19	4	4

Tab. 5-4: Total variance of the results within each standard, each given with number of measurements (n).

device solved this problem). The calculation of the *total variance*[23] for repetitive measurements enables an insight into occurring dispersion within one sample (Tab. 5-4), which is very low in all cases.

5.2.5 Pre-Study on the Effect of Sample Preparation

In addition to the Nok standards, further samples were sent to the laboratory to conduct a pre-study on the effect of sample preparation. This pre-study aimed to reveal any influence of sample preparation, i.e. grinding or sieving, on the obtained outcome. As samples should be processed with minimum effort, questions arose whether and how the use of different grain sizes influences the result. Three additional samples (no. 2, 5 and 11) were sent to the laboratory (see App. 1-4) in order to conduct tests A-C (see Tab. 5-5), which suggested further research on sample preparation was required.

The aim of test A was to reveal the variance within one sample by analyzing two sub-samples with the **same grain-size** of < 125 µm. The estimated total variance of 0.0074 for test A is considered to be typical of the natural occurring inhomogeneity within a sample and helps to assess the outcome of tests B and C. Test B and C dealt with the analysis of **different grain sizes** within one sample. The comparison of the grain sizes < 2 mm and < 125 µm (test B) shows a total variance of 0.0312 and a significant increase of the total variance to 0.2179 was estimated when comparing grain sizes < 2 mm and > 2 mm (test C).

Sample no.	Material analyzed	Test	**Total variance**
8	All grain sizes < 2 mm ground to < 125 µm.	A: Variation among the same grain size	**0.0074**
11			
1	All grain sizes < 2 mm ground to < 125 µm.	B: Variation between different grain sizes (< 2 mm and < 125 µm)	**0.0312**
2	Natural grain size of < 125 µm only.		
4	All grain sizes > 2 mm ground to < 125 µm	C: Variation between different grain sizes (< 2 mm and > 2 mm)	**0.2179**
5	All grain sizes < 2 mm ground to < 125 µm.		

Tab. 5-5: Pre-study on the effect of sample preparation with the objectives A-C. Each sample pair (1+2, 4+5 and 8+11) originates from the same sample and for each pair the total variance between the two values was calculated based on the results shown in App. 1-4. All samples initially consisted of different grain sizes, but were ground and sieved to the size of < 125 µm to guarantee comparability and to meet the requirements of the laboratory.

[23] The total variance is the equivalent of standard deviation for compositional data such as pXRF data (see chapter 8.3.3).

Both tests B and C point to different elemental compositions for different grain-sizes within one sample as indicated by the increased variances, which were greater than the variance considered as 'normal' (test A). It remains unclear whether this is a result of a fundamentally unequal distribution of elements or is caused artificially by the greater amount of crushed stone material within the larger grain sizes. Analyses of the sample preparation methods (chapter 5.3) were employed to find the reason for the occurring variances among different grain-sizes and to avoid inaccurate results.

5.3 Sample Preparation

The aim was to gain consistent results that are representative of the entire sample and yet executed in a time-saving manner. The attempt to find an efficient preparation method was of relevance when considering the number of measured Nok samples (more than 3,000 samples). Thus, the preferred preparation method was to sieve the soil samples and to use the grain size < 125 µm only, which avoids the extremely time-consuming process of grinding. However, since the results of the pre-study (chapter 5.2.5) showed that the results within one sample vary depending on the grain size, it was crucial to avoid inaccurate results by measuring a grain size which is not representative of the samples. It is of fundamental importance to distinguish whether the variances were caused by an unequal element distribution or by the impact of the sample preparation.

Study 1 investigated the grain size required for the analysis to achieve consistent results by comparing the grain sizes < 125 µm, 125-250 µm and 250 µm – 2 mm. Study 2 aimed to reveal the variances between the three mentioned grain sizes. The grain sizes correspond to medium to very coarse sand (250 µm – 2 mm), fine sand (125 – 250 µm) and smaller or equal to very fine sand (< 125 µm) (Wentworth 1922: 381). The utilisation of these grain sizes is based on the comparison of different sand sizes against fine sand and silt. Several definitions for the classification of grain sizes exist (see Scheffer *et al.* 2010: 173), but all have in common that grains larger 2 mm refer to coarse and smaller than 2 mm to fine soil. The transition of sand to silt lies, depending on the classification system, mostly between 63 µm and 125 µm.

5.3.1 Study 1: Consistency of Measurements

The intention of the first study was to determine a grain size which ensures consistency and reproducibility of results. A total of 10 samples from the site *Kusuma 1* were compared. Each of the 10 samples was sieved into three sub-samples consisting of grains < 125 µm, 125-250 µm and 250 µm – 2 mm and measured four times to calculate the total variance; only four samples yielded enough material with the largest grain size (Tab. 5-6).

	Sample no.									
Grain size	**1**	**2**	**3**	**4**	**5**	**6**	**7**	**8**	**9**	**10**
< 125 µm	**0.1003**	**0.0747**	**0.0831**	**0.0397**	**0.0667**	0.0703	**0.1077**	**0.0306**	**0.0288**	**0.0273**
125-250 µm	0.1564	0.122	0.202	0.0688	0.0678	**0.0484**	0.1388	0.1181	0.0753	0.0547
250 µm – 2 mm		0.1565	0.5255	0.3784				0.8745		

Tab. 5-6: Total variance of four measurements for each subsample. Only samples 2, 3, 4 and 8 yielded enough sample material for the grain size 250 µm – 2 mm. The lowest variances of the three grain sizes are highlighted in bold. The total variance was calculated by including the elements Si, Ti, Al, Fe, Mn, K, V, Cr, Zn, Rb, Sr, Y, Zr, Nb, Ba, Ce, La, Pb, Ca, and Cl.

The estimated total variances clearly demonstrate that the variance declines with decreasing grain size. This result is not unexpected as a cause of inconsistent results is the heterogeneity of samples, e.g. when small stone splinters cover the measurement field. Sieving the soil samples increases the homogeneity as finer grain sizes are inherently more homogenous and interfering material like stone splinters will be discarded. In accordance with this, the differences in variances between the two finer grain sizes are significantly smaller than those of the largest grain size.

Using a grain size of < 125 µm is meaningful to produce consistent results as it yields the lowest total variance; a grain size < 125 µm can be achieved by either using the natural grain size < 125 µm or by grinding larger grains to that size. As the preferred method is using only the natural grain size < 125 µm, the crucial question of whether there is a loss or distortion of information was the objective of study 2.

5.3.2 Study 2: Representativeness of Grain Sizes

The objective of study 2 was to ascertain if the use of the natural grain sizes finer than 125 µm is representative for the entire sample or if this procedure causes a loss of information. Comparisons of the elemental concentrations among different grain sizes have proven that the results are in most cases similar and using only the grain size < 125 µm is suitable.

Origin and Treatment of Samples

The ability of the grain sizes < 125 µm to represent the entire sample was verified by comparisons to the other two grain sizes, which, all together, represent the entire sample. The significance of the information, however, lies not in the equality of values but in the similarities of trends, i.e. the differentiation of samples.

Figure 5-3 shows the position of the samples 1-10 taken from the site *Kusuma 1*. According to the excavation documentation, **samples 9 and 10 originate from a pit** (feature 2). Thus, the crucial information lies in the comparison of samples 9 and 10 to the remaining samples representing the surroundings.

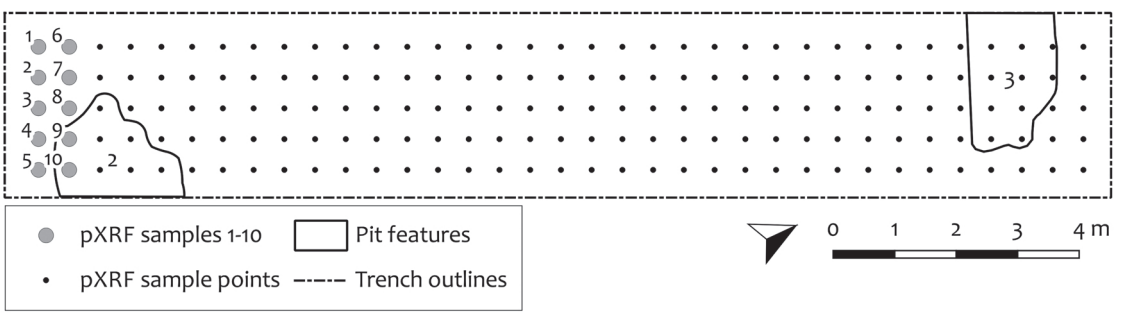

Fig. 5-3: Top-view of the site *Kusuma 1* with pXRF sampling scheme at a depth of 60 cm. The samples 1-10 are used for studies 1 and 2. Sample 9 and 10 originate from pit feature 2 according to the feature outlines obtained from the documentation.

Like in study 1, each of the 10 samples was sieved into three subsamples of < 125 µm, 125-250 µm and 250 µm – 2 mm. However, in order to ensure comparability, the subsamples of 125-250 µm and 250 µm – 2 mm were in a second step ground to the same grain size of < 125 mm. To distinguish the grain sizes, they will be denoted with their original grain size.

To ensure an acceptable level of homogeneity *after* grinding, all samples were measured four times to calculate the total variance (Tab. 5-7). The result clearly shows the lowest variance for the natural grain size < 125 µm. The samples artificially ground in a ball mill to < 125 µm reveal a higher variance. However, in all cases the total variance was acceptable.

	Sample no.									
Grain size *before* grinding	**1**	**2**	**3**	**4**	**5**	**6**	**7**	**8**	**9**	**10**
< 125 µm	**0.0284**	**0.0203**	**0.0251**	**0.0394**	**0.0311**	**0.0220**	**0.0260**	**0.0481**	**0.0328**	**0.0119**
125-250 µm	0.2669	0.2665	0.1072	0.0888	0.0741	0.1654	0.1065	0.1028	0.0986	0.1458
250 µm – 2 mm	0.6759	0.0309	0.2629	0.2158	0.0797	0.1009	0.1365	0.0918	0.0580	0.0343

Tab. 5-7: Total variance of the different subsamples given with their original grain size. The two larger grain sizes were ground to < 125 µm to ensure comparability. The total variance was calculated for the same elements as in study 1 (Tab. 5-6).

Results of Study 2

The data were plotted in a diagram with points and interpolated curve progressions to display and reveal trends (App. 1-5). All three grain sizes yield similar trends for most elements; the distinction of samples 9 and 10 was successful in most cases for all three grain sizes. The same trend and almost the same values for all grain sizes were obtained for Mn (Fig. 5-4a). Very similar trends distinguishing samples within and outside the pit were, in the case of the grain sizes < 125 µm and 125-250 µm obtained for Fe (Fig. 5-4b), V, Cr, Zn, Rb, Sr, Y, Zr, Pb, Ca, and P. Furthermore, in the case of P, it appears that the grain size < 125 µm incorporates the highest elemental concentration.

A dissimilar trend, however, was observed for the samples 3 and 5: the two larger grain sizes show higher values of Si, Ti, Al, K, Sr, and Nb (for Al see Fig. 5-4c) and lower values of the balance (Fig. 5-4d), which sums up the elements not quantifiable by the pXRF device. The overall result of the balance differs significantly as lower values occur for coarser grain sizes and higher values for finer material. The largest grain size, 250 µm – 2 mm, comprises additional differences for specific elements, e.g. V, or for specific samples, such as sample 1 in the case of Rb, Zn and Y. The elements Ba, Ce, La, As, and Cl differ significantly, although they show partly the same trend.

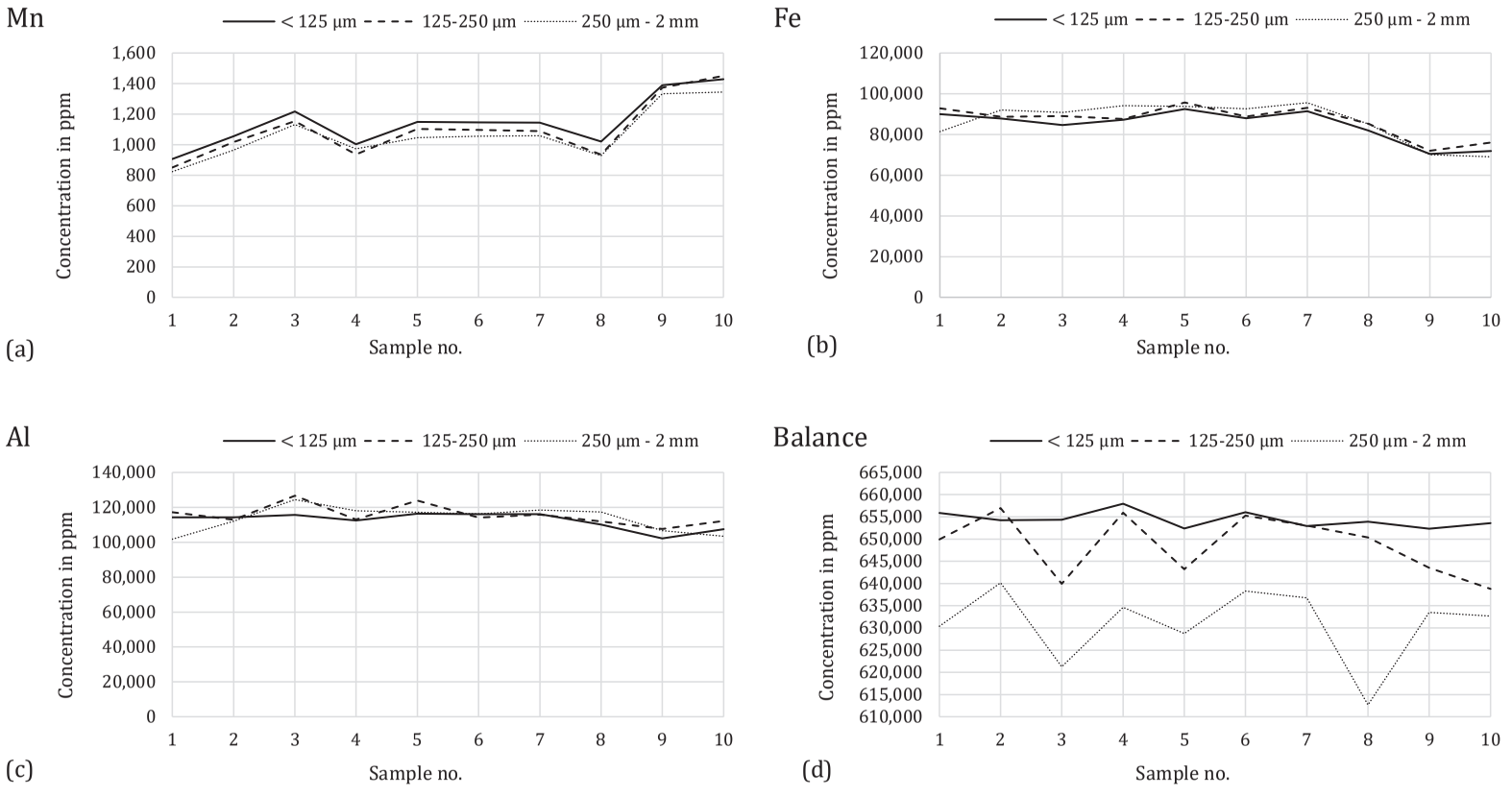

Fig. 5-4: Differences in elemental concentrations in ppm for the three grain sizes. According to the excavation documentation, samples 9 and 10 are from feature 2, the others from the surrounding soil. For the other elements see App. 1-5.

Interpretation of Results

It is of fundamental importance whether the observed irregularities of the two larger grain sizes are caused by technical issues or whether they are indicative of general differences in the distribution of elements. To understand and interpret the differences, the fact that pXRF data are compositional data must be considered (see chapter 8.1). Compositional data are data with a constant sum, which is 10^6 parts in the case of pXRF analysis as the elemental concentrations are given in parts per million (ppm). The peculiarity of these data is that if the concentration of a specific element changes (e.g. there is more Si), the concentration of all other elements changes as well so that the sum of 1,000,000 will be constant. This means for the analysis of different grain sizes that if one element changes, the other elements will counterbalance this change. This constraint can explain the behaviour of the elements for samples 3 and 5, as observed for the two larger grain sizes: the increased values for several elements is accompanied by a decreased balance value.

The crucial information, however, is the origin of this irregularity. Do the dissimilarities in sample 3 and 5 reflect a 'noise' or an 'anomaly' in the soil, e.g. an extension of feature 2? One likely explanation for noise is the higher presence of stone material within the samples of the larger grain sizes *before* grinding. For example, grinding a sample that contains granite splinters may cause an increase in measured concentrations for elements such as Si, Ti and Al (see Scheffer *et al.* 2010: 29, Tab. 2.3-1). In particular the overall increase of Si within the largest grain size can be explained by a higher occurrence of quartz splinters. The interpretation of the irregularities as an anomaly, i.e. the extension of feature 2, is unlikely. The elemental compositions of sample 3 and 5 are different to those within the feature (sample 9 and 10), e.g. in case of the balance values, which are much lower for sample 3 and 5 compared to samples 9 and 10. It appears that sample 8 is in fact part of the feature when considering its similarity to samples 9 and 10 (e.g. in case of Fe in Fig. 5-4b).

The outcome of both studies favours the use of the natural grain size < 125 µm due to its lowest total variance and its simple extraction by sieving, which requires considerably less effort than grinding the samples. There is no loss of information with respect to the key question: the distinction of the samples inside (sample 9, 10) and outside of features. Ultimately, the origin of the irregularities within the two coarser grain sizes remains unknown. The possibility that these anomalies represent features, which will remain unidentified when omitting the larger grain sizes is rather unlikely; the probability is higher that these irregularities reflect noise caused by stone material and that this noise, in consequence, might even conceal further features.

5.3.3 Technical Notes

All Nok samples were air dried for several days to weeks, depending on whether the sampling took place during the rainy or dry season, sieved to < 125 µm, poured into small sample cups (Ø 30 mm) and covered with a thin film (Prolene® 4.0 µm) to allow light elements to pass. After the sample cups were labelled the samples were measured and stored to enable re-measurements.

It was considered sufficient to measure each sample once because of the low total variance of the measurements for the grain size < 125 µm and because the spatial character of the data allows both the visualisation and elimination of outliers (see chapter 8.3.1.3).

5.4 Summary

Measurements using the pXRF device with configured **factory calibration** turned out to be suitable, compared with the results obtained by the laboratory. However, applying an empirical calibration by using linear corrections can be worthwhile as the results become more precise for some elements.

The outcome of the studies on sample preparation suggests the use of the **grain size sieved to < 125 µm**. Study 1 has shown the lowest total variance, and thus the most consistent results, for the grain size < 125 µm. Study 2 indicated that using only the sizes < 125 µm is representative for the entire sample and there is no loss of information. Although some irregularities were observed, the key information required to distinguish samples inside and outside of features is provided. The use of the natural grain sizes finer than 125 µm also has the advantage of being easy to obtain by sieving and avoids the laborious process of grinding.

The low total variance of grain sizes < 125 µm allows the **measurement of Nok samples once**, which results in an enormous saving of time. Furthermore, as these samples are spatially related, it is possible to visualise and eliminate outliers.

6 Elemental Analysis

6.1 Technical Evolution and Application on Soils

Elemental analysis as an aid for archaeological research began in the early 20th century with pioneering work such as the study by the Swedish biochemist Olof Arrhenius, who discovered a correlation between abandoned farmsteads and increased phosphate content in the soil (Arrhenius 1931: 427; Abrahams *et al.* 2010: 234). Since the 1950s, further elements came to the fore through the use of chemical analysis (Lutz 1951), although the main focus remained on phosphorus. Multi-element approaches emerged in the following decade with the enhancement of techniques capable of simultaneous multi-element analysis. Instruments using inductively coupled plasma, e.g. mass spectrometry (ICP-MS) and atomic emission spectroscopy (ICP-AES), became particularly important for the detection of trace elements (Abrahams *et al.* 2010: 235).

The onset of portable XRF devices (pXRF) was concurrent with these methodological developments, although their use in archaeological studies initially concentrated on metallurgical analysis (see e.g. Helmig *et al.* 1989). Nowadays, pXRF multi-element analysis provides information on a wide range of materials such as pottery, metals, stones and sediments, porcelain, glass, paintings, and coins (Shugar & Mass 2012; Mantler & Schreiner 2000). Studies involving archaeological soil analysis that utilise ICP-AES or ICP-MS commenced in the 1990s (Middleton & Price 1996; Entwistle *et al.* 1998), although soil analyses with pXRF have proven their usefulness in the meantime (Gauss *et al.* 2013; van Zwieten *et al.* 2017).

On the African continent, however, multi-element analysis of archaeological soils are rare and successful case studies have employed ICP-based techniques rather than pXRF (Sulas *et al.* 2017; Fleisher 2014). In the context of West and Central Africa, there is a shortage of literature with regards to archaeological multi-element analysis on soils in general and in particular using a pXRF device.

6.2 Archaeological Studies

In order to compare and interpret the results obtained from Nok sites, a review of archaeological studies that involved similar research tasks was carried out. This included elemental analysis of grave soils and pits. Comparable pit analyses, however, were absent in West and Central Africa, apart from one study in southern Cameroon. To gather information on characteristic enrichments and depletions of elements on archaeological sites and within features in spite of this, this literature review encompasses studies from all over the world. This review was not intended to aspire for completeness, but aimed to identify 'chemical fingerprints' that are characteristic of specific activities.

Pits & Burials

Elemental analysis of burials and pits, as conducted in the course of this thesis, are rare, especially on the African continent. Regarding pit analyses, only one noteworthy study from southern Cameroon was found (though not obtained by pXRF), which aimed to reconstruct the former use of pit features[24]. In addition, grave features were also the subject of analysis. In the case of the pit features, enrichments of P, Ca and K at *Campo* indicated the use as dump pits, probably caused by the infill of ashy soil (Mbida Mindzie & Mvondo Ze 2016: 147–150; Seidensticker 2010: 61). Additional samples at *Campo* revealed an increase in P in relation to higher depths (Seidensticker 2016: 151, 154; Seidensticker 2010: 108), which was also observed at *Akonéyte* (Seidensticker 2010: 61, Tab. 30-31), *Nkang* (Mbida Mindzie 1995: 722–724, Fig. 1-6; Seidensticker 2016: 154) and several other sites (Meister & Eggert 2008: 198–199, Tab. 4; Seidensticker 2016: 154; Seidensticker 2013: 55). The origin and interpretation of these P enrichments, however, remained unclear; possible explanations are the infill of organic matter, such as decomposed plant material (Meister & Eggert 2008: 198–199; Seidensticker 2016: 155), or the use as a latrine, which was formerly suggested for *Nkang* (Mbida Mindzie *et al.* 2000: 159). However, remains of entire vessels or pottery packages could also have indicated a non-ritual use (Seidensticker 2016: 154; Seidensticker 2010: 55, 107) and a comprehensive interpretation of a ritual or non-ritual use remains unsolved (Meister & Eggert 2008: 198–199).

At *Campo*, rectangular grave features void of bone material (see chapter 4.2.1) were also subjected to multi-element analysis. The results comprised low pH values and a lower content of P and Ca compared to the pit features, but higher values of Na and organic C. The abundances of soil elements were more variable within the graves compared to the pits (Mbida Mindzie & Mvondo Ze 2016: 147, 149; Seidensticker 2010: 61). Evidence of decayed bone remains was derived from correlations of low P concentrations with organic C and K. Unlike the pits, P did not correlate with Ca within the grave features (Mbida Mindzie & Mvondo Ze 2016: 150).

Further archaeological studies of grave soils revealed other elements associated with burials. For example, enrichments of P, Mn and Cu were found in a grave soil indicated by a dark stain forming a soil silhouette (Keeley *et al.* 1977: 23). Mn, however, presumably derived not from the body but from the soil (Keeley *et al.* 1977: 24), as Mn appears to be attracted to the body during decay (Bethell & Carver 1987: 17–18; Dent *et al.* 2004: 581).

[24] Among them were the sites of *Nkang*, *Akonétye* and *Campo* (see chapter 4.2.2 for more information about these features).

	Site or feature	Element enrichments
Burials	Burials/graves	P, Cu, Mn, Ca
	Decomposition of bones, teeth, hairs, nails or skin	Rare earth elements, such as Y, La, Ce
Fire exposure	Hearths	P, K, (Mg)
	In situ burning	P, K, Ca, Fe, also high concentrations of other elements
	Wood ash, fire application	P, K, Ca, (Mg), Mn, Sr, also high concentrations of other elements
	Burning firewood	(Mg)
	Burning organic materials	P
	Human habitation, particularly in ashes	K, (Th), Rb, (Cs)
Food processing	Food preparation	P, Ca, Sr
	Cooking areas	K, Mn, P
	Plant remains	K, Mn
Occupation	Activity areas, occupation	High alkaline earth metals, (Na), Ca, Sr
	Human activities	Ca, Cu, Zn
	General archaeological sites/ archaeological soils	(B), Cu, (Mg), Mn, Ni, P, (Se), Zn, K, Ba, Ca, (Na)
	Large amounts of organic matter, human occupation	Cu, Zn, depletion of Fe/Mn
	Rubbish pit	Zn
	Disposal of excrement/faeces, waste, organic decay	P
	Disposal or storage of organic material	P
	Middens	P, K, Ca
	Utilised exterior areas	Low in all concentrations but higher than off-site
	High-traffic areas	Low concentrations of all elements, maybe even lower than off-sites
Working area	Mining, metal smelting and production sites	Cu, Pb, Mn, Fe
	Production and use of coins, jewellery, and pigments	Cu, Pb
Farms	(Farm)houses	P, Ca, (Mg), Fe, K, (Th), Rb, (Cs), Pb, Zn, Sr, Ba
	Former farms	Cu, Pb, Zn, Sr, Ba
Animal husbandry	(Mineralised) manure	Heavy metals e.g. (As), (Cd), Cu, Ni, Zn; also P, K, Ca
	Animal penning	Sr

Tab. 6-1: Overview of enrichments (and a few depletions) of elements within archaeological sites and features. Elements shown in brackets cannot be quantified by the pXRF device. Information obtained from compilations (especially Oonk *et al.* 2009a: 38, Tab. 1) and numerous other compilations and case studies provided by (in alphabetical order): Abrahams *et al.* 2010: 240; Bethell & Smith 1989: 48–49; Cook *et al.* 2006: 638; Cook *et al.* 2010: 879; Davies *et al.* 1988: 397; Entwistle *et al.* 1998: 64; Entwistle *et al.* 2000: 296; Fleisher 2014: 9; Gauss *et al.* 2013: 2951; Hao & Chang 2003: 102; Haslam & Tibbett 2004: 731–732; Keeley *et al.* 1977: 23–24; Middleton 2004: 53, 56; Middleton & Price 1996: 677; Oonk *et al.* 2009b: 1223–1224; Sulas *et al.* 2017: 62; Terry *et al.* 2004: 1244; van Zwieten *et al.* 2017: 2–3; Wilson *et al.* 2005: 1097; Wilson *et al.* 2009: 2332–2333.

These body silhouettes, so-called *pseudomorphs*, were also attested from medieval graves in East Anglia and revealed enrichments of P and Cu, although Cu probably originated from the adjacent copper grave goods (Bethell & Carver 1987: 17). One of these sites, *Sutton Hoo*, showed enrichments of P, but neither Cu nor Mn (Bethell & Smith 1989: 54). Enrichments of Ca, caused by the breakdown of bones when the mineral phase dissolves and both Ca and P leach out (Bethell & Carver 1987: 17; Carter *et al.* 2007: 18), were reported as well (Oonk *et al.* 2009a: 38, Tab. 1). Rare earth elements such as Y, La and Ce were found associated with bones, teeth, hairs, nails and skin (Cook *et al.* 2006: 638; Oonk *et al.* 2009b: 1223; Entwistle *et al.* 1998: 64).

Compilation of Elemental Signatures

A compilation of elemental signatures identified at case studies from all over the world for different time periods is presented in Table 6-1. It shows the information obtained for roughly 20 elements characteristic of archaeological sites and features.

Generally, archaeological sites, activity areas or occupation layers show enrichments of P and high levels of alkaline metals and alkaline earth elements such as Ca and K (Oonk *et al.* 2009a: 41; Middleton 2004: 56). Cu and Zn, although less abundant, are also found on archaeological sites (Oonk *et al.* 2009a: 38). Depending on the scale of impact, areas can show a significant decrease in elements, e.g. in high-traffic areas (Middleton 2004: 56). Furthermore, areas associated with human activity but free of (organic) waste have lower concentrations of P and K, but higher abundances of Ca and Sr (Middleton & Price 1996: 677; Fleisher 2014: 9).

P is beyond doubt the most important element in proving human impact as it is a key element in organisms (Middleton 2004: 53). Anthropogenic P originates from both organic and inorganic material, caused by microbial and fungal decay. Inorganic P derives from ashes, bones (apatite) and microbial mineralization of organic P, although the majority of P is organic (Oonk *et al.* 2009a: 40). It enters the soil by manifold processes (Holliday & Gartner 2007: 325), such as burning, food preparation, disposal or decay of organic material, including burial remains, or manure. **K** is, besides P, the main indicator for archaeological sites (Oonk *et al.* 2009a: 37). It occurs in ash and plant tissues, and thus is an indicator for in situ burning and wood ash (Middleton 2004: 56), as well as in manures (Hao & Chang 2003: 102; Oonk *et al.* 2009a: 41). **Ca** is the third most important element indicating site occupation, human activities or farmlands (Oonk *et al.* 2009a: 37). Ca originates from bones or teeth and is abundant in manure (Oonk *et al.* 2009a: 41). Both Ca and **Sr** point to animal husbandry or animal penning. Ca and Sr are associated with fire exposure, including in situ burning or wood ash, and occur in the process of food preparation (Middleton 2004: 56).

Of similar significance are the following elements, albeit less frequently attested. **Mn** derives, for example, from plant remains (van Zwieten *et al.* 2017: 3), burials (Bethell & Smith 1989: 48–49) and wood ash (Gauss *et al.* 2013: 2951). Like **Fe**, its depletion indicates large amounts of organic matter associated with human occupation (Oonk *et al.* 2009b: 1223–1224), and Fe can also indicate in situ burning (Middleton 2004: 56). **Ni**, **Zn** and **Cu** occur generally on archaeological sites and in (mineralised) manure (Oonk *et al.* 2009b: 1223–1224). Zn is also known from rubbish pits (van Zwieten *et al.* 2017: 2). **Cu** was associated with working areas for e.g. coin production, together with **Pb** (Davies *et al.* 1988:

397; Haslam & Tibbett 2004: 732). Enrichments of Pb also occur on former farms (Wilson *et al.* 2005: 1097; Wilson *et al.* 2009: 2332).

Rare earth elements such as **La**, **Ce** and **Y** are less frequently present. These elements derive from the decomposition of bones, teeth, hairs, nails and skin (Cook *et al.* 2006: 638; Oonk *et al.* 2009b: 1223; Entwistle *et al.* 1998: 64). La and Ce occur together with the enrichment of other elements on former settlements and are associated with arable soils (Abrahams *et al.* 2010: 240; Entwistle *et al.* 1998: 64; Cook *et al.* 2006: 638). **Ba** and **Rb** are also known to be indicators for archaeological sites and farms (Wilson *et al.* 2005: 1097; Oonk *et al.* 2009a: 38; Entwistle *et al.* 2000: 296). Depletion of **Cr** was observed on former settlements (Abrahams *et al.* 2010: 240; Entwistle *et al.* 1998: 64) and its enrichment was observed in a Scottish byre (Wilson *et al.* 2005: 1097).

Rarely or not associated with human impact are the elements **Al**, **Ti**, **V**, **Zr**, and **Nb.** Some of these correlate negatively with P and variations in their concentration are considered to be related to geology (Wilson *et al.* 2009: 2327; Wilson *et al.* 2005: 1096; Gauss *et al.* 2013: 2951). Enrichments in Ti, for example, have been identified as floor fill consisting of sand rich in Ti, which was transported from river beds into the settlement (Middleton & Price 1996: 677). Information on **Cl** within archaeological soils or features is absent, which is probably due to the fact that information on halogens are often not provided by ICP-based techniques, as they are expensive to evaluate.

Based on the lack of information for West and Central Africa, this information was obtained from all over the world throughout different time periods, e.g. from Çatalhöyük during the 8th to 7th millennium BCE, prehistoric house floors from Mexico dating to *c.* 250 to 750 CE (Middleton & Price 1996), footprints of houses in the Netherlands during the late Bronze Age and Roman period (Oonk *et al.* 2009b), pit features of the late Iron Age/early Roman period in England (van Zwieten *et al.* 2017) and former settlements in the Central Highlands of Scotland during the 17th/18th century CE (Abrahams *et al.* 2010). Furthermore, the number of multi-element analyses of soil are few (Gauss *et al.* 2013: 2951) and the majority of studies employed techniques such as ICP-MS rather than pXRF devices.

6.3 Fulani Village

Although considerable information about elemental signatures on archaeological sites and features exists (chapter 6.2), it derives from many different contexts and – apart from the analyses carried out in southern Cameroon – it is far removed from the Nok Culture. A suitable method for understanding elemental signatures is to follow an inductive approach (from the known to the unknown), e.g. by obtaining information from ethno-archaeological studies (Middleton *et al.* 2010: 205–206). To gain insight into the inherent elemental signatures of specific activities and for a close comparison to the soil properties of our research area, a field study on a Nigerian Fulani village was conducted. The study aims to identify and interpret elemental signatures for specific activity areas by pXRF analysis (for results see chapter 9.3).

Fig. 6-1: Part of the sampled Fulani village with the two hut types, which are torn down every few years and re-built on nearby locations. In the foreground a typical fireplace is visible.

The Hausa word *Fulani* refers to the nomadic pastoralists mainly found in West Africa, who nowadays live as full-time cattle pastoralists or with a sedentary lifestyle in villages and cities (Danver 2015: 31). The sampled village *Rugan Bature* (9°33'31" North and 7°41'28" East), comprising roughly two dozen huts, is located ca. 1.5 km to the northeast of the Nok project's research station at Janjala (see chapter 2.2, Fig. 2-1).

In this village, only the young are nomadic herdsmen, herding some of the cattle across the landscape, whilst the others stay within the village and some cultivate crops. They live in small dome-shaped huts built up with branches and leaves or within larger

huts made from unburnt mudbricks (Fig. 6-1). Both hut types are torn down after a few years and re-built in close proximity in a continuous process, resulting in a shift of the village by a few hundred metres every few years.

The areas sampled for the study comprised different activity zones such as the interior of several huts, sheds for cattle or other animals, hearths, as well as on-site and off-site samples for reference (see Appendix 4-1 and 4-2 for details on the sampling). On-site samples originated from the village itself, but from areas with no designated function. Off-site samples represented the soil outside the village. In order to prove whether the method is capable of identifying a village that was abandoned for some years, samples from old huts and former on-site areas were taken as well.

The modern lifestyle, however, has a certain impact on the village and must be considered when analysing and interpreting the results. Plastic, metal objects, batteries, chemical fertilisers, oil and fuel as well as other pollutants are frequently used and stored within the settlement. Contamination with these substances can distort the outcome and render the samples useless. In spite of these issues, sampling a Fulani village within the core region of the research area was the best available option. It makes it possible to gain insight into the elemental patterns occurring as a result of settlement activities in soil conditions similar to those at Nok sites.

6.4 Forensic Studies

Human decomposition changes the soil and its chemical, biological and physical properties (Lühe 2016: 2; Carter *et al.* 2007; Dent *et al.* 2004), which lays the foundation for the detection of enrichments in certain elements. In order to verify that the identified elemental signatures in the Nok features originate from a human body, it is crucial to understand the process of decomposition and the elements involved. Only a few archaeological studies contain information on elements associated with grave soils, and thus the exploitation of knowledge derived from forensic studies is useful.

Decomposition of the Human Body

The decomposition of the human body comprises six stages. The first stage, *Fresh*, refers to the cessation of the heart and depletion of oxygen (Carter *et al.* 2007: 14). With the onset of putrefaction, in the *Bloated* stage, fluids leave the body through the mouth, nose and anus (Carter *et al.* 2007: 15; Powers 2005: 6). *Active Decay* is linked with rapid mass loss when maggot activity is the highest and massive amounts of cadaveric fluids are released into the soil (Carter *et al.* 2007: 15). *Advanced Decay* commences when the maggots start to pupate and soil nitrogen increases significantly (Carter *et al.* 2007: 15, 17). The transition to the final stages *Dry* and *Remains* are difficult to distinguish but comprise another period of slow mass loss (Carter *et al.* 2007: 17) with only bones remaining (Powers 2005: 6). Depending on the circumstances, bodies not buried in tombs or coffins can disappear completely, after the bone material is dissolved (Dent *et al.* 2004: 583).

The human body consists of both organic and inorganic matter, of which water, comprising 64% of the body mass, is the main component, together with 20% proteins, 10% fat, 1% carbohydrate, and 5% minerals (Dent *et al.* 2004: 577; Janaway *et al.* 2009: 317). The decay of the body comprises the liquefaction and disintegration of soft tissue, i.e. proteins, carbohydrates and fats, as well as the decalcification and dissolution of inorganic components, i.e. the bones. Under low oxygen levels, fatty acids can remain as adipocere in the soil, a greyish-white and waxy substance, which can become very solid and resistant (Janaway *et al.* 2009: 317–321). Bones consist of, aside from organic components, a resistant biological apatite (hydroxyapatite) (Janaway *et al.* 2009: 321; Dent *et al.* 2004: 583–584). Low pH, however, dissolves the inorganic matrix of the biological apatite, as Ca ions migrate into the soil solution when they are replaced by protons. Thus, acidic soils are most destructive to bones as they can dissolve their inorganic matrix (Janaway *et al.* 2009: 322; Dent *et al.* 2004: 584).

Elemental Enrichments and Soil pH of Grave Soils

A total of 25 different elements occur in the body, of which oxygen, carbon, hydrogen, and nitrogen comprise ca. 96% of the mass of an adult human body of 70 kg (Schaal *et al.* 2016: 268, 271). Calcium and phosphorus occur in significant amounts of 1000 g and 700 g, respectively. Potassium, sulphur, chlorine, sodium, magnesium and iron occur, in descending order, in amounts of between 3-170 g. Between 100-300 mg of copper and manganese are also present. The remaining elements occur in marginal quantities (Schaal *et al.* 2016: 271).

Forensic studies of both animal cadavers and human bodies, including terrestrial decomposition (i.e. exposed to air) and decomposition during burial, found an increase in base cations (potassium, sodium, calcium, magnesium) as well as phosphorus, nitrogen, ammonium, sulphate, and chloride within grave soils (Lühe 2016: 2; Aitkenhead-Peterson *et al.* 2012: 133; Stokes *et al.* 2013; Benninger *et al.* 2008; Melis *et al.* 2007; Carter *et al.* 2007). Theoretically, all elements of the human body will be released into the soil. However, some light elements cannot be quantified by the pXRF device, such as organic carbon, which is frequently found in grave soils (Fiedler *et al.* 2004: 563; Fiedler *et al.* 2009: 311; Hopkins *et al.* 2000: 285; Benninger *et al.* 2008: 74; Carter *et al.* 2007: 18). Other elements occur in too low concentrations in the body (in μg to a few grams), so that they can either not be quantified by the pXRF device or they are concealed by their natural occurrence in the soil.

Forensic studies have also confirmed the enrichment of phosphorus, calcium and potassium, which were already attested by archaeological studies (see chapter 6.2). Enrichments in **phosphorus** are retained most frequently within grave soils and have been proven in different contexts. The identification of a former mass grave from the Second World War demonstrated its strong retention in the soil, since the bodies were lying within the mass grave for only roughly 10 months before they received a decent burial in a cemetery after the end of the war. The location of the former position of the bodies, however, was indicated by enrichment of phosphorus at the bottom of the two large pits. The estimated position was confirmed by characteristic finds such as a dental prosthesis (Fiedler *et al.* 2009: 311). Notably high amounts of P were also attested for a soil associated with adipocere beneath a coffin (Fiedler *et al.* 2004: 563). Several terrestrial analyses of both human bodies and carcasses confirmed the enrichment of P within grave soils (Carter *et al.* 2007: 17; Melis *et al.* 2007: 810; Stokes *et al.* 2013: 586), although in some cases the enrichment persisted for only a short time and declined back to basal levels (Benninger *et al.* 2008: 73). Enrichments of **calcium and potassium** were also found in terrestrial studies on human bodies and animal cadavers (Carter *et al.* 2007: 17; Melis *et al.* 2007: 810; Stokes *et al.* 2013: 586). However, long-term studies on a bison cadaver have shown that after an initial increase of Ca, its concentration declined back to basal after a few years (Melis *et al.* 2007: 810).

The reliability of **soil pH** as an indicator for burials is equivocal, although long-term studies suggest a lower pH value for grave soils. Several terrestrial studies of both human bodies and animals cadavers revealed ambiguous outcomes with either higher or lower pH values for the grave soil (Aitkenhead-Peterson *et al.* 2012: 132), or even fluctuating values depending on the moment of sampling (Melis *et al.* 2007: 809–810; Benninger *et al.* 2008: 73; Stokes *et al.* 2013: 586). However, the occurrence of high pH values was considered to be a result of incomplete decomposition (Fiedler *et al.* 2004: 563).

Information obtained from forensic studies are beneficial, but when utilising the evidence, the specific conditions have to be taken into account. The objectives of the analyses often focus on determining the post-mortem interval and information relating to elemental concentrations are merely a by-product of these studies. Furthermore, the replacement of dead bodies with animal cadavers or study of the decay in terrestrial conditions rather than during burial may alter the outcome.

6.5 Properties and Behaviour of Elements

One major issue relating to the elemental analysis of soil is the distinction between anthropogenically and naturally caused elemental signatures. All elements that can be characteristic of archaeological sites and features are inherent components of the soil. Thus, natural enrichments, caused e.g. by soil formation processes, can conceal archaeological patterns or can be misinterpreted as such. Both the formation and transformation of elemental signatures are influenced by the behaviour and properties of the elements in the soil such as their mobility, affinity to other elements or their behaviour during weathering. Although soils contain all natural chemical elements of the periodic table (Strawn *et al.* 2015: 41), only elements relevant for this thesis will be discussed.

6.5.1 General Remarks

Important processes for the formation, transformation and preservation of elemental signatures in the soil are the mobility of elements. The **mobility** and bioavailability of elements are highly variable and depend on many factors (Strawn *et al.* 2015: 56). In general, alkali and alkaline earth metals are relatively soluble elements and thus quite mobile. Transition metals have a lower solubility than alkali and alkaline earth metals, although their mobility is variable and depends upon factors such as valence state. Rare earth elements are, unlike alkali and alkaline earth metals, relatively insoluble and due to their immobility their concentrations often remain unchanged, e.g. during weathering (White 2013: 274–275, 278).

Weathering of igneous and metamorphic rocks is an important process in our research area, where, among others, granites, gneisses and migmatites are found as part of the *Basement Complex* (Obaje 2009: 9; Bennett *et al.* 1979: 13, see also chapter 3.1). The breakdown of igneous and metamorphic rocks during weathering has a significant impact on the elements. When these rocks transform into soil, they release alkali and alkaline earth cations (Ca^{2+}, Mg^{2+}, Na^{+}, K^{+}), some of which are retained by plants, but most of which are leached from the soil (Strawn *et al.* 2015: 165–166). The leaching of these base cations leads to an enrichment of exchangeable Al^{3+} in the soil, which, in turn, results in soil acidification (Strawn *et al.* 2015: 319). Weathering also releases silica (SiO_2) to the soil solution, which partly forms secondary minerals such as kaolinite. Although the phosphate content of soils remains quite constant during soil formation, the form of phosphate changes from apatite ($Ca_5(OH,F)(PO_4)_3$) in igneous rocks to Al(III) and Fe(III) phosphates in weathered soils. Al and Fe hydroxides, as well as Ti and Mn oxides, are insoluble and tend to accumulate in the soil (Strawn *et al.* 2015: 165–167). In general, weathering has two stages as it initially produces some alkalinity and then it produces acidity (Strawn *et al.* 2015: 165). **Resistance** against processes such as weathering is controlled by the molecular bonds – a stronger bond is more resistant, e.g. that of SiO_2. Although silica is affected by weathering processes as mentioned before (Strawn *et al.* 2015: 165–166), the Si-O bonds in quartz are strong (Strawn *et al.* 2015: 33–34). K-O bonds in mica, in contrast, are most susceptible to weathering and the bond breaks easily, leading to a release of K^{+} (Strawn *et al.* 2015: 34).

The **affinity of elements** can explain their mutual occurrence or similar behaviour. Trace elements have an affinity for metal oxides, phosphates and organic matter (Oonk *et al.* 2009a: 42). Fe and Al commonly co-occur in soils, Ca and Sr are closely related chemically

and thus behave similarly. Ba is also related to Ca, but to a lesser extent; this might be the reason why Ba also follows the behaviour of Sr, since Sr follows Ca. Furthermore, a strong correlation exists between P and K (Middleton & Price 1996: 675).

6.5.2 Non-Metals (P and Cl)

Phosphorus occurs geologically as phosphate rocks (Kabata-Pendias 2011: 73; Jones *et al.* 2013: 33) and the content of P in soils is determined by the parent material (Scheffer *et al.* 2010: 412). The main source of phosphate in the soil is Ca phosphate apatite $Ca_5(PO_4)_3(OH,F,CO_3)$ (Scheffer *et al.* 2010: 28; Kabata-Pendias 2011: 74). Anions of phosphoric acid (H_3PO_4), in addition to being found in Ca phosphates, can bond with Al and Fe to form phosphates, which are hard to dissolve (Scheffer *et al.* 2010: 416; Kabata-Pendias 2011: 73). P can also occur in rarer minerals such as monazite (White 2013: 280). High soil acidity leads to an increased solubility of P in Ca phosphates, whereas the solubility of P in Al and Fe phosphates decreases in soils with higher acidity (Scheffer *et al.* 2010: 417). This means that low soil pH and high levels of Fe and Al oxides can immobilise phosphorus (Jones *et al.* 2013: 33).

Chlorine is classified as a halogen element and is common in the terrestrial environment. Its concentration varies considerably, but it is more prevalent in igneous rocks (Kabata-Pendias 2011: 393). In soils with pH values > 5, chlorides are usually not adsorbed. At lower pH values, the adsorption increases with decreasing pH, especially in soils rich in Fe oxides (Scheffer *et al.* 2010: 442).

6.5.3 Alkali Metals (K and Rb)

Alkali metals are, due to their solubility, quite mobile in geochemical processes (White 2013: 274). They are closely associated with the major crustal components and are likely to enter silicate minerals (Kabata-Pendias 2011: 123). Alkali metals tend to form weaker bonds compared to other elements (White 2013: 11).

Potassium occurs mainly in minerals such as micas and feldspars. K is highly mobile and K levels are low in old and strongly weathered soils, where the micas, feldspars and clay have been converted to K-free kaolinite and Fe and Al oxides (Jones *et al.* 2013: 33; Scheffer *et al.* 2010: 423).

Rubidium occurs in acidic igneous rocks. The Rb content depends on the parent rock, and is highest in soils with granites and gneisses as the parent material. However, Rb is a dispersed element and like K is also associated with micas and feldspars. Rb is closely linked with K, but its bond to silicates is stronger, which is why the K:Rb ratio decreases during soil formation. Rb is generally active in soil processes (Kabata-Pendias 2011: 127).

6.5.4 Alkaline Earth Metals (Ca, Sr and Ba)

Alkaline earth metals have similar characteristics to alkali metals (White 2013: 11) and, like them, they are relatively mobile (White 2013: 274). The physical properties of Ca, Sr, and Ba are akin, which is why they behave similarly (Kabata-Pendias 2011: 135).

Calcium is widely absent in soils and often leached out (Jones *et al.* 2013: 33). Ca dissolves with increasing acidity, e.g. as carbonate calcite ($CaCO_3$), which is easily weathered. Ca occurs mostly in an exchangeable form (Scheffer *et al.* 2010: 427).

Strontium and its content in the soil depends on the parent rocks. It is geochemically very similar to Ca and associated with it, which is why the Sr:Ca ratio is relatively stable. Sr is moderately mobile, but like Ca it is more mobile in acid soils, where it can leach down. Soil organic matter, however, can concentrate Sr in the upper horizons (Kabata-Pendias 2011: 138–139).

Barium is, in general, a common element and concentrates in acidic igneous rocks. It is associated with K in geochemical processes and also has a great affinity to Mn. It is not very mobile, although its mobility increases, like Ca and Sr, within acidic soils. Fe and Mn hydrous oxides can fix and immobilise Ba (Kabata-Pendias 2011: 142–143).

6.5.5 Metalloids, Transition and Post-Transition Metals

The metalloids, transition and post-transition metals comprise the elements Al, Si, Ti, V, Cr, Mn, Fe, Ni, Cu, Zn, Y, Zr, Nb, and Pb (arranged by atomic number), the majority of which belong to the transitional elements. Transition metals are very complex and their solubility is variable, but generally lower than that of alkali and alkaline earth metals (White 2013: 278). Furthermore, some transition metals can form strong bonds, generally with O (White 2013: 12).

Aluminium is the third most abundant element in the Earth's crust. Its concentration in the soil depends on the parent rocks (Kabata-Pendias 2011: 325–326). Al increases the acidity and concentration of cations (Jones *et al.* 2013: 33). In acidic soils Al is more soluble, in soils with soil pH < 5.5 in particular, its mobility increases significantly (Kabata-Pendias 2011: 325). As Al hydroxide it is insoluble and tends to accumulate in soils, especially within the clay mineral fraction (Strawn *et al.* 2015: 165, 168).

Silicon, especially in combination with O, is the basic non-metallic component of all rocks. After oxygen, it is the most prevalent and most stable element in the lithosphere. In the soil, Si is the most abundant element and occurs mainly as silicates and oxides (Kabata-Pendias 2011: 333; Scheffer *et al.* 2010: 443). It is the basis of all silicates such as feldspar and Al silicate minerals. As SiO_2 it is a very resistant mineral and in acidic soils, silicate and phosphate ions can form insoluble precipitates (Kabata-Pendias 2011: 333–334). The abundance of Si in the soil solution is mainly controlled by weathering processes (Scheffer *et al.* 2010: 443).

Titanium is common and occurs in several rocks. It is very resistant to weathering and Ti minerals are the most stable minerals in soils (Kabata-Pendias 2011: 167–168). An increase of Ti in upper horizons can be a result of its limited solubility (Kabata-Pendias 2011: 168; Strawn *et al.* 2015: 165).

Vanadium and its abundance in the soil depends on the parent rock type. It is very often associated with primary minerals, Fe hydrous oxides, soil organic matter and can occur together with phosphates. A strong association of V with Mn and K has also been observed and due to its similar atomic radius to Nb it has similar geochemical properties (Kabata-Pendias 2011: 173, 175).

Chromium and its concentrations in the soil depends on the parent rock type. Its minerals are resistant to chemical weathering. Cr is associated with Fe and Mn. Depending on the proton number of the cations, Cr (Cr^{3+}) can be slightly mobile and only in acidic soils, or it can be very unstable (as hexavalent Cr^{6+}) (Kabata-Pendias 2011: 181–183).

Manganese is one of the most common trace elements in the lithosphere (Kabata-Pendias 2011: 201) and occurs in high concentrations in acidic soils (Jones *et al.* 2013: 33). Mn occurs in soils mostly as Mn oxides and silicates or carbonates and tends to accumulate in the soil (Scheffer *et al.* 2010: 430; Strawn *et al.* 2015: 165). Mn and Fe are closely associated in geochemical processes and Mn often follows the Fe cycles (Kabata-Pendias 2011: 201; Scheffer *et al.* 2010: 430). As a consequence, Mn concentrates where high concentrations of Fe oxides or hydroxides are to be found. Organic matter, however, can bond Mn to the topsoil (Kabata-Pendias 2011: 201, 206). Mn also shows a high degree of affinity to some trace metals and thus accumulations of e.g. Co, Ni, Cu, Zn, Pb, and Ba can be found associated with Mn oxides (Kabata-Pendias 2011: 203; Scheffer *et al.* 2010: 430). Mn is relatively mobile, although it depends on the soil pH (Kabata-Pendias 2011: 203, 205). In the tropics and subtropics, Mn remains as residual deposits, e.g. as concretions or nodules, after weathering has removed all soluble constituents. This is why acidic soils can be poor in Mn (Kabata-Pendias 2011: 201, 203; Scheffer *et al.* 2010: 430). In soils with a higher pH, Mn has an increased adsorption capacity for metals (Kabata-Pendias 2011: 204).

Iron is the most common metal after aluminium in the Earth's crust (Scheffer *et al.* 2010: 434) and one of the major elements in the lithosphere (Kabata-Pendias 2011: 215). Soil colour varies according to the presence of Fe compounds (Kabata-Pendias 2011: 216). Iron mostly originates from chemical weathering of minerals (Jones *et al.* 2013: 33). In general, its geochemistry is very complex and it reacts similarly to Ni. Fe compounds have a great sorption capacity for many trace elements and metals (Kabata-Pendias 2011: 218). Fe is slightly mobile, but Fe compounds become more mobile in acidic soils (Kabata-Pendias 2011: 215). Fe hydroxides are insoluble and tend to accumulate in soils (Strawn *et al.* 2015: 165).

Nickel and its abundance depend on the parent material and are affected by soil-formation processes. Its abundance decreases with increasing acidity of rocks and it is less abundant in e.g. granites (Kabata-Pendias 2011: 238). Ni is associated with Fe, which is why Ni-Fe compounds are common. It can also co-precipitate with Fe and Mn oxides within Fe minerals, e.g. goethite. Furthermore, it is associated with phosphates and silicates (Kabata-Pendias 2011: 237). In general, Ni is only slightly mobile, but easily mobilised during weathering (Kabata-Pendias 2011: 239–240).

Copper and its abundance are higher in acidic soils than in alkaline soils (Jones *et al.* 2013: 33; Oonk *et al.* 2009a: 42). Its concentration is also related to the soil texture, with the lowest concentration found in light sandy soils and the highest in loamy soils (Kabata-Pendias 2011: 253). Cu is rather immobile. It commonly accumulates in upper horizons, although soil organic matter can enhance its retention in deeper layers. Under certain conditions, organic matter can also remove Cu from soil (Oonk *et al.* 2009a: 42; Kabata-Pendias 2011: 254). Phosphates can increase Cu adsorption (Scheffer *et al.* 2010: 436).

Zinc and its abundance in soil is similar to Cu and associated with the soil texture. It is therefore lowest in light sandy soil (Kabata-Pendias 2011: 275). In contrast to Cu, however, Zn is relatively mobile and easily exchanged with other trace metals (Oonk *et al.* 2009a: 42), especially during weathering (Kabata-Pendias 2011: 275). The factors affecting the mobility of Zn, however, are the same as for Cu (Kabata-Pendias 2011: 277), as it can be stabilised through precipitation with soil organic matter, phosphates, carbonates or metal oxides and hydroxides (Oonk *et al.* 2009a: 42). Al, Fe, Mn oxides and hydroxides

can bind Zn, especially goethite (Kabata-Pendias 2011: 278). In soils rich in Ca and P, Zn can become immobile (Kabata-Pendias 2011: 280) and Zn levels increase with lower pH (Scheffer *et al.* 2010: 437).

Zirconium and its abundance depend on the parent rocks. There seems to be a higher mobility of Zr in acidic soils and a strong retention by soil organic matter and Mn oxides (Kabata-Pendias 2011: 170).

Niobium is rather rare. It occurs in higher concentrations in acidic igneous rocks. Nb has an affinity for Fe, Ti, Mn, and Zr (Kabata-Pendias 2011: 173, 178).

Lead and its abundance depend on the parent rocks; it occurs often in acidic igneous rocks (Kabata-Pendias 2011: 338–339). Pb can be strongly retained by organic matter and clay (Oonk *et al.* 2009a: 42) and thus accumulates near the soil surface. It is the least mobile trace metal (Kabata-Pendias 2011: 339–340).

6.5.6 Rare Earth Elements (Y, La and Ce)

Depending on the author, rare earth elements are considered to comprise different elements, both including and not including Y. According to the International Union of Pure and Applied Chemistry (IUPAC), Y and the lanthanides (La, Ce) are part of the rare earth elements (Kabata-Pendias 2011: 150) and will be discussed here. Rare earth elements are, unlike alkali and alkaline earth metals, relatively insoluble and immobile (White 2013: 275, 278).

Yttrium is rather rare in the environment (Kabata-Pendias 2011: 147). It shares the same chemical properties as rare earth elements and shows similar behaviour (Kabata-Pendias 2011: 149; White 2013: 275). Y concentrations are higher when associated with minerals of the rare earth elements and it occurs with them in silicates or phosphates (Kabata-Pendias 2011: 149).

Lanthanum and **cerium** are part of the lanthanides (Kabata-Pendias 2011: 147). They belong to the more basic and more soluble light rare elements and are slightly mobile. They are likely to be concentrated in phosphorites, e.g. in monazite. Acidic soils usually contain less La and Ce than alkaline soils (Kabata-Pendias 2011: 152–154).

6.6 Summary

Multi-element analyses conducted with pXRF are nowadays well-established in archaeological research, although studies on soils are less frequent and less developed. Affirming the Nok stone-pot-arrangements as burials and revealing the former function of the Nok pits, however, requires a fundamental knowledge of elemental signatures. Archaeological studies related to these specific research topics are rare, both in terms of determining elements associated with grave soils, as well as tracing the origin and genesis of pit features.

In order to provide such information, knowledge derived from forensic studies was utilised and attested to enrichments of mainly P, Ca, and K in soils associated with burials. In order to establish the activities that took place within pit features, a compilation of recurring elemental signatures from a wider context was gathered. In addition, a modern Fulani village was sampled and analysed in the scope of this thesis to collect new data originating from the research area.

To differentiate between natural and anthropogenic elemental signatures, basic information about the elements in the soil, their affinities and mobility was reviewed. This information is crucial for the interpretation of the elemental signatures obtained from Nok features.

7 Sites and Sampling

7.1 Selection of Sites

The selection of Nok sites on which to conduct pXRF analysis was based on their suitability to fulfil the objectives of this thesis, i.e. to determine whether stone-pot-arrangements were indeed burials and to reveal the function of pit features. In total, 3,575 samples from seven Nok sites were analysed (Fig. 7-1). When the work for this thesis commenced in 2015, the majority of samples were already collected. Most sites were sampled in 2010 and 2011, when we were inexperienced at sampling and the knowledge and understanding of Nok sites was limited.

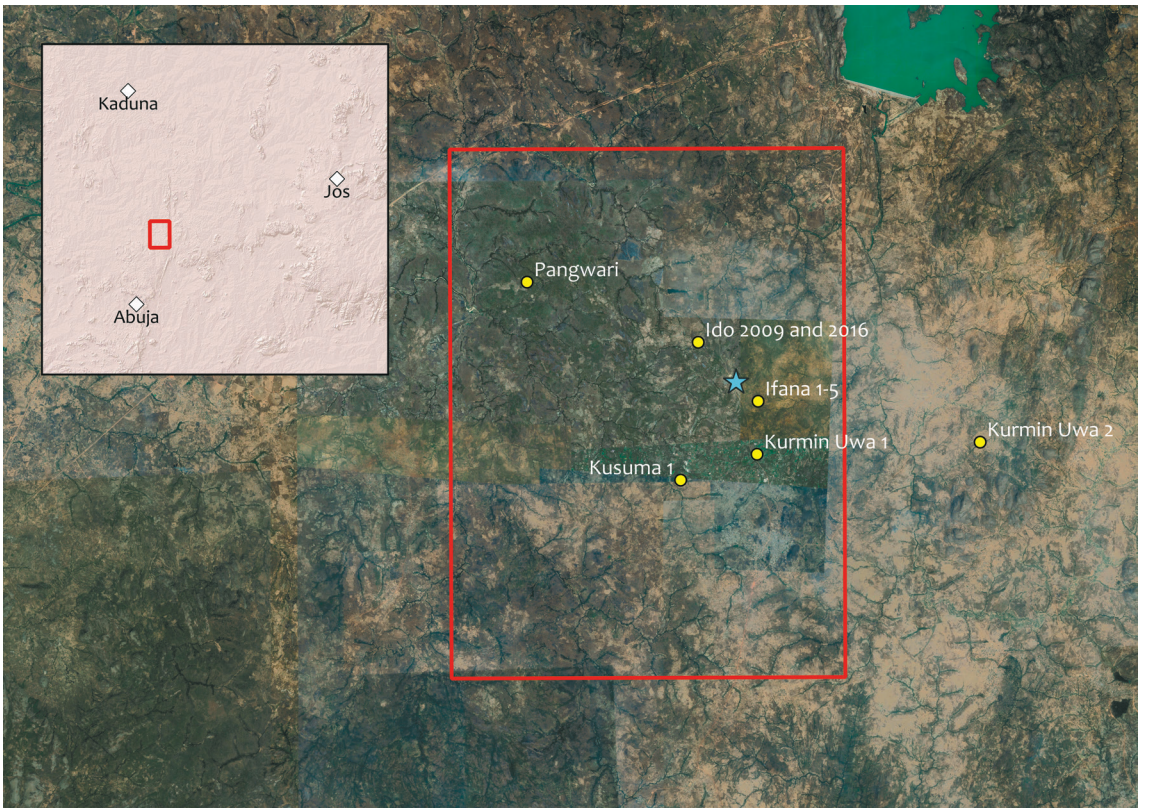

Fig. 7-1: Map with Nok sites where pXRF analyses were carried out. The red box represents the key study area of the Nok project, the blue star refers to the research station in Janjala. Base map from Google Satellite and ESRI Shaded Relief provided by QuickMapsServices (QGIS plugin).

Regarding the **stone-pot-arrangements** (Tab. 7-1), preliminary results from the site of *Kurmin Uwa 2B* seemed promising (Nagel 2014). The samples from *Pangwari* were also considered to be useful. Apart from these two sites, however, none of the other assumed burial sites sampled before 2015 were suitable for pXRF analysis as the number of samples was too low (each site $n < 20$) to be able to distinguish features from the surrounding and reference samples were furthermore absent.

Thus, in the search for further stone-pot-arrangements for sampling, the excavation at *Ido* in 2016 was conducted within the scope of this thesis and yielded further features (Schmidt 2016). In the same year, an excavation at *Ifana 3*, aiming to test the hypothesis that terracotta depositions occur together with stone-pot-arrangements, revealed the largest number of features hitherto uncovered, comprising three terracotta depositions and 18 stone-pot-arrangements (Breunig 2018: 399–400). During the same campaign, a further stone-pot-arrangement was fortuitously discovered within a looting pit at *Kurmin Uwa 2D* and sampled. Potential sampling errors were avoided at those sites excavated in 2016, by applying a dense sampling grid of 25 cm intervals at *Ido* and 10 cm intervals at *Ifana 3* and *Kurmin Uwa 2D*, respectively.

Site	Year of excavation	Sampled and analysed stone-pot-arrangements	Grid size	Analysed samples
Kurmin Uwa 2B	2010	Feature 1	20 cm	40
Pangwari I	2013/14	Feature 18, 20	50 cm	319
Ido 2016	2016	Feature 2 and 9	25 cm	823
Ifana 3	2016	Feature 8, 13, 17, and 18	10 cm	1,384
Kurmin Uwa 2D	2016	One feature (no feat. number)	10 cm	173

Tab. 7-1: Stone-pot-arrangements analysed in the scope of this thesis. *Kurmin Uwa 2B* was already successfully analysed (Nagel 2014), but re-measured for this thesis. Further stone-pot-arrangements were sampled during the excavations in 2016 by engaging an improved sample strategy of 25 cm and 10 cm intervals, respectively.

In terms of the **pit analysis** and the prospection of activity areas, several thousand samples from more than a dozen Nok sites were collected before 2015. This vast number appeared promising for the analysis of activity areas and pits of the Nok Culture. However, during the process of analysis it turned out that sampling was in most cases insufficient due to:

- a lack of reference material,
- only horizontal layers and no profiles were sampled,
- quantities were too small or grid size too large,
- a disturbed layer or layer above the features was sampled,
- problems of reconstructing the sample position, or
- sites or sampled layers were not related to Nok.

Since preliminary results have attested that sampling was in most cases insufficient, an adjusted sampling strategy with focus on vertical sampling was planned for the excavation of *Ifana 4* and *5* in 2017. However, the excavation had to be cancelled after a few days without obtaining samples. Since it was not possible to conduct further excavations after 2017, the analyses are based on the samples taken before 2015.

Those samples considered as promising were taken at *Pangwari D*, *E* and *I*, *Kusuma 1*, *Kurmin Uwa 1*, and *Ifana 1* and *2* (Tab. 7-2). *Ido 2016* was used for both the analysis of stone-pot-arrangements and pit features, although the latter were at that point in time not the subject of the excavation.

The analysed Nok sites and features date mainly to the Middle Nok phase, although activities dating to the Early Nok phase were also attested on most sites (Tab. 7-3).

Site	Year of excavation	Covered area	Measured samples
Kusuma 1	2010	54 m^2	172
Kurmin Uwa 1	2010	60 m^2	223
Ifana 1	2011	54 m^2	205
Ifana 2	2011	10 m^2	65
Pangwari E	2012/13	120 m^2	131
Pangwari D, E and I	2012/13 and 2013/14	Features 8, 9 and 17	40

Tab. 7-2: Sites and features measured in the scope of this thesis in order to ascertain the function of the pits.

Site	Sampled feature or area	Material	Laboratory no.	Radiocarbon age bp	±	δ13C [‰]	Calibrated results 1-sigma 68.2%	2-sigma 95.4%
Ido 2009 and 2016								
Ido 2016	Terracotta-pot-arrangement (feature 16-03)	Pennisetum	Beta-434507	2730	30	-9.9	901-836 BC	**930-812 BCE**
Ido 2016	South of terracotta-pot-arrangement	Pennisetum	MAMS 27395	3029	26	-10.1	1373-1226 BC	**1393-1209 BCE**
Ido 2016	Pit (feature 16-07)	Pennisetum	MAMS 27393	2800	25	-7.7	992-916 BC	**1016-858 BCE**
Ido 2009	Pit (other half of feature 16-07)	Charcoal	MAMS 10702	2708	13	-28.5	894-823 BC	**898-819 BCE**
Ido 2009	Pit (other half of feature 16-07)	Pennisetum	MAMS 10742	2704	23	-22.9	894-816 BC	**901-811 BCE**
Ido 2016	Pit (feature 16-08)	Seed fragment	Beta-434506	2930	30	-24.6	1195-1058 BC	**1220-1025 BCE**
Ido 2009	Pit (other half of feature 16-08)	Pennisetum	MAMS 13664	3036	26	-13.2	1373-1266 BC	**1393-1216 BCE**
Ido 2009	Concentration of charcoal	Charcoal	MAMS 10741	2408	23	-37.7	510-407 BC	**728-403 BCE**
Ifana 1-3								
Ifana 1	Below terracotta deposition (feature 2)	Pennisetum	MAMS 13624	2632	34	-14.6	824-792 BC	**893-772 BCE**
Ifana 2	Pit (feature 3)	Pennisetum	MAMS 13634	2586	25	-15.3	801-775 BC	**811-762 BCE**
Ifana 2	Pit (feature 2)	Pennisetum	MAMS 13635	2550	25	-16.8	795-603 BC	**801-555 BCE**
Ifana 3	Below terracotta deposition (feature 3)	Plant fragment	Beta-445971	2520	30	-28.4	784-558 BC	**794-542 BCE**
Ifana 3	Below terracotta deposition (feature 9)	Plant fragment	Beta-445972	3210	30	-26.0	1503-1446 BC	**1594-1418 BCE**
Ifana 3	Near terracotta deposition (feature 9)	Charcoal	Beta-451381	120	30	-27.2	1685-1927 AD	**1678-1940 CE**
Ifana 3	Below terracotta deposition (feature 19)	Pennisetum/Plant	Beta-445970	2530	30	-25.9	790-571 BC	**797-543 BCE**
Ifana 3	Stone-pot-arrangement (feature 7)	Charcoal	Beta-451380	2500	30	-29.0	766-552 BC	**788-536 BCE**
Ifana 3	Stone-pot-arrangement (feature 13)	Charcoal	Beta-451382	3520	30	-25.8	1894-1775 BC	**1928-1752 BCE**
Ifana 3	Stone-pot-arrangement (feature 17)	Plant fragment	Beta-445775	3420	30	-25.6	1754-1666 BC	**1871-1636 BCE**
Ifana 3	Stone-pot-arrangement (fature 22)	Charcoal	Beta-451383	2490	30	-25.7	761-546 BC	**781-510 BCE**
Ifana 3	Stone-pot-arrangement (feature 29)	Pennisetum/Plant	Beta-445973	3480	30	-24.2	1876-1753 BC	**1888-1696 BCE**
Kurmin Uwa 1								
Kurmin Uwa 1	Next to complete pot (feature 2)	Canarium	MAMS 11163	2464	25	-32.3	750-515 BCE	**763-431 BCE**
Kurmin Uwa 2B								
Kurmin Uwa 2B	Find concentration	Pennisetum	MAMS 11164	2523	24	-10.9	778-571 BC	**792-547 BCE**
Kusuma 1								
Kusuma 1	Pit (feature 2)	Pennisetum	MAMS 11168	2516	32	-8.7	773-553 BC	**794-540 BCE**
Pangwari I								
Pangwari I	Pit (feature 17)	Pennisetum	Beta-431337	2560	30	-9.0	800-598 BC	**805-553 BC**
Pangwari I	Pit (feature 17)	Pennisetum	MAMS 26987	2522	22	-5.2	783-590 BC	**791-548 BC**
Pangwari I	Stone-pot-arrangement (feature 18)	Charcoal	MAMS 26984	2502	23	-25.0	766-556 BC	**780-541 BC**
Pangwari I	Pit (feature 19)	Canarium	Beta-431335	2960	30	-27.4	1218-1124 BC	**1263-1056 BC**
Pangwari I	Pit (feature 19)	Canarium	Beta-477643	2950	30	-23.2	1214-1118 BC	**1260-1051 BC**
Pangwari I	Pit (feature 19)	Canarium	MAMS 26986	2944	24	-25.7	1208-1119 BC	**1221-1054 BC**
Pangwari I	Pit (feature 19)	Charcoal	MAMS 26985	2906	26	-23.8	1127-1038 BC	**1206-1010 BC**

Tab. 7-3: Overview of the relevant ^{14}C dates obtained from the analysed Nok sites. For further dates from *Pangwari* and other Nok sites see Schmidt 2014: 118–121 and Franke 2017: 38–49, App. 3-1. All dates are calibrated in OxCal4.2 using the IntCal13 calibration curve (Bronk Ramsey 2009; Reimer *et al.* 2013).

7.2 Ido 2009 and 2016

The site *Ido*, located on a slight slope close to the research station in Janjala, was discovered and excavated for the first time in 2009 (*Ido 2009*). The most prominent feature was a stone-pot-arrangement with associated stone beads arranged as if on a string between further features consisting of arranged stones (Fig. 7-2).

Based on its appearance, this feature (09-01) was interpreted as a burial due to the archaeological context and it was sampled for pXRF analysis (Rupp 2010: 70–72). However, both the number and mass of samples turned out to be insufficient for pXRF analysis. In order to sample further stone-pot-arrangements with an improved strategy, the old excavation trench was extended and excavated in 2016 (Schmidt 2016).

The excavation trench of 2016 extended from the old trench in 2009 to the north with a trench size of 8.5 x 5 m (Fig. 7-3). The excavation in 2016 yielded two further stone-pot-arrangements (feature 16-02 and 16-09), although with less distinctive stone arrangements compared to the features uncovered in the old trench (Fig. 7-4).

Fig. 7-2: Excavation at *Ido 2009* with a stone-pot-arrangement (feature 09-01) comprising two vessels and a bead necklace (indicated by the black arrow). Further stone-arrangements were found, but without attached pots or other finds. The samples taken for pXRF analysis were not sufficient, since they comprised only one row of samples without reference material.

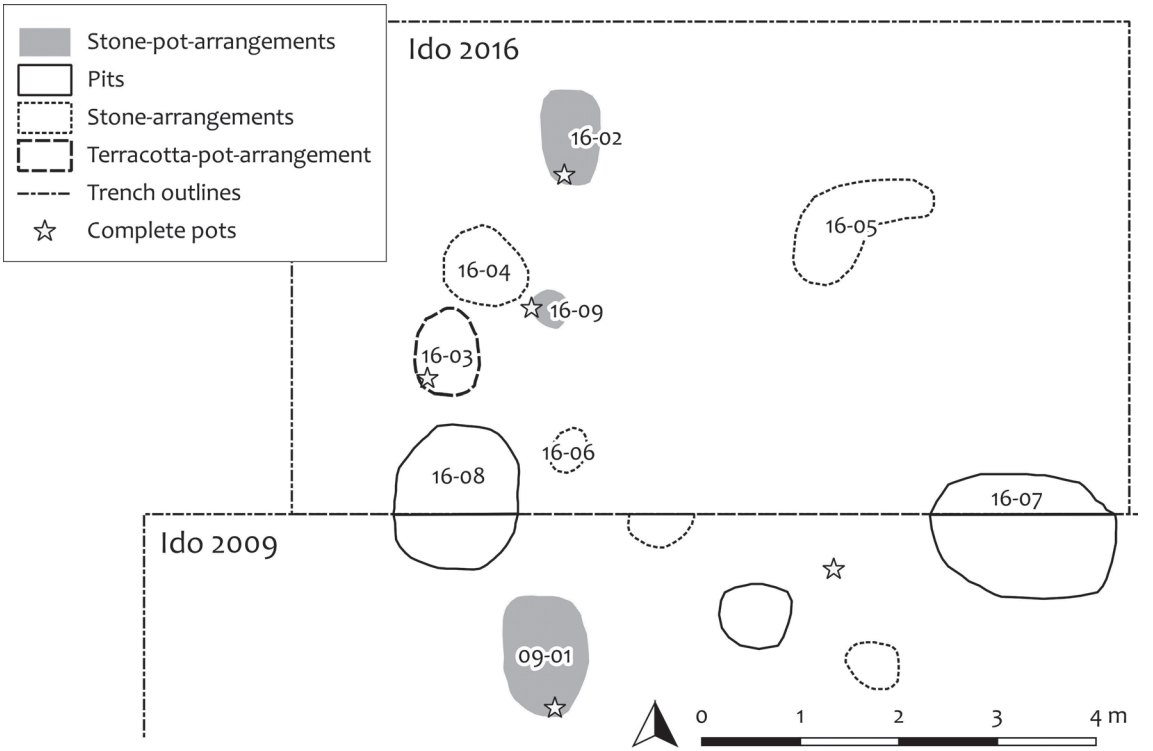

Fig. 7-3: Excavation plan with feature numbers of *Ido 2016* and parts of the excavation in 2009. Feature 09-01 represents the stone-pot-arrangement with the necklace made from stone beads. Features 16-02 and 16-09 were further, but less distinct, stone-pot-arrangements (Fig. 7-4).

Fig. 7-4: Two stone-pot-arrangements (feature 16-02 and 16-09) considered as potential burial features found at *Ido 2016*.

Furthermore, two pits (features 16-07 and 16-08) were located on the southern boundary, which separated the old and new trench. Similar to *Ido 2009*, features consisting of arranged stones, including grinders, were found (features 16-04 to 16-06) but neither pots nor jewellery. In addition, a terracotta-pot-arrangement (feature 16-03) consisting of a stone accumulation with two large terracotta fragments and one vessel beneath was

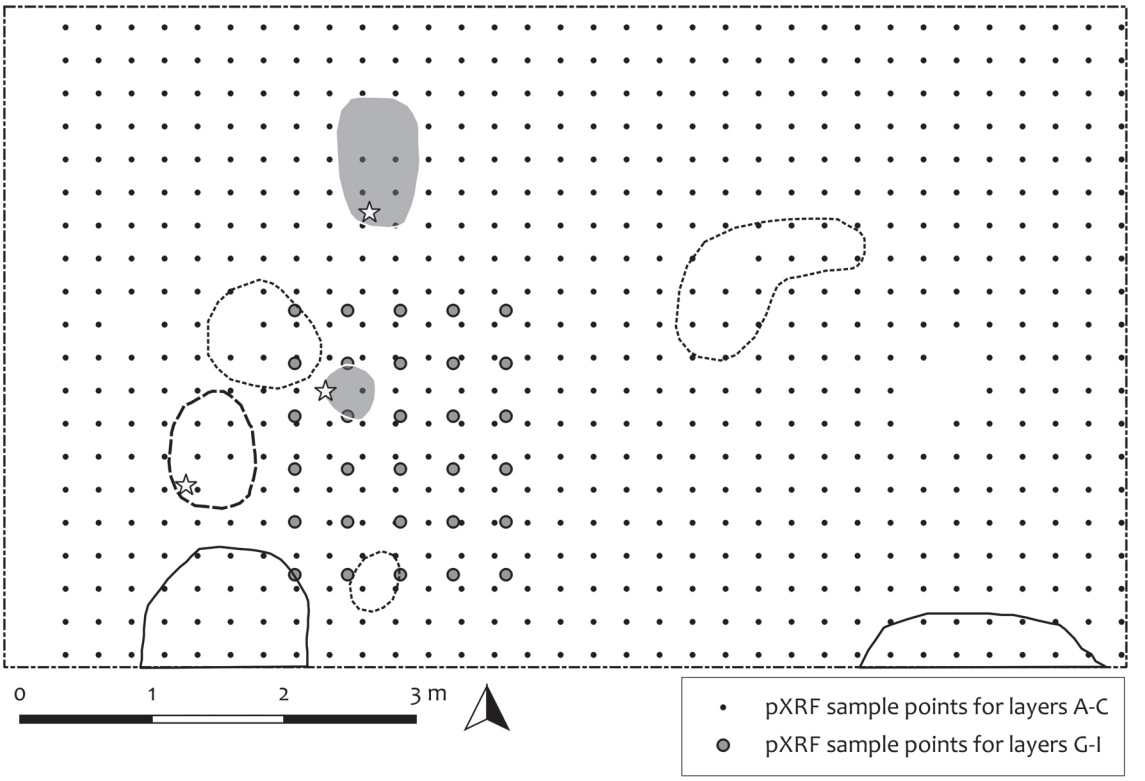

Fig. 7-5: Sampling scheme at *Ido 2016*. Three layers (A-C) covered the whole trench. Three sections encompassed feature 16-09 (G-I), which emerged at a greater depth. For a feature description see Fig. 7-3.

discovered (Schmidt 2016: 65). The find inventory comprised characteristic Nok finds, i.e. mainly pottery and charcoal, a few stone artefacts, and burnt clay. The determination of the size of the stone-pot-arrangements was impeded by the absence of visible outlines. When measuring the extent of the arranged stones and the adjacent pots, the dimensions ranged from *c*. 50 cm (feature 16-09) to *c*. 1.5 m (feature 09-01), whereas the size of the pit features ranged from 1.5 m (feature 16-08) up to 2 m (feature 16-09) in diameter with a minimum depth of 1.2 m below the surface (not fully excavated).

^{14}C dates attested to activities during the Early and Middle Nok, with emphasis on the 10th to 8th century BCE (Tab. 7-3). According to the dates, the two pits (16-07 and 16-08) and the terracotta deposition (16-03) date to that time span. Dates ranging from the 14th to 10th century BCE, together with Early Nok pottery, provided evidence for an early occupation. The Early Nok dates within the pits were probably caused by erosional processes, since they all originated from the upper layers. All stone-pot-arrangements were void of datable material, but the decoration and design of the vessels suggested a contemporaneity with the pits, dating to around 1000-800 BCE.

The sampling strategy focused on the stone-pot-arrangements (Fig. 7-5). Thus, three layers of the whole trench (A-C), sampled in a 25 cm grid, covered feature 09-02. The depths of the layers A-C increased southwards, since *Ido* was located on a slope and layers were excavated perpendicularly. Their depths ranged from north to south between 20 to

50 cm (layer A), 40 to 70 cm (layer B) and 60 to 90 cm (layer C). Three further sections (G-I) from three different depths (100 cm, 120 cm and 130 cm), sampled in a 40 cm grid, covered feature 16-09 (Fig. 7-5). However, since the pXRF results of layer A (Schmidt 2016) revealed that the stone-pot-arrangements were concealed by geogenic interferences, not all layers were measured.

7.3 Ifana 1-5

The site of *Ifana* (IFA) was discovered and excavated for the first time in 2011. The site is located at the southern fringe of a granite hilltop close to the research station in Janjala. Terracotta pieces found on the surface attested to illicit digging activities during the early 2000s. Between 2011 and 2017, a total of 5 trenches were excavated (*Ifana 1-5*), although the excavation at trenches *4* and *5* had to be cancelled after a few days and were not resumed (Fig. 7-6).

Ifana 1 and *2* were both excavated in 2011. At *Ifana 1,* a terracotta deposition was found. In order to test the hypothesis that terracotta depositions and stone-pot-arrangements appear together, the trench at *Ifana 1* was extended in 2016 (*Ifana 3*), in order to find adjacent stone-pot-arrangements. A total of 18 stone-pot-arrangements and a minimum of three further terracotta depositions were discovered (Breunig 2018: 399–400). In 2017, excavations at *Ifana 4* and *5* commenced in order to apply improved sample strategies to the pit features (*Ifana 4*), as well as to reveal further stone-pot-arrangements and terracotta depositions (*Ifana 5*). Since the excavations were interrupted and not resumed, no samples for analysis were obtained.

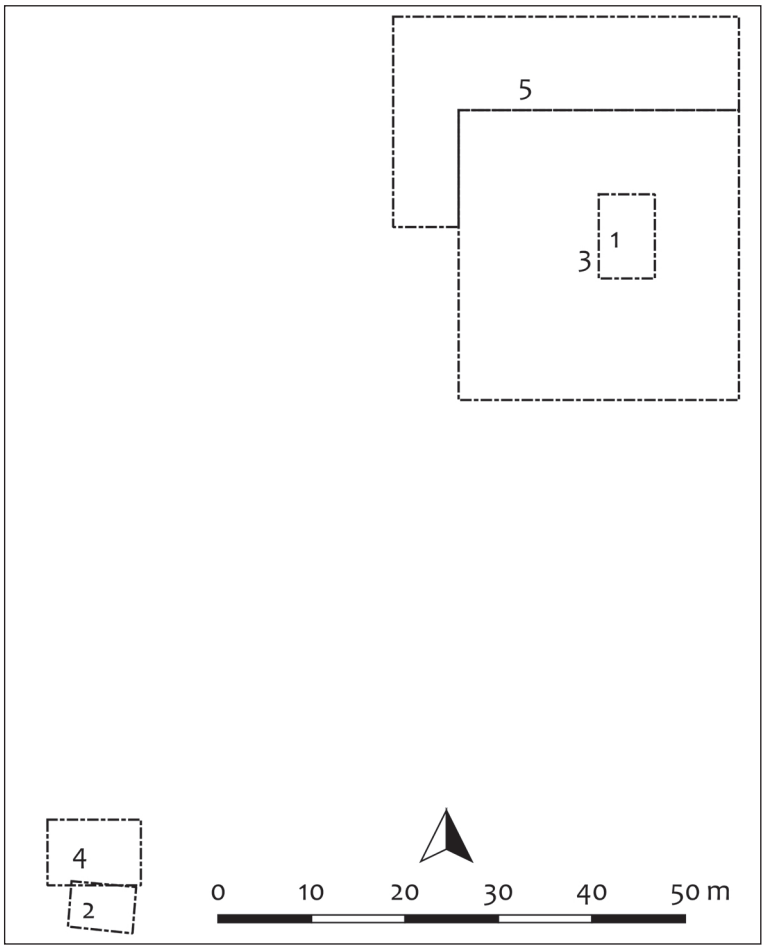

Fig. 7-6: Overview of the site of *Ifana* and the position of the trenches *1-5*. Samples were taken and analysed for *Ifana 1-3*.

7.3.1 Ifana 1

The excavation trench at *Ifana 1* measured 6 x 9 m and yielded five features (Fig. 7-7), among them a terracotta deposition (feature 2), stone-arrangements (features 4, 5) and find concentrations (features 1, 3). Finds of pottery, terracotta fragments, stone artefacts, charcoal, and burnt clay were found throughout the whole trench. Due to the absence of visible outlines, the dimensions of the features were – as in most cases – difficult to determine. When using the extent of the stones as reference, dimensions of the stone-arrangements measured between 1 m up to 2 m in diameter (features 4 and 5, respectively). The terracotta figurines of feature 2 covered an area of *c.* 1 x 2 m. Form and size of the find concentrations ranged from 1.5 m in diameter (feature 1) up to an irregular form measuring 50 cm x 2 m (feature 3).

Both the pottery and one ^{14}C date (Tab. 7-3), between the 9th to 8th century BCE, suggested a Middle Nok date for the features. *Ifana 1* was sampled over three layers, of which one layer (60 cm depth) was at the same height as the features. The grid size was 50 cm; the areas around features 2, 4 and 5 were sampled separately.

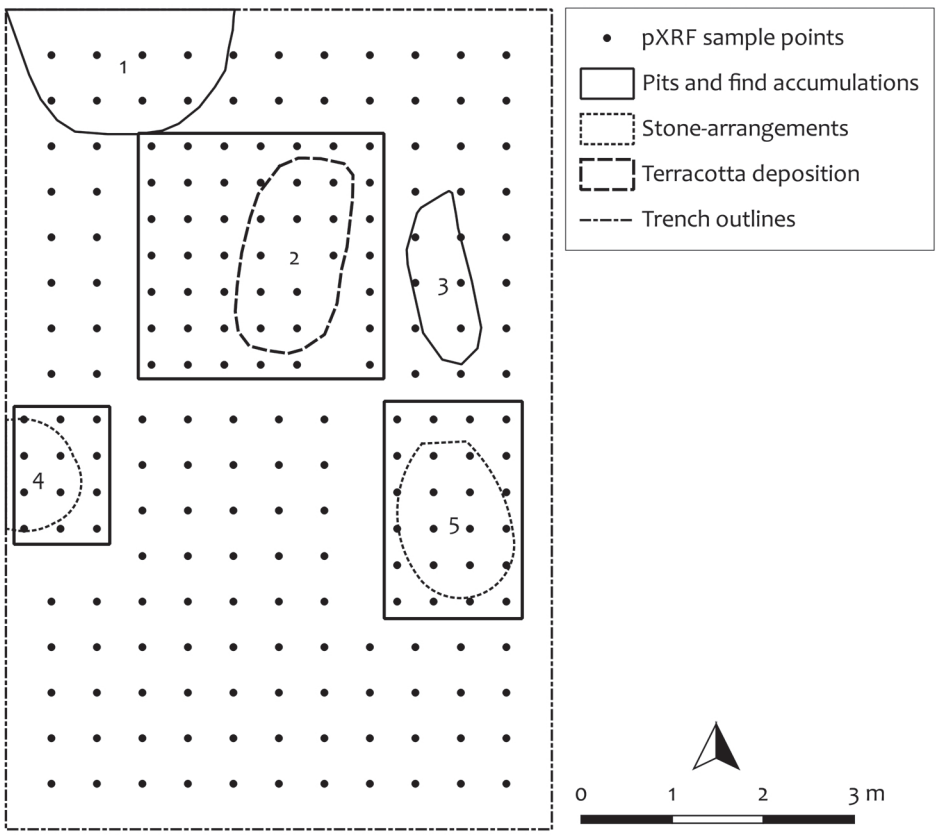

Fig. 7-7: Excavation trench at *Ifana 1* with all features from all depths and the position of the samples taken at a depth of 60 cm. The sampled layer covered features 3 to 5. The areas indicated by the boxes were sampled separately, but on the same layer.

7.3.2 Ifana 2

Two pits (feature 2 and 3) as well as one isolated and complete vessel associated with a single stone (feature 1) were found within the 7 x 5 m large excavation trench at *Ifana 2* (Fig. 7-8 and 7-9). The finds were considered to be characteristic for the Nok Culture. The dimensions of the pits measured 1.5 x 3.5 m (feature 3) and 1.5 x 2 m (feature 2), but were not completely excavated. Both features comprised a 1.2 m thick in situ layer.

Both the pottery and two ^{14}C dates between the end of the 9th century to the 8th and 6th century BCE (Tab. 7-3), respectively, were contemporaneous with *Ifana 1*. Samples for pXRF analyses concentrated on the eastern half and southwest corner of the trench and were taken at a depth of 70 cm, where all features were visible.

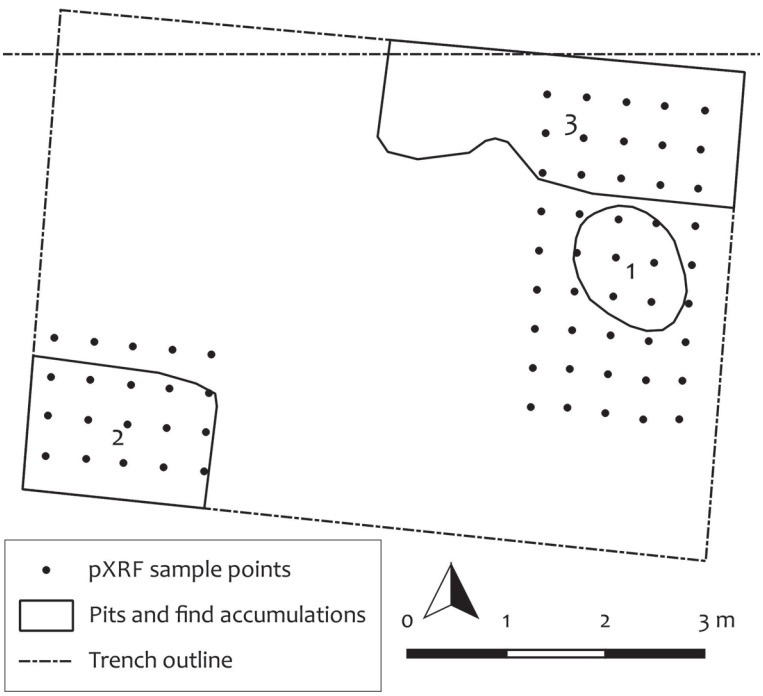

Fig. 7-8: The trench of *Ifana 2* with all features. The samples were taken at a depth of 70 cm below the surface.

Fig. 7-9: Feature 3 with part of the W-E profile. The pit is clearly distinguished by the soil discolouration.

7.3.3 Ifana 3

Ifana 3 is, besides *Pangwari*, the largest Nok excavation conducted by the Nok project. The trench measured 30 x 31 m and yielded more than 30 features (Breunig 2018: 400 Fig. 16), among them several terracotta depositions and stone-pot-arrangements (Fig. 7-10). Characteristic Nok finds, such as pottery, charcoal, stone artefacts, and burnt clay, were scattered across the whole trench but concentrated in the upper layer. The finds at greater depths were mostly restricted to the features. None of the stone-pot-arrangements and terracotta depositions showed clear feature outlines. Depending on the position of the pots and the extents of the arranged stones as well as the terracotta figurines, the dimensions of both feature types ranged between *c*. 50 cm up to 2 m in diameter, although the forms were in most cases irregular.

The obtained ^{14}C dates at *Ifana 3* cluster in two periods (Tab. 7-3). The oldest dates fall between the 20th to 17th century BCE and the 16th to 15th century BCE, the youngest between the 8th to 6th century BCE. Both the older and younger dates originated from stone-pot-arrangements and terracotta depositions. Since the beginning of terracotta use dates to around the 9th century BCE (Franke 2016: 273; Franke 2017: 56) and the pots from the stone-pot-arrangements have a Middle Nok design, both feature types were considered to be Middle Nok and associated with the younger dates. Whether and how the very early ^{14}C dates related to the site of *Ifana 3* is yet to be determined. Four stone-pot-arrangements (features 8, 13, 17, and 18) were sampled for pXRF analysis in a 10 cm grid (Fig. 7-11). Each sampled layer was at the same depth as the bottom edge of the vessels. For technical reasons, features 8 and 18 could only be sampled partially.

Fig 7-10: Part of the excavation at *Ifana 3* with two terracotta depositions and two stone-pot-arrangements. The areas between the features were void of finds, apart from the upper layer.

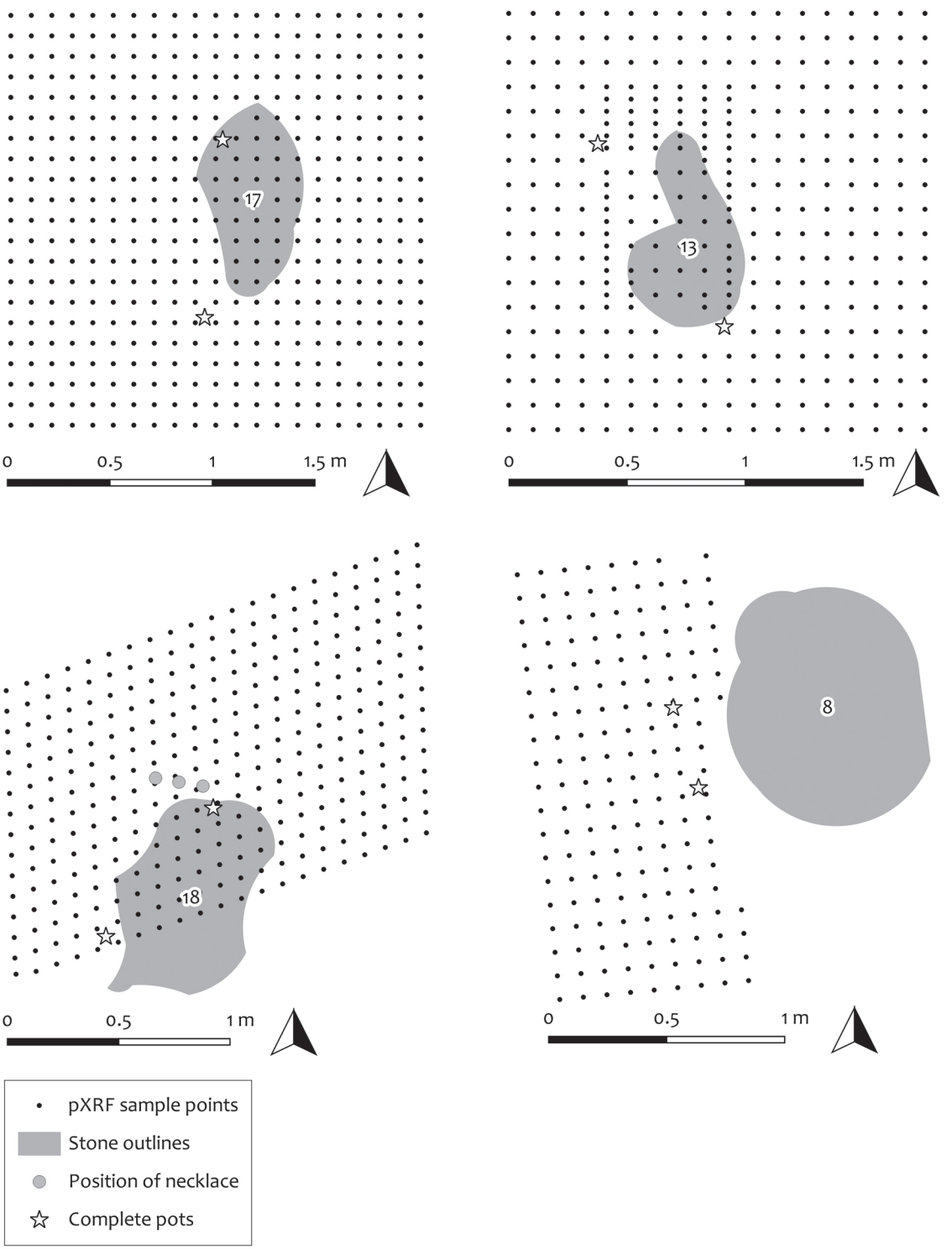

Fig. 7-11: Sampling scheme of features 8, 13, 17, and 18 at *Ifana 3*. The samples were taken in a 10 cm grid. In feature 13, samples were taken both around the arranged stones and beneath the stones. In features 17 and 18 all samples were taken from the layer beneath the arranged stones.

7.4 Kurmin Uwa 1

The site of *Kurmin Uwa 1* (KU 1) was discovered and excavated in 2010. It is located close to the road from Janjala to Kagarko along a slope. Surface holes with characteristic Nok finds inside attested to illicit digging activities. The 6 x 10 m trench yielded three features (Fig. 7-12), among them one reddish discolouration with burnt clay (feature 1), a complete but broken vessel (feature 2) and a pit with fragments of terracotta and a complete but broken vessel associated with further vessel fragments (feature 3, Fig. 7-13). The large pit feature 3 measured 2 m in diameter with a maximum depth of 70 cm, of which at least 30 cm were in situ. Feature 1 measured 50 cm in diameter and disappeared at the sampled layer at 50 cm. Feature 2 consisted of a complete but broken vessel only.

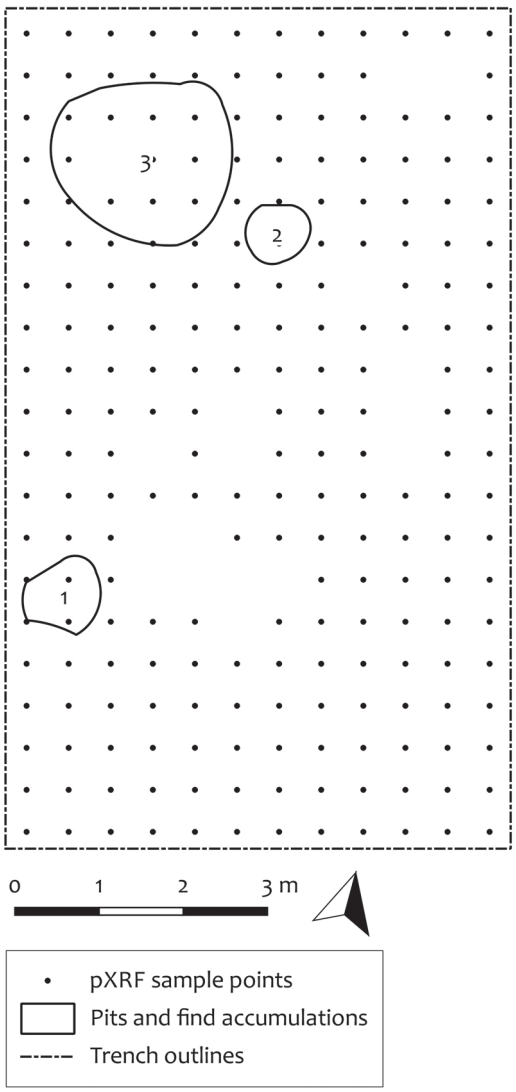

Fig. 7-12: The site of *Kurmin Uwa 1* with the sampled layer at a depth of 50 cm. On the sampled layer only features 2 and 3 were visible. Stones or weathered granite were not sampled, causing the visible voids in the sample grid.

One ^{14}C date between the 8th to 5th century BCE (Tab. 7-3) and Middle Nok pottery date the site of *Kurmin Uwa 1* to this phase. The sampling layer at a depth of 50 cm covered features 2 and 3.

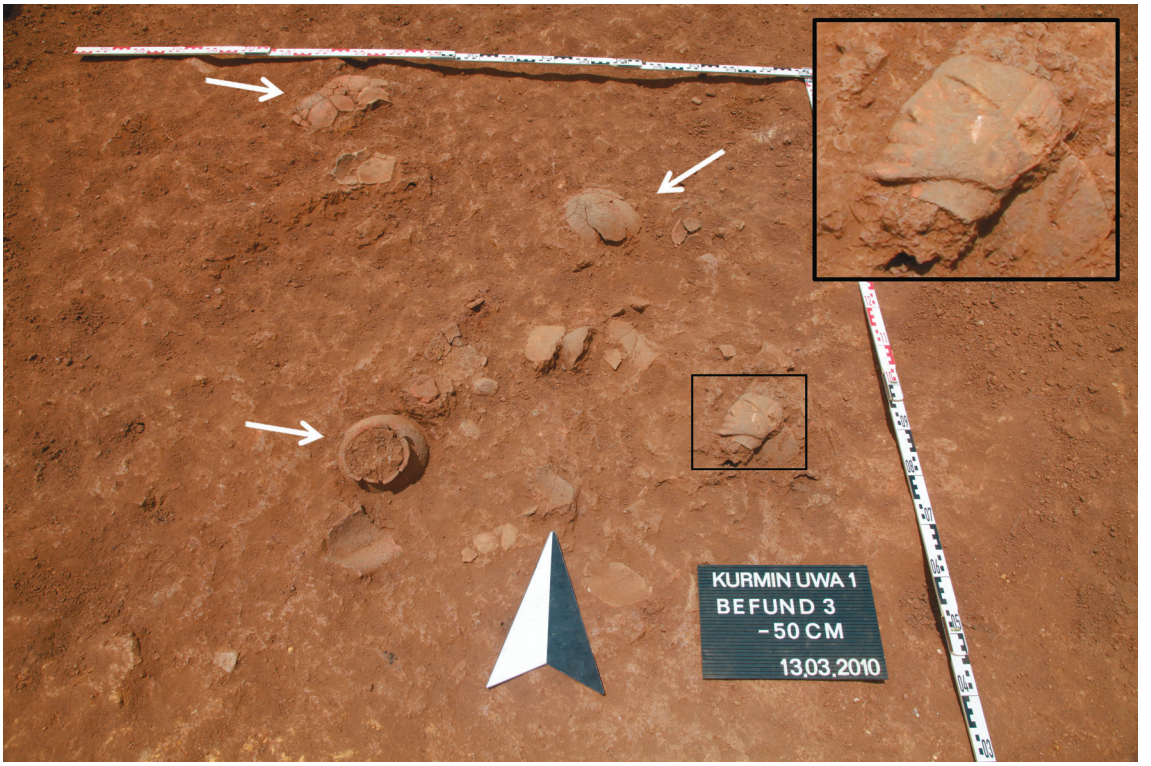

Fig. 7-13: Feature 3 at *Kurmin Uwa 1* at a depth of 50 cm. The pit outlines were barely visible. A complete vessel and further large pot fragments, as indicated by the white arrows, were found associated with a small terracotta head (enlarged section).

7.5 Kurmin Uwa 2B

Kurmin Uwa 2B (KU 2B), excavated in 2010, is located in undulating terrain between granitic outcrops. The area contained several illegal digging holes. The trench, measuring 5 x 9 m (Fig. 7-14), yielded one stone-pot-arrangement with two vessels (feature 1) and a pit feature (feature 2). Most finds were accumulated within feature 2 and contained characteristic Nok finds. According to the accumulated finds, the pit feature 2 measured 1.8 x 2 m (not fully excavated) with a depth of *c.* 70 cm. The stones and pots of feature 1 covered an area of *c.* 1 x 1 m; outlines were not visible.

One ^{14}C date (Tab. 7-3), between the 8th to 6th century BCE, as well as Middle Nok pottery provided evidence for site use at that time. The samples encompassing the stone-pot-arrangement came from a depth of 50 cm and were taken in a 20 cm grid. These samples already had been measured and the results published by Nagel (2014), but were re-measured in the scope of this thesis with customised sample preparation and device settings.

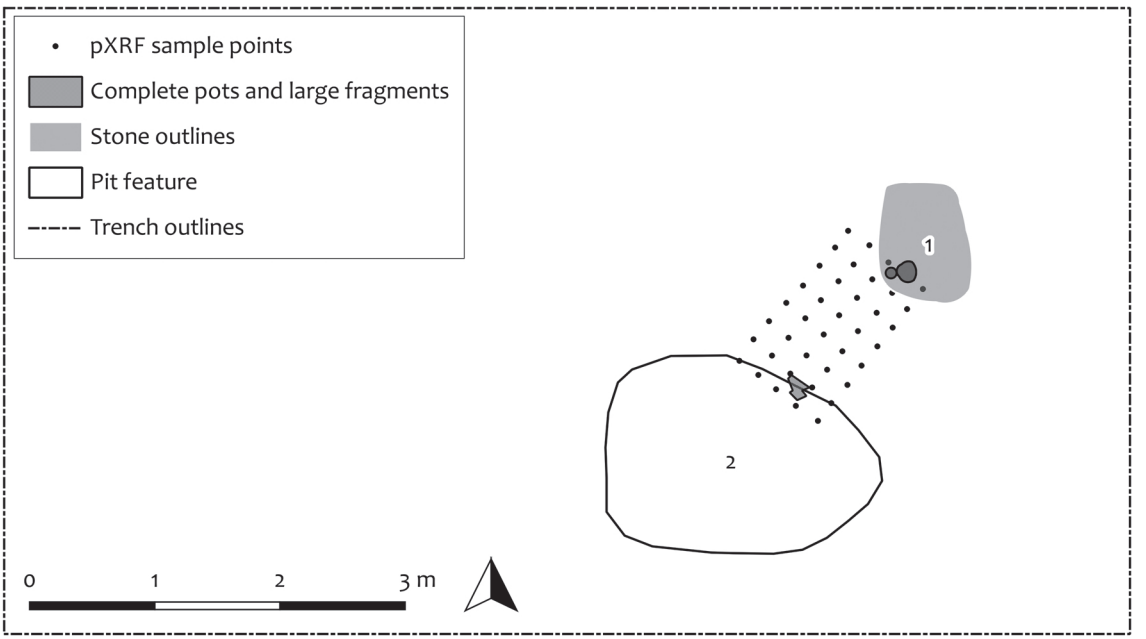

Fig. 7-14: Trench of *Kurmin Uwa 2B* with all features. At the lower edge of the sample grid further remains of a pot were found within an adjacent pit.

7.6 Kurmin Uwa 2D

Kurmin Uwa 2D is part of a site which is known for its intense looting. It was visited in 2016, when a stone setting was discovered within a looting hole and excavated in a 2 x 2 m trench. At a depth of 100 cm, where the pit reached its maximum dimensions of 90 cm x 1.4 m, two complete pots emerged within a pit with sharp outlines (Fig. 7-15). The samples were taken at the bottom of the vessels at a depth of 120 cm in a 10 cm grid (Fig. 7-16); at that depth, the pit was no longer visible. As the pots showed a characteristic Middle Nok design, this feature is considered likely to date to this phase.

Fig. 7-15: View of the small excavation trench measuring 2 x 2 m at *Kurmin Uwa 2D* at a depth of 100 cm. The stone-pot-arrangement was found in between several looting holes.

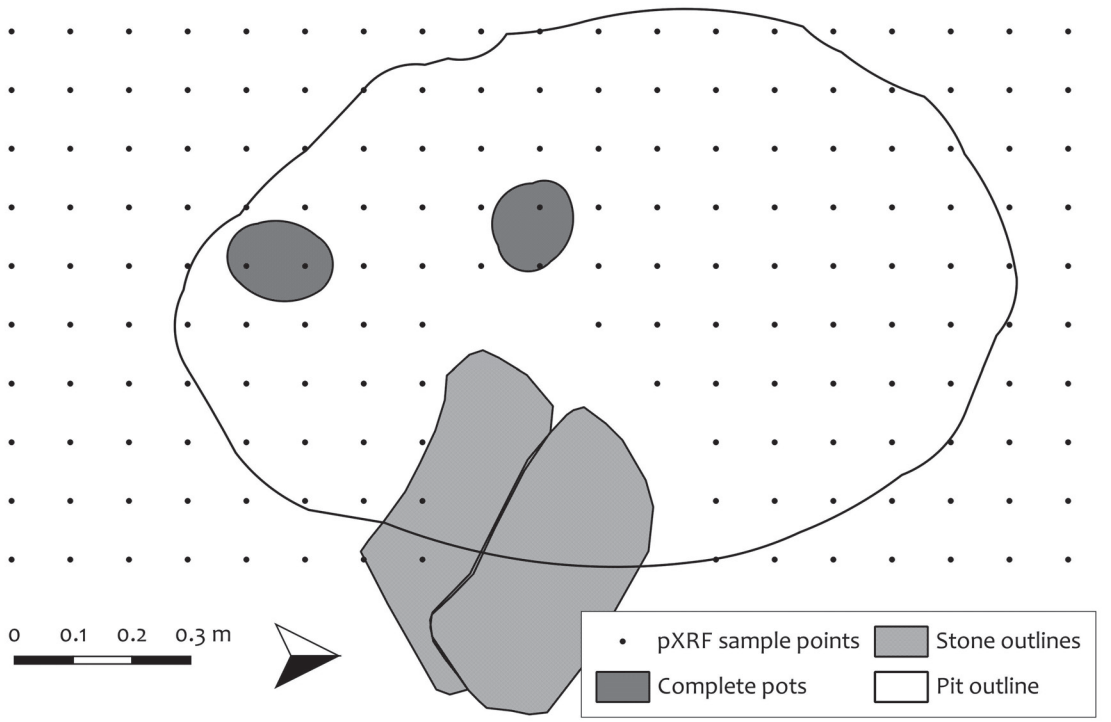

Fig. 7-16: Sampling at *Kurmin Uwa 2D* in a 10 cm grid. The sampling height corresponded with the bottom edges of the pots. The pit was no longer visible at that depth, but its position reconstructed according to its outlines visible in the layer above.

7.7 Kusuma 1

Kusuma (KM), located in flat terrain, was discovered through the occurrence of a few illicit digging holes containing terracotta fragments and was excavated in 2010. Three features were documented within the 3 x 18 m large trench (Fig. 7-17). Besides one stone artefact near the surface (feature 1), two distinctive pits (features 2 and 3) and a charcoal concentration in the middle of the trench were found. The site yielded typical Nok finds such as pottery, burnt clay, stone artefacts, charcoal, and a few terracotta fragments. The majority of finds were concentrated within the pit features, especially at greater depths. The outlines of the pit features 2 and 3 (not fully excavated) measured 1.5 x 2 m with a depth of 50 and 90 cm, respectively. At that time, the excavation at *Kusuma 1* aimed primarily on obtaining organic material for dating, leaving the remains of the pits unexcavated and thus the sampling incomplete.

One ^{14}C date (Tab. 7-3) from feature 2, together with characteristic pottery, dates the site to between the 8th to 6th century BCE. Sampling took place at a depth of 60 cm in a 50 cm grid and covered the features 2 and 3.

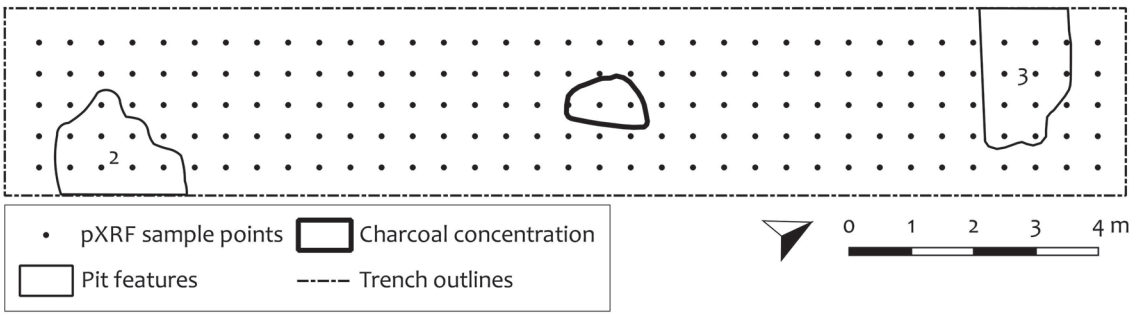

Fig. 7-17: *Kusuma 1* with all features. Features 2 and 3 as well as the charcoal concentration were visible at the sampling depth of 60 cm.

7.8 Pangwari

At *Pangwari* (PGW), discovered almost untouched by lootings in 2011, an area of *c*. 2600 m² was excavated in two campaigns in 2012/13 and 2013/14 (Fig. 7-18) (Schmidt 2014: 25–26). The most prominent features were a terracotta deposition (feature 10) (Schmidt 2014: 73–78; Männel & Breunig 2016) and two stone-pot-arrangements (features 18 and 20) (Schmidt 2014: 97–98, 101–102; Höhn *et al.* 2018: 289–290).

A total of 37 ^{14}C dates and pottery proved that the site was used during all Nok phases, from the 15th century BCE to the decline of the Nok Culture at the end of the 1st century BCE, as well as after the 10th century CE. The majority of dates clustered around 800 BCE (Schmidt 2014: 118–121; Höhn *et al.* 2018: 276–277, Fig. 4). More than 20 additional ^{14}C dates (the relevant dates listed in Tab. 7-3) confirmed this interpretation and provided further evidence for Early Nok features, among them one distinctive pit (feature 19). A further ^{14}C date beneath a stone-pot-arrangement (feature 18) confirmed the age of these feature types as Middle Nok, in accordance with the designation of the pots found within these features.

Samples for analyses were chosen from trenches *D*, *E* and *I*. Samples from the other trenches originated from a disturbed layer, which contained a mixture of older and younger material (Höhn *et al.* 2018: 277–278, Fig. 5).

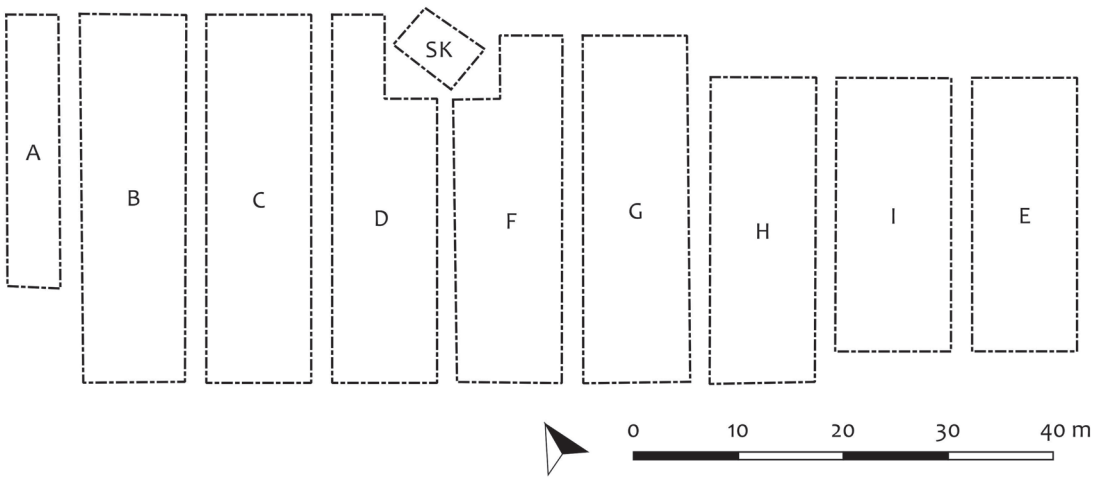

Fig. 7-18: Overview of the ten excavated trenches at *Pangwari*. The trenches were located on a W-E orientated slope. Trench *E* is located on a saddle between two small granitic summits to the north and south. Trench *SK* (located between trenches *D* and *F*) corresponds to a probably contemporary stone circle.

7.8.1 Pangwari D

Finds in trench *D*, located at the lower part of the slope, were found in the upper 20 cm throughout the entire trench but decreased down to a depth of 40 cm beneath the surface, when – aside from feature 8 and 9 – the soil became void of finds. Feature 8 measured *c.* 2 m in diameter with 70 cm being in situ and feature 9 *c.* 2 m to 2.5 m with 1 m being in situ.

A few samples were taken (Fig. 7-19) from both features at a depth of 80 cm (features 8 and 9) and 130 cm (only feature 9). The insufficient amount of reference material (two samples east of feature 8) was unfavourable for interpretation of the pXRF analyses.

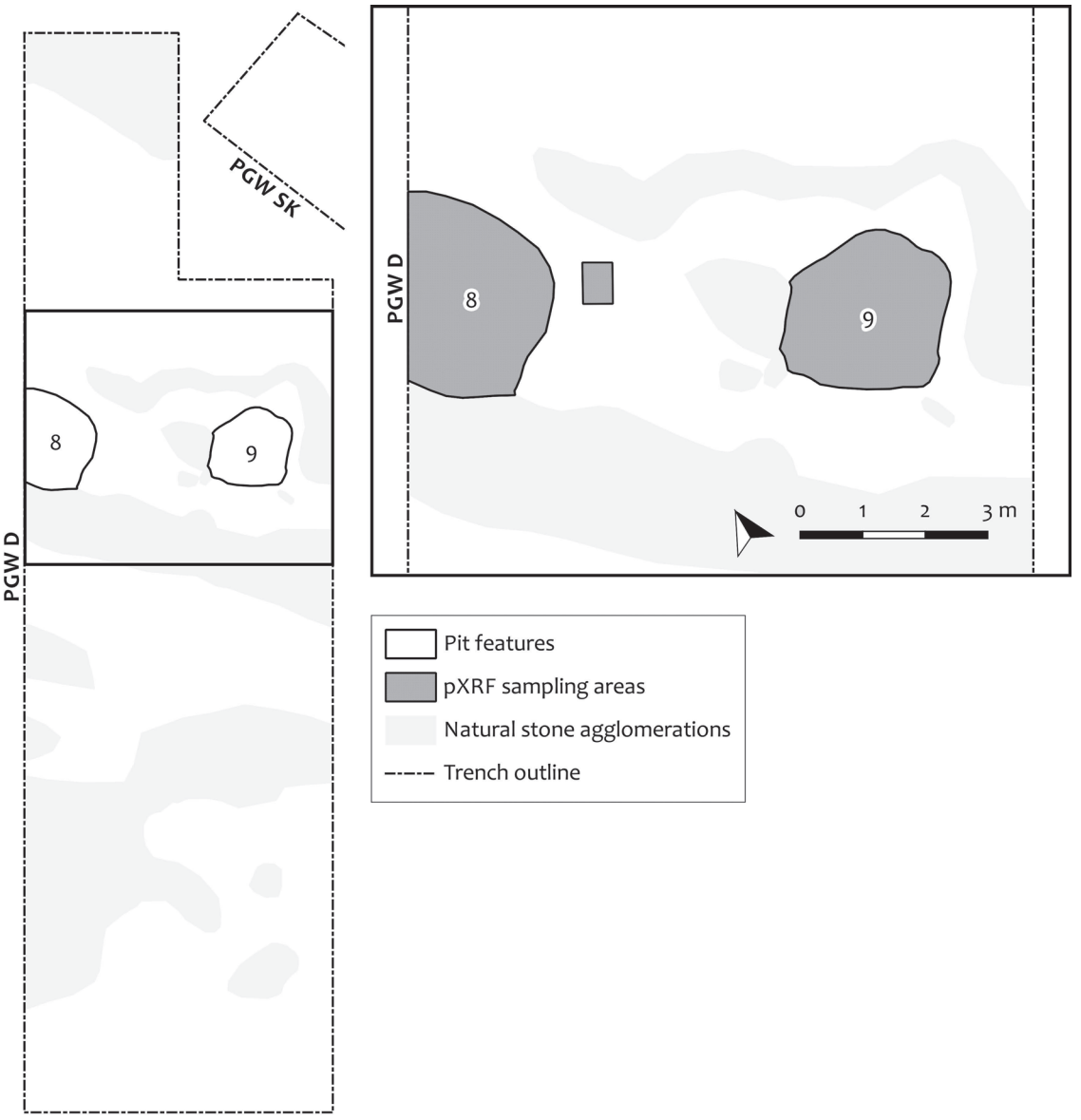

Fig. 7-19: Sampling of features 8 and 9 at *Pangwari D*.

7.8.2 Pangwari E

Located on top of the slope between two low-rise summits, trench *E* had the highest find and feature density (Schmidt 2014: 28, Fig. 8), but was also the most strongly affected by erosional processes leading to an accumulation and mixture of material (Höhn *et al.* 2018: 277–278, Fig. 5). In the north and south of trench *E*, the surface was covered with unworked stones. Finds occurred within the first 20 cm across the entire trench and accumulated at its centre. Four features were discovered, among them one terracotta deposition (feature 10), one large pit (feature 11), a pit-like feature (feature 14) and a disturbed pit (feature 12). The area covered with terracotta figurines (feature 10) measured 1 x 1 m. Outlines of feature 11 were visible and measured *c.* 1.5 x 2.5 m with 1.1 m being in situ. The outlines of feature 12 and 14 were reconstructed by the find distribution and measured both 2 m in diameter with a layer being in situ for 1 m and 70 cm, respectively.

The section of trench *E*, sampled at a depth of 60 cm with a 1 m grid (Fig. 7-20), covered the features 10, 11, and 12, of which the latter two emerged at a depth of 60 cm (Schmidt 2014: 38–39, 73–87). Feature 14 was recorded at a greater depth, although finds concentrated in that area already at a depth of 60 cm (Schmidt 2014: 38–39, 90–92).

7.8.3 Pangwari I

Located at the upper edge of the slope and probably affected by erosional processes, trench *I* yielded only a few finds in the upper 30 cm (Schmidt 2014: 36–37). Notable within this trench were two stone-pot-arrangements (features 18 and 20), an Early Nok pit (feature 19) and another Middle Nok pit (feature 17).

The pit feature 17 measured 2 m in diameter with a 70 cm thick in situ layer. Since no clear outlines were visible, the dimensions of pit feature 19 were defined by its find distribution, extending 70 cm in diameter and depth. The stone-pot-arrangements features 18 and 20 had no visible outlines, but the arrangements covered an area of *c.* 1 x 1.5 m.

The tips of the stone-pot-arrangements were visible at a depth of 70 cm and completely excavated at a depth of 110-120 cm. Due to the significant features 18 and 20, a section of trench *I* was sampled at a depth of 130 cm with a denser grid of 50 cm (Fig. 7-20). This depth corresponded to the height of the bottom edges of the pots and the bottom of feature 19 (Schmidt 2014: 37). A few samples were also taken at a depth of 90 cm around feature 17.

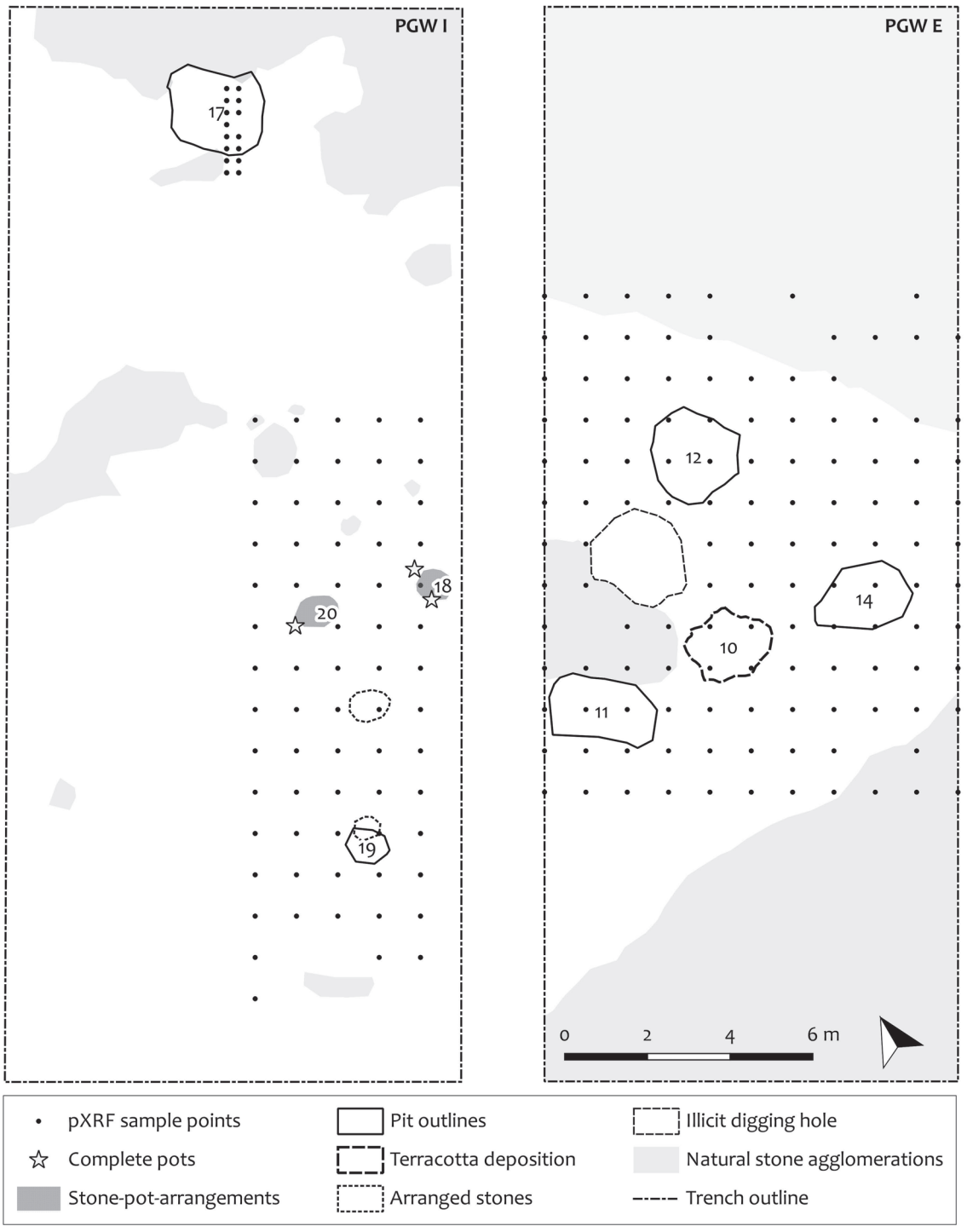

Fig. 7-20: Sampling scheme at *Pangwari E* and *I*. The 1 m sample grid in trench *E* at a depth of 60 cm. The samples from the southeast part of trench *I* were taken at a depth of 130 cm, the samples from feature 17 at a depth of 90 cm.

7.9 Summary

The majority of sites were sampled during excavations in 2010 and 2011, when knowledge of the Nok Culture, the characteristics of Nok sites as well as the knowledge about adequate sampling strategies, especially grid size and extension, were limited. Thus, the selection of features and layers for pXRF analysis was restricted to a few sites, since sampling turned out to be insufficient in most cases.

However, excavations in 2016 at *Ifana 3*, *Kurmin Uwa 2D* and *Ido* provided sufficient material for the analysis of stone-pot-arrangements. Together with the samples from *Pangwari* and *Kurmin Uwa 2B*, a total of ten stone-pot-arrangements were available for pXRF analysis.

In the case of pit features, samples considered to be promising for pXRF analysis were found at *Ifana 1* and *2*, *Kurmin Uwa 1*, *Kusuma 1* and *Pangwari*, and covered more than a dozen features. The utilisation of adjusted sampling strategies, vertical sampling in particular, to enhance the analysis process was precluded when further excavations were ceased in 2017.

8 Statistics

8.1 Geochemical Data

8.1.1 Properties

Compositional Data

Most geochemical data are compositional data and standard statistics, including geostatistics, are not a suitable tool for the analysis of this data type. Compositional data, also called closed data, are by definition **data with non-negative values, which together sum up to a constant**[25] (Pawlowsky-Glahn *et al.* 2015: 8–9). Unlike the 'common' data of our daily life, compositional data do not operate in the unconstrained Euclidean space but in the constrained sample space called the simplex, S^D, where D equals the number of elements making up a composition (Aitchison 1982: 139; Pawlowsky-Glahn & Egozcue 2001; Pawlowsky-Glahn & Egozcue 2016: 30). Since the pXRF data in this thesis were measured in parts per million (ppm), they match these criteria. A sample where D = 20 consists of 20 elements with a constant sum of 10^6 parts and all measurement results are constrained to this sum.

The **constant-sum** is the key constraint of compositional data as calculations with these data in the real space, the Euclidean space, are not appropriate. This is based on the two key principles of compositional data: subcompositional coherence and scale invariance (Pawlowsky-Glahn *et al.* 2015: 12–15). Subcompositional coherence means that deduced inferences should be consistent, regardless of whether analysing subcompositions or the full set (Aitchison 1992: 376, 378; Aitchison & Greenacre 2002: 380). Scale invariance derives from the fact that compositions carry relative instead of absolute information (Aitchison 1981, 1982, 1983 and 1984, cited in Aitchison & Egozcue 2005: 830).

> *'To illustrate this assertion, consider the compositions [5, 65, 30], [10, 60, 30], [50, 20, 30], and [55, 15, 30]. Intuitively, we would say that the difference between [5, 65, 30] and [10, 60, 30] is not the same as the difference between [50, 20, 30] and [55, 15, 30]. The Euclidean distance between them is certainly the same, as there is a difference of 5 units both between the first and the second respective components. But in the first case, the proportion in the first component is doubled, while in the second case, the relative increase is about 10%. This relative difference seems more adequate to describe compositional variability.'*
>
> (Pawlowsky-Glahn *et al.* 2015: 23)

This means that 'any meaningful statement about a composition must be expressible in terms of ratios of components' (Aitchison 1992: 368).

[25] Historically defined they sum up to a constant, more recently compositional data have been defined as 'parts of a whole which only give relative information' (Filzmoser *et al.* 2009: 6100).

Spatial Dependency and Data Quality

Geochemical data are spatially dependent and the data values can include outliers as well as imprecise and missing values (Reimann & Filzmoser 2000: 1001; Filzmoser *et al.* 2009: 6107). Spatial dependency means that two samples close to each other show a higher similarity compared to samples at a greater distance. This dependency limits the choice of statistical approaches as many standard statistics require independent samples (Reimann *et al.* 2005: 3; Reimann *et al.* 2008: 2).

Imprecise and missing values have different reasons. First of all, sampling, sample preparation and analysis technique can cause errors (Reimann & Filzmoser 2000: 1001; Reimann *et al.* 2005: 3). When pXRF is employed as an analysis technique, missing or zero values can occur as the measured concentration of some elements lies below the limit of detection.

Data Distribution

Geochemical data are neither normally nor lognormally distributed and mostly skewed (Reimann & Filzmoser 2000: 1001–1003). A normal distribution of data is a requirement for many statistical analysis (e.g. correlation analysis, factor analysis, discriminant analysis) in order to achieve a reliable outcome (Reimann & Filzmoser 2000: 1001). Skewness can occur when data consist of different statistical populations (Reimann & Filzmoser 2000: 1013), i.e. different groups or clusters of data. The occurrence of more than one population within a dataset is not unusual for soil samples, since soil is influenced by numerous and complex processes, such as parent material, topography, vegetation, and many more (Reimann *et al.* 2005: 3).

A common treatment, especially recommended for right-skewed data, is the log-transformation using the base-10 logarithm. For strongly skewed distributions it is possible to use other tools such as Box-Cox transformations; a family of power transformations which lead to results closer to the normal distribution (Reimann *et al.* 2008: 169–172). In general, neither common transformations (such as logarithm) nor other methods will yield results with a normal distribution (Reimann & Filzmoser 2000: 1013–1014). This impedes the use of statistical approaches, that are based on a normal distribution, which includes most standard methods.

In case of pXRF data, however, tests of normal distribution are pointless as statements on the distribution are only valid for the Euclidean sample space. Compositional data operate in another sample space and thus it is not meaningful to analyse or transform the distribution of these data.

8.1.2 Consequences

Most classical statistics are based on the assumption that the real space endowed with the Euclidean space is the sample space of the performed experiment, but applying these methods to compositional data can result in biases or even nonsensical results (Pawlowsky-Glahn *et al.* 2015: 23–24).

Neglecting these unique properties of compositional data can lead to false results, of which the most dangerous ones are spurious correlations, which Pearson first highlighted at the end of the 19th century (Pearson 1896; Egozcue & Pawlowsky-Glahn 2011: 27).

Classical statistics operating in the Euclidean space include for instance calculations of the arithmetic mean and standard deviation, principal component analysis (Pawlowsky-Glahn *et al.* 2015: 23) and classical correlation analysis with XY plots (Reimann *et al.* 2012: 208).

Applying geostatistics to compositional data causes the same problems as applying classical statistics (Tolosana-Delgado *et al.* 2011: 74). This entails that analysis of single components, e.g. single element plots, hold no significance, as compositional data are never truly univariate data (McKinley *et al.* 2016: 17; Filzmoser *et al.* 2009: 6101; Egozcue & Pawlowsky-Glahn 2005: 796). According to the aforementioned knowledge gained by Aitchison (1981, 1982, 1983 and 1984), the **ratios between the elements hold the information.** Plotting single elements is meaningless when the information provided by the other elements is not taken into account:

> *'Thus no single variable is free to vary separately from the rest of the total composition. […] The relevant information for each single variable in a geochemical dataset thus lies in the ratios between all variables and not in the measured element concentrations as such. An interpretation and statistical evaluation of the observed concentration values is only meaningful if the relationship to the values of the remaining variables is taken into account.'*
>
> (Reimann *et al.* 2012: 196)

8.2 Choice of Methods

Objective

The selection of methods to apply depends both on the research question and the requirements for adequate treatment of the data. According to the research question (see chapter 4) the objective is to compare the elemental compositions of the samples to identify and interpret characteristic elemental signatures. Two different datasets exist: spatial data from Nok sites and groups of data from a Fulani village.

Spatial data from Nok sites enable the mapping of the different elemental compositions and thus the identification of differences between features, the surrounding soil and geogenic interferences. The analysis of the groups of data from the Fulani village aims to distinguish groups, i.e. different activity areas, based on their specific elemental signatures.

However, the use of standard statistics for differentiating groups of data, i.e. using multivariate analysis tools such as PCA or representing spatial data in single element plots, is not an adequate treatment of the obtained pXRF data (see chapter 8.1).

Adequate Treatment

In order to fulfil the objectives and to take into account the properties of the data, the following methods were chosen: multi-element mapping of log-ratio transformed data for the spatial data of Nok sites and clr-biplots for the comparison of the data obtained from the Fulani village.

Multi-element mapping (see chapter 8.3.1) aims to visualise the distribution of elements across the site by interpolating the data. In order to avoid violating the constraints of compositional data, two approaches were pursued: working with **isometric log-ratio transformations** (chapter 8.3.1.1) and the use of **enrichment factors** (chapter 8.3.1.2). Isometric log-ratio transformations enable the representation of the data on Cartesian coordinates, which makes it possible to proceed with standard statistics and to interpolate these coordinates on a map. This **principle of working on coordinates** is based on the representation of data on real orthogonal coordinates (Pawlowsky-Glahn & Egozcue 2001; Egozcue & Pawlowsky-Glahn 2011: 27; Mateu-Figueras *et al.* 2011). This allows the analysis of data with standard statistics and its interpretation as coordinates or back-transformed data to the original unit (Egozcue & Pawlowsky-Glahn 2011: 13; Mateu-Figueras *et al.* 2011). Enrichment factors deal with the ratios of the composition and avoid the constant sum constraint of compositional data (Carranza 2017: 411). The results of both approaches were visualised by mapping them with the interpolation method **inverse distance weighting** (chapter 8.3.1.3) to take into account the spatial character of the data and to eliminate outliers. The visualisation of the data with respect to their geographical position helps to find anomalies originating from e.g. archaeological features or geological interferences.

Clr-biplots (chapter 8.3.2) enable the distinction of groups of data from the Fulani village. In contrast to the Nok samples, these data do not contain spatial information but can be divided into groups (e.g. hearth or cowshed). By comparing these groups

in biplots of clr-transformed data the goal was to reveal different elemental signatures characteristic for each group.

The analysis of the results of sample preparation (see chapter 5.3) was done with exploratory data analysis tools for compositional data. The **total variance** (chapter 8.3.3) which is the equivalent of deviation for compositional data, was of special interest.

The calculations and transformations were executed in CoDaPack Version 2.02.21, a freeware developed by the 'Research Group in Statistics and Compositional Data Analysis at University of Girona' (Thió-Henestrosa & Martín-Fernández 2005; Comas & Thió-Henestrosa 2011; Thió-Henestrosa & Comas 2016). All calculations and graphics were carried out with CoDaPack, apart from the estimation of enrichment factors, calculated with Excel, and interpolations performed with QGIS (qgis.org and QGIS Project 2019).

8.3 Applied Methods

8.3.1 Multi-Element Mapping

8.3.1.1 Isometric Log-Ratio Transformation

As single element plots are not an adequate treatment of compositional data, isometric log-ratio (ilr) transformed data with their corresponding ilr-coordinates were plotted. Working with ilr-coordinates allows geostatistical approaches such as spatial analysis. Applying standard statistics on such ilr-coordinates is allowed for any sample space that has a Euclidean vector space structure if the coordinates are plotted with respect to an orthonormal basis. In case of the compositional data sample space, the simplex, it is possible to define a Euclidean vector space structure with an orthonormal basis.

Log-Ratio Transformations

In the 1980s, John Aitchison (1981, 1982, 1983, 1984 and 1986) realised that the information from compositional data lies in the ratios of components and that transforming them into log-ratios is useful (Aitchison & Egozcue 2005: 830). Nowadays three common types of transformations exist: additive log-ratio (alr), centred log-ratio (clr) and isometric log-ratio (ilr) (Egozcue *et al.* 2003: 279), of which Aitchison developed the additive and centred log-ratio transformations (Aitchison 1986, cited in Egozcue *et al.* 2003: 279). Working with log-ratios is, from a mathematical viewpoint, easier than dealing with ratios. Log-ratios are bijections and can be mapped one-to-one to the unconstrained real space, which is the principle for most standard statistical approaches (Aitchison & Egozcue 2005: 830–831; Egozcue *et al.* 2003: 299). However, both alr and clr have some disadvantages. The outcome of the alr-transformations depends on the chosen denominator. The transformation is asymmetric and the corresponding basis oblique. Clr-transformations result in a singular covariance matrix (Egozcue *et al.* 2003: 280; Bacon-Shone 2011: 6; Filzmoser & Hron 2011: 59), which can cause problems when applying standard statistics. The use of clr-transformations, however, is still recommended for clr-biplots (see chapter 8.3.2).

In the meantime, another approach called isometric log-ratio (ilr) was developed (Egozcue *et al.* 2003), which has some advantages compared to the other two (Bacon-Shone 2011: 6; Filzmoser *et al.* 2009: 6101). Working with isometric log-ratio transformed data is also known as the principle of working on coordinates, which in turn can be used for geostatistical and spatial analysis (Pawlowsky-Glahn & Egozcue 2016: 30, 32).

The Simplex and Working on Coordinates

The simplex S^D is the natural sample space of compositional data and is defined as

$$S^D = \{\mathbf{x} = (x_1, x_2, \dots, x_D): x_i > 0\ (i = 1, 2, \dots, \mathrm{D}), \sum_{i=1}^{D} x_i = k\}$$

with D-parts of the composition, expressed by the vector $\mathbf{x} = (x_1, x_2, \dots, x_D)$, of which all parts are positive numbers. The sum is denoted as the positive constant k (Aitchison 1982: 139; Mateu-Figueras *et al.* 2011: 33; Pawlowsky-Glahn *et al.* 2015: 10). In the case of the pXRF results, the constant sum is 10^6 (as measured in parts per million).

However, the sample space for standard statistics is not the simplex but the real space with its particular algebraic-geometric structure, known as the Euclidean geometry (Mateu-Figueras *et al.* 2011: 31–32). The simplex S^D has an algebraic-geometric structure different from the real space as it is a (D-1)-dimensional subset of a D-dimensional real space (Mateu-Figueras *et al.* 2011: 32–34). In consequence, the use of standard statistics is not adequate (Mateu-Figueras *et al.* 2011: 32, 40).

Although the simplex is different to the real space with its Euclidean geometry, an Euclidean vector space structure of the simplex exists, called *Aitchison geometry* (Pawlowsky-Glahn & Egozcue 2001; Mateu-Figueras *et al.* 2011). The angles and distances of the Aitchison geometry correspond to the angles and distances of the real space (Egozcue *et al.* 2003: 281). This is of great importance as linear algebra allows the safe application of standard statistics in any sample space other than the real space that has a Euclidean vector space structure, if the coordinates are considered with respect to an orthonormal basis (Mateu-Figueras *et al.* 2011: 33). This principle of working on coordinates means that it is possible to apply standard statistics to orthonormal coordinates and, if necessary, return to the simplex (Mateu-Figueras *et al.* 2011: 33, 35, 41). A tool to design such an orthonormal basis for ilr transformation is sequential binary partitioning. Using that, both intra-group and inter-group analysis can be performed (Egozcue & Pawlowsky-Glahn 2005: 823; Mateu-Figueras *et al.* 2011: 35).

Sequential Binary Partitioning

Sequential binary partitioning (SBP), also known as *balances*[26], is a tool to create an orthonormal basis for isometric log-ratio transformations, where the D-parts of the compositions are divided in order to build D-1 ilr-coordinates (Egozcue & Pawlowsky-Glahn 2011: 22).

As explained for the simplex, compositional data with D-parts are vectors with D strictly positive real components with $\mathbf{x} = (x_1, x_2, x_3, \ldots, x_D)$ (Egozcue & Pawlowsky-Glahn 2005: 795; Mateu-Figueras *et al.* 2011: 33). The process of SBP divides these vectors into groups. First, all parts are divided into two groups, marked with (+1, -1), and then sequentially into sub-groups of these two initial groups (see Fig. 8-2) (Egozcue & Pawlowsky-Glahn 2005: 800). By doing so, it is possible to analyse both the relationship between groups and within groups (inter- vs. intra-group) (Egozcue & Pawlowsky-Glahn 2005: 796).

The choice of balances depends on the research question and how to interpret the transformed data. One option is to refer to expert knowledge (Pawlowsky-Glahn & Egozcue 2011: 110) or orient towards affinities, such as minor vs. major elements (Egozcue & Pawlowsky-Glahn 2005: 796). When no relevant criteria exist, exploratory tools help to choose a SBP, namely *variation array* and *clr-biplots* (see chapter 8.3.2) (Pawlowsky-Glahn & Egozcue 2011: 110).

A combination of all three options was chosen for this thesis, with a focus on discovering affinities by examining single element plots together with exploratory tools. Single element plots turned out to be the most successful, although their use can cause biases (see chapter 8.1). However, single element plots were not used to interpret the distribution but to

[26] Not to be confused with the balance value provided by the pXRF device, which sums up all elements that are not quantifiable.

visualize the general influence of the elements. Univariate data analysis can help to gain a deeper understanding of the data before applying multivariate approaches (Reimann *et al.* 2012: 197). This information was processed together with the information obtained by the variation array and clr-biplot in order to adjust the balances.

Example of a Nok Site

At *Ido*, geogenic interferences were accidentally identified during the search for enrichments in P, which are diagnostic of graves (Schmidt 2016). Enrichments in P turned out to be a result of weathered stone material and appeared together with enrichments in Ca, Sr and Mn as well as depletions in K and Rb. This example shows that single element plots can be misleading without considering the other elements: the supposed enrichment of P is not due to the remains of a body but due to geogenic interferences. In order to **illustrate a meaningful mapping of elements and their interpretation**, ilr-coordinates with their balances were plotted.

The ilr-transformation with SBP was conducted in CoDaPack (Thió-Henestrosa & Martín-Fernández 2005; Comas & Thió-Henestrosa 2011; Thió-Henestrosa & Comas 2016) with a manually defined SBP (Thió-Henestrosa & Comas 2016: 9, 10).

The groups are sequentially divided by choosing either '+1' or '-1', starting with all elements until each sub-group ends with two opposed elements. The chosen SBP (Fig. 8-1) of 18 elements resulted in 17 ilr-coordinates. Each ilr-coordinate provides information for each sample point, given as a balance value. It is possible to visualise a coordinate and its balance values for all sample points by interpolating them; the ilr-1 and ilr-5 coordinates were plotted (Fig. 8-2). For the interpolation method see chapter 8.3.1.3.

P	Mn	Sr	Ca	K	Rb	Si	Ti	Al	Fe	V	Cr	Zn	Y	Zr	Nb	Ba	Pb	ilr
+1	**+1**	**+1**	**+1**	-1	-1	-1	-1	-1	-1	-1	-1	-1	-1	-1	-1	-1	-1	**1**
+1	**+1**	-1	-1															**2**
+1	-1																	**3**
		+1	-1															**4**
				+1	**+1**	-1	-1	-1	-1	-1	-1	-1	-1	-1	-1	-1	-1	**5**
				+1	-1													**6**
						+1	-1	-1	-1	-1	-1	-1	-1	-1	-1	-1	-1	**7**
							+1	-1	-1	-1	-1	-1	-1	-1	-1	-1	-1	**8**
								+1	-1	-1	-1	-1	-1	-1	-1	-1	-1	**9**
									+1	-1	-1	-1	-1	-1	-1	-1	-1	**10**
										+1	-1	-1	-1	-1	-1	-1	-1	**11**
											+1	-1	-1	-1	-1	-1	-1	**12**
												+1	-1	-1	-1	-1	-1	**13**
													+1	-1	-1	-1	-1	**14**
														+1	-1	-1	-1	**15**
															+1	-1	-1	**16**
																+1	-1	**17**

Fig. 8-1: SBP of the data from *Ido 2016* (Planum A) with 18 determined elements resulting in 17 ilr-coordinates. Some elements were omitted due to lack of relevance or impreciseness. All elements are separated into groups, with one group (**+1**) opposed to the other (-1). Empty fields indicate that these elements are not involved in the balance of the coordinate. Grey rows are referred to in the text and plots.

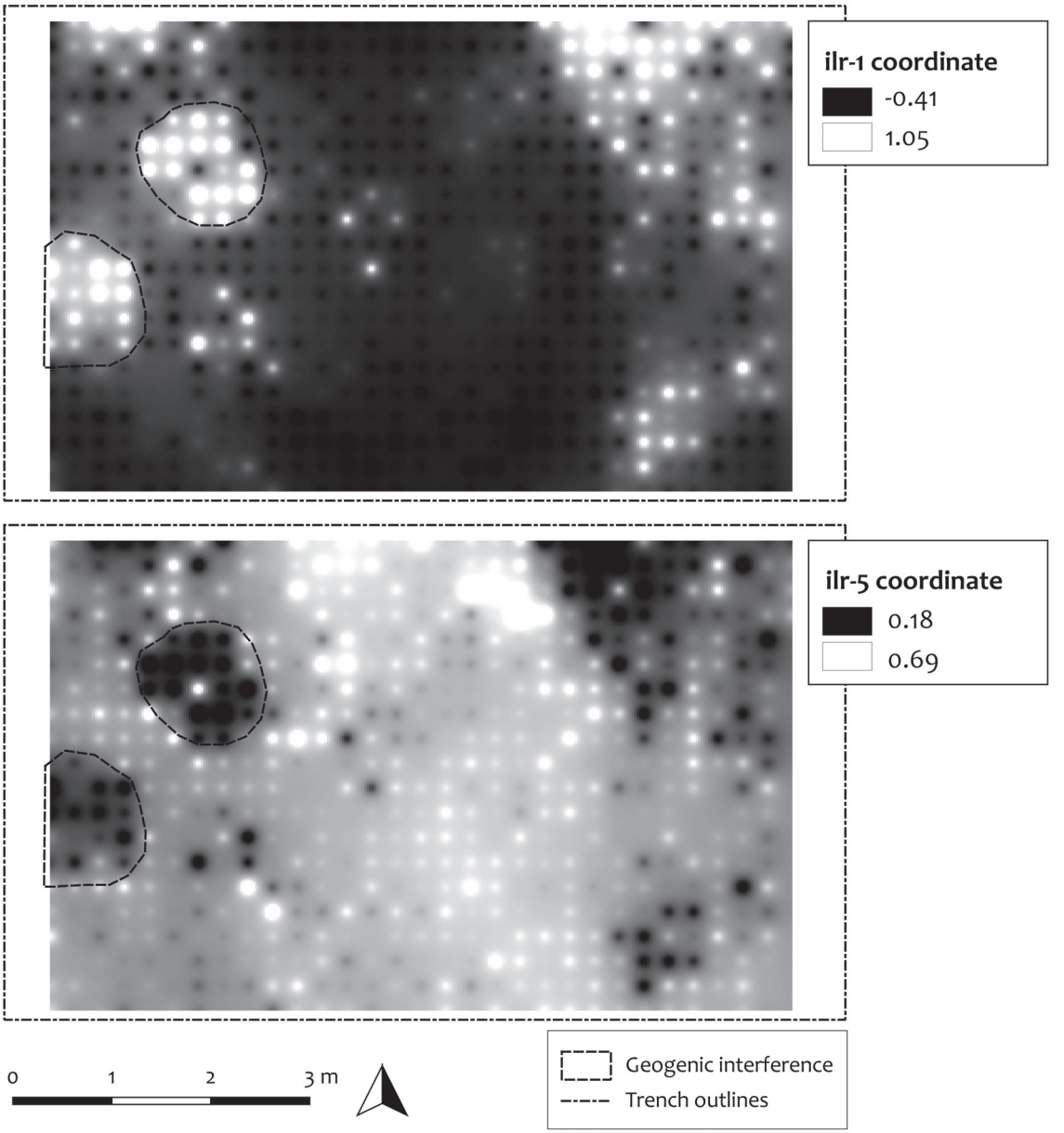

Fig. 8-2: Interpolation of ilr-1 and ilr-5 coordinates. The geogenic interference is visualized by the higher values of the first coordinate and lower values of the fifth coordinate, respectively.

The range of values in the plots is represented from low to high (black to white). A balance value close to zero represents a similar abundance of all elements in this sample (for those elements involved in the balance). If the balance value is highly negative, it indicates that the opposed elements (-1) of the coordinate, the elements in the denominator, are dominant compared to those in the numerator (+1). If the balance value is highly positive, there is a relatively high abundance of the selected elements (+1) (the elements in the numerator), compared to those in the denominator (-1) (Egozcue & Pawlowsky-Glahn 2005; McKinley & Lloyd 2011: 298–299).

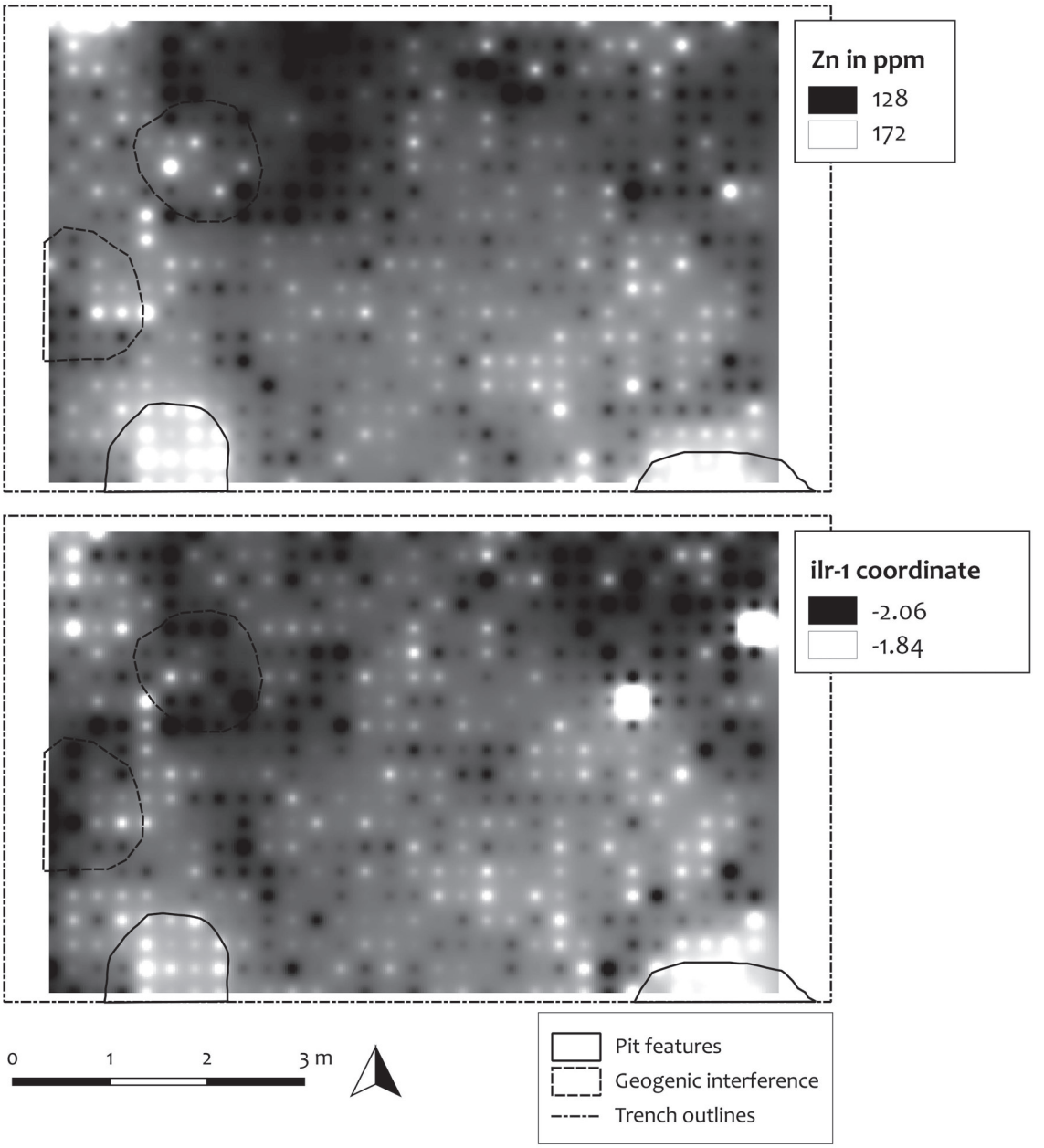

Fig. 8-3: Interpolation of Zn as a single element and the ilr-1 coordinate with Zn opposed to the other elements. Both show higher values within the two pit features, although only in the case of the ilr-coordinate artefacts can be ruled out.

The interpolation of the ilr-1 coordinate shows that the elements P, Ca, Sr, and Mn (+1) are more dominant within the geogenic structure than the remaining 14 elements (-1). The coordinate ilr-5 shows that the elements K and Rb (+1) are less abundant compared to the remaining 12 elements (-1) within the geogenic structure.

Furthermore, the same pattern appears in the upper right and lower right corner. Reviewing the sample material and documentation revealed more traces of weathered

stone in these areas. This proves the use of balance settings for the identification of undetected patterns.

In order to **illustrate the differences between univariate element plots and plots of ilr-transformed data**, both methods are compared (Fig. 8-3). Zn concentration, given in ppm, is visualised in a univariate plot with no other elements taken into account. The balance of the ilr-1 coordinate in Fig. 8-3, however, was adjusted so that the ilr-coordinate is composed of Zn (+1) against all other elements (-1).

In the case of the ilr-1 coordinate all balance values are below zero, which means that the other elements (-1) are more dominant than Zn (+1). However, within the pits the abundance of Zn rises. The enrichment of Zn in the univariate plot appears stronger than the Zn enrichment in the ilr-1 coordinate. However, only the plot of the transformed data can be considered to be a reliable result as it eliminates artefacts. Especially when analysing the stone-pot-arrangements, the use of SBP and ilr-coordinates becomes significant. Although 'only' P and Ca are the elements of interest, single element plots can be erroneous. By using balances, other elements are taken into account leading to a more reliable result.

Ilr-coordinates with their balances, in contrast to raw data, respect the conditions of compositional data. Even when the balance is set to one element (e.g. Zn) against all other elements, the selected element (Zn) is not observed in isolation as is the case in single element plots. Consequently, the interpretation of ilr-coordinates refers to element combinations rather than single elements. Although or *because* it impedes visualisation of single elements isolated from the others, it is the most adequate representation of compositional data.

It is not possible to determine which elements are truly enriched or depleted and which elements are affected by the enrichment or depletion of the other elements (see chapter 8.4). However, the obtained SBP settings are helpful. For example, chosen balances for e.g. geogenic interferences can be applied to other datasets to identify further potential areas of geogenic interferences, regardless of the origin of the enrichments or depletions.

8.3.1.2 Enrichment Factors

A second option for dealing with compositional data is to work with enrichment factors (EF). EFs are not a solution for the 'closed' data problem per se, as the constant-sum constraint is not solved but circumvented by working with ratios rather than log-ratios or the elements' single values (Carranza 2017: 411). Enrichment factors were introduced by Chester & Stoner (1973: 28) in a paper on lead concentrations in particulates. The basic formula was published by Zoller *et al.* 1974 when analysing the origin of trace metals in the atmosphere at the South Pole. The ratios of the element of interest (x) with the reference element (Al) for both the atmosphere (air) and crust ($crust$) were compared:

$$\text{EF } crust = \frac{\left(\frac{\text{X}}{\text{Al}}\right)air}{\left(\frac{\text{X}}{\text{Al}}\right)crust}$$

(Zoller *et al.* 1974: 199)

The study aimed to reveal the origin of the trace metals by comparing the ratios of the atmosphere to the crust as well as the atmosphere to the ocean, respectively (Zoller *et al.* 1974: 189–199). The initial use of EFs for the atmosphere extended to terrestrial analysis (Reimann & Caritat 2005: 105), where soil samples can be compared with the Natural Background Concentration (NBC) of the soil.

'The geochemical or natural background is a relative measure to distinguish between natural element or compound concentrations and anthropogenically-influenced concentrations in real sample collectives.'

(Matschullat *et al.* 2000: 991)

However, the NBC has to be estimated individually for each context and its calculation is not clearly defined; for a discussion of this see Matschullat *et al.* 2000. The main problem of this is the lack of a clear definition for the NBC; it basically means 'absence of anomaly' (Matschullat *et al.* 2000: 990).

Application in Archaeology

In the course of time, the method was applied in archaeological studies as well (see e.g. Entwistle *et al.* 1998, Oonk *et al.* 2009 and Hafez *et al.* 2017). Since the calculation of the NBC remains undefined, different methods to calculate the enrichment factor have emerged. Basic approaches compare on-site data to the mean value of the control samples, without the use of reference elements (Entwistle *et al.* 1998: 57).

The method chosen for this thesis is based on the more complex approach by Hafez *et al.* 2017. The formula for the EF is the same as expressed by Zoller *et al.* (1974: 199) but instead of comparing the ratios of atmosphere and crust, the ratios of archaeological samples and the NBC are compared (Hafez *et al.* 2017: 454). The unique feature of this approach, however, is the estimation of the NBC by calculating the *median + 2*MAD* (MAD denotes the median absolute deviation). Outliers, which are defined as values below *Q1 - 1.5 *IQR* and above *Q3 + 1.5*IQR* – where IQR denotes the interquartile range (Hafez *et al.* 2017: 450), are removed from the calculation, based on the approach developed by Reimann *et al.* (2005) and Rothwell & Cooke (2015).

Example of a Nok Site

For the site of *Kusuma 1* the enrichment factor for Zn was calculated using different reference elements.

The chosen samples for calculating the NBC were on-site, but outside of features (Fig. 8-4), from an area with a low find concentration (red square). Furthermore, no geogenic structures interfered with the samples, unlike in other areas (blue squares). The calculation of the NBC, including the removal of outliers, and the estimation of the EFs were executed according to Hafez *et al.* (2017).

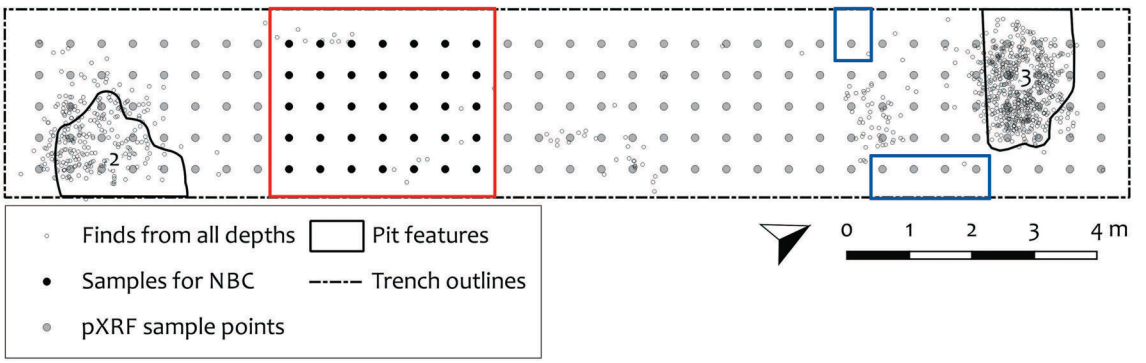

Fig. 8-4: The site *Kusuma 1* with all finds and features from all depths and the sampling points at a depth of 60 cm. The black dots within the red square are the samples used for calculating the NBC in an area without features; at that depth the area was also almost void of finds. The blue squares indicate the location of geogenic interferences.

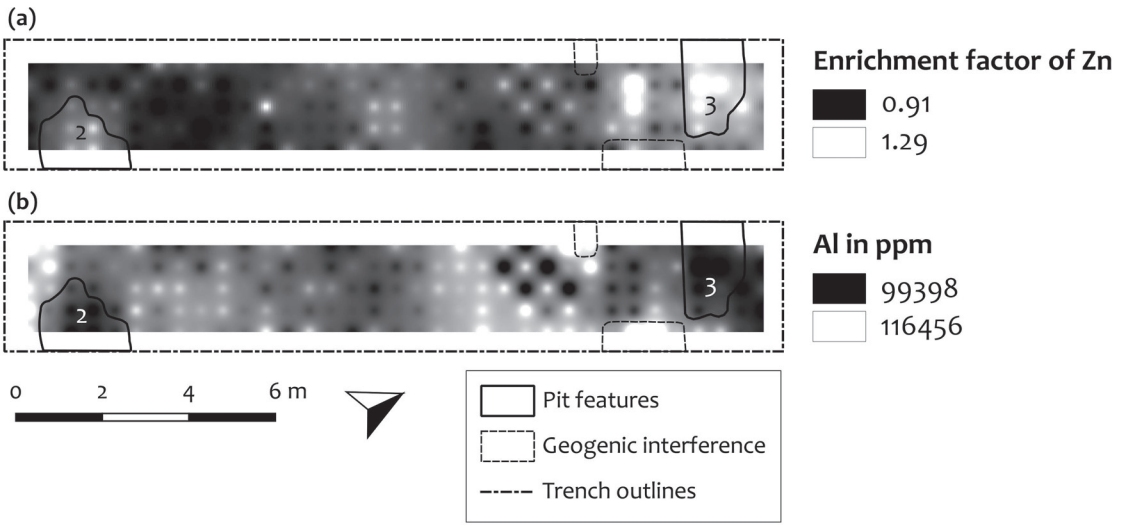

Fig. 8-5: Comparison of the calculated enrichment factor of Zn with Al as the reference element (a) and the single element plot of Al (b). Low values of Al within pits can cause artifical enrichments of Zn.

Fig. 8-5 (a) shows the interpolated EFs of Zn with Al as the reference element. Higher values of the EFs are concentrated within the pit features in the north and south corner. However, the single element plot of Al (Fig. 8-5 b) reveals lower Al values within the pit features compared to the surroundings. As Al is the denominator of the EF formula, the increase of Zn values can be caused by the decrease of Al values. With Al as a reference element it is therefore not possible to judge whether the enrichment of Zn is real or caused by the depletion of Al (see also chapter 8.4).

Other elements as reference elements were also tested and interpolated. Depending on the chosen reference element, the enrichment patterns differ (Tab. 8-1).

Enrichment of Zn	Reference element
Enrichment in pits	Al, Fe, Cr, Y
Enrichment within geogenic structures	Si, Ti, K, Rb, Sr, Nb, Ca, Cl
Enrichment in both	Zr
No enrichments	Mn, V, Ba, Pb

Tab. 8-1: Outcome of Zn distribution patterns using different reference elements.

Apart from the apparent arbitrariness of the outcomes, a closer look has revealed that all enrichments of Zn can be caused by the values of the denominators rather than the element of Zn itself.

Failure of the Method

The example at *Kusuma 1* has shown the hazards of using enrichment factors. Two issues are responsible for this: the choice of the reference element and the calculation of the NBC. The main problem, however, is caused by the inherent properties of compositional data.

A reference element should be stable and not affected by processes such as weathering (Reimann & Caritat 2005: 94). Recommended elements are Al, Fe, Mn, Ti, Sr, or Zr (Hafez *et al.* 2017: 454). In the case of *Kusuma 1*, however, none of these elements has proven stable enough for the analysis. Furthermore, this method has shortcomings for element values below the limit of detection, such as P.

The calculation of the NBC has proven difficult as there is no common definition for it (Matschullat *et al.* 2000: 990). The NBC always depends on the location and its properties; it is also spatially limited as the calculation depends on the used scale (Reimann & Garrett 2005: 24–25; Matschullat *et al.* 2000: 991, 998). The main challenge of the estimation of the NBC is to find homogeneous material undisturbed from both anthropogenic and geogenic influences (Matschullat *et al.* 2000: 991–992).

Although enrichment factors avoid the constant sum constraint of compositional data, their use is affected by the properties of compositional data: it is impossible to determine whether enrichments of a single element are absolute or due to the decreased value of the reference element. As the aim of EFs is to reveal the enrichment of a specific element (e.g. Zn) their application is useless. Furthermore, the calculation of the NBC is not coherent to the restrictions of compositional data (see chapter 8.1.1).

8.3.1.3 Interpolation Methods

As all Nok samples contain spatial information, it is possible to map the results of the ilr-transformations and the calculated enrichment factors with respect to their location on the site. This provides the advantage that further information, such as find density etc. can be taken into account during interpretation.

Interpolation, in contrast to simple representation methods (e.g. differentiation of values by point sizes), extrapolates outliers and missing values. It also allows the differentiation between features and the surrounding soil without precise location of the feature outlines. Regarding the stone-pot-arrangements, no outlines are visible at all (with the exception of the site *KU 2D*), thus the distinction between inside and outside the feature is not possible. Feature outlines of pits exist but often appear blurred and fuzzy; due to e.g. leaching processes it is impossible to determine distinct outlines of the pit. Furthermore, visual representation enables the identification of undetected anomalies, both of anthropogenic and geogenic origin.

Inverse Distance Weighting

Spatial interpolation methods are used to estimate the values at unsampled points by using data from sampled points (Li & Heap 2011: 229). The most common interpolation methods are kriging and inverse distance weighting (IDW). The main advantage of kriging as a geostatistical method compared to non-geostatistical methods is that it provides information on the accuracy of the method (Li & Heap 2011: 240; Reimann *et al.* 2008: 76). Non-statistical methods comprise approaches such as simple point representations to distinguish the different sample values (see Fig. 8-6a). With regards to the compositional character of the data, the most state-of-the-art method is co-kriging (Tolosana-Delgado *et al.* 2011: 76; Pawlowsky-Glahn & Egozcue 2016: 31).

The choice of interpolation method depends, among many others, on factors such as sample density and quality (Li & Heap 2011: 229). The preference for inverse distance weighting (Fig. 8-6b) as the chosen interpolation method is based on the research

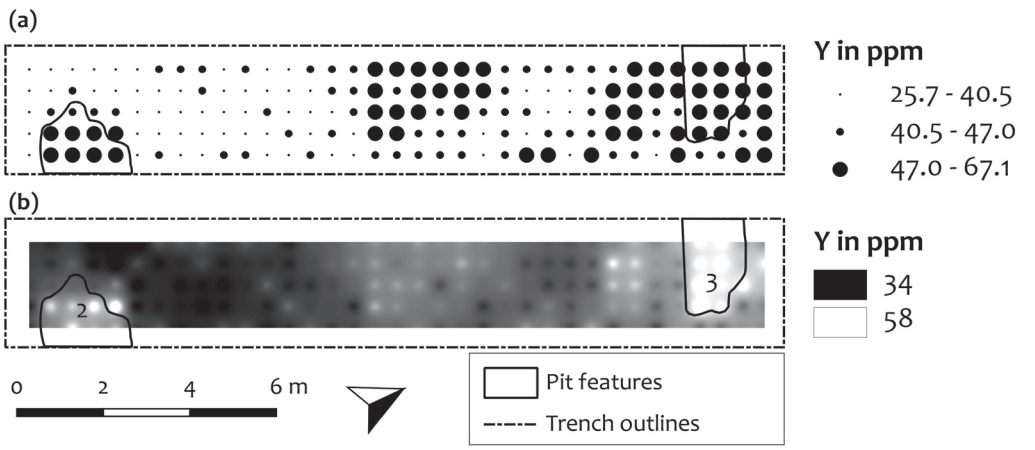

Fig. 8-6: Comparison of representation methods of yttrium for the site *Kusuma 1*. (a) Simple point representation of the data values with different point sizes. The size categories refer to the representation option 'quantiles'. (b) Interpolated data with inverse distance weighting with cumulative pixel count cut from 2.0% – 98.0%.

question. Although co-kriging is more precise, the use of IDW was sufficient to fulfil the objectives. However, employing co-kriging is recommended, especially when the focus is on potential mapping such as in geochemical surveys (Tolosana-Delgado & van den Boogaart 2013).

IDW was also preferred to plain point representations (see Fig. 8-6a). By using IDW the data points are interpolated with a simple formula, enabling a better representation. By weighting the data points, the influence of one point declines towards other points with increasing distance. The method yields the best results when applied to a set of evenly distributed data points (QGIS Project 2019: 435). The interpolation was conducted with QGIS (see qgis.org and QGIS Project 2019) by using the command 'Raster – Interpolation – IDW'. Data values are represented from 'black to white' with extreme values set to 'cumulative pixel count cut 2.0% – 98.0%', which produced the clearest visualisation (QGIS Project 2019: 67, 434–435).

8.3.2 Biplots of Categories

The samples obtained from the Fulani Village are different from the samples taken from Nok sites, since they are not spatially related and were chosen to be representative of a certain category, e.g. from off-site, on-site or hearths. Thus, these samples are assigned to groups. One way to identify differences between groups is to use e.g. principal component analysis (PCA). In case of compositional data, however, classical statistics such as PCA can be misleading and erroneous (see chapter 8.1.1). A proper treatment of compositional data is the use of clr-biplots, which is obtained as a PCA based on the clr of the parts of the composition. An additional tool for the interpretation and distinction of groups is the variation array**.**

Clr-Biplots

Biplots are a method to summarize and display multivariate data sets, where rows can be displayed as individuals and columns as variables (Aitchison & Greenacre 2002: 377). For a proper treatment of compositional data, the biplots consist of log-ratio transformed data. Although ilr-transformations are, in general, preferred to alr- or clr-transformations (see chapter 8.3.1.1), their interpretation within biplots is complex (Aitchison & Greenacre 2002; Egozcue & Pawlowsky-Glahn 2011: 25). The use of clr-transformed data in biplots is the most recommended procedure as it makes it possible to obtain information about simple log-ratios (Aitchison & Greenacre 2002; Filzmoser & Hron 2011: 59).

A biplot is based on the singular value decomposition (SVD) of the rows and columns of the centred log-ratio matrix. The matrix displays which log-ratio combinations contain large or small variabilities (Bacon-Shone 2011: 7). Clr-biplots of the SVD are a projection of the two first principal components, which are orthonormal, together with the centred clr variables as rays (Egozcue & Pawlowsky-Glahn 2011: 24). This means the clr log-ratio coefficients in the first two PCs of the data points are shown together with the centred clr variables in one plot. This enables an insight into the relationship between the elements (Martín-Fernández *et al.* 2015: 185), which is comprehensively explained in Aitchison & Greenacre 2002. The PCs obtained from the SVD of the centred log-ratio matrix are by construction isometric log-ratio coordinates, although not balances, as they involve all parts of the composition.

Interpretation of Clr-Biplots

Two kinds of clr-biplots exist; the form biplot and covariance biplot. Form biplots represent rows in principal co-ordinates and columns in standard co-ordinates; covariance biplots represent rows in standard co-ordinates and columns in principal co-ordinates. Form biplots favour the display of the individuals, covariance biplots favour the display of the variables (Aitchison & Greenacre 2002: 378).

When analysing differences between points, i.e. samples of a group, the use of form biplots is sensible as the distances of the rows (= samples) are approximations, displayed as distances between the individual points on the biplots (Aitchison & Greenacre 2002: 382). In both biplots variables are represented by rays and both their length and direction are of interest (Aitchison & Greenacre 2002: 378; Egozcue & Pawlowsky-Glahn 2011: 24). For example, close vertices of the rays suggest higher proportionality of elements (Martín-Fernández *et al.* 2015: 186) and rays lying perpendicularly to other rays suggest a near zero proportionality (Aitchison & Greenacre 2002: 383). Especially the link between the (vertices of the) rays are more significant than the rays themselves (Aitchison & Greenacre 2002: 388). Care is needed to verify if the relationships derived from the plots are statistically significant or an artefact of the projection. The higher the proportion of variance explained by a biplot, the more confident one can be in those relationships. The use of variation arrays can help to further verify the relationship.

Variation Array

A variation array is an additional tool for data interpretation, especially in combination with the clr-biplot, which helps to understand the proportions of the elements in the sample (Martín-Fernández *et al.* 2015: 185).

The variation array presents estimations of centre and variability (see Fig. 8-8) and provides information on two corresponding elements: the lower triangle of the variation array comprises the sample mean value of simple log-ratios, the upper triangle shows the sample variances of the same log-ratios. Small variance values represent a high proportionality and low values represent low proportionality, respectively (Egozcue & Pawlowsky-Glahn 2011: 23).

Example of the Fulani Village

To illustrate the use and interpretation of clr-biplots and variation arrays for the comparison of different activity areas in the Fulani village, the groups 'off-site', 'on-site' and 'hearth' were analysed (Fig. 8-7). Off-site samples were taken in close proximity to the camp, but outside the village itself. On-site samples represent the village surface from areas without a specific use. The hearth samples originate from inside the fireplace (encircled samples) and adjacent to the fireplace.

The clr-biplot indicates a differentiation between the elemental compositions of all groups, mainly of the hearth samples. Especially the log-ratios of P and Ca versus Fe and Si discriminate all groups quite well. The samples from inside the hearths are more influenced by the log-ratios of P and Ca as well as Ba, V and Sr. The output of the upper triangle in the variation array (Fig. 8-8) shows the highest variances for P, Ca and Sr and, consequently, the absence of proportionality to other elements, expressed by a high number (red fields).

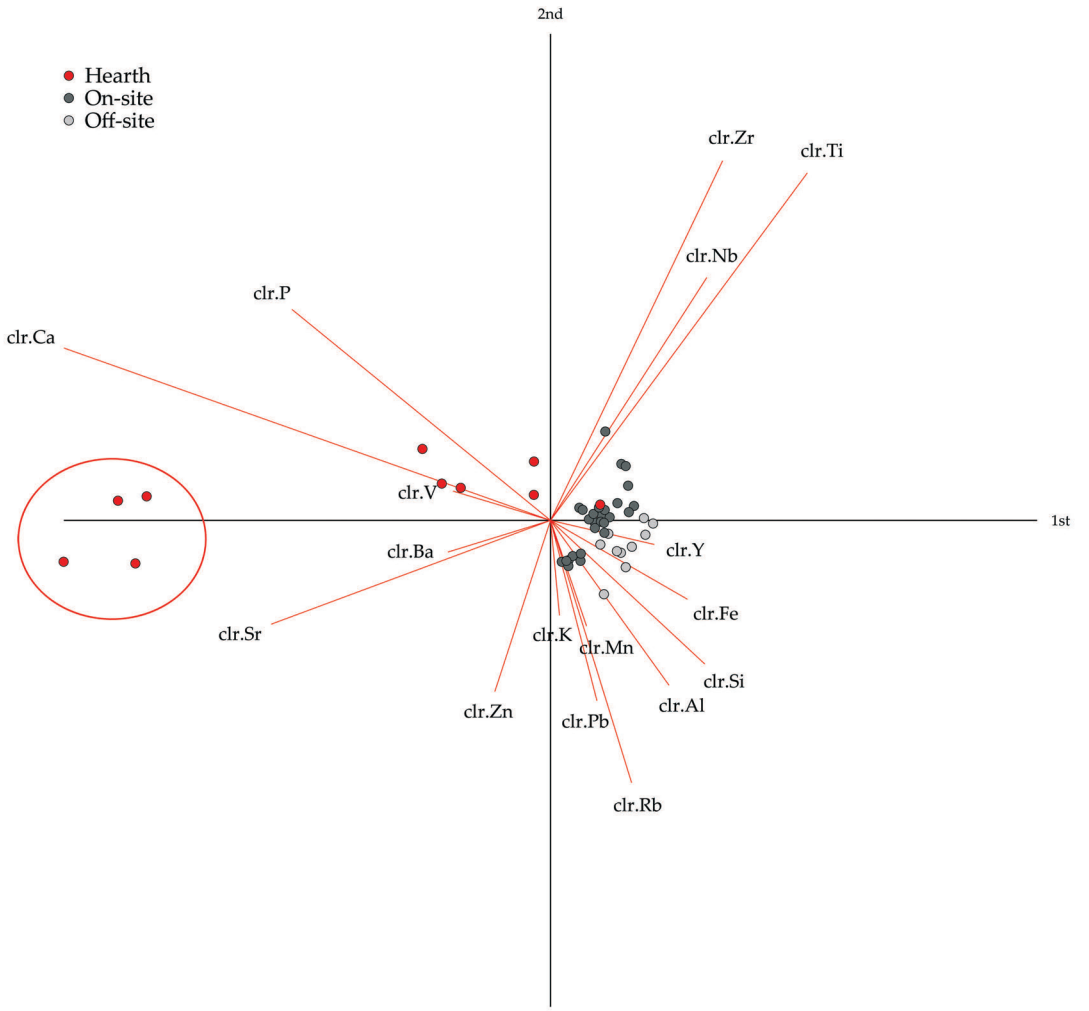

Fig. 8-7: A form biplot of selected elements as clr-transformed data with the first and second axis shown. Displayed are hearth samples (= red) taken from a modern Fulani village with reference samples from both on-site (= dark grey) and off-site (= light grey). The red circle comprises the hearth samples taken from inside the fireplace.

The lack of proportionality between P, Ca and Sr and other elements is also indicated by the fact that their rays are furthest from the others (Fig. 8-7).

Off-site and on-site samples are more influenced by the log-ratios of Fe and Si as well as Al and Y. The high proportion of these elements is also expressed by the smaller variance values of the corresponding elements (blue fields in Fig. 8-8). The influence of these elements on off-site samples appears higher than on the on-site samples.

Furthermore, the hearth samples taken from the soil adjacent to the fireplace are closer to the off- and on-site samples than the samples taken from the middle of the hearth. One of the adjacent hearth samples is even among the on-site samples. This emphasises the success of the applied method as such a result was expected.

Variation array:

Variance ln(Xi/Xj)

Xi\Xj	Si	Ti	Al	Fe	Mn	K	V	Zn	Rb	Sr	Y	Zr	Nb	Ba	Pb	Ca	P	clr variances
Si		0.1256	0.0449	0.0529	0.0727	0.1032	0.2967	0.2172	0.0525	0.7238	0.0428	0.0782	0.0510	0.2760	0.0584	1.5982	0.6830	0.1135
Ti	-2.8671		0.1376	0.1043	0.2405	0.3071	0.5206	0.4485	0.2037	1.1362	0.1338	0.0513	0.0601	0.5431	0.2478	2.0963	1.0187	0.2839
Al	-1.3576	1.5095		0.0065	0.0376	0.0818	0.2055	0.1306	0.0110	0.6107	0.0165	0.0883	0.0544	0.2195	0.0421	1.4080	0.5854	0.0666
Fe	-1.6116	1.2555	-0.2540		0.0571	0.1024	0.2294	0.1554	0.0272	0.6744	0.0234	0.0692	0.0423	0.2520	0.0636	1.4870	0.6330	0.0842
Mn	-5.3649	-2.4979	-4.0074	-3.7534		0.0246	0.0906	0.0493	0.0216	0.3781	0.0251	0.1240	0.0878	0.0891	0.0171	1.0625	0.3561	0.0109
K	-2.4585	0.4086	-1.1009	-0.8469	2.9065		0.0700	0.0614	0.0473	0.3268	0.0571	0.1581	0.1188	0.0549	0.0243	0.9760	0.3067	0.0160
V	-7.5982	-4.7311	-6.2406	-5.9866	-2.2332	-5.1397		0.0326	0.1596	0.1472	0.1721	0.3132	0.2693	0.0181	0.1201	0.6092	0.1311	0.0492
Zn	-7.7145	-4.8475	-6.3569	-6.1029	-2.3496	-5.2561	-0.1163		0.0939	0.2111	0.1198	0.2756	0.2257	0.0435	0.0792	0.7569	0.2100	0.0331
Rb	-7.9853	-5.1182	-6.6277	-6.3737	-2.6203	-5.5268	-0.3871	-0.2707		0.5031	0.0203	0.1273	0.0850	0.1609	0.0209	1.2628	0.4961	0.0438
Sr	-7.4030	-4.5360	-6.0455	-5.7915	-2.0381	-4.9446	0.1952	0.3115	0.5822		0.5587	0.8207	0.7468	0.1284	0.4151	0.1998	0.0308	0.2979
Y	-8.4877	-5.6207	-7.1301	-6.8762	-3.1228	-6.0293	-0.8895	-0.7732	-0.5025	-1.0847		0.0586	0.0353	0.1796	0.0374	1.3381	0.5149	0.0462
Zr	-3.8545	-0.9874	-2.4969	-2.2429	1.5105	-1.3960	3.7437	3.8601	4.1308	3.5486	4.6333		0.0067	0.3286	0.1358	1.6644	0.7129	0.1450
Nb	-8.1591	-5.2921	-6.8015	-6.5475	-2.7942	-5.7007	-0.5609	-0.4446	-0.1739	-0.7561	0.3286	-4.3047		0.2816	0.0948	1.5714	0.6573	0.1082
Ba	-5.6305	-2.7635	-4.2729	-4.0189	-0.2656	-3.1721	1.9677	2.0840	2.3547	1.7725	2.8572	-1.7761	2.5286		0.1089	0.6028	0.1203	0.0505
Pb	-9.2168	-6.3497	-7.8592	-7.6052	-3.8518	-6.7583	-1.6186	-1.5022	-1.2315	-1.8137	-0.7290	-5.3623	-1.0577	-3.5863		1.1170	0.3959	0.0253
Ca	-3.3393	-0.4722	-1.9817	-1.7277	2.0257	-0.8808	4.2589	4.3753	4.6460	4.0638	5.1485	0.5152	4.8199	2.2913	5.8775		0.2250	0.9075
P	-5.0919	-2.2249	-3.7343	-3.4803	0.2730	-2.6335	2.5063	2.6226	2.8933	2.3111	3.3958	-1.2375	3.0672	0.5386	4.1249	-1.7527		0.2664

Mean ln(Xi/Xj)

Fig. 8-8: Screenshot of the variation array of the elements. The lower triangle shows the mean of simple log-ratios, the upper triangle the sample variance of the same log-ratios. Blue fields represent small numbers, thus high proportions of the elements. Red fields represent high numbers, thus low proportions of the elements.

The cumulative proportion explained (Aitchison & Greenacre 2002: 383; Comas & Thió-Henestrosa 2011: 7) has a value of 0.9404 (obtained from the numerical output of the principal components). This means that the first and second principal components together account for 94.04% of the total variance, which means that the data are well represented (Thió-Henestrosa & Daunis-i-Estadella 2011: 334–335).

The data obtained from the Fulani village are fundamentally different from the Nok samples. The activity areas of the village can be separated into distinct groups, e.g. hearth samples vs. off-site samples. This favours the application of clr-biplots. The use of clr-biplots in combination with the variation array has proven to be the best method to find differences in the elemental composition of activity areas (for results see chapter 9.3).

The objective of the analysis of the village is to provide a reference and a basis for interpretation of the Nok samples. However, a simple transfer of the results obtained from the clr-biplot onto Nok data is not meaningful as the origin of elements can be different (see chapter 8.4). Nevertheless, the results of the Fulani data show tendencies and offer possibilities for interpretations, especially in combination with other available data (e.g. knowledge from the literature or pH values).

The analyses were performed in CoDaPack (Thió-Henestrosa & Comas 2016: 27).

8.3.3 Total Variance

The restrictions of compositional data also affect exploratory data analysis. Estimations of the mean or standard deviation are only meaningful for data operating in the Euclidian space, whereas compositional data operate in the simplex. Thus, standard descriptive statistics are not a proper tool for describing compositional data and can be misleading when applied on an inappropriate geometry (Pawlowsky-Glahn *et al.* 2015: 66; Filzmoser *et al.* 2009: 6108).

The equivalent of the mean and standard deviation for compositional data are the *centre* and the *total variance* (Pawlowsky-Glahn *et al.* 2015: 66). A higher *total variance* represents a higher dispersion of the samples around the *centre*, thus a higher deviation. It is a unitless number and enables statements about the stability or homogeneity of the measurements (Filzmoser *et al.* 2009: 6105–6106, 6108).

These statements are especially of interest for the results of the sample preparation (chapter 5.3). The goal is to find a preparation process resulting in a low total variance, i.e. low variation and high homogeneity within a sample. The total variance was calculated with CoDaPack (Thió-Henestrosa & Comas 2016: 18).

The *Chebyshev inequality* can be used in order to describe the total variance (Pawlowsky-Glahn *et al.* 2015: 110). It explains the probability that the distance (in the simplex) of a composition to its centre is lower than the estimated total standard deviation (which is the square root of the total variance). For example, with a given total variance of 0.04 (and thus a total standard deviation of 0.2), the probability is larger than 75% that the distance of one composition to the centre is lower than the estimated twofold total standard deviation (2 x 0.2). This means that approximately 75% of the samples will be at a distance shorter or equal to the twofold total standard deviation of 0.4. For example, when comparing grain sizes, the probability is larger than 75% that the distance of the samples from the centre will be within the twofold standard deviation, which for a grain size < 250 μm is **0.76** and for a grain size < 2 mm is **1.03**. Thus, the smaller grain size has a smaller dispersion of samples.

8.3.4 Zero Values Treatment

A common problem for compositional data analysis are missing or zero values within the dataset. Missing or zero values can have different causes and further steps depend on this information (Martín-Fernández *et al.* 2011: 44). In general, two kinds of zero values can be distinguished: *essential* and *rounded zeros*. Essential zeros refer to absolute absence, rounded zeros refer to values which are present in the sample but below the limit of detection (Martín-Fernández 2003: 255–256). In the case of pXRF measurements, elements with values below the limit of detection occur quite often. However, log-ratio transformations require complete datasets without missing values (Martín-Fernández *et al.* 2015: 188).

Essential zeros are difficult to handle, as a replacement of the value of zero can change the results dramatically; an essential zero means a 'true' zero, which is not caused by e.g. technical issues (Martín-Fernández *et al.* 2011: 53). Rounded zeros, in the classical meaning, describe values that are so small that they were rounded to zero. The zero values of the pXRF data are different as they are caused by the detection limit, but are grouped

together with the 'rounded zeros'. In both cases the traditional approach is a replacement of zero values with a small value. However, this approach harbours dangers as it can distort the covariance structure of the data (Martín-Fernández 2003: 256).

A suitable solution is the replacement of these rounded zeros through a *multiplicative replacement*, which does not distort the structure of compositional data (Martín-Fernández 2003: 276). Each rounded zero is replaced by a small value – and non-zero values are changed in a multiplicative way to maintain the structure of the data (Martín-Fernández *et al.* 2011: 45). This application is available in CoDaPack (Thió-Henestrosa & Comas 2016: 14–15).

8.4 Interpretation of Geochemical Data

In addition to the restrictions associated with the statistical treatment of compositional data, there remains a general problem of interpreting these data.

Methods such as clr-biplots or mapping of ilr-coordinates enable the detection of changes in elemental compositions. However, based on these analyses it is not possible to determine whether the element was enriched or depleted absolutely or relatively. A hypothetical and simplified example of pXRF data helps to illustrate this problem (Fig. 8-9). The obtained pXRF data provide information on more than 20 elements, given in parts per million; the example shows two samples with information on four elements (Si, Al, Fe and P) summing to a constant of 100 (instead of 1,000,000).

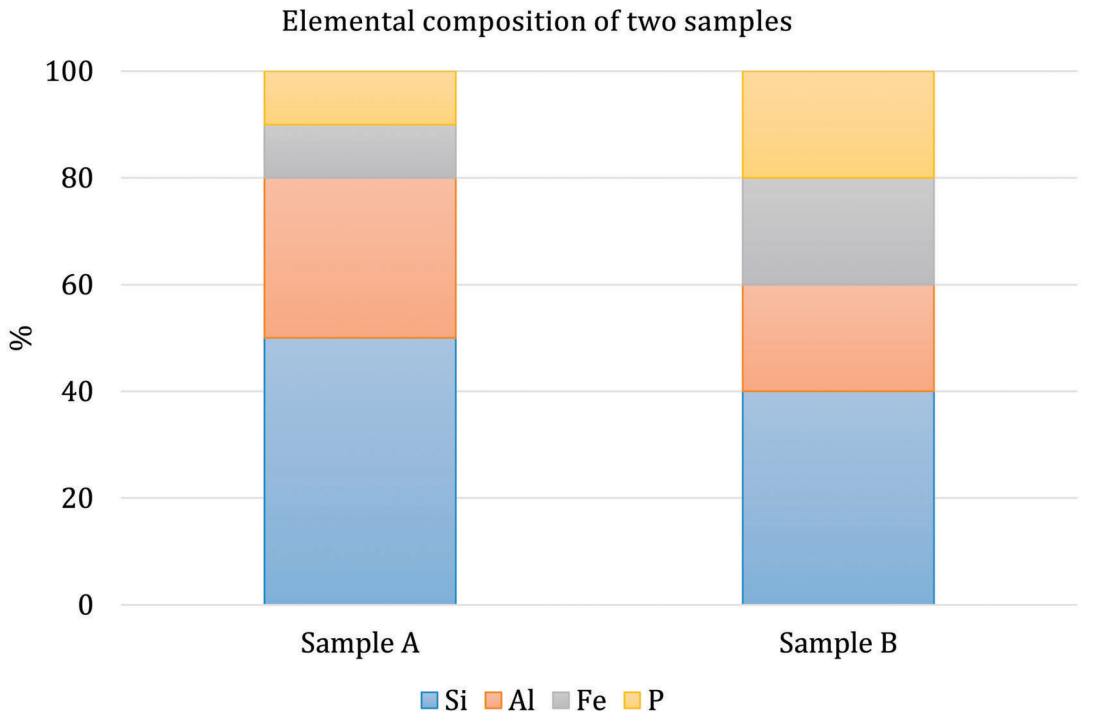

Fig. 8-9: Hypothetical example of two samples consisting of four elements with a constant sum of 100 percent.

In the case of the hypothetical example the obtained measurements show that sample A has, compared to sample B, higher percentages of Si and Al and lower percentages of Fe and P. By applying log-ratio transformations it is possible to measure or to visualise these differences. However, neither the pXRF device nor the log-ratio transformations reveal whether sample B contains more Fe and P because these elements could be **absolutely** or **relatively** enriched. An **absolute** enrichment would be a 'true' enrichment; **relative** enrichments occur when there is a depletion in other elements (in this case Si and Al). Due to the constant sum-constraint the values of Fe and P increase in order to counterbalance the decrease in Si and Al. This means, that in spite of the higher values of Fe and P in

sample B, both sample A and B could contain the same absolute amount of Fe and P. This emphasises why plots of single elements and their interpretation are problematic.

The reciprocal influence of the elements is the reason why the results of the Fulani village cannot be compared directly to the Nok results. If the same elemental signatures occur both in a Nok feature and within the hearths of the Fulani village, it is questionable to interpret the Nok feature as a former hearth. The elemental signatures of both the Fulani hearth and the Nok feature could derive from different origins. For example, the enrichments occurring in the Fulani hearth can be truly (absolutely) enriched whereas the same enrichments in the Nok feature could be caused by depletions of other elements (relative enrichment). By employing pXRF or statistics it is impossible to determine whether elements were absolutely or relatively enriched. However, the probability that a recurring elemental signature is the result of the same process increases with the frequency of its occurrence and the consistency of the signature.

Neither the use of pXRF analysis nor the use of log-ratio transformations enables the distinction between absolute and relative enrichments to be made. It is possible to identify, record and measure changes in the elemental composition of different samples. The interpretation of these specific signatures, however, is another task and can be achieved e.g. by gathering additional information, such as the archaeological context, pH values, or knowledge obtained from the literature. Also, the presence of recurring elemental patterns favours a specific interpretation.

8.5 Summary

The obtained pXRF data are characterised by several properties, which require specific statistical treatment. The main restriction is that they are so-called **compositional data**. The peculiarity of compositional data is that they carry relative rather than absolute information. These data operate in the simplex and not in the unconstrained real space (Euclidean space), which is the sample space for standard statistics. Thus, applying classical statistics is not appropriate and can lead to incorrect, nonsensical results or misinterpretations. Univariate element analysis, such as single element plots, are also affected by this constraint and can be erroneous when observed isolated from the remaining elements. Depending on the type of data, i.e. spatial data from the Nok sites or grouped data from the Fulani village, different approaches were pursued to both fulfil the statistical requirements and answer the research questions.

The Nok samples with their spatial information were investigated **by mapping enrichment factors** and **ilr-coordinates**. When using enrichment factors, the constant-sum constraint of compositional data is avoided by working with ratios. However, due to the lack of a reliable reference material this approach was rejected. Furthermore, this method is not coherent with the compositional character of the data. The method of mapping ilr-coordinates turned out to be successful. This 'principle of working on coordinates' refers to the use of an orthonormal basis within the sample space of compositional data. An orthonormal basis can be designed by sequential binary partitioning, which creates ilr-coordinates represented by balances. These coordinates meet the requirements of standard statistics as well as geostatistics and were employed for spatial analysis, i.e. the creation of multi-element maps.

The analysis of the Fulani village was performed with the help of **variation arrays** and **clr-biplots**. These approaches enable the summary and display of multivariate datasets to reveal variations among groups. However, although different elemental signatures of the activity areas were identified, a one-to-one transfer to the Nok samples is not possible due to the complications of interpreting compositional data.

An **interpretation** of these data is restricted by the inherent properties of compositional data. Compositional data do not carry information on a single element and observations isolated from the remaining parts are meaningless. From a mathematical point of view, it is possible to overcome the restriction of these data with e.g. ilr-transformations. However, the interpretation of these data is limited as the information as to whether enrichments or depletions are true (**absolute**) or caused by other elements (**relative**) is not available. This fact demonstrates the need to reformulate research questions to focus on meaningful changes in log-ratios rather than single elements. For instance, the clr-biplot of the Fulani samples (Fig. 8-7) revealed a clear difference in the log-ratio of P versus Fe between the different sample groups. Only by taking into account all other available information, e.g. derived from the archaeological context, is it possible to achieve a proper interpretation of the change in P or Fe, respectively.

The chosen approaches for overcoming the abovementioned restrictions and problems of compositional data are state-of-the-art. These methods respect the nature of compositional data and provide strategies for its analysis. However, these methods have some shortcomings, and an ideal solution for the treatment of compositional data has yet to be found.

OUTCOME AND SYNTHESIS

9 Results

9.1 Stone-Pot-Arrangements

Analysis of the obtained pXRF data succeeded in revealing enrichments of P within the stone-pot-arrangements that were not caused by soil formation processes. Data exploration took into account the compositional data structure by interpolating so-called isometric log-ratio (ilr) coordinates and examining centred log-ratio (clr) biplots (see chapter 8.3.1.1 and 8.3.2). Ilr-coordinates require balance settings, which enable an analysis of the relationships between and within groups of elements. Three different balance sets were developed and applied at *Ifana 3*, *Kurmin Uwa 2B* and *2D*, *Pangwari I*, and *Ido 2016*. Whether and how the assumed grave soil differed from the surroundings was assessed by employing set 1 and set 2 (chapter 9.1.1). In order to rule out distortions caused by geogenic interferences, a third set as well as clr-biplots were utilised (chapter 9.1.2). The distinction of anthropogenic and geogenic sources furthermore resulted in the identification of another potential burial type at *Pangwari I* (chapter 9.1.3).

9.1.1 Elemental Analysis

Analyses of sets 1 and 2 (Appendix 2-1) demonstrated that **enrichments of P** discerned the assumed grave soil from its surroundings (Fig. 9-1). Set 1 concentrated on all potential elements characteristic of the remains of a body, which are, besides P as the main indicator, Ca, Mn and K, the rare earth elements Y, La and Ce, and Cu[27]. These elements were grouped together and opposed to the remaining elements in the balance settings (set 1, ilr-1). Set 2 assessed both the influence of these elements and aimed to reveal further elements potentially present in the grave. To do so, each element was individually set opposed to the remaining elements in the balance settings (set 2, ilr-1 to ilr-20).

The examination of all potential grave soil elements grouped together in set 1 yielded insignificant or negative results for the majority of features (set 1 in App. 2-2 to App. 2-8). However, when P was opposed to the other elements in set 2, a pattern was revealed that is concordant with the assumed body position (set 2 in App. 2-2 to App. 2-8). According to the principle of balances, this pattern results either from enrichment in P or depletion of the other elements. Evaluations of the other elements[28] ascertained that it was due to an enrichment in P. Such enrichments were revealed in features 8, 13, 17, and 18 at *Ifana 3* next to the vessels, beneath and adjacent to the arranged stones and, in the case of feature 18, extending to the necklace (App. 2-2 to 2-5). The same applied for *Kurmin Uwa 2D* (App. 2-6), *Pangwari* (App. 2-7) and *Kurmin Uwa 2B* (App. 2-8). To rule out a geogenic phenomenon as observed at *Ido 2016* (Schmidt 2016), which also showed enrichments in P (App. 2-9 to App. 2-11), further analyses were conducted (chapter 9.1.2.).

---

[27] Cu was not part of all balance settings, since on some sites its concentration was below the limit of detection for all samples.

[28] Both the potential grave soil elements Ca, K, Mn, Y, La, Ce and the remaining elements Si, Ti, Al, Fe, V, Cr, Zn, Rb, Sr, Zr, Nb, Ba, Pb, and Cl were examined by plotting the ilr-2 to ilr-20 coordinates of set 2 (see App. 2-1 for balance settings).

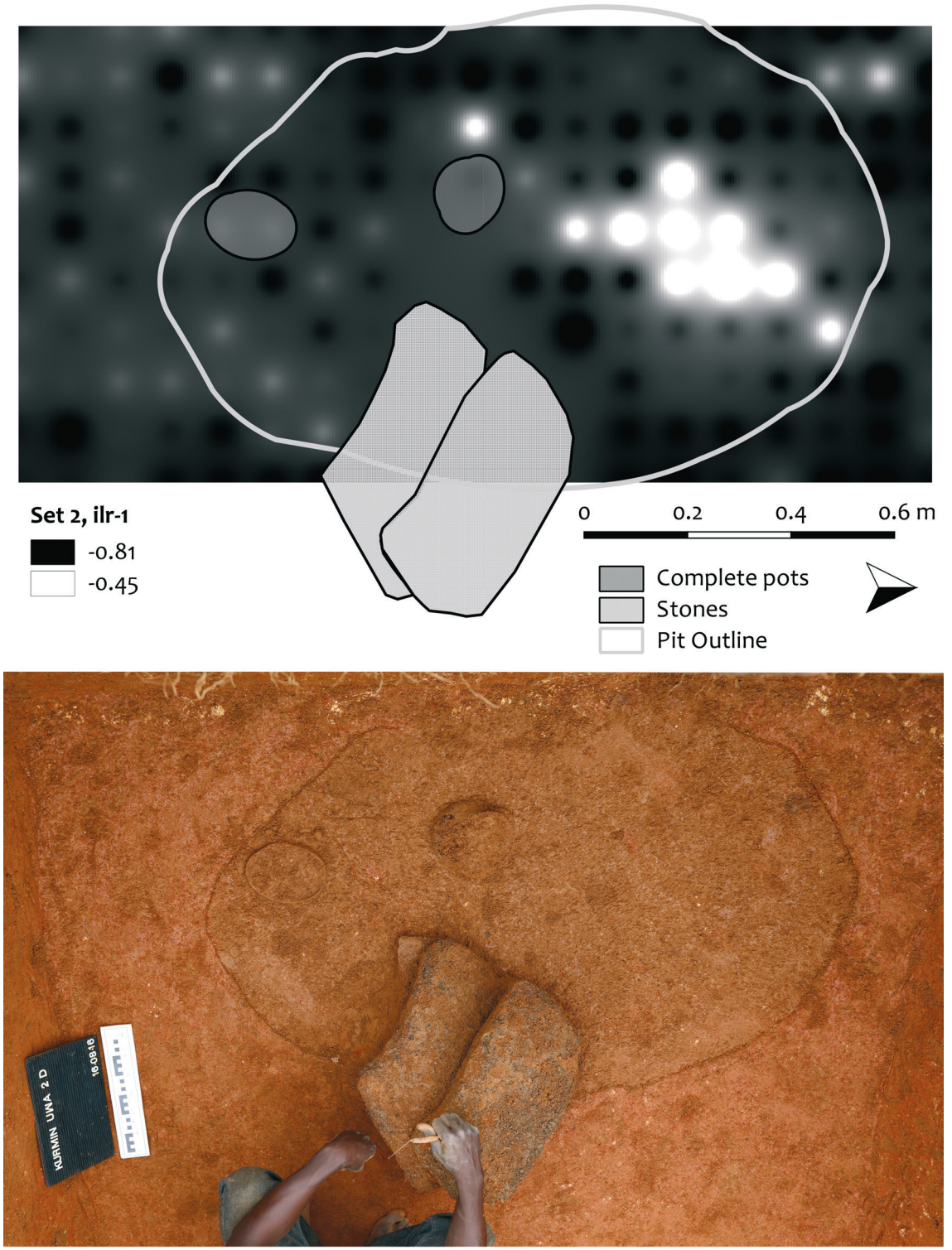

Fig. 9-1: Enrichment pattern of P (top) and top-view of the stone-pot-arrangement at *Kurmin Uwa 2D* (bottom). The enrichment pattern of P derives from the interpolation of coordinate ilr-1, which is composed of P opposed to the remaining elements (set 2 in App. 2-1). The depth of the pXRF samples was *c.* 20 cm below the height seen on the picture, at the bottom edge of the vessels.

9.1.2 Geogenic Interferences

The possibility that P originated from geogenic sources was dismissed for the enrichments at *Ifana 3* (features 8, 13, 17, and 18)[29], *Kurmin Uwa 2D* and *Pangwari I* (feature 18 and 20). In the case of *Kurmin Uwa 2B* the outcome was inconclusive.

At *Ido 2016*, patches of weathered granite adjacent to a stone-pot-arrangement caused enrichments of P, which could be easily misinterpreted as anthropogenic traces (Schmidt 2016). The same pattern was observed at other depths at *Ido 2016* as well (App. 2-9 to 2-11). These geogenic interferences produced a concurrent pattern of enriched P, Ca, Sr,

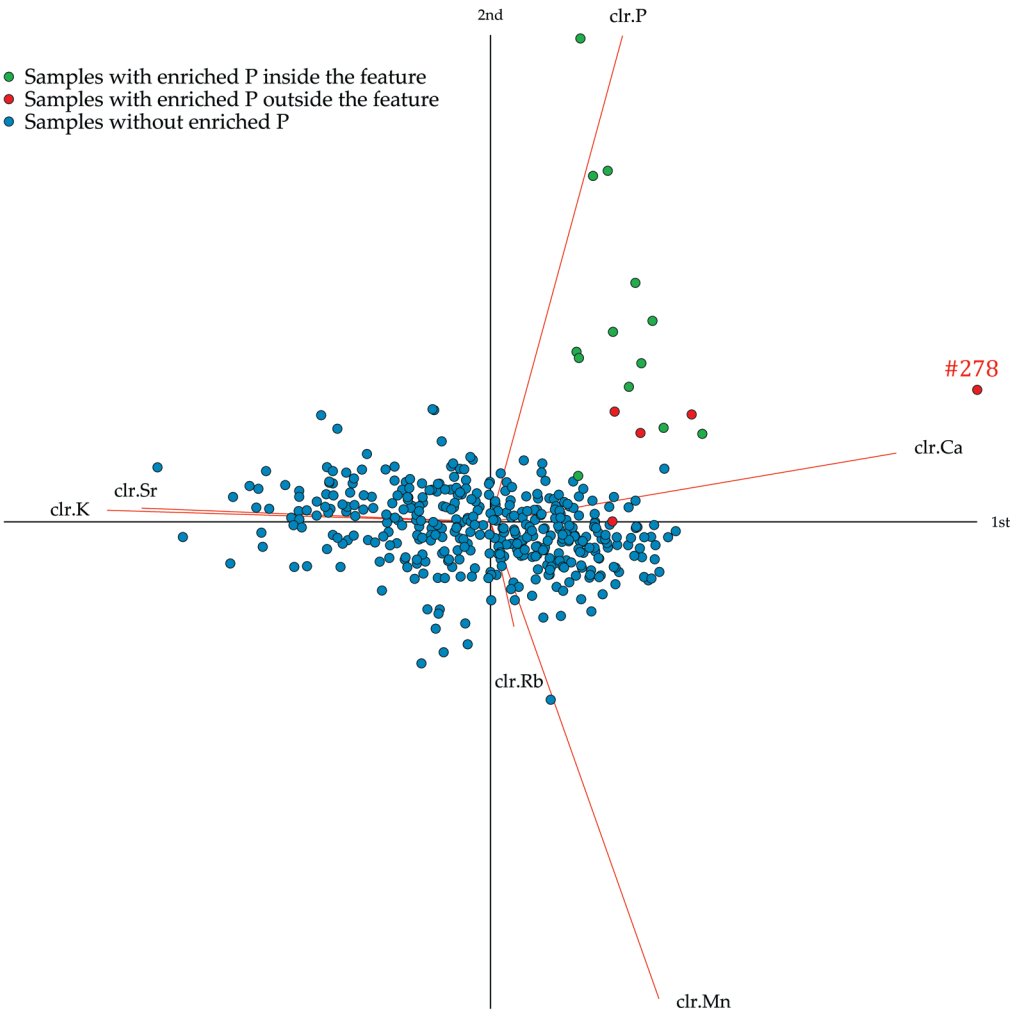

Fig. 9-2: Form clr-biplot for the samples from feature 13 at *Ifana 3* with the log-ratios of the elements P, Ca, Sr, Mn, K, and Rb. Sample #278, considered as having been disturbed by geogenic interferences, clearly separates from the other samples. The cumulative proportion explained is 0.7664, i.e. the first and second principal component together account for 76.64% of the total variance.

[29] The analyses were not conducted for feature 8, since pXRF measurements provided limited information on elements for this feature. However, since the enrichment pattern for P was like the others, a non-geogenic origin seemed plausible.

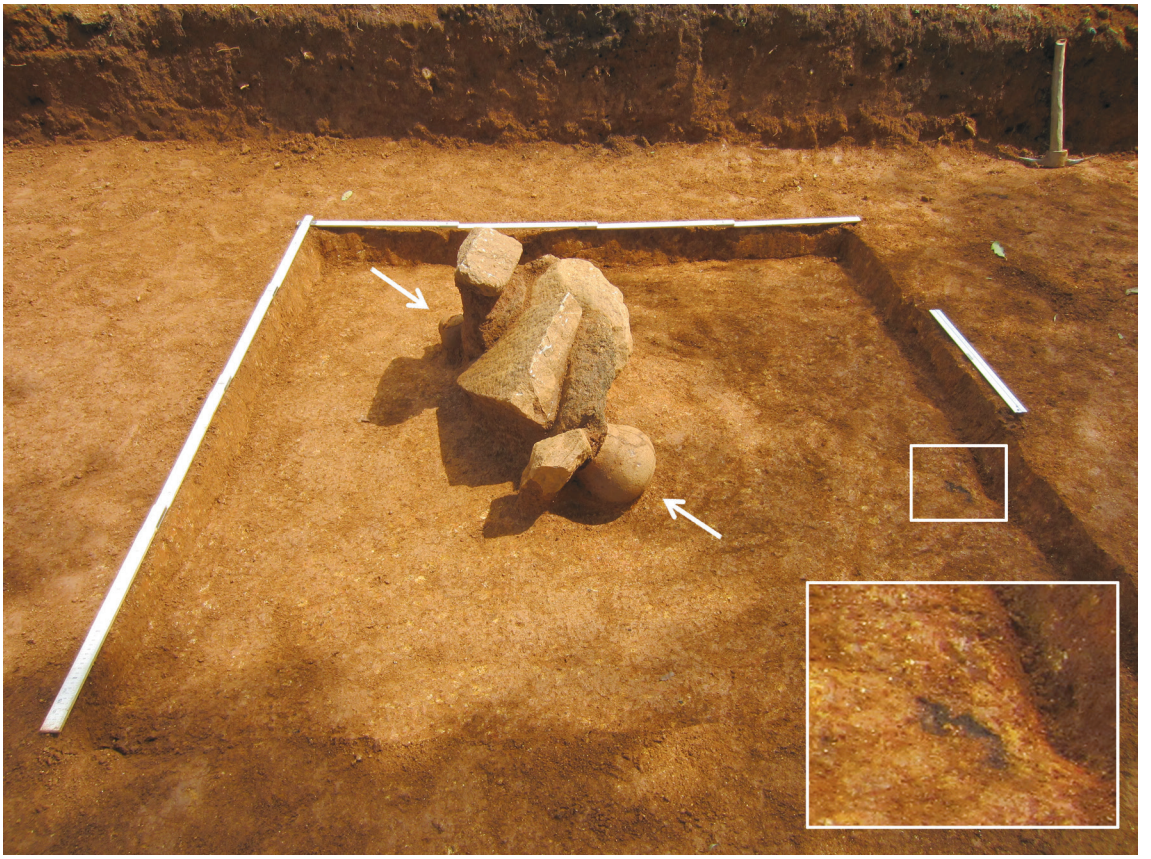

Fig. 9-3: View from the south of feature 13 at *Ifana 3*. The white arrows indicate the position of the vessels in the feature. The enlarged section shows a geogenic interference, probably the remains of weathered granite. Sample #278 (see Fig. 9-2) was taken from that area.

and Mn and depleted K and Rb. Both the enriched and depleted elements were opposed to the remaining elements in set 3 as ilr-1 and ilr-5, respectively (see App. 2-1 for balance settings). When both coordinates revealed a similar interpolation pattern, i.e. enrichments and depletions occurred concurrently, the corresponding samples were considered to have been affected by geogenic interferences. Clr-biplots (for details see chapter 8.3.2) supported the analyses.

The interpolations of set 3 did not reveal concurrent enrichments of P, Ca, Sr, and Mn (ilr-1) and depletions of K and Rb (ilr-5), interpreted as geogenic interferences, within the features at *Ifana 3*, *Kurmin Uwa 2D* and *Pangwari* (set 3 in App. 2-2 to 2-7). However, indications of geogenic interferences were found outside feature 13 at *Ifana 3* (set 3 in App. 2-2). Clr-biplots verified this assumption, since the relevant sample (#278) was separated from the others by a strong influence of Ca (Fig. 9-2) and a closer look revealed material with a geogenic source visible in the soil (Fig. 9-3). The same was observed for feature 18 at *Ifana 3*, where samples outside the feature correlated with weathered material and separated in the clr-biplot (set 3 in App. 2-4). Furthermore, pH values of samples considered as geogenic were higher than those considered as non-geogenic (see chapter 9.4).

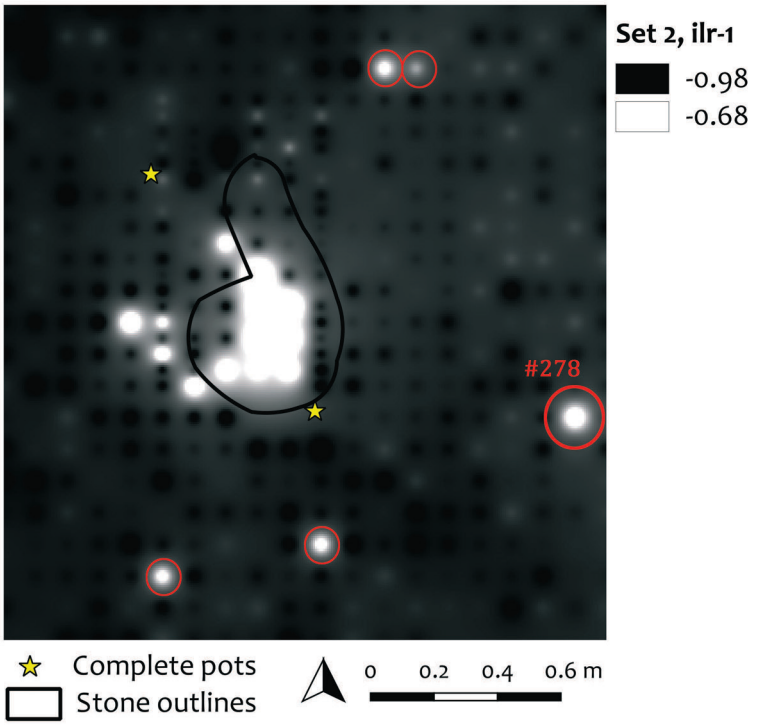

Fig. 9-4: Enrichments of P in feature 13 at *Ifana 3* as indicated by the interpolation of coordinate ilr-1 of set 2. The enrichment concentrates within the feature, besides a few spots outside (circled in red). Sample #278 separated in the clr-biplot (Fig. 9-2) and matched with geogenic material (Fig. 9-3). The other encircled spots clustered with the non-geogenic samples in the clr-biplot. Their origin and significance remains unknown.

At both features 13 and 18, it furthermore appears that not all P enrichments outside the feature originated from geogenic material (Fig. 9-4). Some of these P enrichments clustered in both clr-biplots with non-geogenic samples and comprised neither a geogenic signature nor weathered material in the sample. Whether they indicate further features or biases remains unknown. However, these samples were exceptional – only similar to features at *Pangwari*, which is the subject of chapter 9.1.3. The clr-biplots of feature 17 at *Ifana 3* and *Kurmin Uwa 2D* (App. 2-4 and 2-6) showed a rather homogenous cluster of samples and affirmed the absence of any geogenic interferences.

The results for *Kurmin Uwa 2B* were inconclusive (App. 2-8). The interpolations of set 3 revealed geogenic interferences and the clr-biplot indicated two clusters. A spatial visualisation of these two clusters showed that samples with a higher concentration of P complied with the position of a dead body, whereas samples with a higher concentration of Ca cluster within an adjacent find accumulation. However, since the geogenic signature was present in both areas, it remains unclear whether all samples represent geogenic processes or the signature superimposed the traces of a body as well as the adjacent find concentration.

9.1.3 New Feature Type

At *Pangwari I*, two further features yielded the same P enrichments as those within the stone-pot-arrangements. The prospection for geogenic interferences ruled out a geogenic origin for the enrichments in both the stone-pot-arrangements and two further features.

Prospection for geogenic interferences revealed that three out of seven P enrichments were concordant with the geogenic signature (set 3 in App. 2-7). The clr-biplot (Fig. 9-5) revealed a separation of these three geogenic samples (red) from the others (green). Two of the four non-geogenic samples (green) originated from the stone-pot-arrangements (features 18 and 20). The remaining two samples were also associated with features (see

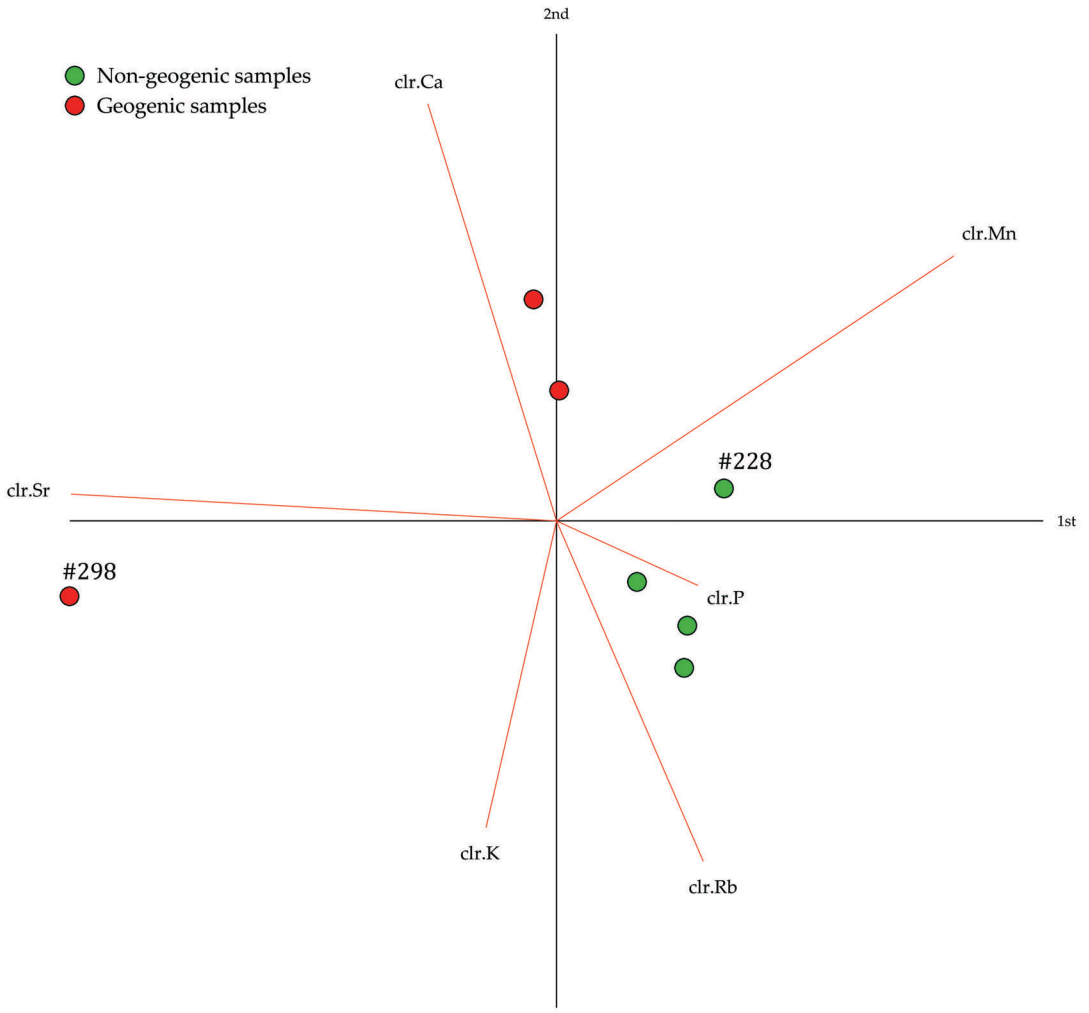

Fig. 9-5: Form clr-biplot for the samples from *Pangwari I* showing enrichments in P. The samples considered as geogenic and non-geogenic (according to the outcome of set 3) separate clearly by the log-ratios of Ca and Rb. Sample #228 originates from a feature consisting of a stone-arrangement and a pit. Sample #298 differs from all samples and may represent a mismeasurement, since the pXRF results for Ti and Mn were below the limit of detection. The cumulative proportion explained is 0.9650, i.e. the first and second principal component together account for 96.50% of the total variance.

Fig. 9-6 and 9-7). However, these two features were – according to the material evidence – not considered to be potential burial features.

The northern feature represents a stone-arrangement with upright standing stones. Since they were less prominent and the feature was void of any finds at all, it was not considered as a potential burial feature. The second feature consists of arranged stones intersecting a pit. Besides one small upright standing stone (Schmidt 2014: 99, Fig. 83) no other similarities to stone-pot-arrangements were found, i.e. no further arranged stones, pots or stone beads. Since the arranged stones truncated a pit[30] (feature 19), the whole feature was classified as such during excavation. Whether the arranged stones were part of the pit feature or represent a second, intersecting feature has to remain unanswered. A truncation and thus a mixture of materials could explain why the sample (#228) in the clr-biplot differs slightly from the other non-geogenic samples.

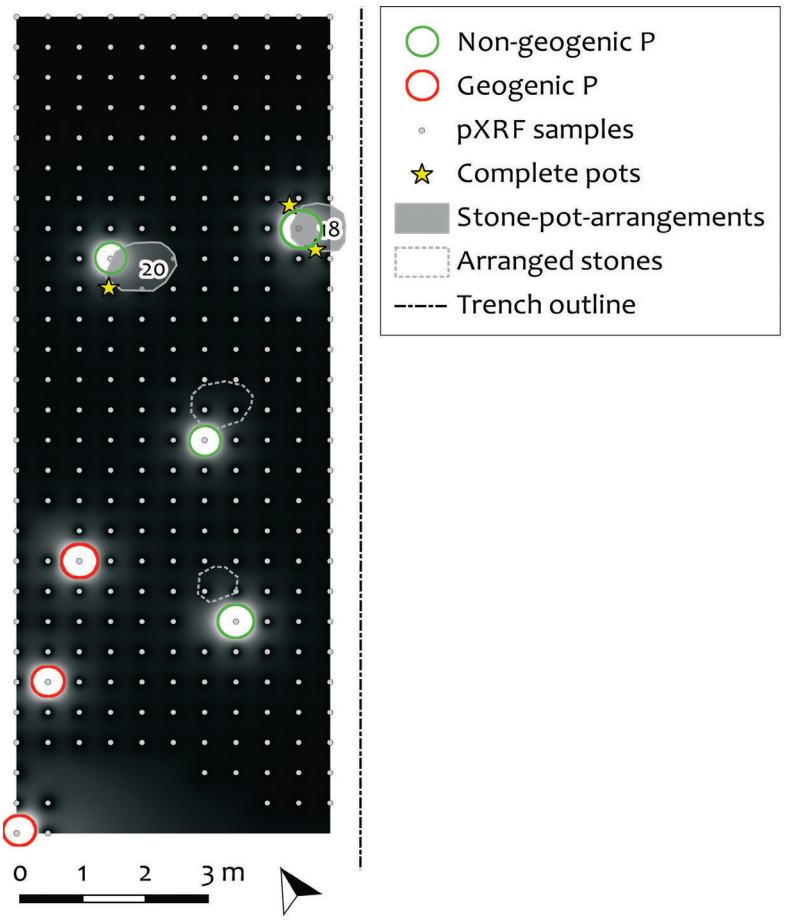

Fig. 9-6: Position of the relevant samples with P enrichments at *Pangwari I*. The samples considered as geogenic (red) lie outside the features. The non-geogenic samples (green) are within the stone-pot-arrangements (features 18 and 20) and within two further features – two stone-arrangements, one of which truncated a pit.

[30] New analysis and dates revealed that the lower in situ layers related to an Early Nok feature.

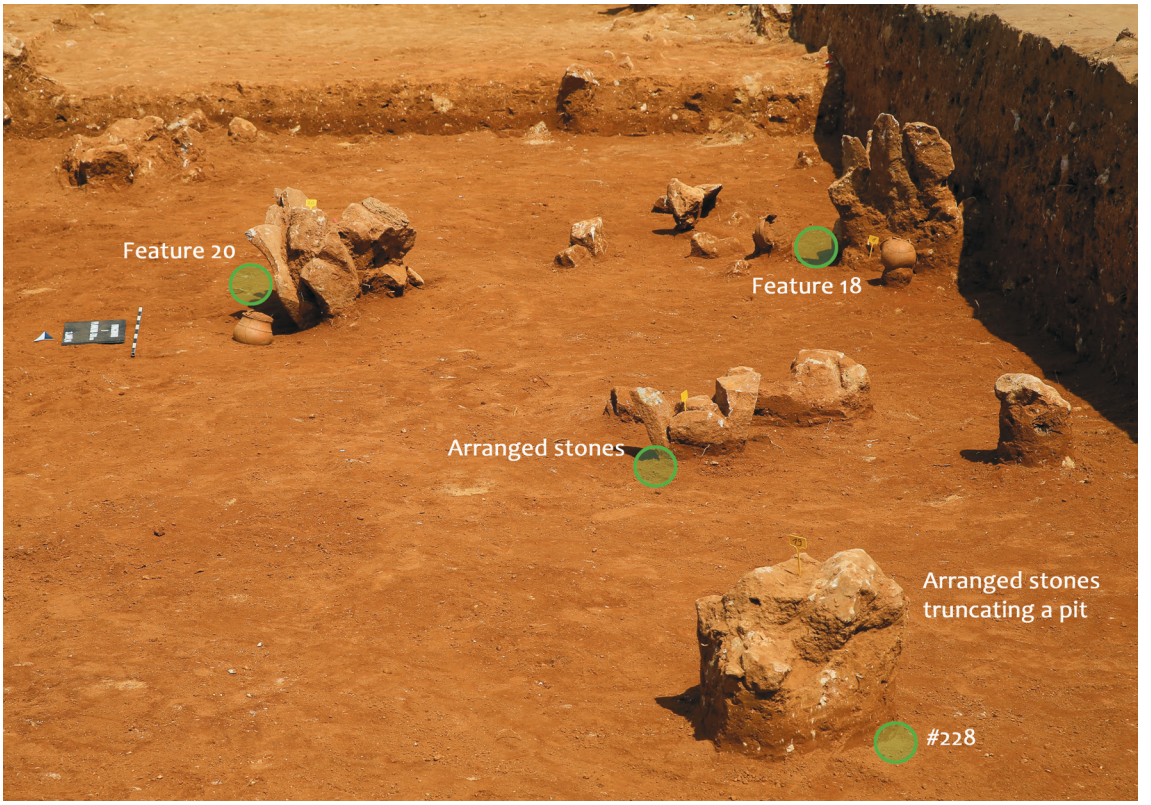

Fig. 9-7: A view of *Pangwari I* corresponding to Fig. 9-6. The samples with P enrichments considered as non-geogenic (green spots) lie within the stone-pot-arrangements (features 18 and 20) and two further features. One sample was adjacent to a stone-arrangement with upright standing stones, the other sample (#228) next to a stone-arrangement that truncated a pit.

The clr-biplot suggests that the P enrichments of these two further features resemble those of the stone-pot-arrangements. Such 'stone-arrangements', i.e. arranged stones without pots or beads, were also found at *Ido 2009 and 2016*. However, those features at *Ido 2009* were not sampled and those at *Ido 2016* were concealed by geogenic interferences. Although these results were exceptional, they might represent another yet unknown type of burial feature.

9.2 Pit Features

A distinct elemental composition with enrichments of P, Y and Zn as well as depletions of Fe, Al, V and Cr characterised some of the Nok pits. This composition was seen at *Kusuma 1* and occurred partly at *Kurmin Uwa 1* and *Ido 2016* as well as in a diminished form at the other sites and features. Apart from this, no other element or elemental composition distinguished features or specific areas from the surroundings.

The pXRF data were transformed and interpolated as ilr-coordinates in order to take the compositional structure of the data into account (see chapter 8.3.1.1). A total of 23 elements was examined by employing balance set 4 (ilr 1-22)[31], with each element opposed to the remaining elements (see App. 3-1 for balance settings). By interpolating each of the 22 ilr-coordinates individually for all sites, patterns associated with the features became visible. Since coordinates are built from balance settings, i.e. two components (elements or groups of elements) opposed to each other, significant patterns can be caused by both components. Clr-biplots of different combinations of elements enabled an assessment of the influence of each element (see chapter 8.3.2). Based on the distinct results at *Kusuma 1*, a signature characteristic of pits (set 5, see Appendix 3-1) was identified and tested on the other sites. Geogenic samples were identified by using balance set 3 developed in chapter 9.1.2 (see Appendix 2-1) and outlined in the excavation trench.

At *Kusuma 1*, several interpolated ilr-coordinates (set 4) revealed enrichments and depletions correlating with the pit features. For example, the interpolations of ilr-1 and ilr-6 indicated an enrichment of P and a depletion of Fe, respectively, within the pits (App. 3-2). Clr-biplots enabled the distinction of pit samples based on specific elements, such as P and Y as well as Fe and Cr (Fig. 9-8). Geogenic material, on the contrary, could be differentiated by the content of Ca, Sr, Ba, and Mn.

The most striking elemental signature to distinguish pits, identified by the interpolations of ilr-coordinates and accompanying clr-biplots, was characterised by enrichments of P, Y and Zn as well as depletions of Al, Fe, Cr, and V. These elements were used to create a pit signature in set 5 (see App. 3-1 for balance settings) and its interpolation revealed a clear pattern that distinguished samples inside and outside of features (App. 3-2). When visualising the position of the samples that clustered in the clr-biplot with the pit samples (encircled in blue in Fig. 9-8), they turned out to be further samples associated with features – they either lay adjacent to the pits or correlated with a charcoal concentration in the middle of the trench. The geogenic samples were identified by applying set 3 (App. 2-1) and confirmed by the clr-biplot.

At *Kurmin Uwa 1* and *Ido 2016*, the interpolations of the 22 ilr-coordinates of set 4 indicated similar enrichments and depletions within the pits as those observed at *Kusuma 1*. At *Kurmin Uwa 1*, the interpolated pit signature (set 5) correlated with the outlines of a pit (feature 3), although the overall pattern appeared rather blurry (App. 3-3). This pattern recurred in the clr-biplot – although the pit samples formed no distinct cluster, they confirmed the influence of Y and Zn as well as Fe, Al, V, and Cr. At *Ido 2016*, the pit signature (set 5) was found within both pits, although it was less distinct. However, the signature also occurred within geogenic spots (App. 3-4). This indistinct picture persisted

[31] Since Ni and Cu were below LOD on most sites, set 4 in App. 3-1 refers to ilr-1 to ilr-20.

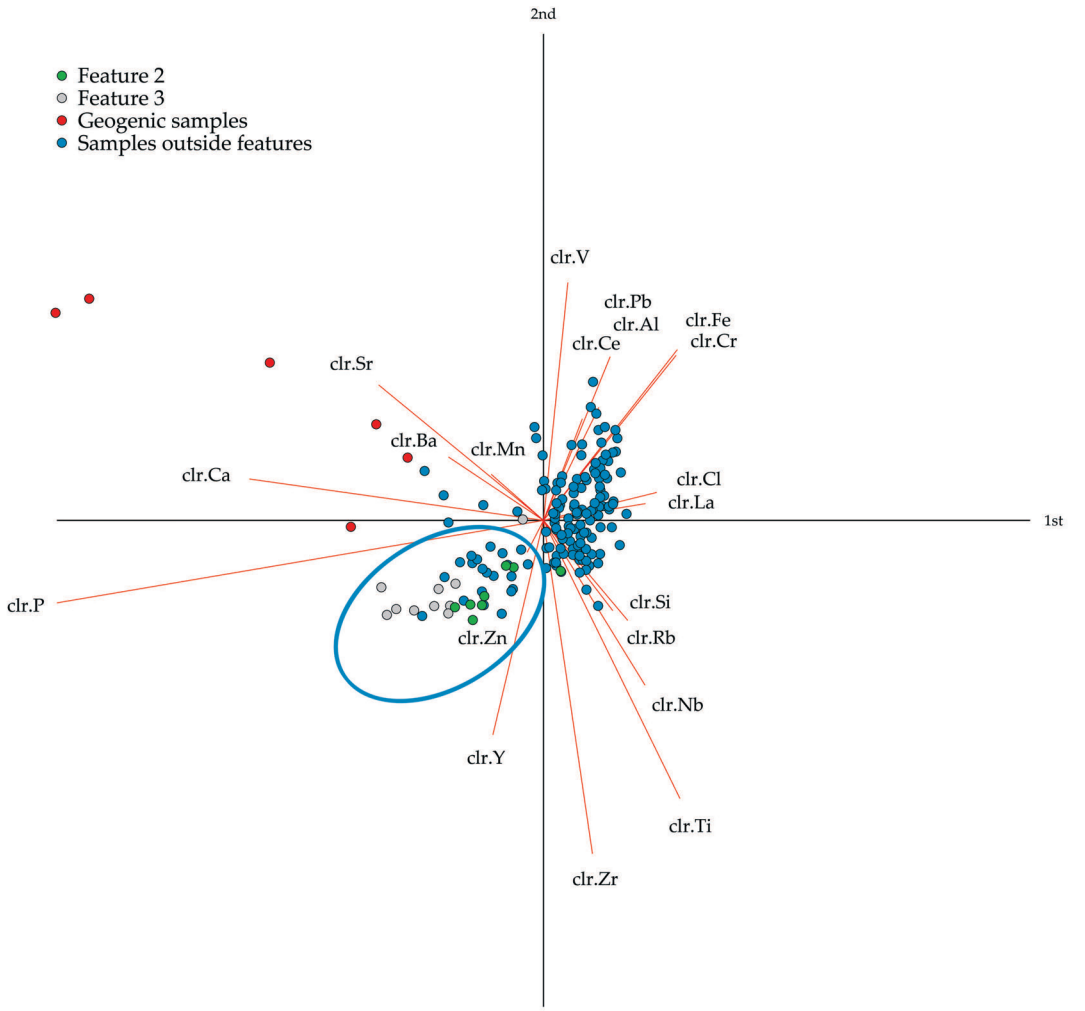

Fig. 9-8: Form clr-biplot for the samples from *Kusuma 1* with log-ratios of all elements. The pit samples are influenced by the log-ratios of P, Y and Zn and separate from both the geogenic (red) and most of the reference (blue) samples. The other (blue encircled) samples that clustered with the pit samples are shown in Fig. 9-9. The cumulative proportion explained is 0.6407, i.e. the first and second principal component together account for 64.07% of the total variance. The low cumulative proportion explained was considered to be sufficient, since the clr-biplot served as supplementary information for the interpretation of the interpolated ilr-coordinates.

in the clr-biplot. The pit samples were influenced by some of the elements of the pit signature, but were not separated from the other samples.

At *Ifana 1*, none of the 23 elements revealed a pattern concordant with the features. The pit signature (set 5), however, correlated to some extent with a charcoal concentration in the southern part of the trench (App. 3-5). Although the clr-biplot showed two clusters separated by their P content, the relevant samples showed no significant distribution in the trench. Ultimately, there was no element or element combination that clearly distinguished features or find concentrations from the surroundings.

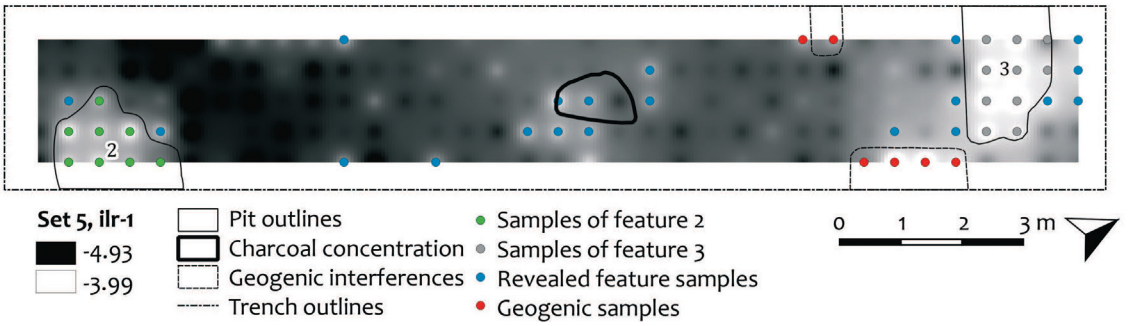

Fig. 9-9: Interpolation of the pit signature at *Kusuma 1*. The samples discussed in Fig. 9-8 are displayed with their position in the trench – those samples that clustered with the pit samples in the clr-biplot turned out to be samples associated with features, as they lie either adjacent to the pits or at the middle of the trench within or close to the charcoal concentration.

At *Pangwari E*, enrichments of P (set 4, ilr-1) as well as the pit signature (set 5) partially correlated with features (App. 3-6). The interpolation patterns indicated differences for features 10, 11, 12, and 14 compared to the surroundings. Although the clr-biplot also indicated a sample cluster distinguished by its P content, the samples of this cluster turned out to be neither associated to the interpolations of set 4 nor to set 5. This ambiguous result is likely due to the condition of the features at that depth – affected by disturbances caused by erosional processes (Höhn *et al.* 2018: 277) and illicit digging (Schmidt 2014: 38, 84–85) – which makes interpretation of these difficult.

At *Ifana 2*, none of the 22 interpolated ilr-coordinates (set 4) rendered a pattern corresponding to the features or find concentrations. The pit signature (set 5) revealed no significant pattern (App. 3-7). The two apparent clusters in the clr-biplot showed, when plotted with their spatial information, no correlations with set 5, the features or find concentrations. The generally small number of reference samples impedes meaningful interpretation.

The low sample number for the features 8, 9 and 17 at *Pangwari D* and *I* was considered insufficient for the interpolation of ilr-coordinates. Clr-biplots turned out to be problematic as well, since adequate reference samples were absent. To compensate for the lack of reference samples for the features 8, 9 and 17 at *Pangwari*, samples considered as sterile from the layer comprising the stone-pot-arrangements at *Pangwari I* were utilised for clr-biplots (App. 3-8). The samples from feature 17 revealed an influence of elements of the pit signature, namely enrichments of Y and Zn as well as depletions of Fe and V. Feature 8 and 9, in contrast, rendered a completely different result. However, whether the differences in the clr-biplot reflected characteristics of the pits or whether the samples were biased by the replacement of reference samples from another depth and area, has to remain unknown. Without adequate reference samples the interpretation cannot be considered reliable.

9.3 Fulani Village

Analyses of the modern Fulani village made it possible to distinguish activity areas by assessing their elemental composition. Soils affected by human impact contained a generally higher concentration of the alkali and alkaline earth metals Ca, Sr and K as well as the lighter elements P and Cl. However, a signature similar to the Nok pits that encompassed enrichments of P, Y and Zn, as well as depletions of Fe, Al, V, and Cr, was not observed and neither any specific activity nor any functional area of the Fulani village revealed a similar pattern.

Different parts of the village were sampled (App. 4-1) to provide information on elemental signatures of functional areas and performed actions (App. 4-2). Samples from on-site and off-site, i.e. the village itself and the surrounding savanna, represent reference samples. On-site samples originated from three sampled village zones and were combined to ensure representativeness. Clr-biplots and variation arrays as analysis tools for compositional data were used to evaluate the influence of the elements on different feature categories (see chapter 8.3.2 for more information).

Hearth samples separated from the reference soil mainly by their increased content of Ca, Sr, P, and Cl as well as their decreased Ti content (App 4-3). The point distances in the biplot of the samples from the centre of the hearth to the reference soil are also larger than for those from the rim of the hearth. Soil with mineralized cow **manure** differs by the elements Ca and K (App. 4-4). A similar pattern was observed for the samples from the chicken coop, where Ca in particular influenced the outcome (App. 4-5). Areas for **food** processing, i.e. the interior of the kitchen hut as well as the soil beneath a large mortar next to the kitchen hut, revealed a strong influence of Cl on the samples (Fig. 9-10). This observation complies with the distribution of samples in the clr-biplot: samples from the interior of the kitchen showed a stronger influence of Cl, whereas the reference samples had a higher Ti content – and samples from the soil next to the kitchen, beneath a mortar, lay in between these two signatures.

The analyses of the **footpath** rendered very satisfying results (App. 4-6), since the distinction of samples from the footpath and samples beside the footpath was consistent with the distinction of on-site and off-site samples. Both the footpath and on-site samples, representative of human impact, were distinguished from the samples taken from beside the footpath and off-site, representative of the absence of human impact, by the elements P, Cl, V, and Ba. The footpath itself was mainly influenced by Ca and Sr.

The interior of a sleeping hut (App. 4-7) and a 'medicine hut' for treating the sick (App. 4-8) both involving **human occupation,** were less distinct than the other activity areas. Nevertheless, the samples differed from the reference samples by their content of Cl, Ca, Sr, Zn, and Cr. Less significant were also the results from the **abandoned village** (App. 4-9). The former cowshed, most recently abandoned, showed a strong influence of Ca, Cl and P as well as K and Sr. Samples from the former village, abandoned for a longer time, differed mainly by Y, Al, Si, Pb, and Zn. Since the land of the abandoned village was re-used for the cultivation of crops it remains unclear whether these elements represent farmland or the abandoned village.

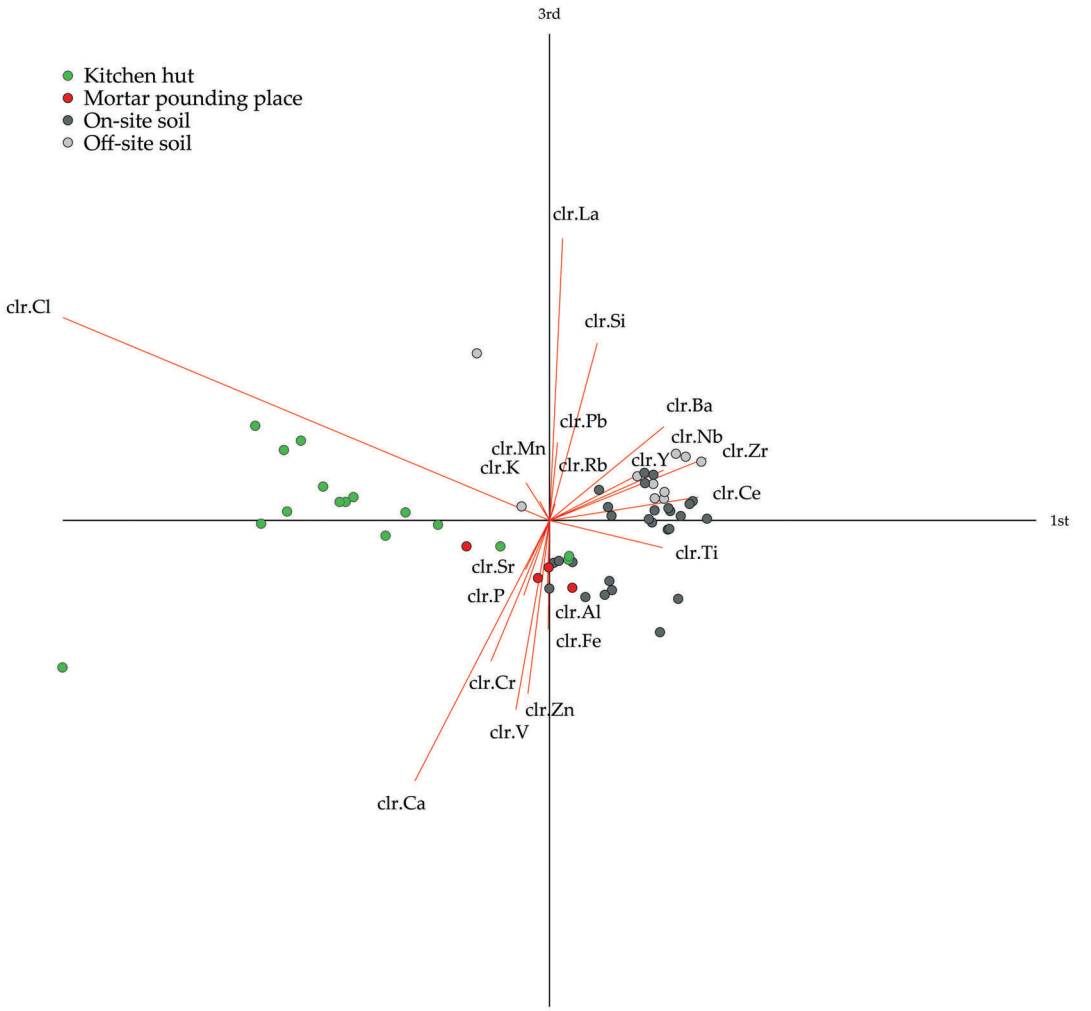

Fig. 9-10: Analysis of samples taken from a modern Fulani village. Form clr-biplot of the samples obtained from the kitchen hut, the soil beneath a pounding place and reference samples. The samples differ by the log-ratio values of Cl – the interior of the kitchen revealed the strongest influence of Cl, the reference samples the lowest. The soil from beneath the mortar, located adjacent to the kitchen hut, lies between both categories. The cumulative proportion explained together accounts for 83.68% of the total variance.

9.4 Soil pH

Analyses of soil pH indicated that the soil within the stone-pot-arrangements had lower pH values than the surroundings. Since soil pH represents one of the basic parameters for the genesis and chemical properties of the soil (Scheffer *et al.* 2010: 151), a total of 21 samples from both inside and outside the features as well as from areas with geogenic interferences were analysed (see Tab. 9-1). The analyses were conducted in the laboratory at the Institute of Physical Geography at Frankfurt, Goethe University. The samples were sieved to < 2 mm and 10 g of the soil sample was added to 25 ml of a 0.01 M $CaCl_2$ solution. The pH of the solution was electronically determined using a combination electrode WTW E 56 and digital meter WTW 740, according to norm DIN 19 684.

In general, the pH values of Nok sites were more acidic than expected, based on the soils occurring in the research area (see chapter 3), which range – by definition – between moderately acidic to slightly alkaline (pH 5.2 to pH 7.6). The obtained pH values, however, ranged from pH 4.48 to pH 5.93, which classified them as very acidic (pH 4.0 to 4.9) to moderately acidic (pH 5.0 to 5.9) (Scheffer *et al.* 2010: 152 Tab. 5.6-1).

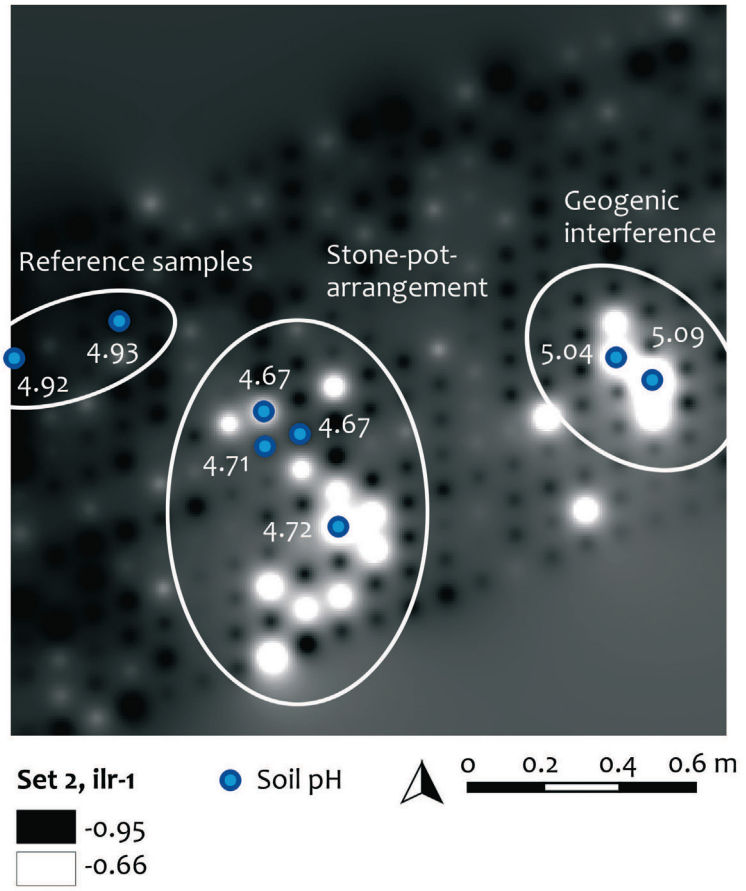

Fig. 9-11: Feature 18 at *Ifana 3* with enrichments of P as indicated by the interpolation of coordinate ilr-1 of set 2 (see chapter 9.1.1) together with the obtained soil pH values. The values within the stone-pot-arrangement were lower than the reference samples, whereas the samples of the geogenic interference were higher.

Kurmin Uwa 2D: Pit with stone-pot-arrangement (no feature number), depth ca. 120 cm

Laboratory no.	XRF no.	pH value	Sample position (inside/outside of feature)	
1	46	4.53	Inside stone-pot-arrangement	
2	53	4.59	Outside	
3	66	4.53	Inside stone-pot-arrangement	
4	84	4.71	Inside stone-pot-arrangement	
5	100	4.89	Inside stone-pot-arrangement	
6	133	4.70	Outside	

Ido 2016: Pit (feature 8), depth ca. 20-50 cm (South-North)

Laboratory no.	XRF no.	pH value	Sample position (inside/outside of feature)	
7	86	5.42	Outside, from geogenic structure	
8	106	5.37	Outside, from geogenic structure	
9	118	4.48	Inside pit feature	
10	119	4.62	Inside pit feature	
11	264	5.43	Outside	
12	277	4.54	Outside	
13	344	5.93	Outside	

Ifana 3: Stone-pot-arrangement (feature 18), depth ca. 90 cm

Laboratory no.	XRF no.	pH value	Sample position (inside/outside of feature)	
14	41	5.09	Outside, from geogenic structure	
15	55	5.04	Outside, from geogenic structure	
16	178	4.72	Inside stone-pot-arrangement	
17	190	4.67	Inside stone-pot-arrangement	
18	204	4.67	Inside stone-pot-arrangement	
19	205	4.71	Inside stone-pot-arrangement	
20	260	4.93	Outside	
21	305	4.92	Outside	

Tab. 9-1: pH values obtained from different sites and features. The sampling depth at the site *Ido 2016* ranges from 20 to 50 cm (from south to north), as the trench was cut perpendicularly to the slope.

The evaluation of the soil pH values from feature 18 (*Ifana 3)* revealed a significant pattern (Fig. 9-11). Compared to the pH of the reference soil (pH 4.92 and 4.93), the values inside the stone-pot-arrangement were **lower** (pH 4.67 to pH 4.72) and the values of the geogenic interference **higher** (pH 5.04 and 5.09).

At *Kurmin Uwa 2D* the values from inside and outside the stone-pot-arrangement were similar, between pH 4.53 to 4.89 and pH 4.59 to 4.70, respectively. Since no samples

originated from geogenic interferences, a verification of the pattern observed at *Ifana 3* is not possible. However, the values for both sites were quite similar, although slightly more acidic at *Kurmin Uwa 2D*, where samples were taken at greater depth.

Greater soil acidity with increasing depth was also observed at *Ido 2016*. Since the trench was located on a slope and excavated perpendicularly, the samples originate from different depths. The values were less acidic in the North (20 cm) and more acidic in the South (50 cm). This meant it was not possible to draw a conclusion about the differences in soil pH between geogenic samples, reference samples and the pit feature and it is unclear why soil pH increased with depth.

9.5 Forensic Approach

Methods applied in forensic science were utilised to seek further evidence of a body within the stone-pot-arrangements. Out of three potential approaches, the analysis of the so-called **soil community** was applied on Nok samples. However, the absence of exploitable material, most probably due to the acidic soil, prevented its application. Due to the adverse soil conditions, the other two approaches suitable for identifying changes over the long-term – aDNA and lipid analyses – were not pursued.

The analysis of so-called soil communities is based on the fact that a decomposing cadaver affects the soil environment. Studies exist on *testate amoebae* (Szelecz *et al.* 2014; Seppey *et al.* 2016) and *soil nematodes* (Szelecz *et al.* 2016). These approaches are employed in forensic investigations to provide evidence of a dead body and to estimate the post-mortem interval. The technique of working with *testate amoebae*, a common group of soil protozoa, is of particular interest as their shells can preserve for millennia (Szelecz *et al.* 2014: 90–91). Abiotic and biotic factors, such as the presence of a decomposing cadaver, can result in changes in their abundance, community composition or shell morphology (Szelecz *et al.* 2014: 91; Seppey *et al.* 2016: 552, 556). Analyses of soil samples from Nok stone-pot-arrangements were conducted by the laboratory of Soil Biology at the University of Neuchâtel. The chosen samples (n=11) were taken from the sites of *Ido 2016*, *Ifana 3* and *Pangwari*, both from inside and outside the features. However, the examination of the samples revealed that no *amobae* were present[32] – the lack of exploitable material in the acidic soil thus precluded any analyses.

Due to the negative outcome, the detection of **ancient DNA** (aDNA) within the Nok samples was considered unlikely and not pursued in the scope of this thesis. Although recovery of DNA without bone material succeeded for Neanderthal mitochondrial DNA from cave sediments (Slon *et al.* 2017), a successful application in the unfavourable soil in our research area, in particular with respect to the age of the burials, is very unlikely[33]. Even in the case of a positive result, detected aDNA does not provide unequivocal evidence of a body as it can originate from other sources, such as faeces[34]. Analysis of **lipid extracts**, as another long-term approach, have proven successful in archaeology for determining the former contents of pots (Evershed *et al.* 2008; Nieuwenhuyse *et al.* 2015); ongoing analyses on Nok potsherds have enabled the identification of beeswax and animal fat[35]. Lipid analysis of soil (Bethell *et al.* 1994; Evershed *et al.* 1997) can be utilised for the identification of fatty acids which correlate with assumed adipocere (Bull *et al.* 2009). However, since the soil conditions were adverse and a success rate considered low, this approach was not pursued in the scope of this thesis.

[32] Pers. comm. Edward Mitchell, Laboratory of Soil Diversity, University Neuchâtel, 18-01-2017.
[33] Pers. comm. Kurt W. Alt, Institute of Anthropology, Johannes Gutenberg University Mainz, 20-10-2017.
[34] Pers. comm. Matthias Meyer, Max-Planck-Institute for Evolutionary Anthropology, Leipzig, 24-09-2018.
[35] Pers. comm. Julie Dunne, Organic Chemistry Unit, University of Bristol, 14-08-2018.

9.6 Summary

Enrichments of P were found within seven **stone-pot-arrangements** at *Ifana 3*, *Kurmin Uwa 2D* and *Pangwari I* and could be distinguished from enrichments caused by geogenic interferences. Such interferences were observed at *Ido 2016* and outside features at *Ifana 3*. The distinction between geogenic and non-geogenic P enrichments enabled the identification of two further potential burial features at *Pangwari I*. These features comprised a different layout than the stone-pot-arrangements, since they consist of arranged stones only – without pots or stone beads. At *Kurmin Uwa 2B*, the results were inconclusive and it remains unclear whether the P enrichments originated from a body or geogenic interferences. Besides enrichments of P, no other elements known from archaeological or forensic studies yielded significant results.

At *Kusuma 1*, two **pit features** and an area of charcoal yielded an elemental signature suggesting enrichments of P, Y, and Zn as well as depletions of Fe, Al, V, and Cr. This signature recurred at other sites, such as *Kurmin Uwa 1* and *Ido 2016*, although less clearly. Apart from this signature, no enrichments or depletions of the 23 observed elements correlated with features. The samples from *Ifana 2* and features 8, 9 and 17 at *Pangwari* demonstrated the need for an adequate sampling strategy, since the low sample number and lack of sufficient reference samples impeded a sensible interpretation.

The analysis of activity areas at the modern **Fulani village** revealed distinct results. Depending on the sampled category, different elements separated the samples from the reference soil, mainly by the elements Ca, Sr, K, P, and Cl. However, none of the functional areas revealed a signature comparable to the Nok features.

Soil pH analyses indicated lower pH values for stone-pot-arrangements compared to the surroundings, and higher pH values for geogenic interferences, respectively.

Utilising **forensic approaches** turned out to be problematic, since only a few possibilities for investigation of long-term changes exist. The method of analysing soil communities was tested but failed as the samples were devoid of exploitable material, probably caused by the acidic soil. Based on this, the two other potential approaches were not pursued.

10 Interpretation and Discussion

10.1 Stone-Pot-Arrangements

Interpretation of Stone-Pot-Arrangements as Burials

Within seven stone-pot-arrangements, pXRF analyses revealed enrichments of phosphorus that are interpreted as residues of decomposed bodies. Based on the spatial distribution of the enrichments and the assumed size of the burial pits, the bodies were most likely buried in a flexed position. This supports the archaeological interpretation of stone-pot-arrangement as burials – assumed as such by their characteristic layout, yet unproven due to the absence of bones and other human remains (Rupp 2010: 70; Nagel 2014; Schmidt 2014: 101–102; Schmidt 2016).

Phosphorus can be considered as the most frequent and most consistent element associated with grave soils (see chapter 6.2 and 6.4). Numerous forensic and archaeological case studies have proven that enrichments of phosphorus are associated with residues of decayed bodies and animal cadavers (Fiedler *et al.* 2004: 563; Fiedler *et al.* 2009: 311; Stokes *et al.* 2013: 586; Carter *et al.* 2007: 17; Melis *et al.* 2007: 810). Such phosphorus enrichments were found in seven stone-pot-arrangements at *Ifana 3, Kurmin Uwa 2D* and *Pangwari* (see chapter 9.1.1).

The spatial distribution of samples containing enrichments of phosphorus and the size of the pit at *Kurmin Uwa 2D* strongly suggest a flexed position for the buried bodies. This assumption derives from both the oval form of the pit with a maximum length of *c.* 140 cm, as well as the distribution of the enrichment patterns at the other sites, which span between 40 and 70 cm in diameter and form either a round or crescent and partly segmented shape. The enrichment patterns furthermore comply with the assumed position of a body as indicated by the grave goods; enrichments of phosphorus accumulate between or next to decorated vessels (Fig. 10-1) and extend to the stone bead necklace in feature 18 at *Ifana 3*. Since some of the enrichments extend beneath the arranged stones, the bodies were either covered by stones or, more likely, the stones were originally set upright, as observed at *Pangwari* and *Ido 2009*, and collapsed onto the body during or after its decay.

A geogenic source of phosphorus was ruled out for the enrichments within the stone-pot-arrangements (see chapter 9.1.2). Prospections for geogenic interferences *within* the burials by utilising a signature identified at *Ido 2016* yielded negative results. Statistical analysis furthermore enabled the identification of different types of phosphorus enrichments, of which only the samples *outside* the burials corresponded with a geogenic signature. Due to the properties of compositional data, enrichments of phosphorus can also be caused by a depletion of other elements, which results in a relative enrichment. Further tests rejected such depletions and therefore the phosphorus enrichments are considered to be absolute. Also, the possibility that phosphorus derived from abrasion of the arranged burial stones contradicts the distribution of enrichments both adjacent and beneath the arranged stones.

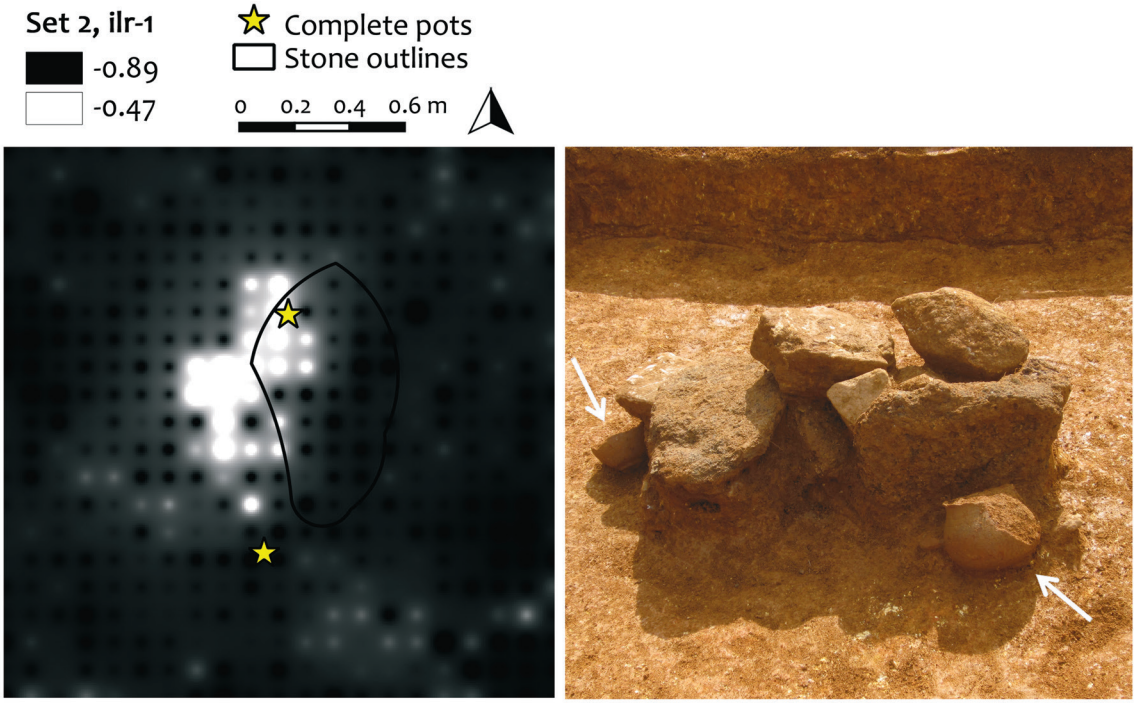

Fig. 10-1: Enrichment of phosphorus within feature 17 at *Ifana 3* (left) and view from the west of the feature (right), with location of pots indicated by the white arrows. The enrichment occurred both next to and beneath the stone arrangements. The interpolation shows not the element phosphorus as such, but the coordinate ilr-1 of set 2, where phosphorus is shown opposed to the other elements. White areas represent a stronger influence of phosphorus or a weaker influence of the remaining elements. Based on further analysis, the first possibility was considered likely.

Soil pH values confirmed the identification of different types of phosphorus enrichments – the soil pH of the geogenic material was higher and the pH of soil associated with the supposed bodies lower than that of the reference soil (chapter 9.4).

According to forensic studies, soil pH values tend to be lower within grave soils, whereas higher pH values occur mostly in short-term studies (Aitkenhead-Peterson *et al.* 2012: 132) or in the context of incomplete decomposition (Fiedler *et al.* 2004: 563). A lower soil pH was also observed within assumed burial features at the Iron Age site of *Campo* (Mbida Mindzie & Mvondo Ze 2016: 147, 149; Seidensticker 2010: 61). Further comparisons with Stone and Iron Age burials from West and Central Africa revealed parallels regarding the layout and finds within the stone-pot-arrangements. These included the presence of stone beads within burials as well as a necklace arranged as if worn (Magnavita S. 2003: 129; Magnavita S. 2015: 175; Connah 1976: 328, 343, 346; Connah 1981: 95, 116), modification or arrangement of stones (Magnavita S. 2009: 84; Magnavita S. 2015: 25, 175–176; Meister & Eggert 2008: 192) and the presence of complete and decorated vessels as grave goods (Meister 2010: 243, 246–247; Eggert & Seidensticker 2016: 25–30, 34–53; González-Ruibal *et al.* 2013).

Alternative Interpretations

Stone-pot-arrangements clearly represent some kind of deposition, since the stones and artefacts were laid down intentionally in recurring patterns. Possible explanations for this deposition, however, are not limited to their use as interments. Depositions with offerings of organic and inorganic goods could also account for the feature layout, the release of phosphorus into the soil as well as the restricted spatial distribution of the enrichment patterns. Furthermore, this could explain the absence of enrichments of other grave soil elements known from forensic and archaeological studies, such as calcium, potassium, manganese, copper, and rare earth elements. Another reason for phosphorus enrichments could be a different soil formation within the associated pit compared to the surroundings.

However, organic offerings as a source for phosphorus are rather unlikely, even though they might explain the restricted extent of the enrichment patterns of phosphorus measuring between 40 to 70 cm. A long-term retention of phosphorus within the soil requires a significant input of phosphorus, which contradicts the source being the decay of organic matter such as that of plants or animal products. A human body of 70 kg, in contrast, contains *c.* 700 g of phosphorus (Schaal *et al.* 2016: 271). Besides, the small spread and segmented dispersion of the enrichment patterns do not contradict a decomposed body. At the site of *Daima II* in northeast Nigeria, for example, a buried body dating to the first centuries CE was so tightly contracted that one knee was within several centimetres of the chin (Connah 1981: 150). Furthermore, the distribution of phosphorus must not necessarily resemble a body in size and form. The lateral and vertical dispersion of cadaveric fluids is based on the size of the skeleton, the extent of the maggot mass, including their migration paths, and the soil texture (Aitkenhead-Peterson *et al.* 2012: 127; Carter *et al.* 2007: 15).

The absence of other enriched elements indicating a decomposed body, including calcium, potassium, manganese, copper, and rare earth elements, is not anomalous. Calcium, as well as phosphorus, is a main component of bones, but is rarely found in forensic studies within grave soils (see chapter 6.4). Long-term studies on animal cadavers have also shown that calcium concentrations decline back to normal values after some time (Melis *et al.* 2007: 810). A low soil pH leads to an increased solubility of calcium phosphates (Scheffer *et al.* 2010: 417), among them hydroxyapatite, the main constituent of bones. The dissolution of the hydroxyapatite results in migration of calcium ions into the soil solution (Janaway *et al.* 2009: 321–322; Dent *et al.* 2004: 583–584) and unbound calcium, which generally leaches out (Jones *et al.* 2013: 33), can migrate to the lower soil levels and adsorb there (Oonk *et al.* 2009a: 42). Phosphorus, as part of this hydroxyapatite, although often referred to as mobile, can be stabilized and immobilised by iron and aluminium oxides within acidic soils (Oonk *et al.* 2009a: 40; Borggaard *et al.* 1990: 448; Jones *et al.* 2013: 33; Scheffer *et al.* 2010: 417). Potassium, known from forensic studies, inherently occurs in small amounts within the body (Schaal *et al.* 2016: 271) and is highly mobile (Jones *et al.* 2013: 33). Manganese, copper and rare earth elements were found as enrichments within grave soils from archaeological studies. However, they are not verified by forensic studies; manganese more likely derives from the soil than from the decomposing body (Keeley *et al.* 1977: 24) and copper rather derives from grave goods (Bethell & Carver 1987: 17). Rare earth elements (e.g. yttrium, lanthanum or cerium) might be concealed by the soil signature itself, since they occur in low quantities (Schaal *et al.* 2016: 271).

Considering phosphorus enrichments as a signature of the pit soil itself[36], i.e. of the soil formation within the pit, is implausible, since the enrichment pattern diverges from the pit outline at *Kurmin Uwa 2D*. The enrichments concentrate in a specific area and resemble neither the form nor the size of the pit.

[36] Although only at *Kurmin Uwa 2D* evidence for a burial pit was found, it is likely that all stone-pot-arrangements comprised burial pits.

10.2 Pit Features

Evidence for Waste Pits (Kusuma 1)

At *Kusuma 1*, the outcome of the pXRF analyses strongly suggests the disposal of waste in the investigated pits. This interpretation is based on the elemental signature that indicates the infill of large amounts of organic matter and complies with the archaeological evidence. The distribution of the signature correlated with two distinct pits with dark discolouration and poorly preserved finds as well as a concentration of charcoal (Fig. 10-2). The same elemental signature, although less significant, was also found at other Nok sites, mainly *Kurmin Uwa 1* and *Ido 2016*, and is interpreted in the same way (see chapter 9.2).

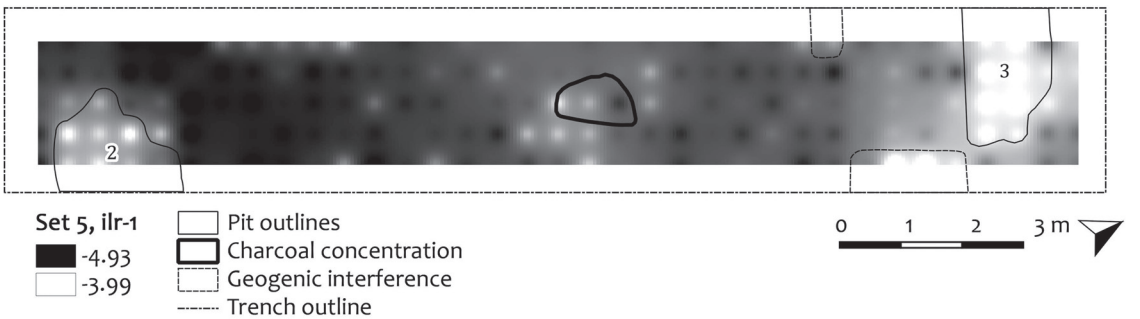

Fig. 10-2: Interpolation of the pit signature at *Kusuma 1*. The pit signature refers to the ilr-coordinate of set 5, which consists of the elements P, Y and Zn as well as Fe, Al, V, and Cr, which indicated enrichments as well as depletions, respectively. The interpolation pattern correlates both with the pits as well as the charcoal concentration in the middle of the trench.

The elemental signature identified at *Kusuma 1* is characterised by enrichments of phosphorus, zinc and yttrium, as well as depletions of iron, vanadium, chromium and aluminium, and can derive from the infill of organic matter.

Enrichments of phosphorus can originate from the disposal and decay of organic materials such as residues from food preparation, faeces or other organic waste (Middleton 2004: 53; Gauss *et al.* 2013: 2951). Zinc is relatively mobile, especially during weathering (Kabata-Pendias 2011: 275) but can be stabilised through complexation reactions with soil organic matter and phosphates (Kabata-Pendias 2011: 277; Oonk *et al.* 2009a: 42). Due to this correlation with organic matter, zinc is considered to be an indicator of rubbish pits (van Zwieten *et al.* 2017: 2). Yttrium occurs in silicates and phosphates (Kabata-Pendias 2011: 149), which can form insoluble precipitates (Kabata-Pendias 2011: 334). Iron and aluminium hydroxides are regarded as insoluble and resistant against weathering (Scheffer *et al.* 2010: 46; Strawn *et al.* 2015: 165), but the majority of iron occurs within iron oxides (Scheffer *et al.* 2010: 23). Iron oxides, in contrast, can deplete through redox reactions – caused by large amounts of organic matter under anaerobic conditions, e.g. during the rainy season (Oonk *et al.* 2009b: 1223; Scheffer *et al.* 2010: 166–167). The loss of vanadium and chromium is probably linked to iron, as they can be incorporated during the formation of iron oxides (Scheffer *et al.* 2010: 24). The depletion of aluminium is probably linked to the depletion of iron.

The infill of large amounts of organic matter interpreted as evidence for waste pits complies with the archaeological record. Besides one charcoal concentration in the middle of the trench, two distinctive pits with dark discolorations correlated with the elemental signature. The pits comprised charcoal, burnt clay as well as small and weathered potsherds – a find inventory concordant with the interpretation as waste. A few terracotta pieces and stone artefacts were found exclusively within the upper layers. The tub- or bowl-shaped form of the pits with a maximum depth of *c.* 50 cm (feature 2) and 80 cm (feature 3) and a maximum width of 2 m, declining to 1 m or less at the bottom, resembles a pit form that is intuitive and easy to dig.

One Pit – Many Explanations?

The interpretation of the pits as refuse dumps at *Kusuma 1* is based on the elemental signature indicating the infill of large amounts of organic matter and the overall archaeological evidence. However, the pXRF results at *Kusuma 1* solely refer to the sampled layer and since the pit stratigraphy indicated more than one layer, the obtained results merely represent a snapshot of the pit rather than the entire pit formation.

When visualising the 3-dimensional measurement data obtained during the excavation at *Kusuma 1*, two layers of the pit can be distinguished by the find composition and distribution (see Fig. 10-3). The evidence for organic infill refers to the lower layers of the pits, where the pXRF samples originated. These layers contained small and weathered potsherds, charcoal and burnt clay – finds consistent with a waste pit. However, the upper layers of the pits each revealed a complete but broken vessel associated with few terracotta fragments and a (fragmented) grinding stone. Even though these finds could also be

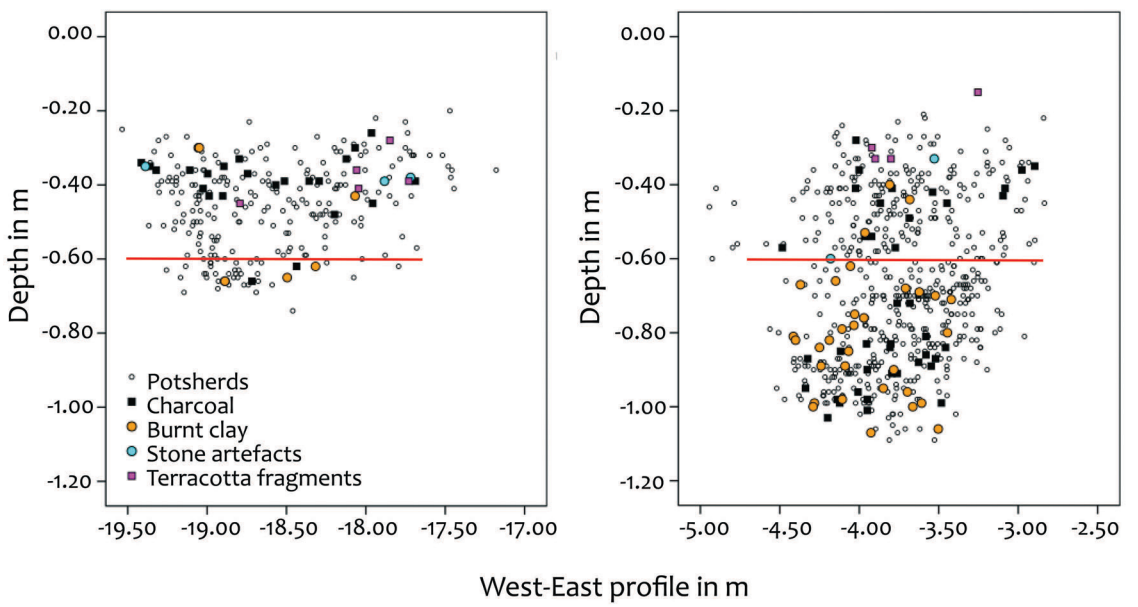

Fig. 10-3: Find composition and distribution in the West-East profiles of features 2 and 3 at *Kusuma 1*. Terracotta fragments are restricted to the upper layer of the pits, together with stone artefacts and remains of complete pots. The sampling (red line) refers to the lower layer, comprising finds of weathered potsherds, charcoal and burnt clay.

considered as waste from a different infill, the peculiarity lies in the recurrence of this find combination at other Nok sites, for example in feature 9 at *Pangwari* (Höhn *et al.* 2018: 293). The combination of (mostly broken) pots, terracotta fragments and single grinding stones is by far not as prominent as the stone-pot-arrangements, but they nevertheless seem to differ from mundane waste. Either way, the pit consists of two layers – regardless of their significance – and since the elemental signature refers to only one of those layers, any statements about the pit, its use and interpretation are thus restricted to this layer.

The lack of information relating to the site context impedes comprehensive interpretation of the pits as well. Even though the disposal of waste is proven as one function, it remains unknown in which context the pits occurred. On one hand, the overall archaeological evidence from the site of *Kusuma 1* suggests an interpretation as a settlement site. There is no evidence for stone-pot-arrangements or terracotta depositions and only twelve small terracotta fragments out of almost 1,000 finds were found. However, settlement remains such as hearths or huts are absent and depending on the trench size of excavated sites, undiscovered burial features could have remained unexcavated – especially since stone-pot-arrangements can occur at large depths within layers void of other finds. Furthermore, the upper layers within the pits indicate a secondary, yet unknown re-use of the pits.

Parts of the elemental signature identified at *Kusuma 1* were also present in pits at *Ido 2016* (see chapter 9.2). In contrast to *Kusuma 1*, the pits were located between stone-pot-arrangements and a terracotta deposition (Schmidt 2016). The presence of the same signature within a different site context demonstrates that it is possible to reconstruct the infill of organic matter as a performed event, but neither the reason nor the intention of the infill. At *Kusuma 1*, the infill could point to settlement waste, whereas the infill at *Ido 2016* could point to activities related to mortuary practices.

10.3 Nok Sites – a Patchwork Model

Based on the outcome of this thesis, it is possible to propose a model that provides a comprehensive explanation for the presumably ambiguous occurrence of finds and features on Nok sites. The model comprehends Nok sites as a patchwork of settlements and burial grounds that were re-visited and re-used throughout time and explains the archaeological record, which comprises multi-phased sites with multi-use pits.

The premise of this model is the concept of settlement burials, a tradition known in West Africa from other sites such as in northeast Nigeria (Connah 1981: 55). Settlement burials contradict a clear distinction of areas used as settlements and burial grounds. In combination with an assumed repetitive exploitation of these places, Nok sites appear as a patchwork of different types of use throughout the time.

This model implies the rejection of concepts that presuppose a separation of ritual and non-ritual areas. It refers to the early Middle Nok phase (*c.* 10th to 8th century), since the relevant feature types are attested for that time, whereas evidence from the Early and Late Nok phases is generally scarce.

The Archaeological Record and its Ambiguity

Pits, stone-pot-arrangements and terracotta depositions emerge in different constellations on Nok sites. Stone-pot-arrangements with nearby terracotta depositions suggest evidence for a burial ground, whereas the presence of adjacent pits with both settlement waste and intentional depositions raise questions about the site use. Such ambiguity also recurs within pits on assumed settlement sites.

Stone-pot-arrangements and nearby terracotta depositions, as observed at *Ifana 3*, are considered to be part of **burial grounds** (Breunig 2018: 399–400). Both feature types date to the Middle Nok phase, with a presumed emphasis during the early stage, between the 10th and 8th centuries BCE (Franke 2017: 56; see also chapter 7, Tab. 7-3). According to the obtained pXRF results and the archaeological evidence, stone-pot-arrangements represent burials. The terracotta depositions are both spatially and chronologically related and are assumed to belong to the same context. These depositions consist of large figurine fragments, which are considered as evidence for mortuary practices or an ancestor cult in a broader sense (Breunig 2018: 400; Wotzka 2017; Männel & Breunig 2016: 327–328; Breunig 2014). One indication for the use of the Nok terracottas as mortuary objects derives from the motif of the inverted pot depicted by some figurines (Wotzka 2017: 285–286) – a motif that recurs in the context of death, e.g. at the necropolis at *Bura-Assinda-Sikka* in Niger, dating between the 3rd and 10th centuries CE, where inverted jars of anthropomorphic design were used as grave markers (Wotzka 2017: 288; Gado 1993: 369–370). The use of terracotta figurines in funeral contexts is a common characteristic found at numerous West African sites[37].

[37] Pers. comm. André Burmann, Nok project, in the scope of his PhD thesis about the terracotta traditions in West Africa.

At other sites, such as *Pangwari* or *Ido 2016,* pits with unclear function are found between or adjacent to the stone-pot-arrangements and terracotta depositions. A representative example is the large pit (feature 11) at *Pangwari* (Schmidt 2014: 79–83): the pit contained finds considered to be settlement waste such as small potsherds, burnt clay and charcoal. However, other finds, such as a terracotta head associated with a grinding stone and a complete but broken pot – a combination that was also found at *Ido 2016* (Schmidt 2016: 65) – contradicts that interpretation. Furthermore, the location of the pit between stone-pot-arrangements and a terracotta deposition render the interpretation as a settlement pit unlikely. The pit and its ambiguity might be explained by funeral feasts, where both artefacts considered as ritual objects and settlement waste were used and afterwards disposed of in the pit (Höhn *et al.* 2018: 294–295; Schmidt 2014: 115). Pits in the context of mortuary practices are known from other sites, such as the site of *Nandá* in Equatorial Guinea, where extant remains were, together with associated objects, placed in small pits as secondary interments (González-Ruibal *et al.* 2013: 122, 140). As is known from the *Fali* in north Cameroon, burial traditions can be very complex and comprise several relocations of the body or bones (Wotzka 1993: 266–268).

Identifying settlement remains on Nok sites is difficult, mainly because hard evidence, such as huts or hearths, is absent (Breunig 2018: 394). Only pits are preserved in the soil and can provide evidence for settlements, in particular when occurring on sites without stone-pot-arrangements and terracotta depositions. Such a site is *Kusuma 1* and – according to the obtained pXRF results – the pits of this site were used for the disposal of waste. However, these pits comprised a second layer that probably developed from another, more ritual context. Similar findings were discovered on other sites in West and Central Africa (see chapter 4.2.2): at the Iron Age site of *Bwambé-Sommet* in Cameroon, large accumulations of potsherds, grinding stones and charred material found in a pit suggested it was used for refuse disposal, but indications of intentional arrangements contradicted this interpretation (Meister 2008: 48; Eggert 2006: 280–281).

Pits and pit-like structures, as potential evidence for settlements, cannot be definitely interpreted as such and hinder the search for settlements, since contents, contexts and the appearance of pits are inconclusive. Nor is it possible to identify other distinct functional areas due to the recurring ambiguity of ritual and non-ritual finds and features on Nok sites. This ambiguity represents the quintessence of problems associated with understanding Nok pits and Nok sites, since it impedes any conclusive interpretation (see chapter 4.1.2).

Nok Sites as a Patchwork – a Model

The perception of Nok sites as a patchwork of settlements and burial grounds, re-used at different times, provides an explanation for the recurring ambiguity within the pits and the occurrence of different feature types in various constellations. The concept of settlement burials, where the people buried their dead close to the living, causes the spatial and temporal superimpositions, which are the fundamentals of the patchwork model. In consequence, dismissing the concept of areas separated by their function or category, such as ritual or non-ritual, is the key to deciphering Nok sites.

The categorisation of ritual and non-ritual areas derives from a concept that is based on an artificial dichotomy. In the early 20th century, Durkheim (1912) postulated in his approach to understanding the basic principles of religion that there exists a dichotomy between two domains – *sacred* and *profane* – and that rites, considered as religious rituals,

embody rules of conduct for the treatment of sacred things (Durkheim 1995: 34–38). Rituals, in their contemporary understanding, are not restricted to religious acts and can, for example, incorporate a social role to meet and sustain the needs of a group (Bell 2009: 27). Rituals are multifaceted and there is no universal understanding of ritual (Bell 2009: 164), but most definitions imply a 'symbolic, non-technical, formal, prescribed, structured, and repetitive nature' (Brück 1999: 314). A key point to distinguish rituals from mundane routines is their symbolic power, which dissociates ritual acts from triviality (D'Orsi & Dei 2018: 116–117; Brück 1999: 315).

In the case of the Nok Culture, the archaeological record provides evidence for rituality on different levels. Beck (2017) stated a ritual complexity for the Nok Culture that is expressed by the manufacture of terracotta figurines as a symbol of identity (Beck 2017: 135–138; Breunig & Rupp 2016: 253). Another, more tangible rituality manifests itself through the destruction of terracotta figurines and their deposition in the ground (Breunig 2014: 266–272; Rupp 2014: 215; Männel & Breunig 2016: 327; Burmann 2016: 124–125). The verification of nearby stone-pot-arrangement as burials through pXRF analysis strengthens the assumption that terracotta figurines (and their destruction) are related to burial rites (Breunig 2018: 400; Wotzka 2017). These rituals can be considered as *rites of passage*, i.e. rituals associated with transitions between life stages – in this case death (Bell 2009: 94).

However, a dissociation of burial grounds as areas of performed rituality – as well as any other ritual areas – from areas with a different function, including non-ritual activities, is not compulsory. The concept of distinct segregation traces back to Durkheim and his perception of a dichotomy that entails exclusivity. The scheme developed by Durkheim originally refers to a conceptual system, although it can impact the tangible world, e.g. expressing itself in distinct spatial patterns. However, without a profound knowledge of the immaterial world it seems impossible to understand a spatial pattern that refers to it. Apart from the non-existent knowledge about the belief system of the Nok Culture, numerous societies, such as the *LaDooga* of northern Ghana (Goody 1961: 151), do not employ distinctions such as 'ritual-secular' or 'sacred-profane' (Brück 1999: 319). Furthermore, rituals can manifest in numerous activities and involve objects that are considered to be mundane or non-ritual (Bell 2009: 138). For example, the disposal of waste can transmit symbolic content (Gifford-Gonzalez 2014: 342) or could have been part of a ritual that we cannot retrace.

Regardless of whether and how the Nok people perceived concepts of rituality, the archaeological record contradicts an exclusivity of ritual and non-ritual areas, i.e. in this case, burial grounds with performed rituality and settlement sites. On the contrary, the composition of finds and features on Nok sites suggests a conjoint occurrence of settlements and burial grounds (and probably other functional areas) that were re-visited and re-used throughout different periods, forming a patchwork. The patchwork model proposes the following scenario: based on the evidence during the Middle Nok phase, it is likely that the people settled at one place for a certain time span in scattered farmsteads or dispersed settlements (Breunig & Rupp 2016: 245; Breunig 2018: 394–395) and the dead were buried within or close to these settlements. Settlements with adjacent cemeteries are also known from Stone and Iron Age sites from northeast Nigeria, where inhumations were often located within settlements (Connah 1981: 55). For example, at *Kursakata* as well as *Daima I* and *II*, the dead were buried in or near the settlement (Connah 1981: 115, 150); at *Borno 38*, parts of the settlement were formerly a cemetery (Connah 1981: 95).

Nok sites did not persist for a long time, since the settlements are considered to have been re-located every few years, as indicated by the brief occupation episodes (Breunig & Rupp 2016: 245) and the shifting cultivation system (Höhn & Neumann 2016: 332). The patchwork model not only assumes the shift of farmland, settlements and burial grounds, but also the subsequent re-visiting and re-use of the formerly abandoned land. The return to abandoned settlements and utilised areas is also proven by the sequence of ^{14}C dates at Nok sites (Franke 2017: 57; Schmidt 2014: 114–115; Breunig & Rupp 2016: 244; Höhn *et al.* 2018). It remains unclear, however, whether the re-visiting of abandoned sites was linked to ancestor cults or whether the sites were economically favourable, e.g. due to soil properties or microclimatic conditions.

The cycle of utilising, abandoning and subsequently re-using land, regardless of function, would result in a patchwork of settlements and burial grounds (and other functional areas) throughout different phases, i.e. in an archaeological record that comprises different find and feature constellations dating to different time periods.

10.4 pXRF Analysis – Potentials & Pitfalls

Multi-element analyses of soils require caution and awareness in order to avoid potential bias and pitfalls. The success of the method on Nok sites is based on the systematic and methodical concept of this thesis, that prevented technical or methodological flaws. This included assessing the limitations of the device and improving the sample preparation (chapter 5), studying the origin, influence and behaviour of elements (chapter 6) as well as an appropriate statistical treatment of the data (chapter 8).

Data Analysis – is there a 'Ground Truth'?

To reveal the relevant information hidden in the soil, a careful and sensible analysis of the data is essential. In chapter 8, different methods of data analysis concordant with the nature of the data were studied. The peculiarity of elemental analysis with soil as a data source lies in a single trait that has manifold consequences: the data are compositional (see chapter 8.1). Having accepted this principle and its consequences, the necessity for an adequate statistical treatment becomes evident.

From the moment of sampling, the soil carries *relative* information about the elements, which reveal their significance only when analysed in relation to the other elements (Aitchison 1992: 368; Aitchison & Egozcue 2005: 830; Pawlowsky-Glahn *et al.* 2015: 23; Tolosana-Delgado 2012: 77). In order to truly understand this premise and its consequences, it is crucial to comprehend that this is not a method-based, but a principle-based constraint. Soil samples carry specific information, regardless of which analytical techniques were applied or whether the results are given in ppm or in mg/g – all values relate to a constant sum and their information lies in the relationship between elements and not within one element (Pawlowsky-Glahn *et al.* 2015: 8–9).

These specific properties of geochemical soil data require statistical approaches that respect the compositional character of the data. Interpolating and interpreting a single element by discarding the remaining elements is tempting and single element maps are often considered as reflecting the 'objective ground truth' (McKinley *et al.* 2016: 17). This is a widespread yet rarely noticed pitfall and is still the subject of discussions (Reimann *et al.* 2012: 197; Filzmoser *et al.* 2009; Filzmoser *et al.* 2010). This statistical issue is stated as a problem for 'mathematical freaks' (Filzmoser *et al.* 2009: 6100), especially as univariate analysis can yield allegedly interpretable and meaningful results (Reimann *et al.* 2012: 208). Besides, problems can evolve even before analysing the data, as e.g. linear calibrations (see chapter 5.2) change the constant sum by aligning the results of measurements. In this thesis, the changes were marginal and have not distorted the outcome. However, this approach should be considered as a potential pitfall and it seems more useful to either rely on the factory calibration or to use a calibration technique which preserves the constant sum.

Most of the pitfalls can be overcome by respecting the nature of the data. According to the state of research, an adequate statistical treatment is using log-ratio transformations (Aitchison 1986; Egozcue *et al.* 2003; Aitchison & Egozcue 2005: 830). Since compositional data cannot be interpreted directly, a careful observation of the data is crucial to extract the relevant information. A combination of different methods, such as ilr-transformations, clr-biplots and variation arrays, has proven to be a suitable approach. Ilr-transformations

are particularly meaningful: they require a re-thinking in terms of balances, i.e. not single elements, but the relationship between these is the subject of the analyses, which resonates with the nature of the data (Egozcue & Pawlowsky-Glahn 2005).

Applying statistics in accordance with the properties of compositional data also circumvents problems of finding adequate reference samples. Other approaches, such as enrichment factors, require a comparison with stable reference samples representing the 'average soil'. This poses a potential source of errors as the reference samples can originate from geochemical variations or anomalies. The lack of a stable element in the soil for reference is the reason why this approach was not useful for this thesis (see chapter 8.3.1.2).

Soil Palimpsests

The soil as an object of study is an open system, constantly affected by changes (Scheffer *et al.* 2010: 5, 43) with an inherent elemental signature that is influenced by numerous factors. These processes can change or superimpose archaeological traces and result in a soil palimpsest, as described by Entwistle *et al.* (1998: 63). The archaeological signature, i.e. the relevant information, is entangled within this soil palimpsest, which is why differentiating natural and anthropogenic signatures is so challenging. To decipher the signatures imprinted in the soil and to differentiate anthropogenic from geogenic signatures, the soils, their characteristics and properties within the research area were examined (chapter 3). Knowledge about the occurrence and behaviour of elements within the soil were also gathered (chapter 6.5) and the representativeness of the samples ensured (chapter 5.3).

Important determinants for the formation of the soil and thus its inherent elemental signature are environmental factors such as climate, vegetation, geomorphology, geology, and lithology (FAO-UNESCO 1977: vii). Site lithology in particular has a significant effect and geochemical background noise can conceal anthropogenic signatures (Oonk *et al.* 2009b; Schmidt 2016). Even under ideal circumstances, the analyses at two very similar sites with the same parameters have proven to yield site-specific outcomes (Wilson *et al.* 2009: 2333). External influences furthermore constantly affect the soil, such as impact from flora and fauna. Termites, for example, can embed a thin layer of material in the soil, which influences the physical and chemical soil properties or they can consume organic matter, which results in low humification with depletions of phosphorus (Eitel 2001: 176–179). Bush fires can cause an enrichment of calcium, potassium and magnesium in strongly chemically weathered soils (Eitel 2001: 176–177). Modern anthropogenic impacts, such as the use of chemical fertilizers, fungicides or insecticides, can be a source of various alkali and alkaline earth metals as well as transitional metals such as chromium, copper, nickel, zinc, and lead (Sutherland 2000: 612, Tab. 1; Kabata-Pendias 2011: 139; Oonk *et al.* 2009a: 36–37).

To understand which and how elements influence the soil and vice versa, key properties of both the soil and the elements were studied (chapter 3 and chapter 6.5). This includes soil acidity and weathering processes as well as the behaviour of elements, such as affinities to other elements or their mobility. Since the samples taken furthermore represent an excerpt of this soil palimpsest and to ensure representativeness, analysis of the effect of the sample preparation were conducted (see chapter 5.3). Sample heterogeneity and sample preparation can also be a source of error (Johnson 2014: 565; Oonk *et al.* 2009a: 37). These

investigations, although costly in terms of labour, prevented technical flaws and saved time and effort[38] without loss of information.

Elemental Signatures – Chemical 'Fingerprint' of an Event?

The interpretation of identified elemental signatures requires knowledge about their formation and occurrence. The review of archaeological signatures in chapter 6.2 illustrated that one process can result in multiple signatures and vice versa. Forensic and archaeological studies of grave soils demonstrated that there is a discrepancy between the elements we assume to find and the elements we find *de facto* (chapter 6.4). By analysing soils from a modern Fulani village, it was possible to assign revealed elemental signatures to specific activities or utilised areas (chapter 6.3). Even though the obtained results were not applicable to the Nok sites, the potential of the method was proven once again.

Soil elemental analyses are based on the premise that human activities or infills inscribe a specific 'fingerprint' in the soil, which enables the identification of the performed events. The literature review of elemental signatures (chapter 6.2, Table 6-1) illustrates that chemical fingerprints, unique elemental signatures resulting from a specific action, do not exist. Even though the event or infill itself incorporates a characteristic signature, e.g. the burning of one specific wood type, this signature is modified and perhaps even concealed by the soil, the environment and modern impacts, which, ultimately, can result in different signatures. Nor does one event always generate the same signature, and a certain element is not restricted to one origin. Furthermore, there is little knowledge about the origin of the elements. Copper, for example, is known to correlate with human impact as reported from different studies, but the archaeological sources are far from confirmed (Oonk *et al.* 2009b: 1224).

Nevertheless, the review of the literature demonstrated that there are common tendencies and recurring patterns, which can help to identify and interpret the original elemental signature. This was affirmed by the results of the Fulani village – although the signatures appear very similar, they differ and can be specified by employing further analysis. Furthermore, context-based knowledge is more reliable than information derived from other contexts. Utilising modern references make it possible to precisely retrace and reconstruct the performed events, which were responsible for the elemental signature (Middleton *et al.* 2010: 205–206). One pitfall when applying knowledge derived from other contexts is misinterpretation based on site-specific parameters. For example, results of a study on former land-use at Scottish sites revealed enrichments of calcium and strontium on former agricultural land – but these enrichments are due to the use of shell sand as a fertilizer (Entwistle *et al.* 1998: 65) and cannot be taken as a generally valid indicator for agricultural land.

Sampling Strategies

The attempt to uncover the use of the Nok Culture pits, to identify activity areas and to decipher the pattern of Nok sites was strongly impeded by the multi-phased and multi-

[38] A grinding of the more than 3,000 measured samples would have required *c.* 250 additional working hours, when calculating 5 minutes/sample, including grinding and cleaning of the ball mill.

used character of the sites. The major reason, however, for the limited results and negative outcomes on most sites was the disadvantageous site selection and sampling strategies.

Apart from the burial sites excavated in 2016 at *Ido*, *Ifana 3* and *Kurmin Uwa 2D*, all samples were taken prior to this thesis[39]. Adjusted sampling of pit features, especially vertically, was planned in 2017 at *Ifana 5* but never conducted since the excavation was cancelled. Most samples were taken in 2010 and 2011, when the majority of Nok sites were excavated in order to establish a refined chronology (see chapter 2.2), which is the reason why numerous, but small-scale excavations were carried out. At that point in time, unawareness of the multi-phased character of the sites adversely affected the sampling. Although the sampling of the large-scale excavation at *Pangwari* (Schmidt 2014) was promising, it turned out that most of the samples originated from a disturbed layer (Höhn *et al.* 2018: 277). In hindsight, the applied sampling strategies on most excavations were insufficient for these adverse conditions on Nok sites: sampling was limited to one layer, which precludes statements about the whole formation history of the sites and features, the grid size was too large as features comprised only a single sample, or suitable reference samples were missing. The sampling strategies in combination with the adverse conditions on Nok sites are thus considered responsible for a negative outcome and the reason why only selected Nok sites were analysed in this thesis (see chapter 7.1).

Sampling, in general, is a difficult topic in terms of choosing the proper sample height and grid size. A dense grid size generates results with a high-resolution, but sampling also delays the excavation and sample preparation and measurements require time and effort. At *Ido 2016*, for example, one trench (*c.* 40 m²), sampled in a 25 cm grid, yielded more than 600 samples, which resulted in *c.* 100 working hours. Sampling has to be adjusted individually – and in case of the pit features, sampling restricted to one layer without vertical sampling turned out to be insufficient. Vertical sampling from several layers in particular can reveal valuable information both about pit use and the formation history of sites and features.

The outcome at *Kusuma 1* has proven a success for the method, if specific site-related parameters are conducive. The site was located on a plain, the find distribution indicated no mixture of material and the sampling was not performed on a disturbed layer. The pXRF element analysis revealed satisfying results in terms of distinguishing pits from the surroundings as well as identifying and interpreting their elemental signature as being derived from large amounts of organic infill.

[39] The samples were taken for a similar PhD thesis carried out by K.-P. Nagel until 2014 (see Nagel 2014).

11 Conclusion and Outlook

Employing pXRF multi-element analysis as a tool in archaeological research can facilitate the identification of human impact on archaeological sites. The conducted analyses successfully verified that stone-pot-arrangements were burials and proved the suitability of the method for reconstructing performed activities by identifying and interpreting pit infills. Nevertheless, a sensible approach is necessary to avoid its possible bias and pitfalls.

The outcome of the pXRF analyses of the **stone-pot-arrangements** supports the archaeological research and proves the benefit of employing pXRF multi-element analyses. The confirmation of this feature type as a burial through phosphorus enrichments grants insight into the mortuary practices of the Nok Culture and enlightens the function and context of the terracotta figurines as part of a death cult. Furthermore, pXRF analyses revealed another potential burial type, in the form of a stone-arrangement without grave goods at *Pangwari*, which otherwise would have remained unidentified. The significance of the results is premised on the lack of alternatives to provide evidence for a dead body. According to the current state of research, only a few forensic methods exist to prove the former presence of a body that has subsequently completely decayed and these are only successful when decay occurred recently[40]. One potential long-term approach was tested but the absence of exploitable material in the acidic soil has eliminated its application. However, since pXRF analyses cannot provide *hard* evidence for a decomposed body and in order to support the obtained pXRF results, additional methods should be employed for future work. Lipid analysis could provide further indications of a decomposed body through evidence of adipocere and ICP-based techniques enable the measurement of further grave soil elements that are not quantifiable by pXRF devices, such as carbon. This information, in combination with soil pH values, can furthermore help to distinguish geogenic anomalies from anthropogenic sources. When utilising supportive methods, the obtained pXRF results also serve as a useful indicator for promising samples, especially since the mentioned techniques are expensive and labour-intensive. Furthermore, sampling in a dense 10 cm grid both horizontally and vertically, which enables the rendering of a 3-dimensional distribution pattern, should also be considered for future studies.

Elemental analysis of **pits** confirmed the potential of the method and its suitability for future analyses. The method supports the archaeological research as it enables the reconstruction of performed actions on sites and within features, such as the infill of organic matter at *Kusuma 1*. The analyses succeeded in spite of adverse conditions, when considering the age of the sites, the soil properties and strong erosion of the research area. The difficulties of revealing a definite function of the pits trace back to their multi-phased use and multiple uses. Limitations were set by the sampling scheme, since the results referred to the sampled layer and represent a snapshot rather than the entire pit formation. By employing an improved strategy, in particular vertical sampling, information on all layers can be obtained. In combination with pedological analysis to understand soil formation and further approaches to specify the pit content, such as archaeobotanical studies, it could be possible to both reconstruct the entire pit formation and its multiple functions. Furthermore, future analysis should take into account the possibility that pits represented a further potential burial type or were used for secondary interments. The approach of

[40] Pers. comm. Jens Amendt from 14-03-2017 and Marcel A. Verhoff from 13-12-2017, Institute for Legal Medicine, University Hospital Frankfurt.

pXRF analysis, in particular in combination with supplementary studies, may also help to unravel the *pit phenomenon* of West and Central Africa.

The **patchwork model** proposed in this thesis offers an explanation for the formation and layout of Nok sites. Through the process of re-visiting and re-using previously abandoned settlements and burial grounds, Nok sites appear as a patchwork of areas and features used in several contexts at different times. A key property of this model is the assumption that areas with performed rituality, such as burial grounds, were not spatially separated from other, allegedly non-ritual areas, such as settlements. The usage of such settlement burials in combination with repetitive exploitation of these sites explains the presumed ambiguity of finds and feature compositions on Nok sites. The discussion around concepts of rituality has lasted for more than a century and this thesis does not aim to solve but to reiterate these issues. In accordance with the pXRF analyses, it appears more rewarding to concentrate on concrete evidence rather than elusive perceptions such as rituality and to focus on 'rationality', i.e. on what the actions tell us (Brück 1999: 326–327). The reconstruction of infills, e.g. derived from organic matter or fire exposure, grants insight into performed actions and can reveal former usage. This seems more relevant and fruitful than the attempt to decipher activities and intentions in terms of being ritual or non-ritual.

Multi-element analyses with pXRF are a powerful tool to reveal hidden information, as proven by the obtained results. In general, the prominence and use of pXRF devices in archaeological research has grown continually over the last few years. Convincing advantages are its rapid analysis with suitable precision for many elements, its portability which allows in situ analysis and the non-destructive character of the method (Goodale *et al.* 2012: 882). However, multi-element analyses of soils can be challenging and there is a danger of misuse and misinterpretations. There is still a lack of basic research on the methodology of pXRF analysis, especially for its application on archaeological soils. With the growing use of this device, operating and analysis errors have also increased, resulting in misinterpretations. This has been the topic of many discussions throughout the last decade, addressing aspects such as the measurement of standards, system reliability and qualitative versus quantitative analysis (Shackley 2010: 19). Geological materials are problematic to measure due to effects of lithic materials, e.g. grain size or mineralogy, as well as the occurrence of light elements (Goodale *et al.* 2012: 882). Especially for soil analysis, the acceptance of this method is not fully established, mainly due to the low amount of peer-reviewed papers, the complex influence of soil chemistry, the lack of knowledge about the source of elements and whether anomalies are caused naturally or anthropogenically (Oonk *et al.* 2009: 35–36). Nevertheless, most of the problems and pitfalls can be overcome with a better understanding of the soil properties, the elements and their behaviour as well as proper data treatment. The knowledge about elemental signatures grows with every conducted case study and future work on ethnoarchaeological studies can help to retrace and reconstruct element formations. When applying a sensible data treatment, most statistical pitfalls can be avoided. A re-thinking of the statistical method that complies with the compositional data structure is the key – instead of single elements, the relation *between* elements should be studied. This can be achieved by combining approaches such as ilr-transformations, clr-biplots and variation arrays.

12 Summary

pXRF multi-element analysis of features of the Nigerian Nok Culture, dating from *c.* the 15th century BCE until the end of the 1st century BCE, succeeded in identifying and interpreting elemental signatures associated with human impact. The confirmation of assumed burials grants insight into burial rites and the reconstruction of performed activities sheds light on the use of pit features. Both outcomes culminated in a model that perceives Nok sites as a patchwork of settlements and burial grounds without distinctive functional zones or areas segregated into ritual or non-ritual activities.

The discovery of phosphorus enrichments within seven stone-pot-arrangements, features considered to be burials but without preserved bones or other human remains, strongly suggest the presence of decomposed bodies. The feature layout and the spatial distribution of phosphorus furthermore indicate the interment of bodies in a flexed position.

Elemental signatures of pits facilitated the reconstruction of the use of some pits for the disposal of waste by identifying the infill of organic matter. However, since sampling was restricted to one layer, the obtained results reflect a snapshot of the pit use rather than the entire formation history.

The proposed patchwork model for Nok sites assumes a repetitive cycle of utilising land for farming, settlements and burials, followed by abandonment and subsequent re-visiting and re-use of the formerly abandoned land. It favours the concept of settlement burials and rejects a dissociation of areas with performed rituality, such as burial grounds, from areas with unproven rituality, such as settlement sites.

The systematic approach of this thesis prevented potential flaws and misinterpretations. Use of the pXRF device factory calibration settings as well as sieving the sample soil to < 125 µm turned out to be sufficient. The selected statistical approach, taking into consideration the compositional structure of the data, comprised log-ratio transformations, in particular isometric log-ratio transformations, and centred log-ratio biplots.

Bibliography

Abaje, I., Ishaya, S. & Usman, S. 2010. An Analysis of Rainfall Trends in Kafanchan, Kaduna State, Nigeria. *Research Journal of Environmental and Earth Sciences* 2(2), 89–96.

Abaje, I., Sawa, B., Iguisi, E. & Ibrahim, A. 2016. Impacts of Climate Change and Adaptation Strategies in Rural Communities of Kaduna State, Nigeria. *Ethiopian Journal of Environmental Studies and Management* 9(1), 97–108.

Abrahams, P., Entwistle, J. & Dodgshon, R. 2010. The Ben Lawers Historic Landscape Project: Simultaneous Multi-Element Analysis of Former Settlement and Arable Soils by X-Ray Fluorescence Spectrometry. *Journal of Archaeological Method and Theory* 17(3), 231–248.

Aitchison, J. 1981. A New Approach to Null Correlations of Proportions. *Mathematical Geology* 13(2), 175–189.

Aitchison, J. 1982. The Statistical Analysis of Compositional Data. *Journal of the Royal Statistical Society. Series B (Methodological)* 44(2), 139–177.

Aitchison, J. 1983. Principal Component Analysis of Compositional Data. *Biometrika* 70(1), 57–65.

Aitchison, J. 1984. The Statistical Analysis of Geochemical Compositions. *Mathematical Geology* 16(6), 531–564.

Aitchison, J. 1986. *The Statistical Analysis of Compositional Data.* Chapman and Hall, London.

Aitchison, J. 1992. On Criteria for Measures of Compositional Difference. *Mathematical Geology* 24(4), 365–379.

Aitchison, J. & Egozcue, J. 2005. Compositional Data Analysis. Where Are We and Where Should We Be Heading? *Mathematical Geology* 37(7), 829–850.

Aitchison, J. & Greenacre, M. 2002. Biplots of Compositional Data. *Journal of the Royal Statistical Society: Series C (Applied Statistics)* 51(4), 375–392.

Aitkenhead-Peterson, J., Owings, C., Alexander, M., Larison, N. & Bytheway, J. 2012. Mapping the Lateral Extent of Human Cadaver Decomposition with Soil Chemistry. *Forensic Science International* 216(1-3), 127–134.

Arrhenius, O. 1931. Die Bodenanalyse im Dienst der Archäologie. *Zeitschrift für Pflanzenernährung, Düngung, Bodenkunde* 10, 427–439.

Atangana, C. 1988. *Archéologie du Cameroun Méridional: Étude du Site d'Okolo.* PhD thesis, Université Panthéon-Sorbonne, Paris.

Bacon-Shone, J. 2011. A Short History of Compositional Data Analysis. In: Pawlowsky-Glahn, V. & Buccianti, A. (eds.) *Compositional Data Analysis. Theory and Applications.* Wiley, Hoboken, 3–11.

Beck, C. 2017. *The Value of Art. Studies in the Material Character of the Terracotta Figurines of the Nok Culture of Central Nigeria.* Verlag Dr. Hut, München.

Beckhoff, B. 2006. *Handbook of Practical X-ray Fluorescence Analysis.* Springer, Berlin/New York.

Bell, C. 2009. *Ritual. Perspectives and Dimensions.* Oxford University Press, Oxford.

Bennett, J., Blair Rains, A., Gosden, P., Howard, W., Hutcheon, A., Kerr, W., Mansfield, J., Rackham, L. & Rose Innes, R. 1979. *Land Resources of Central Nigeria. Agricultural Development Possibilities. Volume 5B Kaduna Plains.* Ministry of Overseas Development, Surrey.

Benninger, L., Carter, D. & Forbes, S. 2008. The Biochemical Alteration of Soil Beneath a Decomposing Carcass. *Forensic Science International* 180(2-3), 70–75.

Bethell, P. & Carver, M. 1987. Detection and Enhancement of Decayed Inhumations at Sutton Hoo. In: Boddington, A. (ed.) *Death, Decay and Reconstruction. Approaches to Archaeology and Forensic Science.* Manchester University Press, Manchester, 10–21.

Bethell, P., Goad, L., Evershed, R. & Ottaway, J. 1994. The Study of Molecular Markers of Human Activity: The Use of Coprostanol in the Soil as an Indicator of Human Faecal Material. *Journal of Archaeological Science* 21(5), 619–632.

Bethell, P. & Smith, J. 1989. Trace-Element Analysis of an Inhumation from Sutton Hoo, Using Inductively Coupled Plasma Emission Spectrometry: An Evaluation of the Technique Applied to Analysis of Organic Residues. *Journal of Archaeological Science* 16(1), 47–55.

Borggaard, O., Jørgensen, S., Møberg, J. & Raben-Lange, B. 1990. Influence of Organic Matter on Phosphate Adsorption by Aluminium and Iron Oxides in Sandy Soils. *Journal of Soil Science* 41(3), 443–449.

Boullier, C. 2001. *Recherches Méthodologiques sur la Sculpture en Terre Cuite Africaine: Application à un Corpus de Sculptures Archéologiques - en Contexte et Hors Contexte - De la Culture Nok (Nigéria).* PhD thesis, Université Panthéon-Sorbonne, Paris.

Boullier, C. 2008. Nok, Sokoto and Katsina Archaeological Cultures. In: Anquandah, J., Morin, F. & Wastiau, B. (eds.) *African Terra Cottas. A Millenary Heritage: in the Barbier-Mueller Museum Collections.* Somogy éditions d'art, Musée Barbier-Mueller, Paris, Genève, 188–201.

Breunig, P. 2009a. Cultural Change in the First Millenium BC – Evidence from Nigeria, West Africa. In: Magnavita S. (ed.) *Crossroads/Carrefour Sahel. Cultural and Technological Developments in First Millennium BC/AD West Africa.* Africa Magna, Frankfurt am Main, 15–26.

Breunig, P. 2009b. Die früheisenzeitliche Nok-Kultur in Zentral-Nigeria, Westafrika. Neues archäologisches Langfristprojekt der Deutschen Forschungsgemeinschaft. *Archäologisches Nachrichtenblatt* 14(4), 341–360.

Breunig, P. 2012. Understanding Nok Terracotta Art. *Tribal Art* 65, 84–99.

Breunig, P. 2013. *Nok. Ein Ursprung afrikanischer Skulptur.* Africa Magna, Frankfurt am Main.

Breunig, P. 2014a. *Nok – African Sculpture in Archaeological Context.* Africa Magna, Frankfurt am Main.

Breunig, P. 2014b. Some Thoughts on the Purpose of the Nok Sculptures. In: Breunig, P. (ed.) *Nok – African Sculpture in Archaeological Context.* Africa Magna, Frankfurt am Main, 256–272.

Breunig, P. 2018. Die Skulpturen der Nok-Kultur Nigerias. Ein Beispiel für hoch spezialisiertes Handwerk einer vor-staatlichen Gesellschaft. In: Meller, H., Gronenborn, D. & Risch, R. (eds.) *Überschuss ohne Staat – Politische Formen in der Vorgeschichte (Tagungen des Landesmuseums für Vorgeschichte Halle 18).* Landesamt f. Denkmalpflege u. Archäologie Sachsen-Anhalt, Halle, 387–405.

Breunig, P. & Rupp, N. 2010. Outline of a New Research Project on the Nok Culture of Central Nigeria, West Africa. *Nyame Akuma* 73, 46–54.

Breunig, P. & Rupp, N. 2016. An Outline of Recent Studies on the Nigerian Nok Culture. *Journal of African Archaeology* 14(3), 237–255.

Bronk Ramsey, C. 2009. Bayesian Analysis of Radiocarbon Dates. *Radiocarbon* 51(1), 337–360.

Brück, J. 1999. Ritual and Rationality: Some Problems of Interpretation in European Archaeology. *European Journal of Archaeology* 2(3), 313–344.

Bull, I., Berstan, R., Vass, A. & Evershed, R. 2009. Identification of a Disinterred Grave by Molecular and Stable Isotope Analysis. *Science & Justice: Journal of the Forensic Science Society* 49(2), 142–149.

Burmann, A. L. R. F. 2016. *Die archäologischen Fundkontexte von Terrakotten der Nok-Kultur Zentralnigerias (1500 v. Chr. bis um die Zeitenwende) an ausgewählten Befunden.* M.A. thesis, Goethe-Universität Frankfurt.

Carranza, E. 2017. Geochemical Mineral Exploration. Should We Use Enrichment Factors or Log-Ratios? *Natural Resources Research* 26(4), 411–428.

Carter, D., Yellowlees, D. & Tibbett, M. 2007. Cadaver Decomposition in Terrestrial Ecosystems. *Naturwissenschaften* 94(1), 12–24.

Casey, J. 2000. *The Kintampo Complex. The Late Holocene on the Gambaga Escarpment, Northern Ghana.* Archaeopress, Oxford.

Chester, R. & Stoner, J. 1973. Pb in Particulates from the Lower Atmosphere of the Eastern Atlantic. *Nature* 245(5419), 27–28.

Clist, B. 2005. *Des Premiers Villages aux Premiers Europeens Autour de L'Estuaire du Gabon. Quatre Millenaires d'Interactions entre l'Homme et son Milieu.* PhD thesis, Université Libre de Bruxelles.

Comas, M. & Thió-Henestrosa, S. 2011. CoDaPack 2.0: A Stand-Alone, Multi-Platform Compositional Software. In: Egozcue, J. J., Tolosana-Delgado, R. & Ortego, M. I. (eds.) *Proceedings of the 4th International Workshop on Compositional Data Analysis (2011),* 1–10.

Connah, G. 1976. The Daima Sequence and the Prehistoric Chronology of the Lake Chad Region of Nigeria. *The Journal of African History* 17(3), 321–352.

Connah, G. 1981. *Three Thousand Years in Africa.* Cambridge University Press, Cambridge.

Cook, D., Kovacevich, B., Beach, T. & Bishop, R. 2006. Deciphering the Inorganic Chemical Record of Ancient Human Activity Using ICP-MS: a Reconnaissance Study of Late Classic Soil Floors at Cancuén, Guatemala. *Journal of Archaeological Science* 33(5), 628–640.

Cook, S., Banerjea, R., Marshall, L.-J., Fulford, M., Clarke, A. & van Zwieten, C. 2010. Concentrations of Copper, Zinc and Lead as Indicators of Hearth Usage at the Roman Town of Calleva Atrebatum (Silchester, Hampshire, UK). *Journal of Archaeological Science* 37(4), 871–879.

D'Orsi, L. & Dei, F. 2018. What is a Rite? Émile Durkheim, a Hundred Years Later. *Open Information Science* 2(1), 115–126.

Danver, S. L. 2015. *Native Peoples of the World.* Taylor and Francis, Hoboken.

Davies, B., Bintliff, J., Gaffney, C. & Water, A. 1988. Trace Metal Residues in Soil as Markers of Ancient Site Occupation in Greece. In: Hemphill, D. D. (ed.) *Proceedings of the 22nd Trace Substances in Environmental Health Symposium.* University of Missouri, St. Louis, 391–398.

Davies, O. 1980. The Ntereso Culture in Ghana. In: Swartz, B. K. & Dumett, R. E. (eds.) *West African Culture Dynamics. Archaeological and Historical Perspectives.* Mouton, The Hague, 205–225.

Dent, B., Forbes, S. & Stuart, B. 2004. Review of Human Decomposition Processes in Soil. *Environmental Geology* 45(4), 576–585.

Dewitte, O., Jones, A., Spaargaren, O., Breuning-Madsen, H., Brossard, M., Dampha, A., Deckers, J., Gallali, T., Hallett, S., Jones, R., Kilasara, M., Le Roux, P., Michéli, E., Montanarella, L., Thiombiano, L., van Ranst, E., Yemefack, M. & Zougmore, R. 2013. Harmonisation of the Soil Map of Africa at the Continental Scale. *Geoderma* 211-212, 138–153.

Durkheim, É. 1912. *Les Formes Élémentaires de la Vie Religieuse: le Système Totémique en Australie.* Librairie Félix Alcan, Paris.

Durkheim, É. 1995. *The Elementary Forms of Religious Life.* The Free Press, New York.

Eggert, M. K. H. 2006. Pits, Graves and Grains: Archaeological and Archaeobotanical Research in Southern Cameroon. *Journal of African Archaeology* 4(2), 273–298.

Eggert, M. K. H. 2014. Early Iron in West and Central Africa. In: Breunig, P. (ed.) *Nok – African Sculpture in Archaeological Context.* Africa Magna, Frankfurt am Main, 50–59.

Eggert, M. K. H. & Seidensticker, D. 2016. *Campo.* Heinrich-Barth-Institut, Köln.

Egozcue, J. & Pawlowsky-Glahn, V. 2005. Groups of Parts and Their Balances in Compositional Data Analysis. *Mathematical Geology* 37(7), 795–828.

Egozcue, J. & Pawlowsky-Glahn, V. 2011. Basic Concepts and Procedures. In: Pawlowsky-Glahn, V. & Buccianti, A. (eds.) *Compositional Data Analysis. Theory and Applications.* Wiley, Hoboken, 12–28.

Egozcue, J., Pawlowsky-Glahn, V., Mateu-Figueras, G. & Barceló-Vidal, C. 2003. Isometric Logratio Transformations for Compositional Data Analysis. *Mathematical Geology* 35(3), 279–300.

Eitel, B. 2001. *Bodengeographie.* Westermann, Braunschweig.

Entwistle, J., Abrahams, P. & Dodgshon, R. 1998. Multi-Element Analysis of Soils from Scottish Historical Sites. Interpreting Land-Use History Through the Physical and Geochemical Analysis of Soil. *Journal of Archaeological Science* 25(1), 53–68.

Entwistle, J., Abrahams, P. & Dodgshon, R. 2000. The Geoarchaeological Significance and Spatial Variability of a Range of Physical and Chemical Soil Properties from a Former Habitation Site, Isle of Skye. *Journal of Archaeological Science* 27(4), 287–303.

Evershed, R., Bethell, P., Reynolds, P. & Walsh, N. 1997. 5ß-Stigmastanol and Related 5ß-Stanols as Biomarkers of Manuring: Analysis of Modern Experimental Material and Assessment of the Archaeological Potential. *Journal of Archaeological Science* 24(6), 485–495.

Evershed, R., Payne, S., Sherratt, A., Copley, M., Coolidge, J., Urem-Kotsu, D., Kotsakis, K., Ozdoğan, M., Ozdoğan, A., Nieuwenhuyse, O., Akkermans, P., Bailey, D., Andeescu, R.-R., Campbell, S., Farid, S., Hodder, I., Yalman, N., Ozbaşaran, M., Biçakci, E., Garfinkel, Y., Levy, T. & Burton, M. 2008. Earliest Date for Milk Use in the Near East and Southeastern Europe Linked to Cattle Herding. *Nature* 455(7212), 528–531.

Fagg, B. 1956. The Nok Culture. *West African Review* 27, 1083–1087.

Fagg, B. 1959. The Nok Culture in Prehistory. *Journal of the Historical Society of Nigeria* 1, 288–293.

Fagg, B. 1968. The Nok Culture: Excavations at Taruga. *The West African Archaeological Newsletter* 10, 27–30.

Fagg, B. 1969. Recent Work in West Africa. New Light on the Nok Culture. *World Archaeology* 1, 41–50.

Fagg, B. 1990. *Nok Terracottas.* Ethnographica Ltd., National Commission for Museums and Monuments, London/Lagos.

Fagg Rackham, A. 1972. A Preliminary Report on an Occupation Site in the Nok Valley, Nigeria: Samun Dukiya, AF/70/1. *West African Journal of Archaeology* 2, 75–79.

Fagg Rackham, A. 2014. Discovery an Early Research on the Nok Culture in Nigeria. In: Breunig, P. (ed.) *Nok – African Sculpture in Archaeological Context.* Africa Magna, Frankfurt am Main, 80–90.

Fagg Rackham, A. 2017. Revisiting Samun Dukiya – New Dates and Interpretation for a Nok Culture Site. In: Rupp, N., Beck, C. & Franke, G. & Wendt, K. P. (eds.) *Winds of Change. Archaeological Contributions in Honour of Peter Breunig.* Verlag Dr. Rudolf Habelt, Bonn, 247–254.

Fagg Rackham, A., Franke, G., Junius, H., Männel, T. & Beck, C. 2017. Early West African Iron Smelting: The Legacy of Taruga in Light of Recent Nok Research. *African Archaeological Review* 34(3), 321–343.

FAO 2014. *World Reference Base for Soil Resources.* FAO, Rome.

FAO/IIASA/ISRIC/ISS-CAS/JRC 2012. *Harmonized World Soil Database (Version 1.2).* FAO/IIASA, Rome/Laxenburg.

FAO-UNESCO 1974. *Soil Map of the World, 1:5000000.* Tipolitografia F. Failli, Rome.

FAO-UNESCO 1977. *Soil Map of the World, 1:5000000.* Tipolitografia F. Failli, Rome.

FAO-UNESCO 1997. *Soil Map of the World.* ISRIC, Wageningen.

Fiedler, S., Berger, J., Stahr, K. & Graw, M. 2009. Localisation of a Mass Grave from the Nazi Era. In: Ritz, K., Dawson, L. & Miller, D. (eds.) *Criminal and Environmental Soil Forensics.* Springer Netherlands, Dordrecht, 303–314.

Fiedler, S., Schneckenberger, K. & Graw, M. 2004. Characterization of Soils Containing Adipocere. *Archives of Environmental Contamination and Toxicology* 47(4), 561–568.

Filzmoser, P. & Hron, K. 2011. Robust Statistical Analysis. In: Pawlowsky-Glahn, V. & Buccianti, A. (eds.) *Compositional Data Analysis. Theory and Applications.* Wiley, Hoboken, 59–72.

Filzmoser, P., Hron, K. & Reimann, C. 2009. Univariate Statistical Analysis of Environmental (Compositional) Data. Problems and Possibilities. *The Science of the Total Environment* 407(23), 6100–6108.

Filzmoser, P., Hron, K. & Reimann, C. 2010. The Bivariate Statistical Analysis of Environmental (Compositional) Data. *The Science of the Total Environment* 408(19), 4230–4238.

Filzmoser, P., Hron, K. & Templ, M. 2018. *Applied Compositional Data Analysis. With Worked Examples in R.* Springer, Cham.

Fleisher, J. 2014. The Complexity of Public Space at the Swahili Town of Songo Mnara, Tanzania. *Journal of Anthropological Archaeology* 35, 1–22.

Franke, G. 2016. A Chronology of the Central Nigerian Nok Culture – 1500 BC to the Beginning of the Common Era. *Journal of African Archaeology* 14(3), 257–289.

Franke, G. 2017. *Potsherds in Time – The Pottery of the Nigerian Nok Culture and its Chronology.* Verlag Dr. Hut, München.

Franke, G. & Beck, C. 2017. "Early Nok" or Not? Linking Sites of the Second Millennium BC in Central Nigeria to the Nok Culture. In: Rupp, N., Beck, C. & Franke, G. & Wendt, K. P. (eds.) *Winds of Change. Archaeological Contributions in Honour of Peter Breunig.* Verlag Dr. Rudolf Habelt, Bonn, 263–273.

Franke, G. & Breunig, P. 2014. How Old is the Nok Culture? In: Breunig, P. (ed.) *Nok – African Sculpture in Archaeological Context.* Africa Magna, Frankfurt am Main, 131–136.

Gado, B. 1993. Un Village des Morts à Bura en République du Niger. In: Devisse, J., Polet, J. & Sidibé, S. (eds.) *Vallées du Niger.* Editions de la Réunion des Musées Nationaux, Paris, 365–374.

Garba, A. 1999. Ethnoarchaeology of Architecture of Storage Facilities at Dufuna, Yobe State, Northeast Nigeria. *Nyame Akuma* 52, 50–54.

Gauss, R., Bátora, J., Nowaczinski, E., Rassmann, K. & Schukraft, G. 2013. The Early Bronze Age Settlement of Fidvár, Vráble (Slovakia): Reconstructing Prehistoric Settlement Patterns Using Portable XRF. *Journal of Archaeological Science* 40(7), 2942–2960.

Gifford-Gonzalez, D. 2014. Constructing Community Through Refuse Disposal. *African Archaeological Review* 31(2), 339–382.

González-Ruibal, A., Sánchez-Elipe, M. & Otero-Vilariño, C. 2013. An Ancient and Common Tradition. Funerary Rituals and Society in Equatorial Guinea (First–Twelfth Centuries AD). *African Archaeological Review* 30(2), 115–143.

Goodale, N., Bailey, D., Jones, G., Prescott, C., Scholz, E., Stagliano, N. & Lewis, C. 2012. PXRF: a Study of Inter-Instrument Performance. *Journal of Archaeological Science* 39(4), 875–883.

Goody, J. 1961. Religion and Ritual: The Definitional Problem. *The British Journal of Sociology* 12(2), 142–164.

Gouem Gouem, B. 2011. *Des Premières Communautés Villageoises aux Sociétés Complexes sur le Littoral Méridional du Cameroun.* PhD thesis, Université Libre de Bruxelles.

Gronenborn, D. 1997. An Ancient Storage Pit in the SW Chad Basin, Nigeria. *Journal of Field Archaeology* 24(4), 431–439.

Hafez, I., Sorrentino, G., Faka, M., Cuenca-García, C., Makarona, C., Charalambous, A., Nys, K. & Hermon, S. 2017. Geochemical Survey of Soil Samples from the Archaeological Site Dromolaxia-Vyzakia (Cyprus), by Means of Micro-XRF and Statistical Approaches. *Journal of Archaeological Science: Reports* 11, 447–462.

Hahn-Weinheimer, P., Hirner, A. & Weber-Diefenbach, K. 1995. *Röntgenfluoreszenzanalytische Methoden. Grundlagen und praktische Anwendung in den Geo-, Material- und Umweltwissenschaften.* Vieweg, Braunschweig.

Hao, X. & Chang, C. 2003. Does Long-Term Heavy Cattle Manure Application Increase Salinity of a Clay Loam Soil in Semi-Arid Southern Alberta? *Agriculture, Ecosystems and Environment* 94(1), 89–103.

Hartmann, L. 2013. *Are Environmental Conditions Predisposing to Calcium-Deficiency Rickets in Developing Countries? A Community-Based Case Study from Rural Kaduna, Northern Nigeria.* PhD thesis, Goethe-Universität Frankfurt.

Haslam, R. & Tibbett, M. 2004. Sampling and Analyzing Metals in Soils for Archaeological Prospection. A Critique. *Geoarchaeology* 19(8), 731–751.

Helfert, M., Mecking, O., Lang, F. & von Kaenel, H.-M. 2011. Neue Perspektiven für die Keramikanalytik. Zur Evaluation der portablen energiedispersiven Röntgenfluoreszenzanalyse (P-ED-RFA) als neues Verfahren für die geochemische Analyse von Keramik in der Archäologie. *Frankfurter elektronische Rundschau zur Altertumskunde* 14, 1–30.

Helmig, D., Jackwerth, E. & Hauptmann, A. 1989. Archaeometallurgical Fieldwork and the Use of a Portable X-Ray Spectrometer. *Archaeometry* 31(2), 181–191.

Höhn, A., Franke, G. & Schmidt, A. 2018. Pits at Pangwari: Charcoal Taphonomy at a Multi-Phased Nok Site, Central Nigeria. In: Mercuri, A. M., D'Andrea, A. C. & Fornaciari, R. & Höhn, Alexa (eds.) *Plants and People in the African Past: Progress in African Archaeobotany*, 271–299.

Höhn, A. & Neumann, K. 2014. Millet and More: Farming and Food in the Time of the Nok Culture. In: Breunig, P. (ed.) *Nok – African Sculpture in Archaeological Context.* Africa Magna, Frankfurt am Main, 178–185.

Höhn, A. & Neumann, K. 2016. The Palaeovegetation of Janruwa (Nigeria) and its Implications for the Decline of the Nok Culture. *Journal of African Archaeology* 14(3), 331–353.

Holliday, V. & Gartner, W. 2007. Methods of Soil P Analysis in Archaeology. *Journal of Archaeological Science* 34(2), 301–333.

Hopkins, D.W., Wiltshire, P.E.J. & Turner, B.D. 2000. Microbial Characteristics of Soils from Graves. An Investigation at the Interface of Soil Microbiology and Forensic Science. *Applied Soil Ecology* 14(3), 283–288.

Janaway, R., Percival, S. & Wilson, A. 2009. Decomposition of Human Remains. In: Percival, S. L. (ed.) *Microbiology and Aging.* Humana Press, Totowa, 313–334.

Jemkur, J. 1992. *Aspects of the Nok Culture.* Ahmadu Bello University Press, Zaria.

Jemkur, J. 2014. My Adventure with the Nok Culture. In: Breunig, P. (ed.) *Nok – African Sculpture in Archaeological Context.* Africa Magna, Frankfurt am Main, 92–103.

Johnson, J. 2014. Accurate Measurements of Low Z Elements in Sediments and Archaeological Ceramics Using Portable X-Ray Fluorescence (PXRF). *Journal of Archaeological Method and Theory* 21(3), 563–588.

Jones, A. *et al.* 2013. *Soil Atlas of Africa.* Publications Office of the European Union, Luxembourg.

Junius, H. 2016a. Nok Early Iron Production in Central Nigeria – New Finds and Features. *Journal of African Archaeology* 14(3), 291–311.

Junius, H. 2016b. *Nok Iron Production in Central Nigeria in the Middle of the First Millennium BCE.* PhD thesis, Goethe-Universität Frankfurt.

Kabata-Pendias, A. 2011. *Trace Elements in Soils and Plants.* CRC Press, Boca Raton.

Kahlheber, S. 2009. Archaeobotanical Studies at Nok Sites: An Interim Report. *Nyame Akuma* 71, 2–17.

Kahlheber, S., Eggert, M. K. H., Seidensticker, D. & Wotzka, H.-P. 2014. Pearl Millet and Other Plant Remains from the Early Iron Age Site of Boso-Njafo (Inner Congo Basin, Democratic Republic of the Congo). *African Archaeological Review* 31(3), 479–512.

Keeley, H., Hudson, G. & Evans, J. 1977. Trace Element Contents of Human Bones in Various States of Preservation. 1. The Soil Silhouette. *Journal of Archaeological Science* 4(1), 19–24.

Li, J. & Heap, A. 2011. A Review of Comparative Studies of Spatial Interpolation Methods in Environmental Sciences. Performance and Impact Factors. *Ecological Informatics* 6(3-4), 228–241.

Livingstone Smith, A., Cornelissen, E., Francquen, C. de, Nikis, N., Mees, F., Tshibamba Mukendi, J., Beeckman, H., Bourland, N. & Hubau, W. 2017. Forests and Rivers. The Archaeology of the North Eastern Congo. *Quaternary International* 448, 95–116.

Lühe, B. 2016. *The Fate of Human Decomposition Products in Soils.* PhD thesis, Johannes Gutenberg-Universität, Mainz.

Lutz, H. 1951. The Concentration of Certain Chemical Elements in the Soils of Alaskan Archaeological Sites. *American Journal of Science* 249(12), 925–928.

Magnavita C. 2008. *Studien zur endsteinzeitlichen und früheisenzeitlichen Besiedlung im südwestlichen Tschadbecken (1300 BC-700 AD).* PhD thesis, Goethe-Universität Frankfurt.

Magnavita C., Breunig, P., Ameje, J. & Posselt, M. 2006. Zilum. A Mid-First Millennium BC Fortified Settlement Near Lake Chad. *Journal of African Archaeology* 4(1), 153–169.

Magnavita C. & Magnavita S. 2001. New Evidence of Proto-Urban Settlements in the Lake Chad Area. *Nyame Akuma* 55, 46–50.

Magnavita S. 2003. The Beads of Kissi, Burkina Faso. *Journal of African Archaeology* 1(1), 127–138.

Magnavita S. 2009. Sahelian Crossroads: Some Aspects on the Iron Age Sites of Kissi, Burkina Faso. In: Magnavita S. (ed.) *Crossroads/Carrefour Sahel. Cultural and Technological Developments in First Millennium BC/AD West Africa.* Africa Magna, Frankfurt am Main, 79–104.

Magnavita S. 2015. *1500 Jahre am Mare de Kissi. Eine Fallstudie zur Besiedlungsgeschichte des Sahel von Burkina Faso.* Africa Magna, Frankfurt am Main.

Magnavita S., Hallier, M., Pelzer, C., Kahlheber, S. & Linseele, V. 2002. Nobles, Guerriers, Paysans. Une Nécropole de l'Age de Fer et son Emplacement dans l'Oudalan Pré- et Protohistorique. *Beiträge zur Allgemeinen und Vergleichenden Archäologie* 22, 21–64.

Männel, T. & Breunig, P. 2016. The Nok Terracotta Sculptures of Pangwari. *Journal of African Archaeology* 14(3), 313–329.

Mantler, M. & Schreiner, M. 2000. X-Ray Fluorescence Spectrometry in Art and Archaeology. *X-ray Spectrometry* 29(1), 3–17.

Martín-Fernández, J. 2003. Dealing with Zeros and Missing Values in Compositional Data Sets Using Nonparametric Imputation. *Mathematical Geology* 35(3), 253–278.

Martín-Fernández, J., Buxeda i Garrigós, J. & Pawlowsky-Glahn, V. 2015. Logratio Analysis in Archaeometry: Principles and Methods. In: Barceló i Alvarez, J. Anton & Bogdanovic, I. (eds.) *Mathematics and Archaeology.* Taylor & Francis Group, Boca Raton, 178–189.

Martín-Fernández, J., Palarea-Albaladejo, J. & Olea, R. 2011. Dealing with Zeros. In: Pawlowsky-Glahn, V. & Buccianti, A. (eds.) *Compositional Data Analysis. Theory and Applications.* Wiley, Hoboken, 43–58.

Mateu-Figueras, G., Pawlowsky-Glahn, V. & Egozcue, J. 2011. The Principle of Working on Coordinates. In: Pawlowsky-Glahn, V. & Buccianti, A. (eds.) *Compositional Data Analysis. Theory and Applications.* Wiley, Hoboken, 31–42.

Matschullat, J., Ottenstein, R. & Reimann, C. 2000. Geochemical Background - Can We Calculate It? *Environmental Geology* 39(9), 990–1000.

Mbida Mindzie, C. 1995. *L'Emergence de Communautes Villageoises au Cameroun Meridional. Etude Archeologique des Sites de Nkang et de Ndindan.* PhD thesis, Université Libre de Bruxelles.

Mbida Mindzie, C. 2002. Ndindan: Synthèse Archéologique d'un Site Datantde Trois Millénaires à Yaoundé (Cameroun). *L'Anthropologie* 106(1), 159–172.

Mbida Mindzie, C. & Mvondo Ze, A. 2016. Chemical Analysis of Soil Samples from Campo-Église and Campo-Center. In: Eggert, M. K. H. & Seidensticker, D. *Campo. Archaeological Research at the Mouth of the Ntem River (South Cameroon).* Heinrich-Barth-Institut, Köln, 147–150.

Mbida Mindzie, C., van Neer, W., Doutrelepont, H. & Vrydaghs, L. 2000. Evidence for Banana Cultivation and Animal Husbandry During the First Millennium BC in the Forest of Southern Cameroon. *Journal of Archaeological Science* 27(2), 151–162.

McIntosh, S. 1999. Pathways to Complexity: An African Perspective. In: McIntosh, S. Keech (ed.) *Beyond Chiefdoms. Pathways to Complexity in Africa.* Cambridge University Press, Cambridge, 1–30.

McKinley, J., Hron, K., Grunsky, E., Reimann, C., Caritat, P. de, Filzmoser, P., van den Boogaart, K. & Tolosana-Delgado, R. 2016. The Single Component Geochemical Map. Fact or Fiction? *Journal of Geochemical Exploration* 162, 16–28.

McKinley, J. & Lloyd, C. 2011. Multivariate Geochemical Data Analysis in Physical Geography. In: Pawlowsky-Glahn, V. & Buccianti, A. (eds.) *Compositional Data Analysis. Theory and Applications.* Wiley, Hoboken, 290–301.

Meister, C. 2008. Recent Archaeological Investigations in the Tropical Rain Forest of South-West Cameroon. In: Runge, J. (ed.) *Dynamics of Forest Ecosystems in Central Africa During the Holocene: Past – Present – Future: Palaeoecology of Africa 28.* CRC Press, Boca Raton, 43–57.

Meister, C. 2010. Remarks on Early Iron Age Burial Sites from Southern Cameroon. *African Archaeological Review* 27(3), 237–249.

Meister, C. & Eggert, M. K. H. 2008. On the Early Iron Age in Southern Cameroon: The Sites of Akonétye. *Journal of African Archaeology* 6(2), 183–202.

Melis, C., Selva, N., Teurlings, I., Skarpe, C., Linnell, J. & Andersen, R. 2007. Soil and Vegetation Nutrient Response to Bison Carcasses in Białowieża Primeval Forest, Poland. *Ecological Research* 22(5), 807–813.

Middleton, W. 2004. Identifying Chemical Activity Residues on Prehistoric House Floors: A Methodology and Rationale for Multi-Elemental Characterization of a Mild Acid Extract of Anthropogenic Sediments. *Archaeometry* 46(1), 47–65.

Middleton, W., Barba, L., Pecci, A., Burton, J., Ortiz, A., Salvini, L. & Suárez, R. 2010. The Study of Archaeological Floors: Methodological Proposal for the Analysis of Anthropogenic Residues by Spot Tests, ICP-OES, and GC-MS. *Journal of Archaeological Method and Theory* 17(3), 183–208.

Middleton, W. & Price, T. 1996. Identification of Activity Areas by Multi-Element Characterization of Sediments from Modern and Archaeological House Floors Using Inductively Coupled Plasma-Atomic Emission Spectroscopy. *Journal of Archaeological Science* 23(5), 673–687.

Nagel, K.-P. 2014. The Chemistry of a Nok Site. In: Breunig, P. (ed.) *Nok – African Sculpture in Archaeological Context.* Africa Magna, Frankfurt am Main, 151–155.

Ngomanda, A., Neumann, K., Schweizer, A. & Maley, J. 2009. Seasonality Change and the Third Millennium BP Rainforest Crisis in Southern Cameroon (Central Africa). *Quaternary Research* 71(3), 307–318.

Nieuwenhuyse, O., Roffet-Salque, M., Evershed, R., Akkermans, P. & Russell, A. 2015. Tracing Pottery Use and the Emergence of Secondary Product Exploitation Through Lipid Residue Analysis at Late Neolithic Tell Sabi Abyad (Syria). *Journal of Archaeological Science* 64, 54–66.

Nlend Nlend, P. 2013. *Les Traditions Ceramiques dans leur Contexte Archéologique sur le Littoral Camerounais (Kribi-Campo) de 3000 a 500 BP.* PhD thesis, Université Libre de Bruxelles.

Obaje, N. 2009. *Geology and Mineral Resources of Nigeria.* Springer-Verlag, Berlin/ Heidelberg.

Odeh, I.O.A., Leenaars, J., Hartemink, A. & Amapu, I. 2012. The Challenges of Collating Legacy Data for Digital Mapping of Nigerian Soils. In: Minasny, B., Malone, B. P. & McBratney, A. B. (eds.) *Digital Soil Assessments and Beyond. Proceedings of the 5th Global Workshop on Digital Soil Mapping, 2012, Sydney, Australia, 10-13 April 2012.* CRC Press, Boca Raton, 453–458.

Oonk, S., Slomp, C. & Huisman, D. 2009a. Geochemistry as an Aid in Archaeological Prospection and Site Interpretation: Current Issues and Research Directions. *Archaeological Prospection* 16(1), 35–51.

Oonk, S., Slomp, C., Huisman, D. & Vriend, S. 2009b. Effects of Site Lithology on Geochemical Signatures of Human Occupation in Archaeological House Plans in the Netherlands. *Journal of Archaeological Science* 36(6), 1215–1228.

Pawlowsky-Glahn, V. & Egozcue, J. 2001. Geometric Approach to Statistical Analysis on the Simplex. *Stochastic Environmental Research and Risk Assessment* 15(5), 384–398.

Pawlowsky-Glahn, V. & Egozcue, J. 2011. Exploring Compositional Data with the CoDa-Dendrogram. *Australian Journal of Statistics* 40(1-2), 103–113.

Pawlowsky-Glahn, V. & Egozcue, J. 2016. Spatial Analysis of Compositional Data. A Historical Review. *Journal of Geochemical Exploration* 164, 28–32.

Pawlowsky-Glahn, V., Egozcue, J. & Tolosana-Delgado, R. 2015. *Modeling and Analysis of Compositional Data.* Wiley, Chichester.

Pearson, K. 1896. Mathematical Contributions to the Theory of Evolution. On a Form of Spurious Correlation Which May Arise When Indices Are Used in the Measurement of Organs. *Proceedings of the Royal Society of London* 60, 489–498.

Pollard, A. & Heron, C. 2008. *Archaeological Chemistry.* Royal Society of Chemistry, Cambridge.

Powers, R. 2005. The Decomposition of Human Remains: A Biochemical Perspective. In: Rich, J., Dean, D. E. & Powers, R. H. (eds.) *Forensic Medicine of the Lower Extremity. Human Identification and Trauma Analysis of the Thigh, Leg, and Foot.* Humana Press, Totowa, 3–16.

QGIS Project. 2019. *QGIS User Guide. Release 2.18*. Last visited on January 10, 2019.

Quickert, N., Godfrey-Smith, D. & Casey, J. 2003. Optical and Thermoluminescence Dating of Middle Stone Age and Kintampo Bearing Sediments at Birimi, a Multi-Component Archaeological Site in Ghana. *Quaternary Science Reviews* 22(10-13), 1291–1297.

Reimann, C. & Caritat, P. de. 2005. Distinguishing Between Natural and Anthropogenic Sources for Elements in the Environment. Regional Geochemical Surveys Versus Enrichment Factors. *The Science of the Total Environment* 337(1-3), 91–107.

Reimann, C. & Filzmoser, P. 2000. Normal and Lognormal Data Distribution in Geochemistry. Death of a Myth. Consequences for the Statistical Treatment of Geochemical and Environmental data. *Environmental Geology* 39(9), 1001–1014.

Reimann, C., Filzmoser, P., Fabian, K., Hron, K., Birke, M., Demetriades, A., Dinelli, E. & Ladenberger, A. 2012. The Concept of Compositional Data Analysis in Practice – Total Major Element Concentrations in Agricultural and Grazing Land Soils of Europe. *The Science of the Total Environment* 426, 196–210.

Reimann, C., Filzmoser, P. & Garrett, R. 2005. Background and Threshold. Critical Comparison of Methods of Determination. *The Science of the Total Environment* 1-3, 1–16.

Reimann, C., Filzmoser, P., Garrett, R. & Dutter, R. 2008. *Statistical Data Analysis Explained. Applied Environmental Statistics with R.* Wiley, Chichester.

Reimann, C. & Garrett, R. 2005. Geochemical Background – Concept and Reality. *The Science of the Total Environment* 350(1-3), 12–27.

Reimer, P., Bard, E., Bayliss, A., Beck, J., Blackwell, P., Ramsey, C., Buck, C., Cheng, H., Edwards, R., Friedrich, M., Grootes, P., Guilderson, T., Haflidason, H., Hajdas, I., Hatté, C., Heaton, T., Hoffmann, D., Hogg, A., Hughen, K., Kaiser, K., Kromer, B., Manning, S., Niu, M., Reimer, R., Richards, D., Scott, E., Southon, J., Staff, R., Turney, C. & van der Plicht, J. 2013. IntCal13 and Marine13 Radiocarbon Age Calibration Curves 0–50,000 Years cal BP. *Radiocarbon* 55(4), 1869–1887.

Rothwell, K. & Cooke, M. 2015. A Comparison of Methods Used to Calculate Normal Background Concentrations of Potentially Toxic Elements for Urban Soil. *The Science of the Total Environment* 532, 625–634.

Rupp, N. 2010. Beyond Art. Archaeological Studies on the Nok Culture, Central Nigeria. In: Allsworth-Jones, P. (ed.) *West African Archaeology. New Developments, New Perspectives.* Archaeopress, Oxford, 67–78.

Rupp, N. 2014a. Communing with the Ancestors? The Mystery of Utak Kamuan Garaje Kagoro. In: Breunig, P. (ed.) *Nok – African Sculpture in Archaeological Context.* Africa Magna, Frankfurt am Main, 215–231.

Rupp, N. 2014b. Tradition and Innovation. In: Breunig, P. (ed.) *Nok – African Sculpture in Archaeological Context.* Africa Magna, Frankfurt am Main, 156–166.

Rupp, N. 2014c. Well Hidden and Densly Spread: The Sites of the Nok Culture. In: Breunig, P. (ed.) *Nok – African Sculpture in Archaeological Context.* Africa Magna, Frankfurt am Main, 138–149.

Sawatzky, R. 1998. *Kintampo Architecture.* Unpublished M.A. thesis, University of South Carolina.

Schaal, S.; Kunsch, K. & Kunsch, S. (eds.) 2016. *Der Mensch in Zahlen.* Springer, Berlin/ Heidelberg.

Scheffer, F., Schachtschabel, P. & Blume, H.-P. 2010. *Lehrbuch der Bodenkunde.* Spektrum Akademischer Verlag, Heidelberg/Berlin.

Schmidt, A. 2014. *Studien zur Struktur der Nok-Fundstelle Pangwari in Zentralnigeria anhand der Befunde und der Fundverteilung.* M.A. thesis, Goethe-Universität Frankfurt.

Schmidt, A. 2016. Excavation 2016 and XRF Analysis at the Nok Site of Ido in Central Nigeria. *Nyame Akuma* 86, 65–70.

Schultz, J. 2005. *The Ecozones of the World. The Ecological Divisions of the Geosphere.* Springer, Berlin.

Seidensticker, D. 2010. *Grubenbefunde in Campo (Südkamerun).* M.A. thesis, Eberhard Karls Universität Tübingen.

Seidensticker, D. 2013. Die Nutzung und Funktion von Gruben in Zentralafrika. In: Karl, R. & Leskovar, J. (eds.) *Interpretierte Eisenzeiten. Fallstudien, Methoden, Theorie: Tagungsbeiträge der 5. Linzer Gespräche zur interpretativen Eisenzeitarchäologie.* Oberösterreichisches Landesmuseum, Linz, 51–59.

Seidensticker, D. 2016. Chemical Analysis of further soil samples from Campo-Église and Campo-Center. In: Eggert, M. K. H. & Seidensticker, D. *Campo. Archaeological Research at the Mouth of the Ntem River (South Cameroon).* Heinrich-Barth-Institut, Köln, 151–155.

Seppey, C., Fournier, B., Szelecz, I., Singer, D., Mitchell, E. & Lara, E. 2016. Response of Forest Soil Euglyphid Testate Amoebae (Rhizaria Cercozoa) to Pig Cadavers Assessed by High-Throughput Sequencing. *International Journal of Legal Medicine* 130(2), 551–562.

Shackley, M. 2010. Is there Reliability and Validity in Portable X-Ray Fluorescence Spectrometry (PXRF)? *The SAA Archaeological Record* 10(5), 17–20.

Shugar, A. & Mass, J. 2012. *Handheld XRF for Art and Archaeology.* Leuven University Press, Leuven.

Slon, V., Hopfe, C., Weiss, C., Mafessoni, F., La Rasilla, M. de, Lalueza-Fox, C., Rosas, A., Soressi, M., Knul, M., Miller, R., Stewart, J., Derevianko, A., Jacobs, Z., Li, B., Roberts, R., Shunkov, M., Lumley, H. de, Perrenoud, C., Gušić, I., Kućan, Ž., Rudan, P., Aximu-Petri, A., Essel, E., Nagel, S., Nickel, B., Schmidt, A., Prüfer, K., Kelso, J., Burbano, H., Pääbo, S. & Meyer, M. 2017. Neandertal and Denisovan DNA from Pleistocene Sediments. *Science* 356(6338), 605–608.

Spaargaren, O., Schad, P., Micheli, E. & Jones, A. 2010. *Guidelines for Constructing Small-Scale Map Legends Using the World Reference Base for Soil Resources.* FAO, Rome.

Stokes, K., Forbes, S. & Tibbett, M. 2013. Human Versus Animal. Contrasting Decomposition Dynamics of Mammalian Analogues in Experimental Taphonomy. *Journal of Forensic Sciences* 58(3), 583–591.

Strawn, D., Bohn, H. & O'Connor. 2015. *Soil Chemistry.* Wiley, Hoboken.

Sulas, F., Fleisher, J. & Wynne-Jones, S. 2017. Geoarchaeology of Urban Space in Tropical Island Environments. Songo Mnara, Tanzania. *Journal of Archaeological Science* 77, 52–63.

Sutherland, R. 2000. Bed Sediment-Associated Trace Metals in an Urban Stream, Oahu, Hawaii. *Environmental Geology* 39(6), 611–627.

Szelecz, I., Fournier, B., Seppey, C., Amendt, J. & Mitchell, E. 2014. Can Soil Testate Amoebae be Used for Estimating the Time Since Death? A Field Experiment in a Deciduous Forest. *Forensic Science International* 236, 90–98.

Szelecz, I., Sorge, F., Seppey, C., Mulot, M., Steel, H., Neilson, R., Griffiths, B., Amendt, J. & Mitchell, E. 2016. Effects of Decomposing Cadavers on Soil Nematode Communities Over a One-Year Period. *Soil Biology and Biochemistry* 103, 405–416.

Terry, R., Fernández, F., Parnell, J.J. & Inomata, T. 2004. The Story in the Floors: Chemical Signatures of Ancient and Modern Maya Activities at Aguateca, Guatemala. *Journal of Archaeological Science* 31(9), 1237–1250.

Thió-Henestrosa, S. & Comas, M. 2016. *CoDaPack v2 User's Guide*. Last visited on January 10, 2019.

Thió-Henestrosa, S. & Daunis-i-Estadella, J. 2011. Exploratory Analysis Using CoDaPack 3D. In: Pawlowsky-Glahn, V. & Buccianti, A. (eds.) *Compositional Data Analysis. Theory and Applications.* Wiley, Hoboken, 329–340.

Thió-Henestrosa, S. & Martín-Fernández, J. 2005. Dealing with Compositional Data. The Freeware CoDaPack. *Mathematical Geology* 37(7), 773–793.

Tolosana-Delgado, R. 2012. Uses and Misuses of Compositional Data in Sedimentology. *Sedimentary Geology* 280, 60–79.

Tolosana-Delgado, R. & van den Boogaart, K. 2013. Joint Consistent Mapping of High-Dimensional Geochemical Surveys. *Mathematical Geosciences* 45(8), 983–1004.

Tolosana-Delgado, R., van den Boogaart, K. & Pawlowsky-Glahn, V. 2011. Geostatistics for Compositions. In: Pawlowsky-Glahn, V. & Buccianti, A. (eds.) *Compositional Data Analysis. Theory and Applications.* Wiley, Hoboken, 73–86.

van Zwieten, C., Cook, S., Voss, J., Fulford, M., Pankhurst, N. & Barnett, C. 2017. Waste Disposal in Late Iron Age and Early Roman Silchester: A Geochemical Comparison of Pits, Post Holes, Ditches and Wells in Insula IX. *Journal of Archaeological Science: Reports* 15, 1–7.

Watson, D. 2010. Within Savanna and Forest. A Review of the Late Stone Age Kintampo Tradition, Ghana. *Azania: Archaeological Research in Africa* 45(2), 141–174.

Wendt, K. 2007. *Gajiganna. Analysis of Stratigraphies and Pottery of a Final Stone Age Culture of Northeast Nigeria.* Africa Magna, Frankfurt am Main.

Wentworth, C. 1922. A Scale of Grade and Class Terms for Clastic Sediments. *The Journal of Geology* 30(5), 377–392.

White, F. 1983. *The Vegetation of Africa. A Descriptive Memoir to Accompany the Unesco/AETFAT/UNSO Vegetation Map of Africa.* Unesco, Paris.

White, W. 2013. *Geochemistry.* Wiley, Hoboken.

Wilson, C., Davidson, D. & Cresser, M. 2005. An Evaluation of Multielement Analysis of Historic Soil Contamination to Differentiate Space Use and Former Function in and around Abandoned Farms. *The Holocene* 15(7), 1094–1099.

Wilson, C., Davidson, D. & Cresser, M. 2009. An Evaluation of the Site Specificity of Soil Elemental Signatures for Identifying and Interpreting Former Functional Areas. *Journal of Archaeological Science* 36(10), 2327–2334.

Wotzka, H.-P. 1993. Zur Tradition der Keramikdeponierung im äquatorialen Regenwald Zaires: Ein Bekenntnis zur allgemeinvergleichenden Analogie. *Ethnographisch-Archäologische Zeitschrift* 34(2), 251–283.

Wotzka, H.-P. 2017. The Inverted Pot: A Leitmotiv in Nok Terracotta. In: Rupp, N., Beck, C. & Franke, G. & Wendt, K. P. (eds.) *Winds of Change. Archaeological Contributions in Honour of Peter Breunig.* Verlag Dr. Rudolf Habelt, Bonn, 285–294.

Zoller, W., Gladney, E. & Duce, R. 1974. Atmospheric Concentrations and Sources of Trace Metals at the South Pole. *Science* 183(4121), 198–200.

Appendix 1 – Calibration & Sample Preparation

Tables & Figures

Appendix 1-1

• Laboratory results of samples 1-11

Appendix 1-2

• pXRF measurement series with employed factory calibration

Appendix 1-3

• Comparison of the results of the laboratory, pXRF measurements and after applying the empirical calibration

Appendix 1-4

• Laboratory results used for test A-C

Appendix 1-5

• Comparison of different grain sizes

Appendix 1-1

ActLabs (actlabs.com) laboratory results of samples 1-11 with information on employed analysis method and detection limit. Samples 2, 5 and 11 were only used for laboratory analysis, the other samples numbers correspond to the Nok standards. Some of the element concentrations (e.g. Ni, Cu) were rounded up by the laboratory. For the element Cl no value was provided. Concentrations of the major elements were given in weight percent oxides. All elements sorted in the order provided by the laboratory. All element concentrations listed with quality control (QC) information.

Laboratory results of samples 1-11. Report Number: A15-02933. Report Date: 19/5/2015.

Analyte Symbol	SiO2	Al2O3	Fe2O3(T)	MnO	MgO	CaO	Na2O	K2O	TiO2	P2O5	LOI	Total	Sc	Be	V	Ba	Sr
Unit Symbol	%	%	%	%	%	%	%	%	%	%	%	%	ppm	ppm	ppm	ppm	ppm
Detection Limit	0.01	0.01	0.01	0.001	0.01	0.01	0.01	0.01	0.001	0.01		0.01	1	1	5	3	2
Analysis Method	FUS-ICP	FUS-ICP	FUS-ICP	FUS-ICP	FUS-ICP	FUS-ICP	FUS-ICP	FUS-ICP	FUS-ICP	FUS-ICP	FUS-ICP	FUS-ICP	FUS-ICP	FUS-ICP	FUS-ICP	FUS-ICP	FUS-ICP
Sample 1	52.39	20.95	10.53	0.175	0.38	0.14	0.16	1.7	2.355	0.13	11.54	100.4	20	3	113	577	72
Sample 2	50.01	20.93	10.47	0.179	0.4	0.13	0.14	1.59	2.269	0.15	11.93	98.2	20	3	110	538	68
Sample 3	43.95	22.53	15.33	0.249	0.77	0.59	0.36	1.59	2.615	0.43	12.03	100.4	25	3	198	830	85
Sample 4	53.98	18.54	10.2	0.171	0.36	0.2	0.22	1.86	2.466	0.35	10.81	99.16	17	3	105	676	78
Sample 5	50.61	20.33	10.1	0.178	0.4	0.17	0.16	1.74	2.345	0.16	11.93	98.13	19	3	107	617	74
Sample 6	46.16	21.7	15.08	0.143	0.52	0.16	0.2	2.3	1.804	0.11	11.26	99.45	16	3	137	797	88
Sample 7	44.48	24.28	14.15	0.178	0.31	0.1	0.08	1.17	1.799	0.11	12.53	99.18	17	3	147	429	53
Sample 8	41.87	21.88	15.18	0.229	0.71	0.64	0.34	1.49	2.201	0.43	14.06	99.02	25	3	189	868	88
Sample 9	44.14	22.16	15.41	0.27	0.75	0.54	0.31	1.56	2.61	0.41	12.32	100.5	26	3	199	759	90
Sample 10	53.29	19.32	10.31	0.131	0.51	0.29	0.38	2.69	2.024	0.13	11.1	100.2	16	3	98	991	108
Sample 11	42.09	22.57	15.57	0.231	0.73	0.66	0.34	1.47	2.224	0.44	14.07	100.4	25	4	191	870	89

Analyte Symbol	Y	Zr	Cr	Co	Ni	Cu	Zn	Ga	Ge	As	Rb	Nb	Mo	Ag	In	Sn	Sb
Unit Symbol	ppm	ppm	ppm	ppm	ppm	ppm	ppm	ppm	ppm	ppm	ppm	ppm	ppm	ppm	ppm	ppm	ppm
Detection Limit	2	4	20	1	20	10	30	1	1	5	2	1	2	0.5	0.2	1	0.5
Analysis Method	FUS-ICP	FUS-ICP	FUS-MS	FUS-MS	FUS-MS	FUS-MS	FUS-MS	FUS-MS	FUS-MS	FUS-MS	FUS-MS	FUS-MS	FUS-MS	FUS-MS	FUS-MS	FUS-MS	FUS-MS
Sample 1	48	1849	50	30	30	40	120	34	2	< 5	115	53	3	4.8	< 0.2	4	0.9
Sample 2	53	1824	40	31	30	40	130	35	2	< 5	115	53	2	5.1	< 0.2	4	< 0.5
Sample 3	44	911	40	59	50	60	170	34	2	< 5	94	38	3	2.4	< 0.2	3	< 0.5
Sample 4	47	1640	40	27	30	30	110	31	2	< 5	106	50	2	4.5	< 0.2	3	< 0.5
Sample 5	56	1985	40	28	30	40	120	32	2	< 5	113	52	2	5.5	< 0.2	3	0.6
Sample 6	28	1162	30	38	20	40	130	36	2	< 5	108	42	3	3.2	< 0.2	4	< 0.5
Sample 7	30	1069	50	73	30	30	90	37	2	< 5	85	42	4	2.8	< 0.2	3	< 0.5
Sample 8	40	584	40	55	50	60	180	35	2	< 5	84	34	2	1.4	< 0.2	3	< 0.5
Sample 9	45	823	40	58	50	60	200	35	2	< 5	93	38	2	2.1	< 0.2	3	0.6
Sample 10	51	1440	30	23	< 20	40	120	31	2	< 5	119	46	2	3.7	< 0.2	4	< 0.5
Sample 11	40	696	40	55	50	60	180	35	2	< 5	83	34	2	1.7	< 0.2	3	< 0.5

Laboratory results of samples 1-11. Report Number: A15-02933. Report Date: 19/5/2015.

Analyte Symbol	Cs	La	Ce	Pr	Nd	Sm	Eu	Gd	Tb	Dy	Ho	Er	Tm	Yb	Lu	Hf	Ta
Unit Symbol	ppm	ppm	ppm	ppm	ppm	ppm	ppm	ppm	ppm	ppm	ppm	ppm	ppm	ppm	ppm	ppm	ppm
Detection Limit	0.5	0.1	0.1	0.05	0.1	0.1	0.05	0.1	0.1	0.1	0.1	0.1	0.05	0.1	0.04	0.2	0.1
Analysis Method	FUS-MS	FUS-MS	FUS-MS	FUS-MS	FUS-MS	FUS-MS	FUS-MS	FUS-MS	FUS-MS	FUS-MS	FUS-MS	FUS-MS	FUS-MS	FUS-MS	FUS-MS	FUS-MS	FUS-MS
Sample 1	4	73.9	137	17.3	67.6	13.7	3.34	11.9	1.8	9.8	1.9	5.5	0.79	5.1	0.82	45.1	3.4
Sample 2	4.2	77	154	17.9	70.6	14.6	3.56	12.6	1.9	10.8	2	5.9	0.86	5.6	0.9	46.2	3.4
Sample 3	2.9	68.6	128	16	63	13	3.57	11.4	1.7	9.2	1.8	5	0.7	4.4	0.69	22.2	2.6
Sample 4	3.4	68.3	124	15.7	62.4	12.6	3.19	11.2	1.7	9.6	1.9	5.3	0.81	5.4	0.84	39.9	3.5
Sample 5	3.7	78.7	141	18.7	72.8	14.6	3.86	13.3	2	11.2	2.1	6.2	0.92	5.9	0.92	49	3.3
Sample 6	4.6	57	226	11.8	45.2	8.6	2.18	7.1	1.1	6.3	1.2	3.5	0.51	3.3	0.54	28.9	2.6
Sample 7	3.2	57.5	442	12	44.7	8.2	2.06	7.3	1.2	6.3	1.2	3.5	0.53	3.4	0.55	26.9	2.6
Sample 8	2.7	64	124	14.4	56.9	11.3	3.38	10.1	1.5	8.3	1.5	4.3	0.59	3.8	0.57	14.2	2
Sample 9	2.8	63	126	14.8	59.6	12.5	3.51	11.2	1.7	9.4	1.7	4.7	0.66	4.2	0.65	20.1	2.4
Sample 10	4.6	74.5	117	18	71.2	14.1	3.49	12.4	1.8	10.1	1.9	5.3	0.77	5	0.75	34.6	2.9
Sample 11	2.7	65.3	126	14.7	58.1	11.5	3.39	10.5	1.5	8.2	1.6	4.4	0.6	3.9	0.59	16.8	2

Analyte Symbol	W	Tl	Pb	Bi	Th	U
Unit Symbol	ppm	ppm	ppm	ppm	ppm	ppm
Detection Limit	1	0.1	5	0.4	0.1	0.1
Analysis Method	FUS-MS	FUS-MS	FUS-MS	FUS-MS	FUS-MS	FUS-MS
Sample 1	3	0.5	27	< 0.4	16.2	5.5
Sample 2	2	0.5	29	< 0.4	16.3	5.8
Sample 3	2	0.4	23	< 0.4	8.5	2.8
Sample 4	8	0.5	26	< 0.4	13.1	4.9
Sample 5	2	0.5	24	< 0.4	14.9	5.1
Sample 6	7	0.5	33	< 0.4	10.6	5.7
Sample 7	6	0.5	46	< 0.4	12.2	5.3
Sample 8	3	0.4	22	< 0.4	7.8	2.6
Sample 9	2	0.4	24	< 0.4	8.3	2.4
Sample 10	10	0.5	21	< 0.4	10.6	4.7
Sample 11	3	0.4	22	< 0.4	8.1	2.7

Quality control information. Report Number: A15-02933. Report Date: 19/5/2015.

Analyte Symbol	SiO2	Al2O3	Fe2O3(T)	MnO	MgO	CaO	Na2O	K2O	TiO2	P2O5	LOI	Total	Sc	Be	V	Ba
Unit Symbol	%	%	%	%	%	%	%	%	%	%	%	%	ppm	ppm	ppm	ppm
Detection Limit	0.01	0.01	0.01	0.001	0.01	0.01	0.01	0.01	0.001	0.01		0.01	1	1	5	3
Analysis Method	FUS-ICP	FUS-ICP	FUS-ICP	FUS-ICP	FUS-ICP	FUS-ICP	FUS-ICP	FUS-ICP	FUS-ICP	FUS-ICP	FUS-ICP	FUS-ICP	FUS-ICP	FUS-ICP	FUS-ICP	FUS-ICP
NIST 694 Meas	11.17	1.92	0.74	0.01	0.35	43.69	0.89	0.56	0.12	30.18					1657	
NIST 694 Cert	11.2	1.8	0.79	0.0116	0.33	43.6	0.86	0.51	0.11	30.2					1740	
DNC-1 Meas	46.76	18.49	9.83	0.15	10	11.31	1.95	0.23	0.48	0.08			31		149	106
DNC-1 Cert	47.15	18.34	9.97	0.150	10.13	11.49	1.890	0.234	0.480	0.070			31		148	118
GBW 07113 Meas	71.93	12.87	3.17	0.14	0.14	0.58	2.44	5.35	0.28	0.05			5	4	6	501
GBW 07113 Cert	72.8	13	3.21	0.14	0.16	0.59	2.57	5.43	0.3	0.05			5	4	5	506
LKSD-3 Meas																
LKSD-3 Cert																
TDB-1 Meas																
TDB-1 Cert																
W-2a Meas	52.54	15.37	11.05	0.17	6.32	11	2.24	0.63	1.08	0.15			36	< 1	264	176
W-2a Cert	52.4	15.4	10.7	0.163	6.37	10.9	2.14	0.626	1.06	0.13			36	1.3	262	182
SY-4 Meas	49.39	20.78	6.16	0.11	0.51	7.88	6.97	1.67	0.29	0.13			< 1	3	9	344
SY-4 Cert	49.9	20.69	6.21	0.108	0.54	8.05	7.10	1.66	0.287	0.131			1.1	2.6	8.0	340
CTA-AC-1 Meas																
CTA-AC-1 Cert																
BIR-1a Meas	47.23	15.42	11.37	0.17	9.59	13.25	1.86	0.02	0.97	0.02			44	< 1	316	8
BIR-1a Cert	47.96	15.50	11.30	0.175	9.700	13.30	1.82	0.030	0.96	0.021			44	0.58	310	6
NCS DC86312 Meas																
NCS DC86312 Cert																
NCS DC70009 (GBW07241) Meas																
NCS DC70009 (GBW07241) Cert																
OREAS 100a (Fusion) Meas																
OREAS 100a (Fusion) Cert																
OREAS 101a (Fusion) Meas																
OREAS 101a (Fusion) Cert																
OREAS 101b (Fusion) Meas																
OREAS 101b (Fusion) Cert																
JR-1 Meas																
JR-1 Cert																
Method Blank																

Quality control information. Report Number: A15-02933. Report Date: 19/5/2015.

Analyte Symbol	Sr	Y	Zr	Cr	Co	Ni	Cu	Zn	Ga	Ge	As	Rb	Nb	Mo	Ag	In
Unit Symbol	ppm	ppm	ppm	ppm	ppm	ppm	ppm	ppm	ppm	ppm	ppm	ppm	ppm	ppm	ppm	ppm
Detection Limit	2	2	4	20	1	20	10	30	1	1	5	2	1	2	0.5	0.2
Analysis Method	FUS-ICP	FUS-ICP	FUS-ICP	FUS-MS	FUS-MS	FUS-MS	FUS-MS	FUS-MS	FUS-MS	FUS-MS	FUS-MS	FUS-MS	FUS-MS	FUS-MS	FUS-MS	FUS-MS
NIST 694 Meas																
NIST 694 Cert																
DNC-1 Meas	148	16	35	270	61		90	70								
DNC-1 Cert	144.0	18.0	38	270	57		100	70								
GBW 07113 Meas	43	47	387													
GBW 07113 Cert	43	43	403													
LKSD-3 Meas				90	32	50						75		< 2		
LKSD-3 Cert				87	30	47						78		2		
TDB-1 Meas				260		90	330	160								
TDB-1 Cert				251		92	323	155								
W-2a Meas	201	20	90	90	45	70	110		18	2		19		< 2	< 0.5	
W-2a Cert	190	24	94	92	43	70	110		17	1		21		0.6	0.046	
SY-4 Meas	1179	123	538													
SY-4 Cert	1191	119	517													
CTA-AC-1 Meas							60	40								
CTA-AC-1 Cert							54.0	38.0								
BIR-1a Meas	111	13	15	380	55	170	120	70	16				< 1			
BIR-1a Cert	110	16	18	370	52	170	125	70	16				0.6			
NCS DC86312 Meas																
NCS DC86312 Cert																
NCS DC70009 (GBW07241) Meas				30			930	100	18	11					1.7	1.2
NCS DC70009 (GBW07241) Cert				30			960	100	16.5	11.2					1.8	1.3
OREAS 100a (Fusion) Meas					19		170									
OREAS 100a (Fusion) Cert					18.1		169									
OREAS 101a (Fusion) Meas					50		410							23		
OREAS 101a (Fusion) Cert					48.8		434							21.9		
OREAS 101b (Fusion) Meas					48		430							21		
OREAS 101b (Fusion) Cert					47		416							20.9		
JR-1 Meas						< 20		< 30				259	15	3	< 0.5	< 0.2
JR-1 Cert						1.67		30.6				257	15.2	3.25	0.031	0.028
Method Blank				< 20	< 1	< 20	< 10	< 30	< 1	< 1	< 5	< 2	< 1	< 2	< 0.5	< 0.2

Quality control information. Report Number: A15-02933. Report Date: 19/5/2015.

Analyte Symbol	Sn	Sb	Cs	La	Ce	Pr	Nd	Sm	Eu	Gd	Tb	Dy	Ho	Er	Tm	Yb
Unit Symbol	ppm	ppm	ppm	ppm	ppm	ppm	ppm	ppm	ppm	ppm	ppm	ppm	ppm	ppm	ppm	ppm
Detection Limit	1	0.5	0.5	0.1	0.1	0.05	0.1	0.1	0.05	0.1	0.1	0.1	0.1	0.1	0.05	0.1
Analysis Method	FUS-MS	FUS-MS	FUS-MS	FUS-MS	FUS-MS	FUS-MS	FUS-MS	FUS-MS	FUS-MS	FUS-MS	FUS-MS	FUS-MS	FUS-MS	FUS-MS	FUS-MS	FUS-MS
NIST 694 Meas																
NIST 694 Cert																
DNC-1 Meas							4.8		0.55							1.8
DNC-1 Cert							5.20		0.59							2.0
GBW 07113 Meas																
GBW 07113 Cert																
LKSD-3 Meas			2.3		85.8		41.1	7.6				4.7				2.6
LKSD-3 Cert			2.3		90		44	8				4.9				2.7
TDB-1 Meas				16.5	38.9		23.5		2							3.2
TDB-1 Cert				17	41		23		2.1							3.4
W-2a Meas				10.9	23.4		12.4	3.2	1.1		0.6	3.7	0.8			2
W-2a Cert				10	23		13	3.3	1		0.63	3.6	0.76			2.1
SY-4 Meas																
SY-4 Cert																
CTA-AC-1 Meas				> 2000	> 3000		1160	164	44.2	126	14.4					10.5
CTA-AC-1 Cert				2176	3326		1087	162	46.7	124	13.9					11.4
BIR-1a Meas		0.6			1.8			1								1.6
BIR-1a Cert		0.58			1.9			1.1								1.7
NCS DC86312 Meas				> 2000	175		1530			231	31.7	183	34.6	101	13.5	84
NCS DC86312 Cert				2360	190		1600			225.0	34.6	183	36	96.2	15.1	87.79
NCS DC70009 (GBW07241) Meas		2.9	45.1	22.8	57.7	7.7	30.5	11.9		15	3	20.7	4.2	13.5	2.1	15.2
NCS DC70009 (GBW07241) Cert		3.1	41	23.7	60.3	7.9	32.9	12.5		14.8	3.3	20.7	4.5	13.4	2.2	14.9
OREAS 100a (Fusion) Meas				260	467	47.2	150	24	3.65		3.6	23.8	5	15.7	2.35	15.5
OREAS 100a (Fusion) Cert				260	463	47.1	152	23.6	3.71		3.80	23.2	4.81	14.9	2.31	14.9
OREAS 101a (Fusion) Meas				764	1320	125	376	47.8	7.67			31.1	6.3	19.5	2.7	17.3
OREAS 101a (Fusion) Cert				816	1396	134	403	48.8	8.06			33.3	6.46	19.5	2.90	17.5
OREAS 101b (Fusion) Meas				799	1380	124	380	49	8.09		5.3	32	6.4	19.1	2.79	18.2
OREAS 101b (Fusion) Cert				789	1331	127	378	48	7.77		5.37	32.1	6.34	18.7	2.66	17.6
JR-1 Meas	2		21.4	18.7	44.7	5.7	22.5	5.8		5.3	0.9	6.2			0.63	4.4
JR-1 Cert	2.86		20.8	19.7	47.2	5.58	23.3	6.03		5.06	1.01	5.69			0.67	4.55
Method Blank	< 1	< 0.5	< 0.5	< 0.1	< 0.1	< 0.05	< 0.1	< 0.1	< 0.05	< 0.1	< 0.1	< 0.1	< 0.1	< 0.1	< 0.05	< 0.1

Quality control information. Report Number: A15-02933. Report Date: 19/5/2015.

Analyte Symbol	Lu	Hf	Ta	W	Tl	Pb	Bi	Th	U
Unit Symbol	ppm	ppm	ppm	ppm	ppm	ppm	ppm	ppm	ppm
Detection Limit	0.04	0.2	0.1	1	0.1	5	0.4	0.1	0.1
Analysis Method	FUS-MS	FUS-MS	FUS-MS	FUS-MS	FUS-MS	FUS-MS	FUS-MS	FUS-MS	FUS-MS
NIST 694 Meas									
NIST 694 Cert									
DNC-1 Meas									
DNC-1 Cert									
GBW 07113 Meas									
GBW 07113 Cert									
LKSD-3 Meas	0.41	4.7	0.7					10.5	4.6
LKSD-3 Cert	0.4	4.8	0.7					11.4	4.6
TDB-1 Meas								2.5	
TDB-1 Cert								2.7	
W-2a Meas	0.33			< 1	< 0.1	9	< 0.4		0.5
W-2a Cert	0.33			0.3	0.2	9.3	0.03		0.53
SY-4 Meas									
SY-4 Cert									
CTA-AC-1 Meas	1.16							24	4.1
CTA-AC-1 Cert	1.08							21.8	4.4
BIR-1a Meas	0.28					< 5			
BIR-1a Cert	0.3					3			
NCS DC86312 Meas	12.4								
NCS DC86312 Cert	11.96								
NCS DC70009 (GBW07241) Meas	2.28			2220	2			28.6	
NCS DC70009 (GBW07241) Cert	2.4			2200	1.8			28.3	
OREAS 100a (Fusion) Meas	2.29							54.4	144
OREAS 100a (Fusion) Cert	2.26							51.6	135
OREAS 101a (Fusion) Meas	2.49							35.2	404
OREAS 101a (Fusion) Cert	2.66							36.6	422
OREAS 101b (Fusion) Meas	2.73							37.6	406
OREAS 101b (Fusion) Cert	2.58							37.1	396
JR-1 Meas	0.7	4.4	1.9			18	0.6	26.7	8.9
JR-1 Cert	0.71	4.51	1.86			19.3	0.56	26.7	8.88
Method Blank	< 0.04	< 0.2	< 0.1	< 1	< 0.1	< 5	< 0.4	< 0.1	< 0.1

Appendix 1-2

Estimated median of four pXRF measurement series with employed factory calibration (without applied empirical calibration). All units in ppm. Samples 2, 5 and 11 were not measured as the samples were only sent to the laboratory for comparison studies. All elements sorted in original order provided by the pXRF device.

Element	Si	Si Error	Ti	Ti Error	Al	Al Error	Fe	Fe Error	Mn	Mn Error
Sample 1	185643	782	10585	92	57817	599	77999	306	1436	48
Sample 3	162571	714	11489	105	58116	647	114195	409	2224	55
Sample 4	190226	792	11065	93	55927	592	75961	297	1374	47
Sample 6	160352	709	9654	97	56553	629	115016	413	1151	45
Sample 7	160574	699	9087	92	65781	663	107972	382	1512	48
Sample 8	155198	693	10213	99	60601	656	116322	408	2026	53
Sample 9	162125	711	11775	107	60571	659	112796	400	2322	55
Sample 10	178616	766	10523	92	53731	588	80537	300	1005	42

Element	K	K Error	V	V Error	Cr	Cr Error	Ni	Ni Error	Cu	Cu Error
Sample 1	16246	262	389	31	148	28	< LOD		< LOD	
Sample 3	14427	278	550	38	195	33	43		29	
Sample 4	18382	274	407	32	150	28	< LOD		< LOD	
Sample 6	22208	338	508	36	205	33	< LOD		< LOD	
Sample 7	11554	246	507	34	228	33	< LOD		< LOD	
Sample 8	13273	268	526	37	195	34	49	16	35	8
Sample 9	14542	279	543	38	207	33	46	16	34	8
Sample 10	25698	325	447	32	148	28	< LOD		< LOD	

Element	Zn	Zn Error	Rb	Rb Error	Sr	Sr Error	Y	Y Error	Zr	Zr Error
Sample 1	76	5	44	1	392	9	46	1	1239	7
Sample 3	129	6	36	1	456	10	41	1	562	5
Sample 4	71	5	41	1	447	10	43	1	1271	7
Sample 6	77	5	40	1	484	10	26	1	760	5
Sample 7	56	5	32	1	289	8	29	1	728	5
Sample 8	135	6	32	1	474	10	38	1	406	4
Sample 9	143	6	35	1	492	10	42	1	528	4
Sample 10	85	5	46	1	588	11	48	1	945	6

Element	Nb	Nb Error	Ba	Ba Error	Ce	Ce Error	La	La Error	Cd	Cd Error
Sample 1	38	1	575	24	287	23	192	19	< LOD	
Sample 3	29	1	817	27	354	25	212	21	< LOD	
Sample 4	42	1	632	24	278	23	179	19	< LOD	
Sample 6	31	1	810	27	392	26	224	21	< LOD	
Sample 7	32	1	531	25	465	26	201	20	< LOD	
Sample 8	25	1	810	27	326	25	208	21	< LOD	
Sample 9	29	1	720	27	314	25	204	21	< LOD	
Sample 10	34	1	763	25	258	23	154	19	< LOD	

Element	Ag	Ag Error	Bal	Bal Error	Th	Th Error	Bi	Bi Error	As	As Error
Sample 1	< LOD		645379	1751	< LOD		< LOD		< LOD	
Sample 3	< LOD		626526	1952	< LOD		< LOD		4	4
Sample 4	< LOD		639187	1767	< LOD		< LOD		< LOD	
Sample 6	< LOD		629454	1901	< LOD		< LOD		< LOD	
Sample 7	< LOD		639625	1840	< LOD		< LOD		< LOD	
Sample 8	< LOD		631484	1922	< LOD		< LOD		< LOD	
Sample 9	< LOD		626308	1928	< LOD		< LOD		< LOD	
Sample 10	< LOD		643097	1765	< LOD		< LOD		< LOD	

Element	Se	Se Error	Pb	Pb Error	Hg	Hg Error	Co	Co Error	Ca	Ca Error
Sample 1	< LOD		13	2	< LOD		< LOD		524	41
Sample 3	< LOD		8	2	< LOD		< LOD		2615	74
Sample 4	< LOD		12	2	< LOD		< LOD		825	46
Sample 6	< LOD		14	2	< LOD		< LOD		627	52
Sample 7	< LOD		25	2	< LOD		< LOD		333	38
Sample 8	< LOD		8	2	< LOD		< LOD		2999	78
Sample 9	< LOD		8	2	< LOD		< LOD		2405	72
Sample 10	< LOD		11	2	< LOD		< LOD		1193	56

Element	P	P Error	Cl	Cl Error	S	S Error	Mg	Mg Error
Sample 1	603	122	541	24	< LOD		< LOD	
Sample 3	3486	158	638	25	< LOD		< LOD	
Sample 4	3306	152	536	24	316		< LOD	
Sample 6	< LOD		586	25	< LOD		< LOD	
Sample 7	< LOD		590	24	< LOD		< LOD	
Sample 8	3520	158	630	25	< LOD		< LOD	
Sample 9	3376	158	659	26	< LOD		< LOD	
Sample 10	493	124	591	25	< LOD		< LOD	

Appendix 1-3

Comparison of the results of the laboratory (ICP-MS), pXRF measurements of device 1 (FC pXRF 1) and 2 (FC pXRF 2) as well as the results after applying the empirical calibration (Calibrated pXRF 1). All data given in ppm. Elements sorted by atomic number. Data for the standards 2, 5 and 11 were not provided as these samples were used for laboratory analysis only.

For the calibration of Ni the factory calibration of device 1 (FC pXRF 1) was used, since the values were close to the results from the laboratory. In case of Cr the results of both pXRF devices appeared more reliable compared with the results from the laboratory.

Al

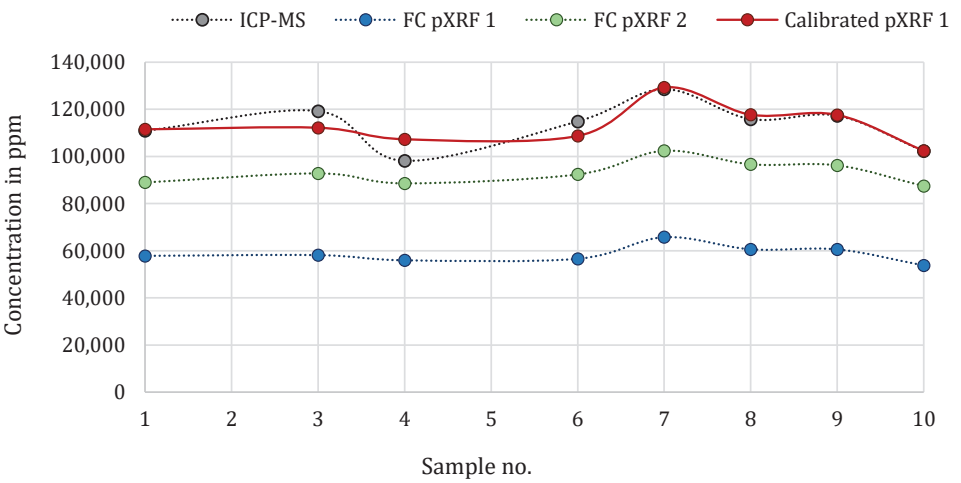
ICP-MS
FC pXRF 1
FC pXRF 2
Calibrated pXRF 1
Concentration in ppm
140,000
120,000
100,000
80,000
60,000
40,000
20,000
0
1
2
3
4
5
6
7
8
9
10
Sample no.

Si

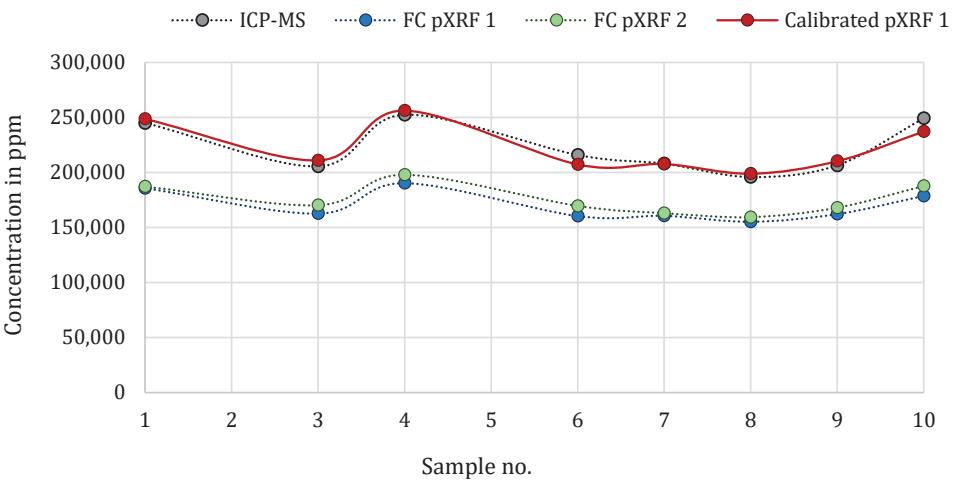
ICP-MS
FC pXRF 1
FC pXRF 2
Calibrated pXRF 1
Concentration in ppm
300,000
250,000
200,000
150,000
100,000
50,000
0
1
2
3
4
5
6
7
8
9
10
Sample no.

P

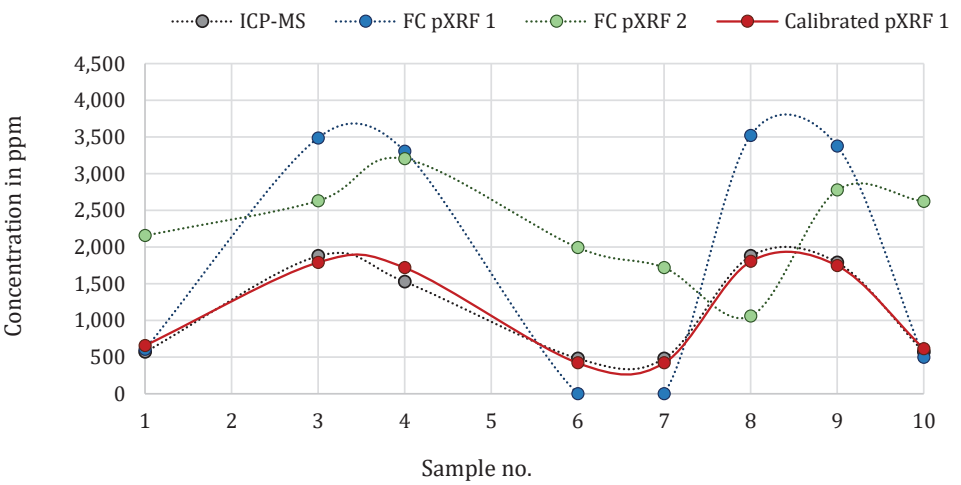
ICP-MS
FC pXRF 1
FC pXRF 2
Calibrated pXRF 1
Concentration in ppm
4,500
4,000
3,500
3,000
2,500
2,000
1,500
1,000
500
0
1
2
3
4
5
6
7
8
9
10
Sample no.

K

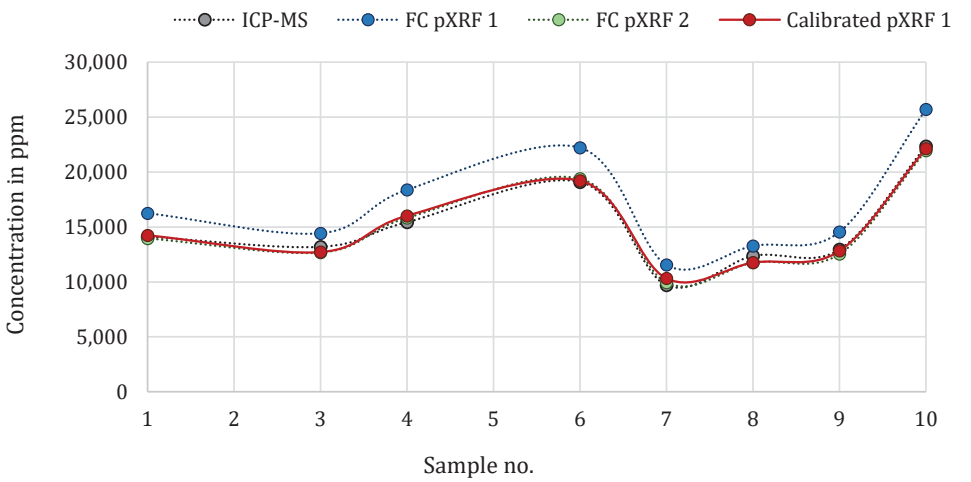
ICP-MS
FC pXRF 1
FC pXRF 2
Calibrated pXRF 1
Concentration in ppm
30,000
25,000
20,000
15,000
10,000
5,000
0
1
2
3
4
5
6
7
8
9
10
Sample no.

Ca

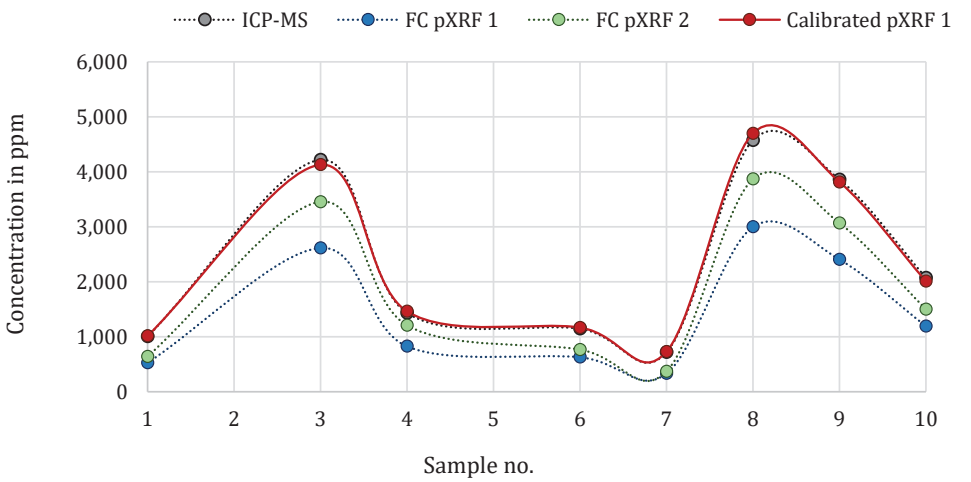
ICP-MS
FC pXRF 1
FC pXRF 2
Calibrated pXRF 1
Concentration in ppm
6,000
5,000
4,000
3,000
2,000
1,000
0
1
2
3
4
5
6
7
8
9
10
Sample no.

Ti

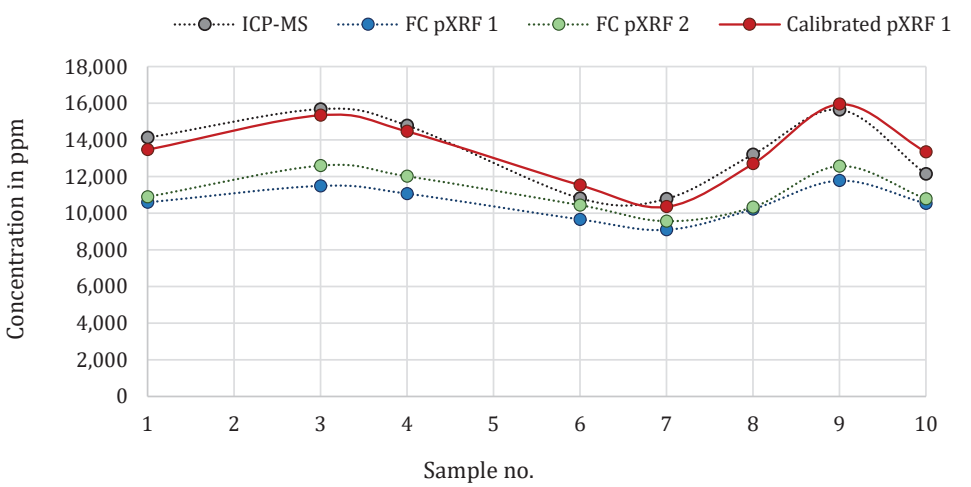
ICP-MS
FC pXRF 1
FC pXRF 2
Calibrated pXRF 1
Concentration in ppm
18,000
16,000
14,000
12,000
10,000
8,000
6,000
4,000
2,000
0
1
2
3
4
5
6
7
8
9
10
Sample no.

V

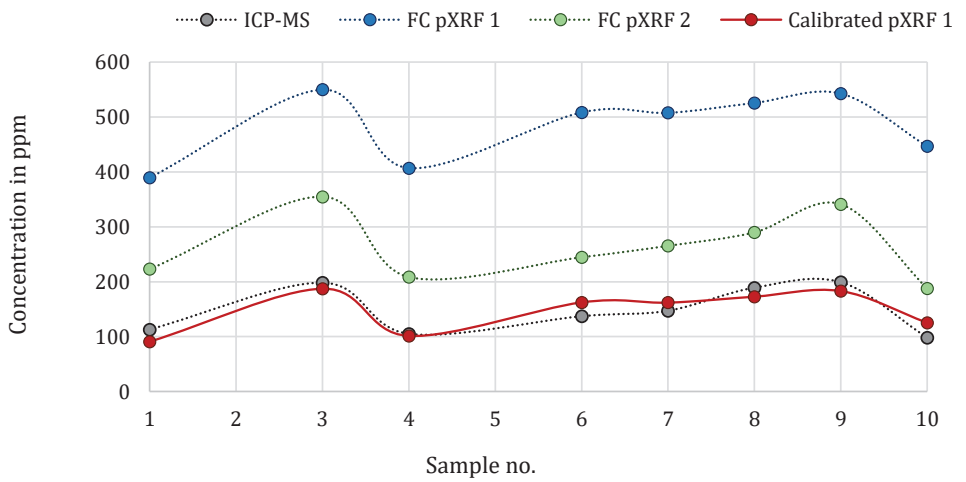
ICP-MS
FC pXRF 1
FC pXRF 2
Calibrated pXRF 1
Concentration in ppm
600
500
400
300
200
100
0
1
2
3
4
5
6
7
8
9
10
Sample no.

Cr

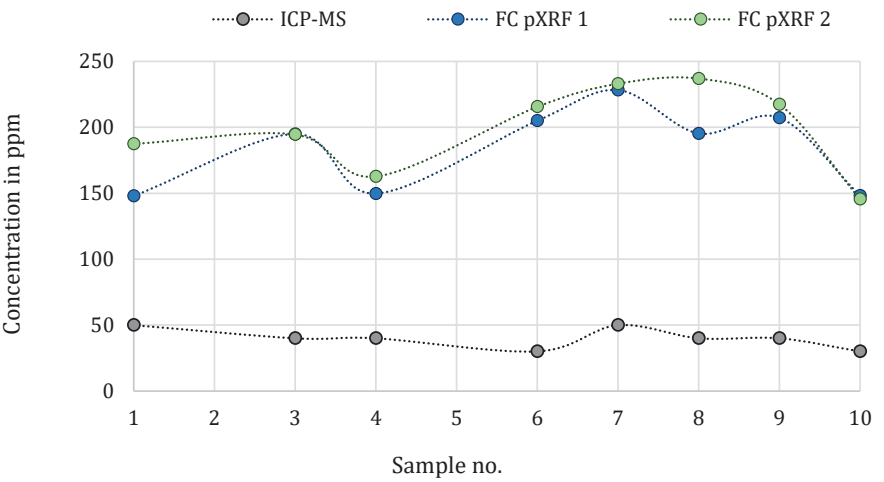
ICP-MS
FC pXRF 1
FC pXRF 2
Concentration in ppm
250
200
150
100
50
0
1
2
3
4
5
6
7
8
9
10
Sample no.

Mn

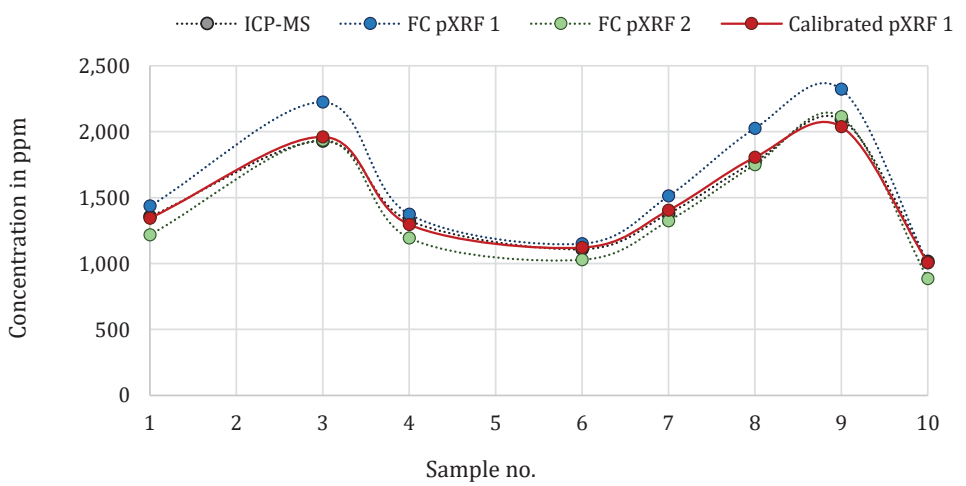
ICP-MS
FC pXRF 1
FC pXRF 2
Calibrated pXRF 1
Concentration in ppm
2,500
2,000
1,500
1,000
500
0
1
2
3
4
5
6
7
8
9
10
Sample no.

Fe

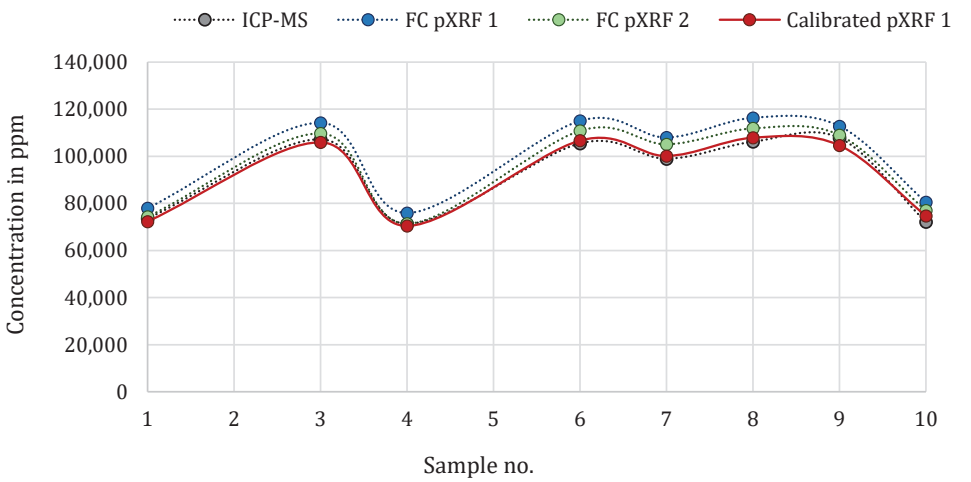
ICP-MS
FC pXRF 1
FC pXRF 2
Calibrated pXRF 1
Concentration in ppm
140,000
120,000
100,000
80,000
60,000
40,000
20,000
0
1
2
3
4
5
6
7
8
9
10
Sample no.

Ni

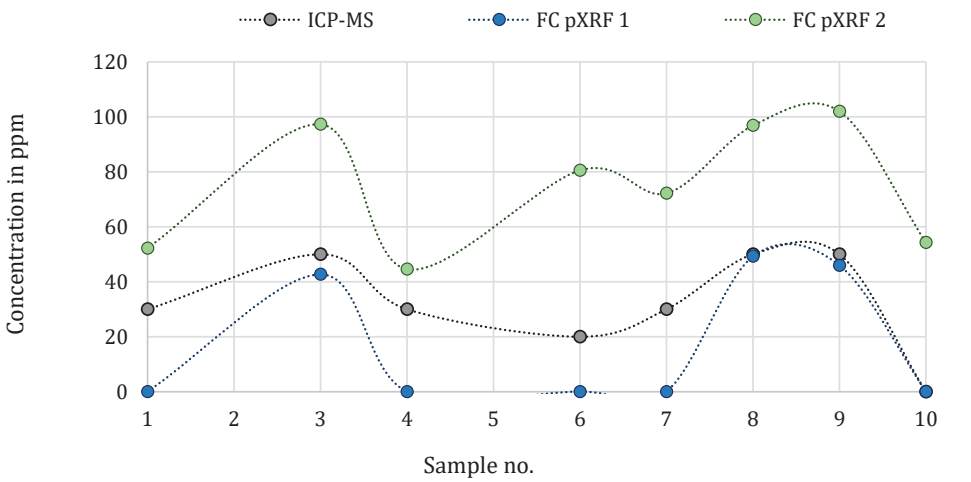
ICP-MS
FC pXRF 1
FC pXRF 2
Concentration in ppm
120
100
80
60
40
20
0
1
2
3
4
5
6
7
8
9
10
Sample no.

Cu

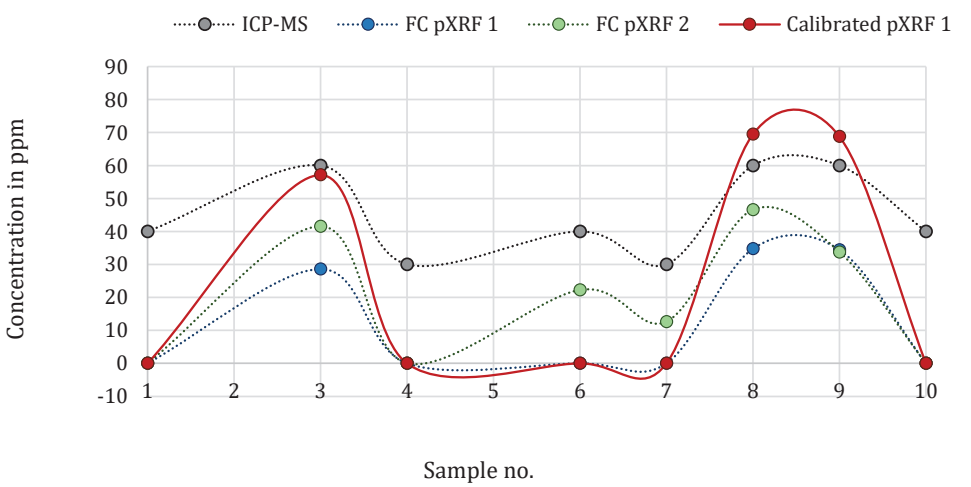
ICP-MS
FC pXRF 1
FC pXRF 2
Calibrated pXRF 1
Concentration in ppm
90
80
70
60
50
40
30
20
10
0
-10
1
2
3
4
5
6
7
8
9
10
Sample no.

Zn

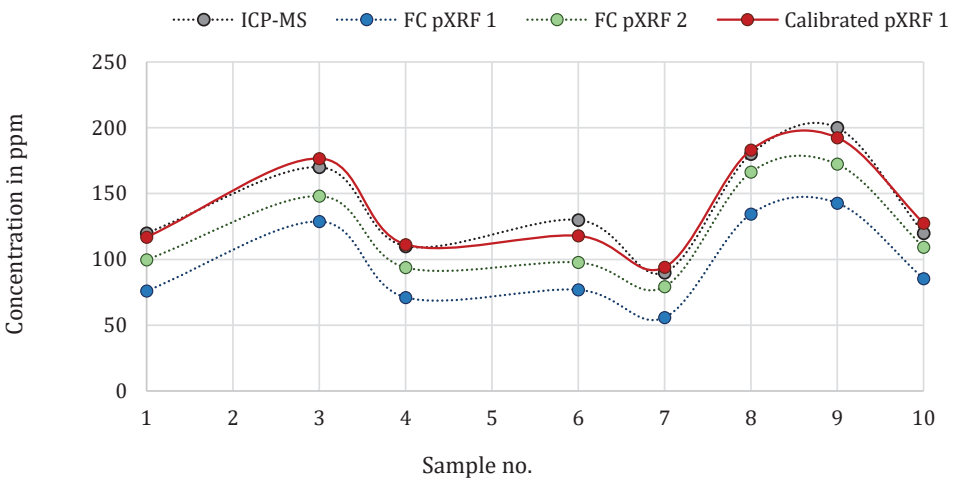
ICP-MS
FC pXRF 1
FC pXRF 2
Calibrated pXRF 1
Concentration in ppm
250
200
150
100
50
0
1
2
3
4
5
6
7
8
9
10
Sample no.

Rb

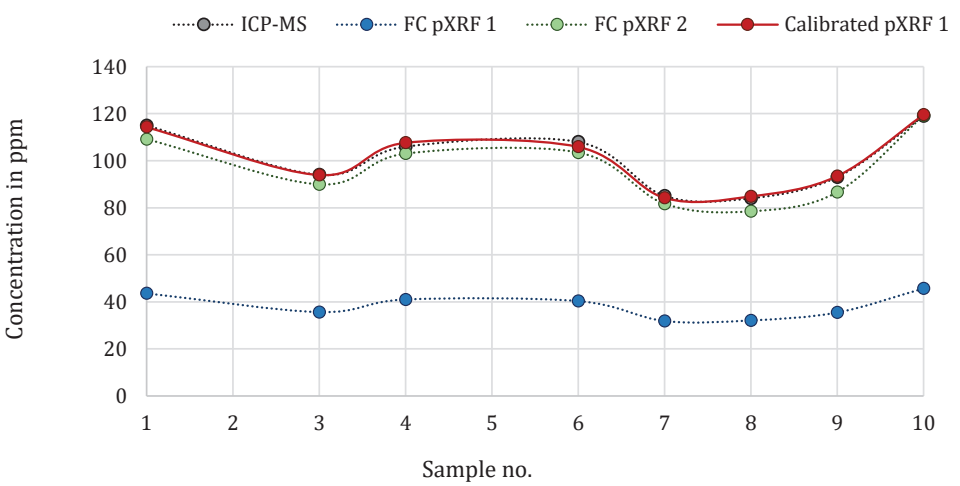
ICP-MS
FC pXRF 1
FC pXRF 2
Calibrated pXRF 1
Concentration in ppm
140
120
100
80
60
40
20
0
1
2
3
4
5
6
7
8
9
10
Sample no.

Sr

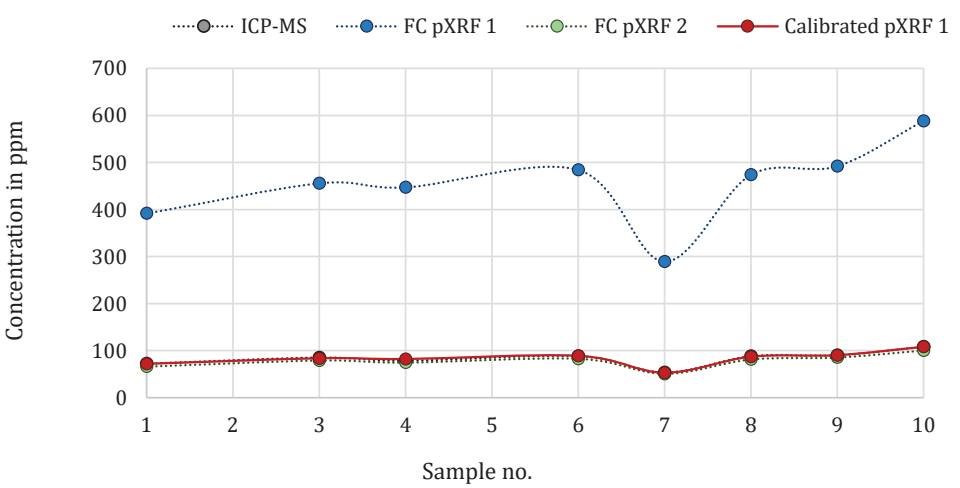
ICP-MS
FC pXRF 1
FC pXRF 2
Calibrated pXRF 1
Concentration in ppm
700
600
500
400
300
200
100
0
1
2
3
4
5
6
7
8
9
10
Sample no.

Y

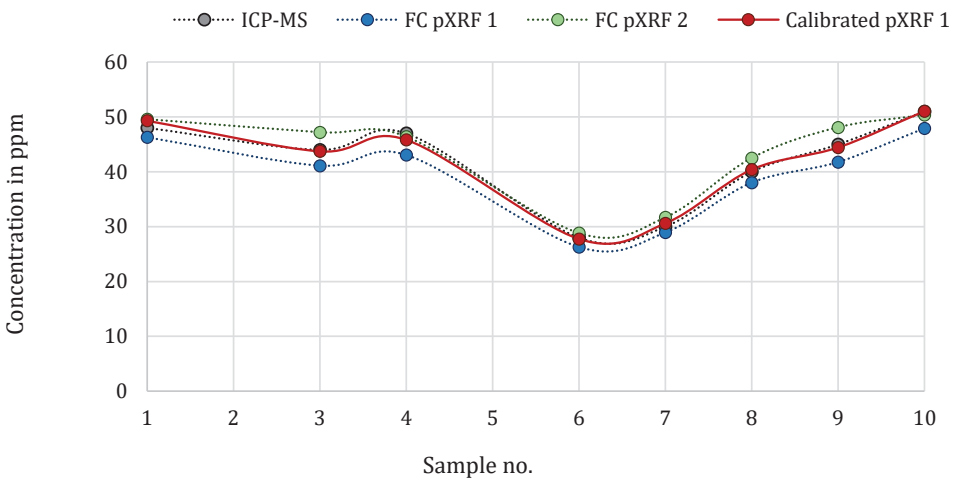
ICP-MS
FC pXRF 1
FC pXRF 2
Calibrated pXRF 1
Concentration in ppm
0
10
20
30
40
50
60
1
2
3
4
5
6
7
8
9
10
Sample no.

Zr

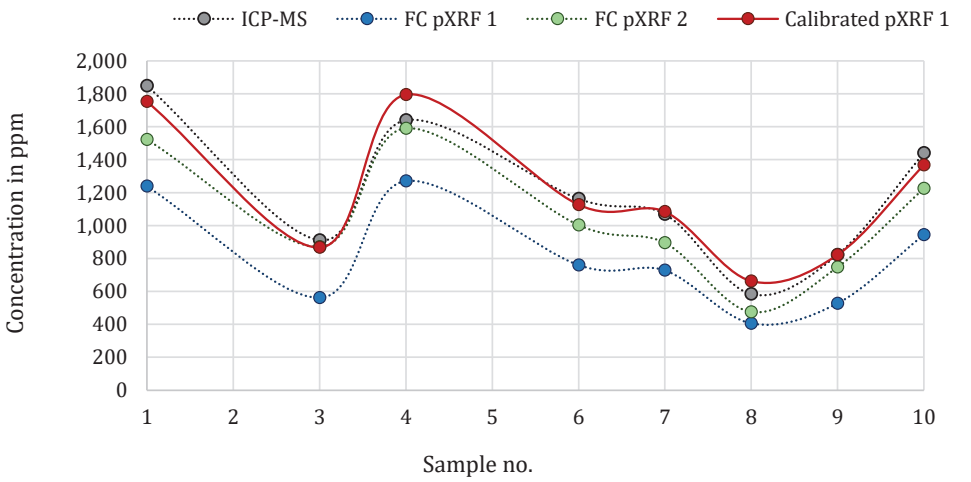
ICP-MS
FC pXRF 1
FC pXRF 2
Calibrated pXRF 1
Concentration in ppm
0
200
400
600
800
1,000
1,200
1,400
1,600
1,800
2,000
1
2
3
4
5
6
7
8
9
10
Sample no.

Nb

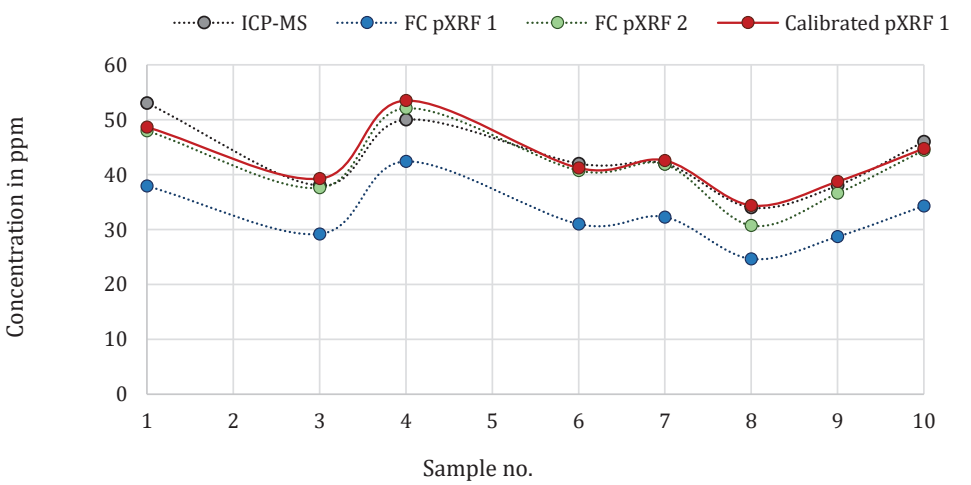
ICP-MS
FC pXRF 1
FC pXRF 2
Calibrated pXRF 1
Concentration in ppm
0
10
20
30
40
50
60
1
2
3
4
5
6
7
8
9
10
Sample no.

Ba

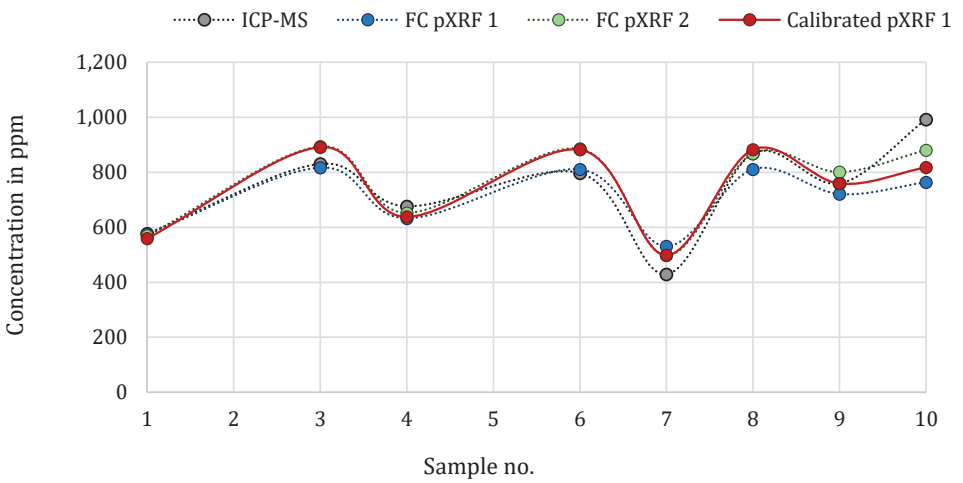
ICP-MS
FC pXRF 1
FC pXRF 2
Calibrated pXRF 1
Concentration in ppm
1,200
1,000
800
600
400
200
0
1
2
3
4
5
6
7
8
9
10
Sample no.

La

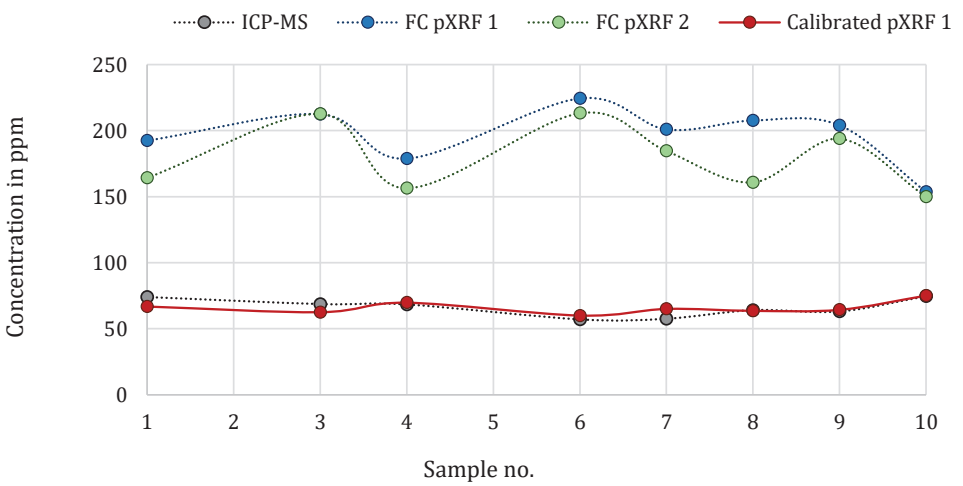
ICP-MS
FC pXRF 1
FC pXRF 2
Calibrated pXRF 1
Concentration in ppm
250
200
150
100
50
0
1
2
3
4
5
6
7
8
9
10
Sample no.

Pb

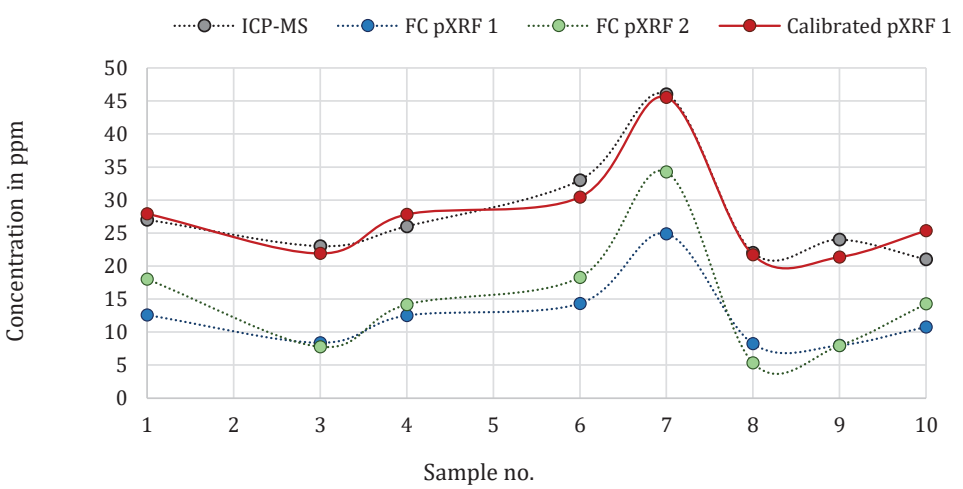
ICP-MS
FC pXRF 1
FC pXRF 2
Calibrated pXRF 1
Concentration in ppm
50
45
40
35
30
25
20
15
10
5
0
1
2
3
4
5
6
7
8
9
10
Sample no.

Appendix 1-4

Excerpt of the laboratory results (converted to ppm) used for test A-C for the pre-study on sample preparation. Only elements that can be obtained by the pXRF device were selected.

	Test A		Test B		Test C	
Element	**Sample 8**	**Sample 11**	**Sample 1**	**Sample 2**	**Sample 4**	**Sample 5**
Si	195718	196747	244893	233768	252326	236573
Ti	13195	13333	14119	13603	14784	14059
Al	115798	119450	110876	110770	98121	107595
Fe	106154	108881	73636	73217	71329	70629
Mn	1774	1789	1355	1386	1324	1379
K	12369	12203	14113	13199	15441	14445
V	189	191	113	110	105	107
Cr	40	40	50	40	40	40
Zn	180	180	120	130	110	120
Rb	84	83	115	115	106	113
Sr	88	89	72	68	78	74
Y	40	40	48	53	47	56
Zr	584	696	1849	1824	1640	1985
Nb	34	34	53	53	50	52
Ba	868	870	577	538	676	617
Ce	124	126	137	154	124	141
La	64	65.3	73.9	77	68.3	78.7
Pb	22	22	27	29	26	24
Ca	4574	4717	1001	929	1429	1215
P	567	655	1527	698	1877	1920
Ni	30	30	30	30	50	50
Cu	40	40	30	40	60	60

Appendix 1-5

Comparison of different grain sizes and their elemental composition displayed with their 'original' grain size. For comparison reasons, the grain sizes of 125-250 μm and 250 μm – 2 mm were ground and sieved to < 125 μm. All samples taken from the site of Kusuma 1, with samples 9 and 10 from feature 2. All data given in ppm and elements sorted by atomic number.

Al

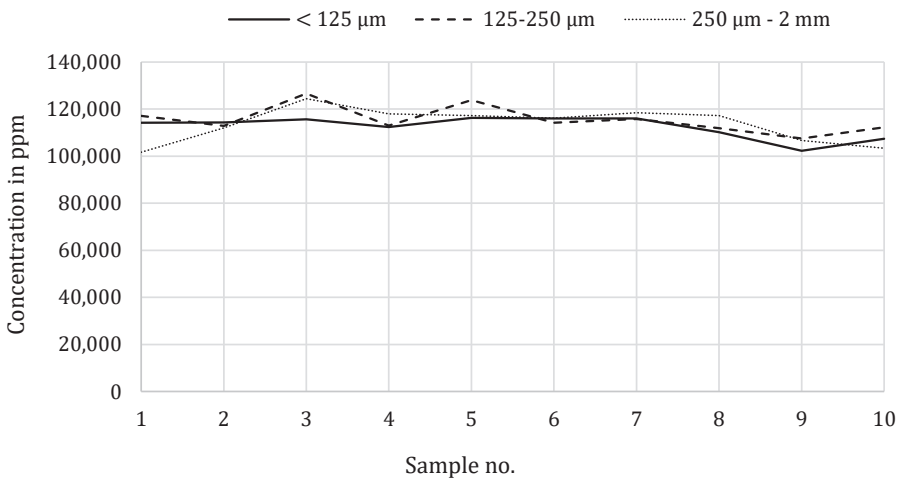
< 125 µm
125-250 µm
250 µm - 2 mm
140,000
120,000
100,000
80,000
60,000
40,000
20,000
0
Concentration in ppm
1
2
3
4
5
6
7
8
9
10
Sample no.

Si

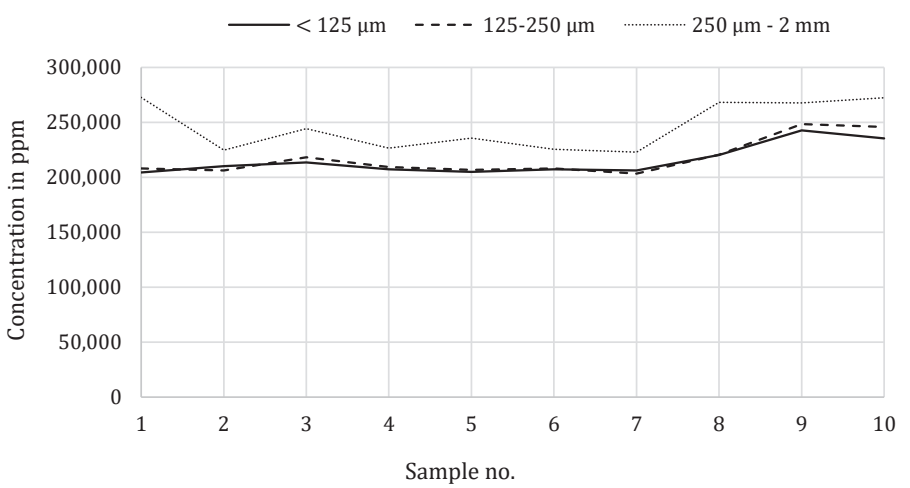
< 125 µm
125-250 µm
250 µm - 2 mm
300,000
250,000
200,000
150,000
100,000
50,000
0
Concentration in ppm
1
2
3
4
5
6
7
8
9
10
Sample no.

P

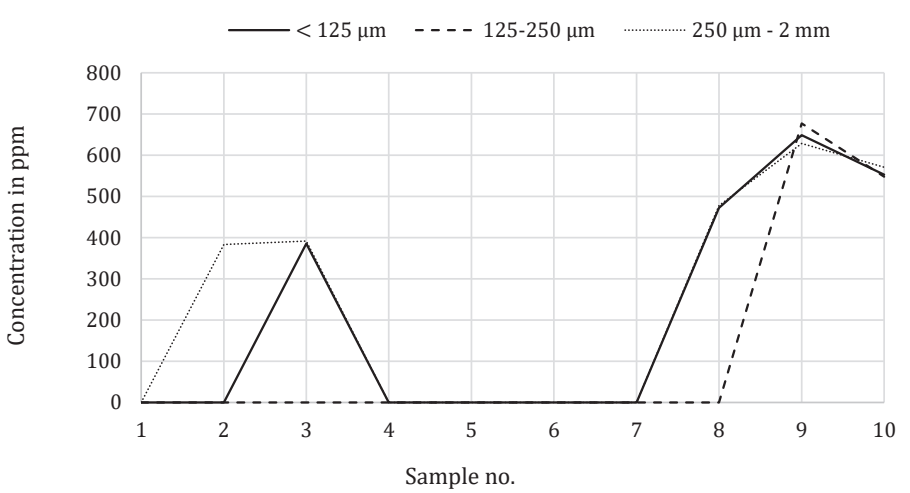
< 125 µm
125-250 µm
250 µm - 2 mm
800
700
600
500
400
300
200
100
0
Concentration in ppm
1
2
3
4
5
6
7
8
9
10
Sample no.

Cl

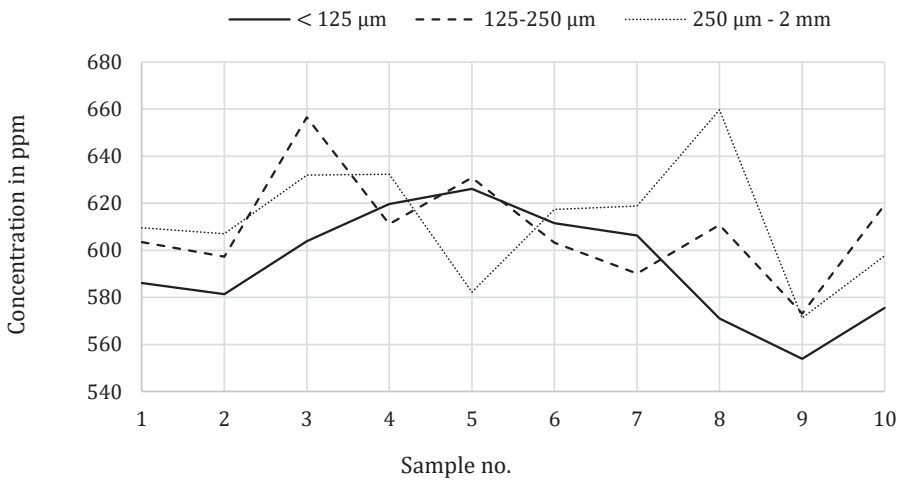
< 125 µm
125-250 µm
250 µm - 2 mm
Concentration in ppm
680
660
640
620
600
580
560
540
1
2
3
4
5
6
7
8
9
10
Sample no.

K

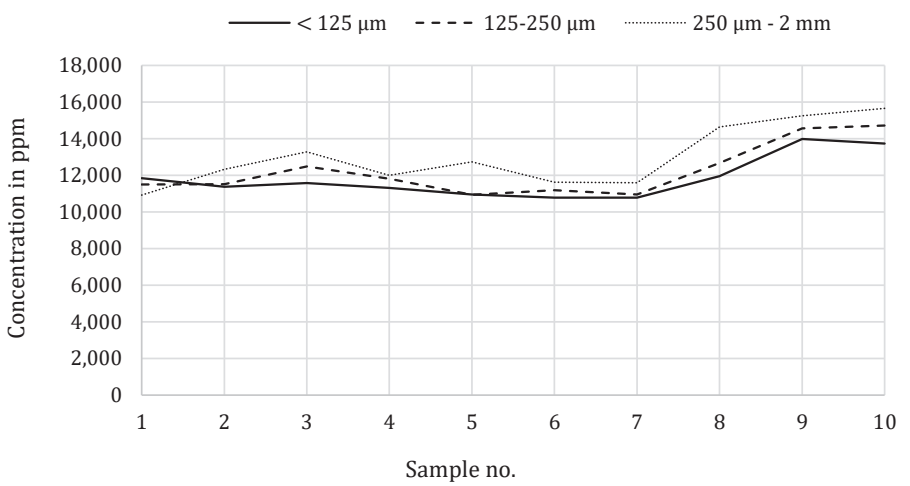
< 125 µm
125-250 µm
250 µm - 2 mm
Concentration in ppm
18,000
16,000
14,000
12,000
10,000
8,000
6,000
4,000
2,000
0
1
2
3
4
5
6
7
8
9
10
Sample no.

Ca

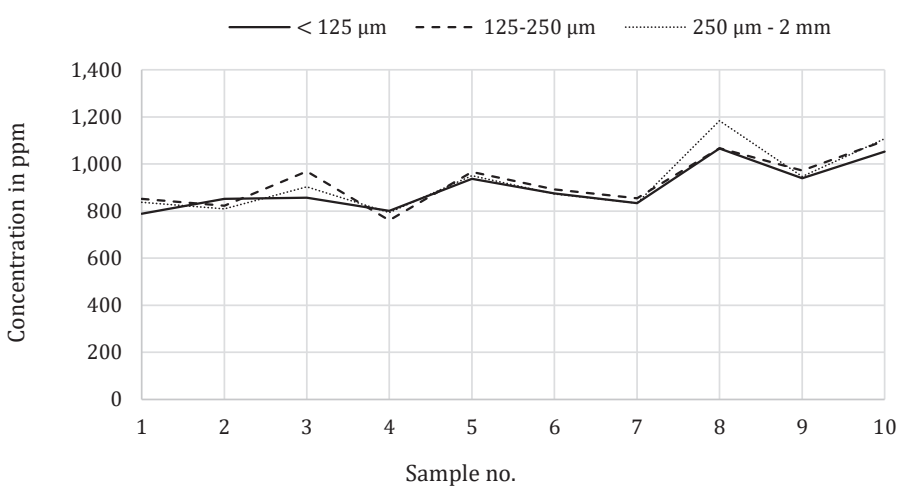
< 125 µm
125-250 µm
250 µm - 2 mm
Concentration in ppm
1,400
1,200
1,000
800
600
400
200
0
1
2
3
4
5
6
7
8
9
10
Sample no.

Ti

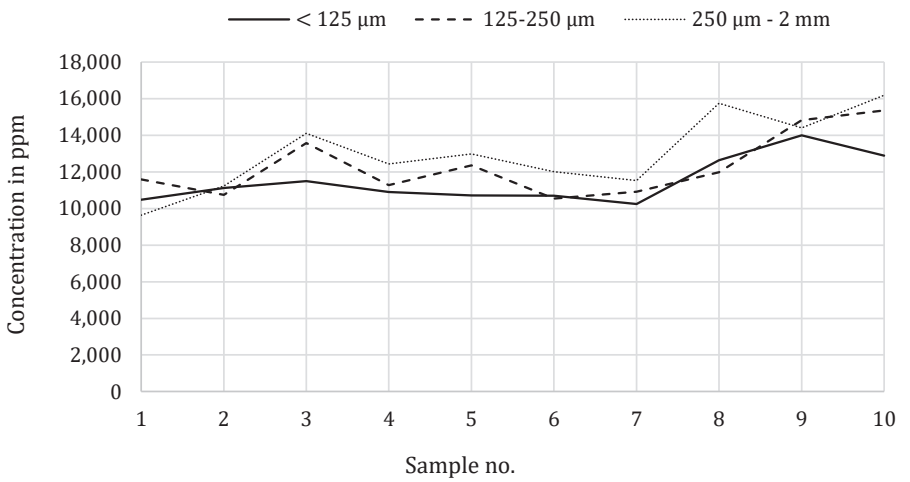
< 125 µm
125-250 µm
250 µm - 2 mm
Concentration in ppm
18,000
16,000
14,000
12,000
10,000
8,000
6,000
4,000
2,000
0
1
2
3
4
5
6
7
8
9
10
Sample no.

V

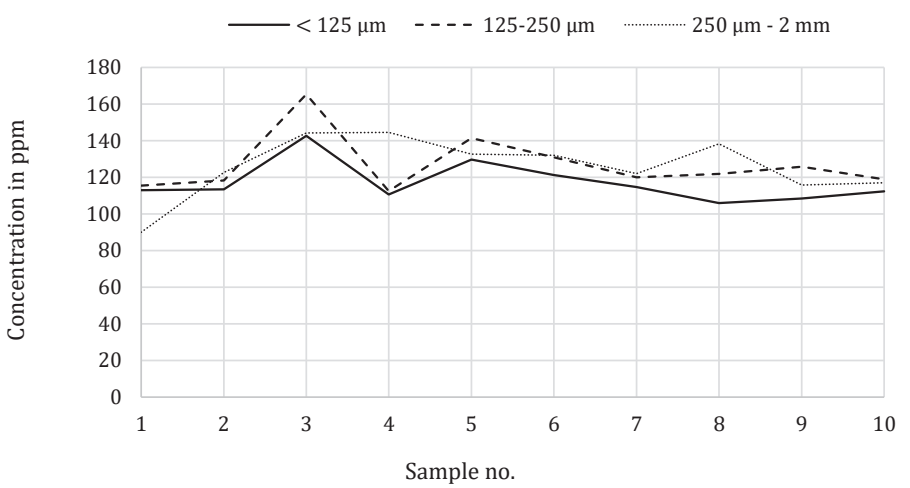
< 125 µm
125-250 µm
250 µm - 2 mm
Concentration in ppm
180
160
140
120
100
80
60
40
20
0
1
2
3
4
5
6
7
8
9
10
Sample no.

Cr

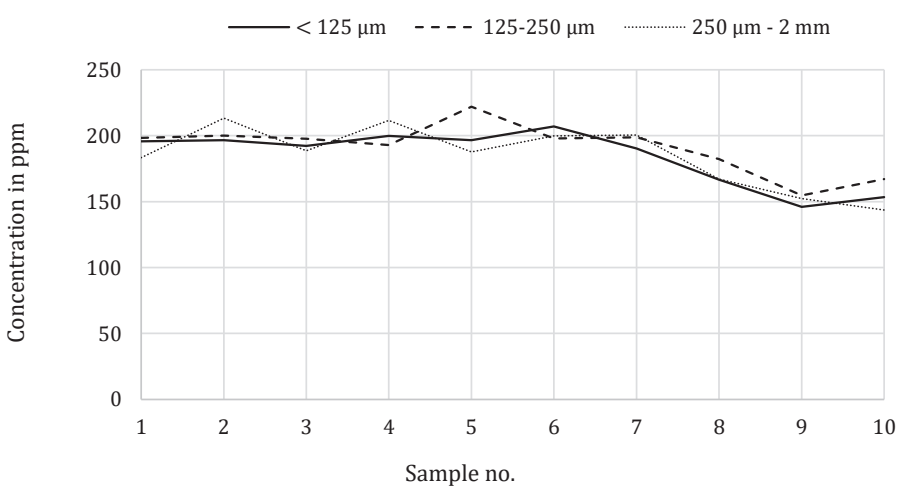
< 125 µm
125-250 µm
250 µm - 2 mm
Concentration in ppm
250
200
150
100
50
0
1
2
3
4
5
6
7
8
9
10
Sample no.

Mn

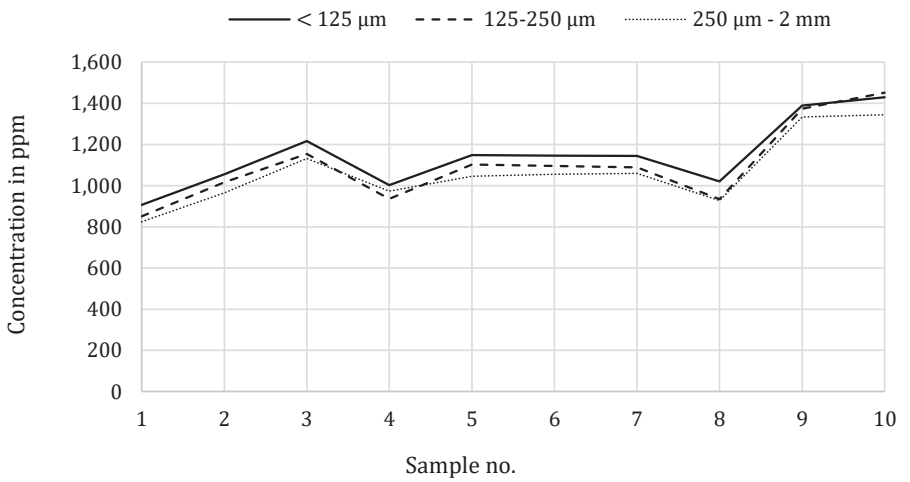
< 125 µm
125-250 µm
250 µm - 2 mm
Concentration in ppm
1,600
1,400
1,200
1,000
800
600
400
200
0
1
2
3
4
5
6
7
8
9
10
Sample no.

Fe

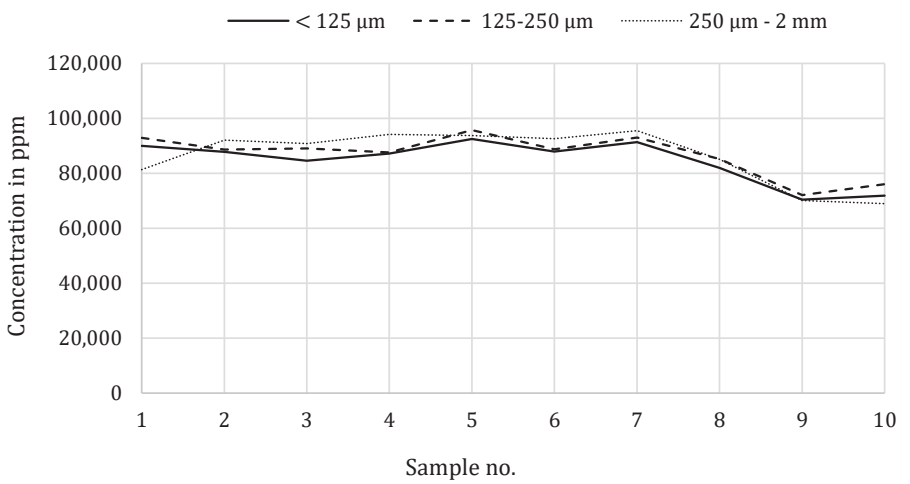
< 125 µm
125-250 µm
250 µm - 2 mm
Concentration in ppm
120,000
100,000
80,000
60,000
40,000
20,000
0
1
2
3
4
5
6
7
8
9
10
Sample no.

Zn

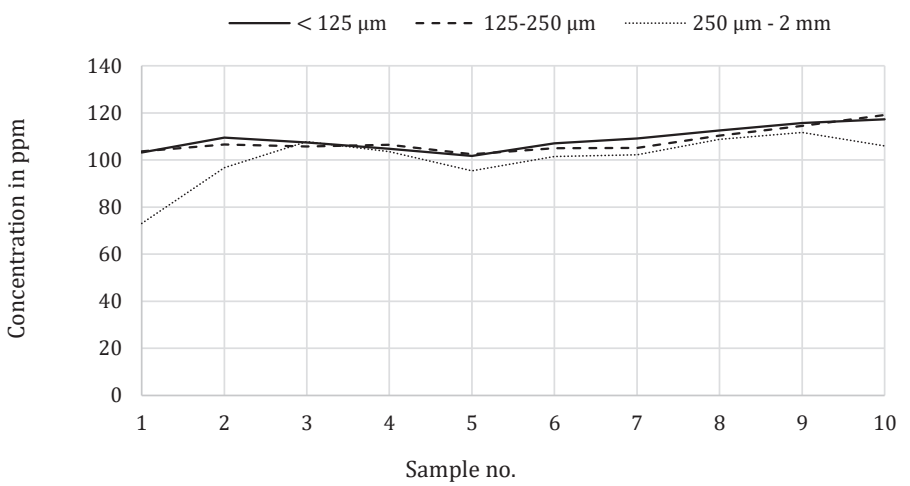
< 125 µm
125-250 µm
250 µm - 2 mm
Concentration in ppm
140
120
100
80
60
40
20
0
1
2
3
4
5
6
7
8
9
10
Sample no.

As

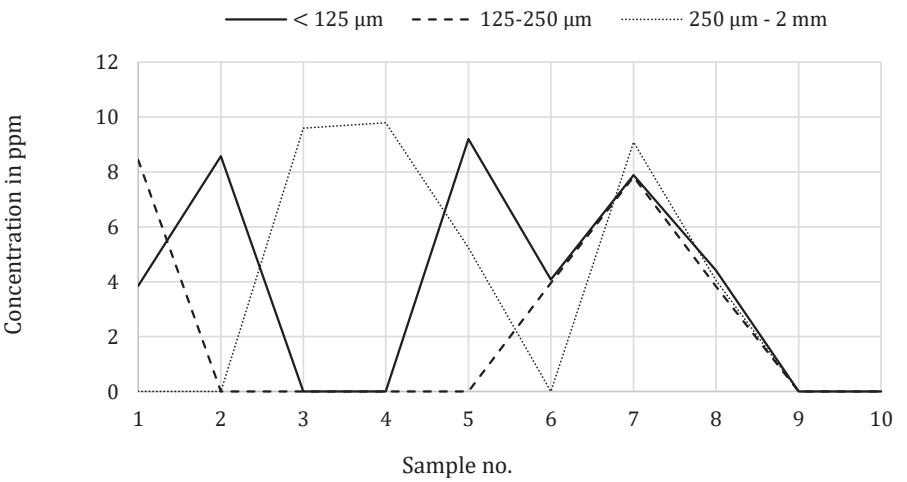
< 125 µm
125-250 µm
250 µm - 2 mm
Concentration in ppm
0
2
4
6
8
10
12
1
2
3
4
5
6
7
8
9
10
Sample no.

Rb

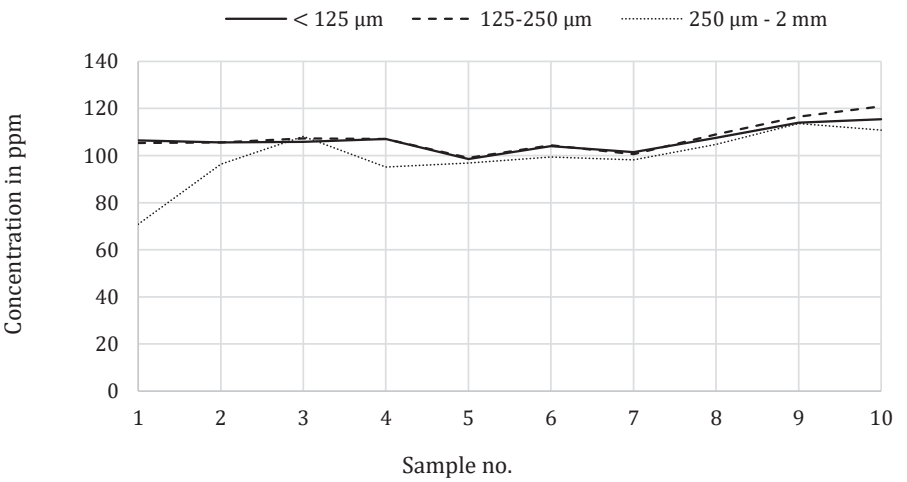
< 125 µm
125-250 µm
250 µm - 2 mm
Concentration in ppm
0
20
40
60
80
100
120
140
1
2
3
4
5
6
7
8
9
10
Sample no.

Sr

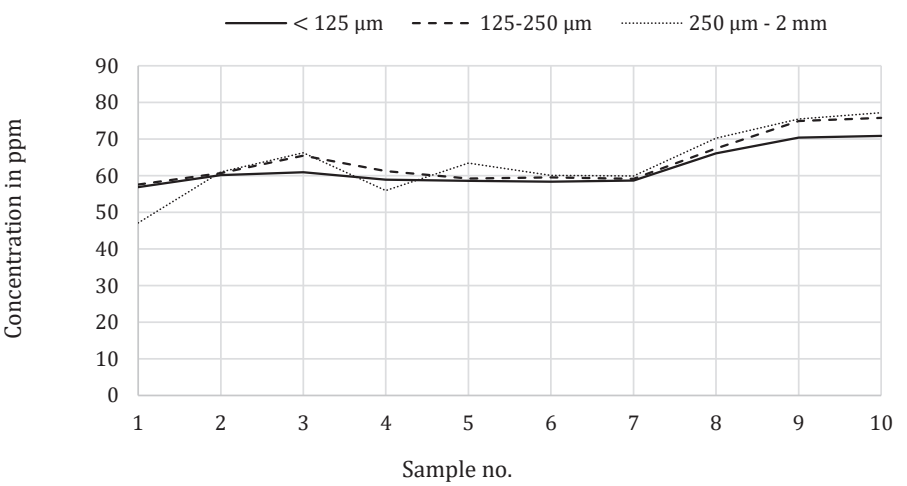
< 125 µm
125-250 µm
250 µm - 2 mm
Concentration in ppm
0
10
20
30
40
50
60
70
80
90
1
2
3
4
5
6
7
8
9
10
Sample no.

Y

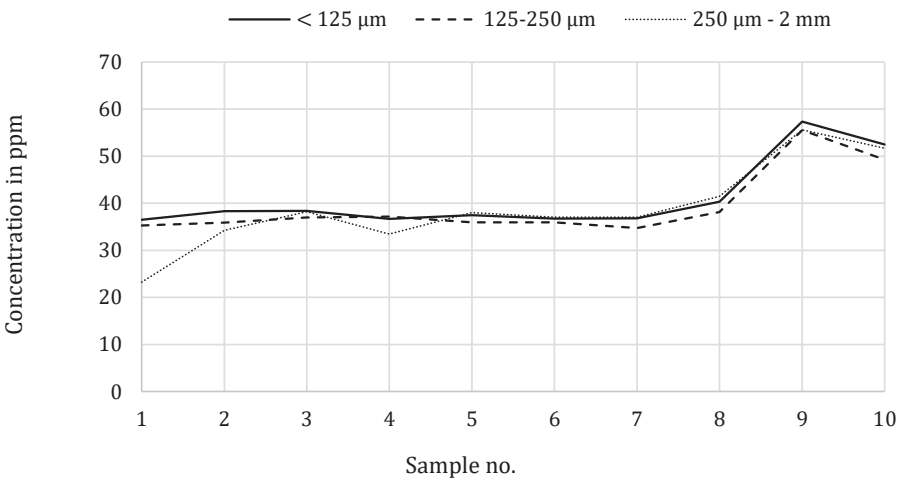
< 125 µm
125-250 µm
250 µm - 2 mm
Concentration in ppm
70
60
50
40
30
20
10
0
1
2
3
4
5
6
7
8
9
10
Sample no.

Zr

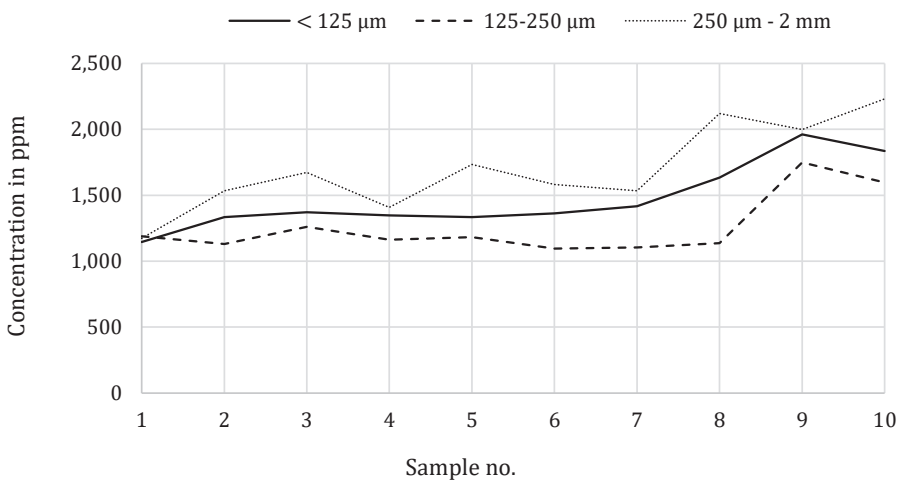
< 125 µm
125-250 µm
250 µm - 2 mm
Concentration in ppm
2,500
2,000
1,500
1,000
500
0
1
2
3
4
5
6
7
8
9
10
Sample no.

Nb

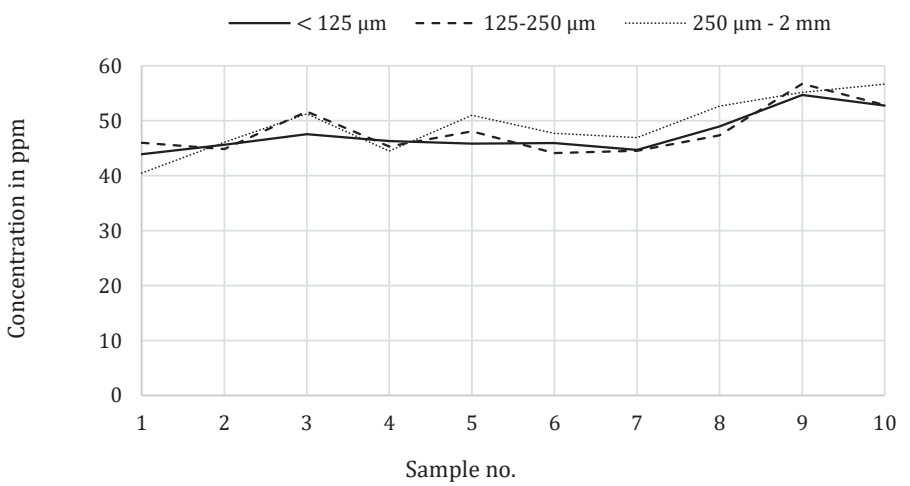
< 125 µm
125-250 µm
250 µm - 2 mm
Concentration in ppm
60
50
40
30
20
10
0
1
2
3
4
5
6
7
8
9
10
Sample no.

Ba

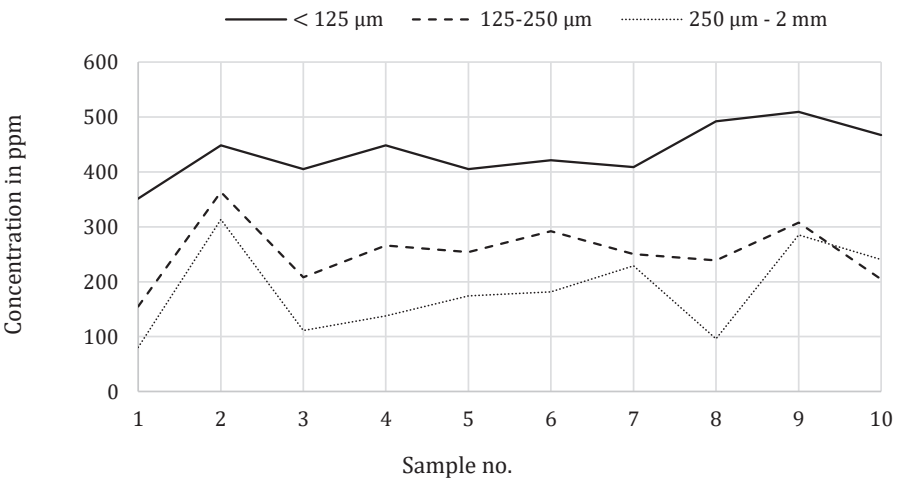
< 125 µm
125-250 µm
250 µm - 2 mm
Concentration in ppm
600
500
400
300
200
100
0
1
2
3
4
5
6
7
8
9
10
Sample no.

La

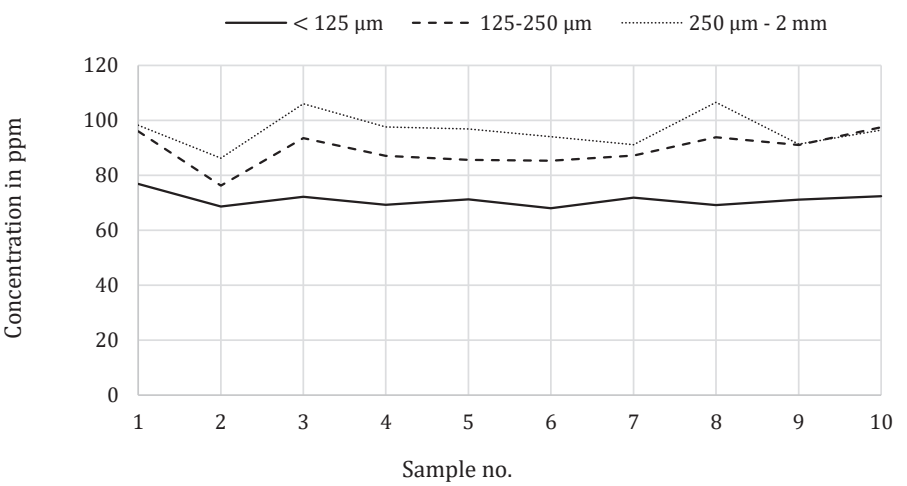
< 125 µm
125-250 µm
250 µm - 2 mm
Concentration in ppm
120
100
80
60
40
20
0
1
2
3
4
5
6
7
8
9
10
Sample no.

Ce

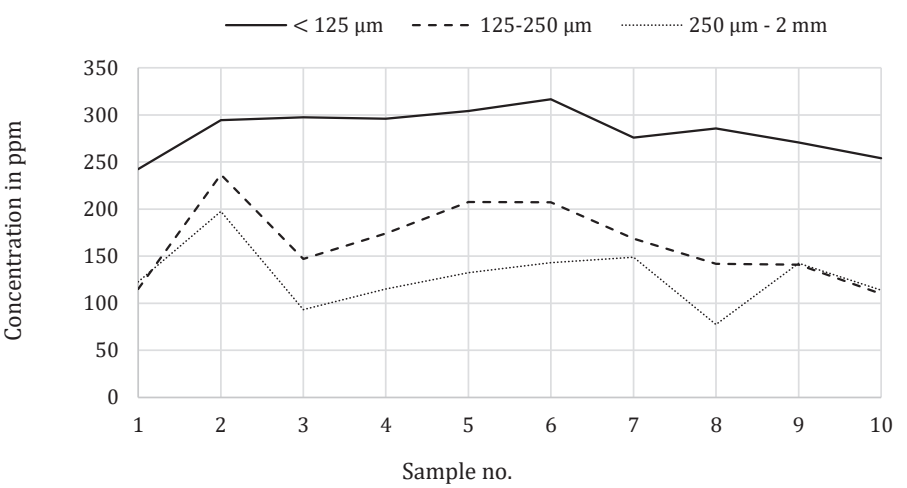
< 125 µm
125-250 µm
250 µm - 2 mm
Concentration in ppm
350
300
250
200
150
100
50
0
1
2
3
4
5
6
7
8
9
10
Sample no.

Pb

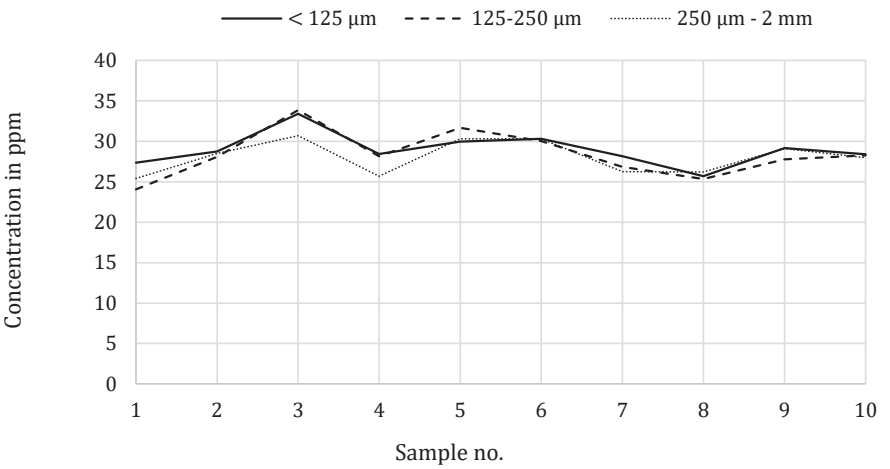
< 125 µm
125-250 µm
250 µm - 2 mm
Concentration in ppm
40
35
30
25
20
15
10
5
0
1
2
3
4
5
6
7
8
9
10
Sample no.

Balance

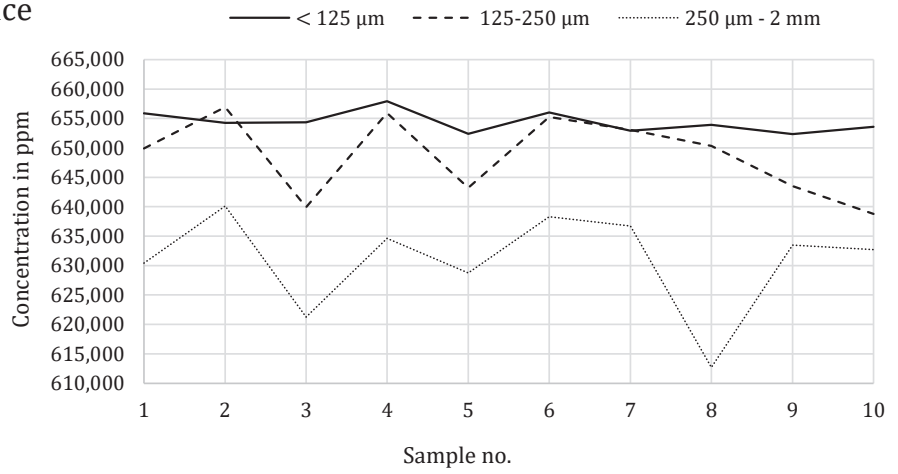
< 125 µm
125-250 µm
250 µm - 2 mm
Concentration in ppm
665,000
660,000
655,000
650,000
645,000
640,000
635,000
630,000
625,000
620,000
615,000
610,000
1
2
3
4
5
6
7
8
9
10
Sample no.

Appendix 2 – Stone-Pot-Arrangements

Balance Settings, Interpolations and Biplots

Appendix 2-1

- Balance Settings of Set 1, 2 and 3

Appendix 2-2

- Ifana 3, feature 13 – Set 1, 2 and 3

Appendix 2-3

- Ifana 3, feature 18 – Set 1, 2 and 3
- Ifana 3, feature 18 – Clr-Biplot

Appendix 2-4

- Ifana 3, feature 17 – Set 1, 2 and 3
- Ifana 3, feature 17 – Clr-Biplot

Appendix 2-5

- Ifana 3, feature 8 – Set 2

Appendix 2-6

- Kurmin Uwa 2D – Set 1, 2 and 3
- Kurmin Uwa 2D – Clr-Biplot

Appendix 2-7

- Pangwari I – Set 1, 2 and 3

Appendix 2-8

- Kurmin Uwa 2B – Set 1, 2 and 3
- Kurmin Uwa 2B – Clr-Biplot and Visualisation of Sample Cluster

Appendix 2-9

- Ido 2016 (layer A) – Set 1, 2 and 3

Appendix 2-10

- Ido 2016 (layer B) – Set 1, 2 and 3

Appendix 2-11

- Ido 2016 (layer G) – Set 1, 2 and 3

Appendix 2-1: Balance Settings of Set 1 and 2

P	Ca	K	Mn	Y	La	Ce	Si	Ti	Al	Fe	V	Cr	Zn	Rb	Sr	Zr	Nb	Ba	Pb	Cl	ilr
+	+	+	+	+	+	+	-	-	-	-	-	-	-	-	-	-	-	-	-	-	1
-	-	-	-	+	+	+															2
				+	-	-															3
					+	-															4
+	+	-	-																		5
+	-																				6
		-	+																		7
							+	-	-	-	-	-	-	-	-	-	-	-	-	-	8
								+	-	-	-	-	-	-	-	-	-	-	-	-	9
									+	-	-	-	-	-	-	-	-	-	-	-	10
										+	-	-	-	-	-	-	-	-	-	-	11
											+	-	-	-	-	-	-	-	-	-	12
												+	-	-	-	-	-	-	-	-	13
													+	-	-	-	-	-	-	-	14
														+	-	-	-	-	-	-	15
															+	-	-	-	-	-	16
																+	-	-	-	-	17
																	+	-	-	-	18
																		+	-	-	19
																			+	-	20

Set 1: All potential grave soil elements are grouped together (+), opposed to the other elements (-) in coordinate ilr-1 (grey row). At those sites where Cu was present, it was added to the elements (+) in ilr-1. For methodological approach see Egozcue & Pawlowsky-Glahn 2005.

P	Ca	K	Mn	Y	La	Ce	Si	Ti	Al	Fe	V	Cr	Zn	Rb	Sr	Zr	Nb	Ba	Pb	Cl	ilr
+	-	-	-	-	-	-	-	-	-	-	-	-	-	-	-	-	-	-	-	-	1
	+	-	-	-	-	-	-	-	-	-	-	-	-	-	-	-	-	-	-	-	2
		+	-	-	-	-	-	-	-	-	-	-	-	-	-	-	-	-	-	-	3
			+	-	-	-	-	-	-	-	-	-	-	-	-	-	-	-	-	-	4
				+	-	-	-	-	-	-	-	-	-	-	-	-	-	-	-	-	5
					+	-	-	-	-	-	-	-	-	-	-	-	-	-	-	-	6
						+	-	-	-	-	-	-	-	-	-	-	-	-	-	-	7
							+	-	-	-	-	-	-	-	-	-	-	-	-	-	8
								+	-	-	-	-	-	-	-	-	-	-	-	-	9
									+	-	-	-	-	-	-	-	-	-	-	-	10
										+	-	-	-	-	-	-	-	-	-	-	11
											+	-	-	-	-	-	-	-	-	-	12
												+	-	-	-	-	-	-	-	-	13
													+	-	-	-	-	-	-	-	14
														+	-	-	-	-	-	-	15
															+	-	-	-	-	-	16
																+	-	-	-	-	17
																	+	-	-	-	18
																		+	-	-	19
																			+	-	20

Set 2: Each element is individually set (+) opposed to the remaining elements (-). Coordinate ilr-1 (grey row), where P is opposed to the other elements, revealed significant patterns within the stone-pot-arrangements. For methodological approach see Egozcue & Pawlowsky-Glahn 2005.

Appendix 2-1: Balance Settings of Set 3

P	Ca	Sr	Mn	K	Rb	Si	Ti	Al	Fe	V	Cr	Zn	Y	Zr	Nb	Ba	Ce	La	Pb	Cl	ilr
+	+	+	+	-	-	-	-	-	-	-	-	-	-	-	-	-	-	-	-	-	1
+	+	-	-																		2
+	-																				3
		+	-																		4
				+	+	-	-	-	-	-	-	-	-	-	-	-	-	-	-	-	5
				+	-																6
						+	-	-	-	-	-	-	-	-	-	-	-	-	-	-	7
							+	-	-	-	-	-	-	-	-	-	-	-	-	-	8
								+	-	-	-	-	-	-	-	-	-	-	-	-	9
									+	-	-	-	-	-	-	-	-	-	-	-	10
										+	-	-	-	-	-	-	-	-	-	-	11
											+	-	-	-	-	-	-	-	-	-	12
												+	-	-	-	-	-	-	-	-	13
													+	-	-	-	-	-	-	-	14
														+	-	-	-	-	-	-	15
															+	-	-	-	-	-	16
																+	-	-	-	-	17
																	+	-	-	-	18
																		+	-	-	19
																			+	-	20

Set 3: Ilr-1 and ilr-5 (grey rows) represent the geogenic signature observed at *Ido 2016* (Schmidt 2016). When an area revealed both an enrichment of ilr-1 and a depletion of ilr-5, the area was considered to have been disturbed by geogenic interferences. For methodological approach see Egozcue & Pawlowsky-Glahn 2005.

Appendix 2-2: Ifana 3, feature 13 – Set 1, 2 and 3

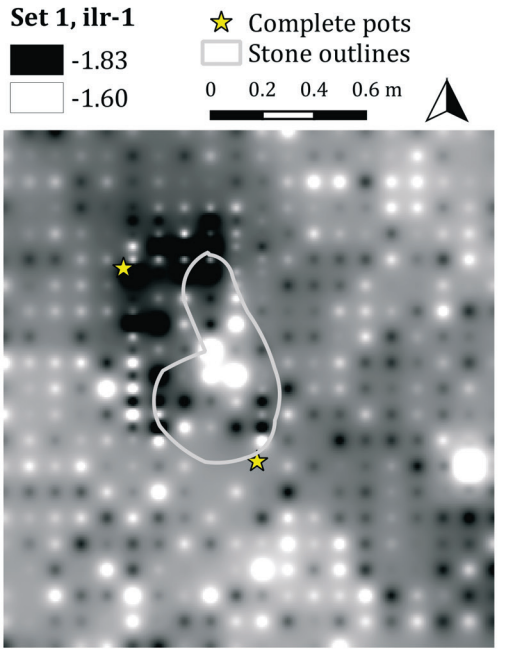

The interpolation of coordinate ilr-1 indicates either a depletion of the grave soil elements or an enrichment of the remaining elements between the two pots.

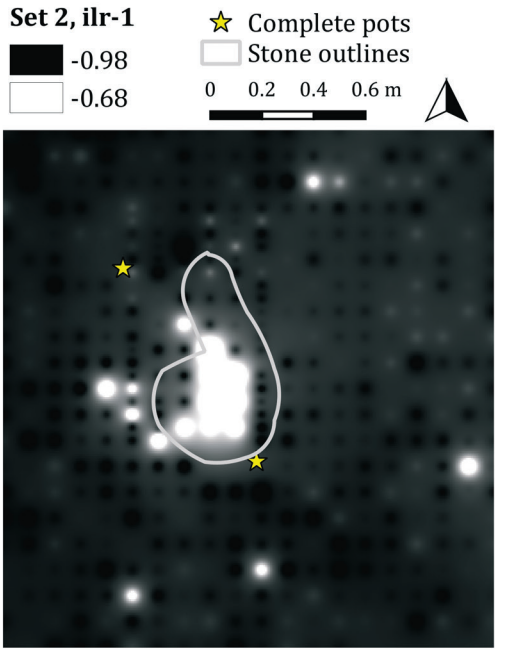

Within the feature, between the pots, the interpolation pattern of coordinate ilr-1 suggests an enrichment of P.

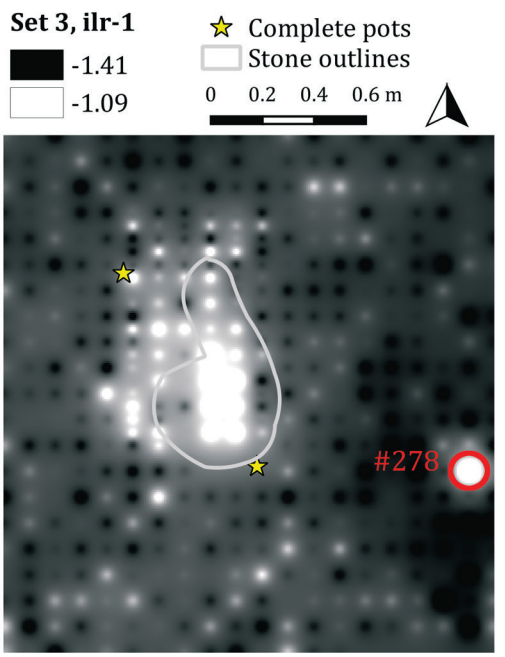

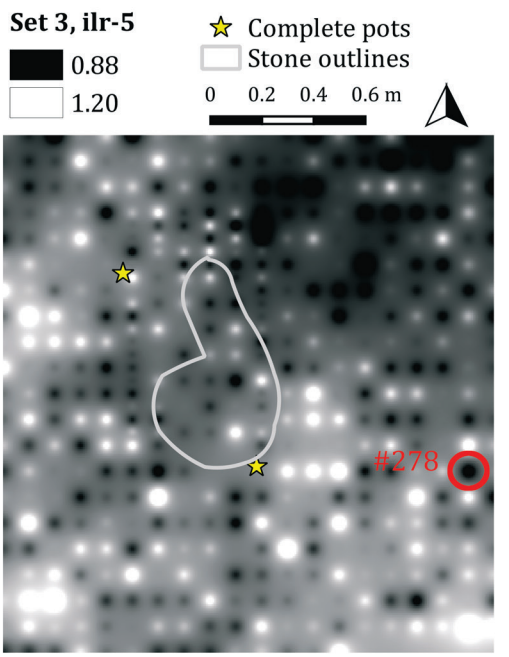

The interpolation of coordinate ilr-1 and ilr-5 do not indicate any geogenic interference within the feature. The concurrent pattern for both coordinates at sample #278, however, suggests geogenic disturbances.

Appendix 2-3: Ifana 3, feature 18 – Set 1, 2 and 3

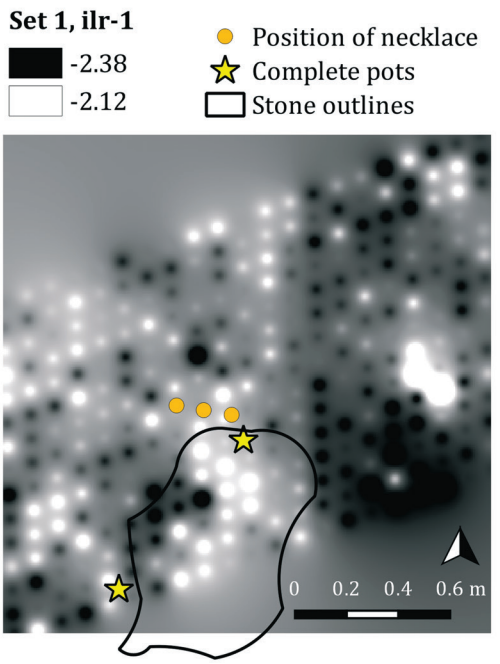

The interpolation indicates enrichments of the grave soil elements within the feature and to the east of it.

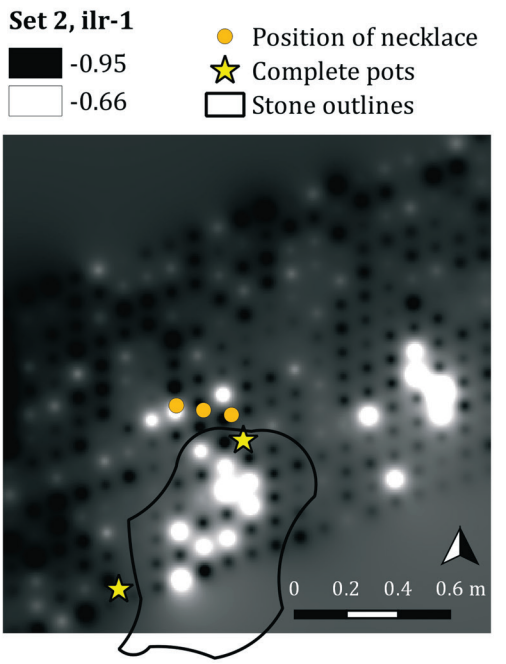

Both within the feature and to the east of it, the interpolation of ilr-1 reveals enrichment of P.

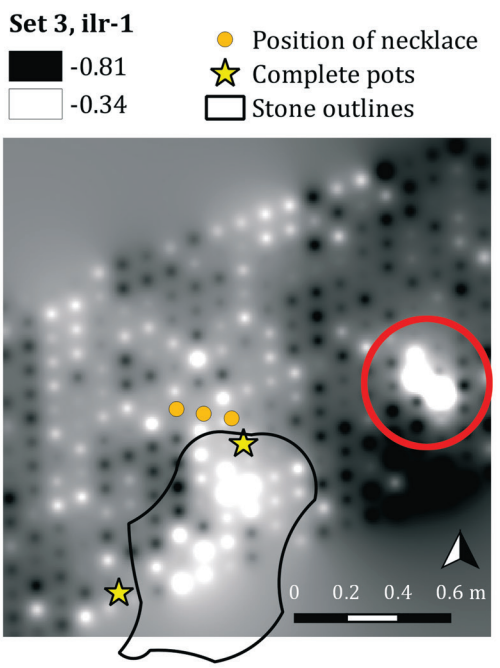

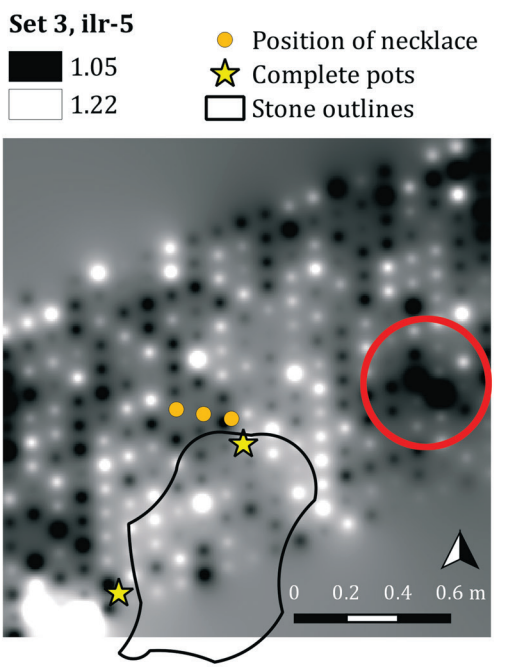

Some of the enrichment in P outside the feature turned out to be geogenic interferences as indicated by the concurrent enrichment of ilr-1 and depletion of ilr-5. The encircled area refers to the encircled samples in the clr-biplot.

Appendix 2-3: Ifana 3, feature 18 – Clr-Biplot

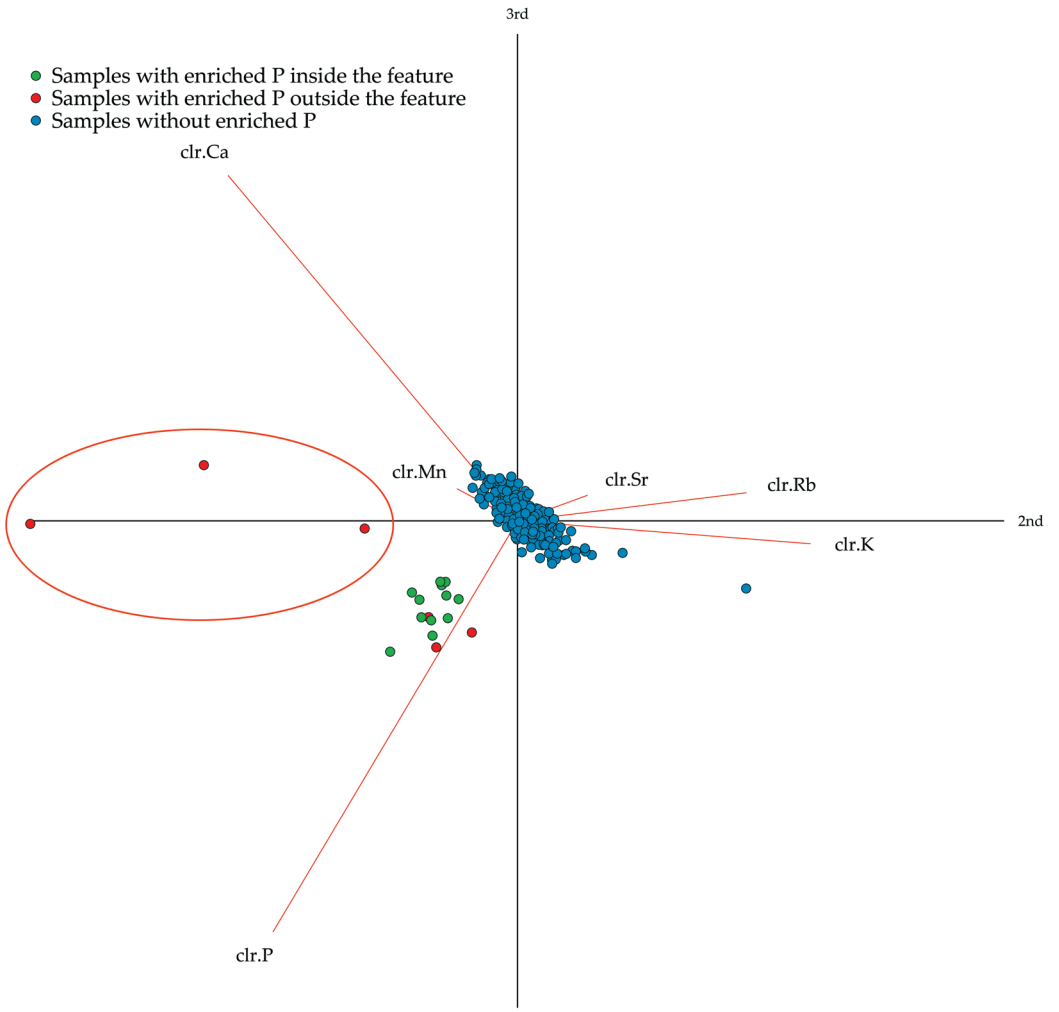

Form clr-biplot for the samples from feature 18 at *Ifana 3* with the log-ratios of the elements P, Ca, Sr, Mn, K, and Rb. The samples coloured in red refer to samples with P enrichments located outside the feature. Three of those samples (encircled) are considered to have been affected by geogenic interferences and refer to the encircled area in set 3. This area furthermore revealed a higher pH value compared to both the surrounding and the feature soil (see chapter 9.4). To gain a better insight into the data, the second and third axis are shown. The cumulative proportion explained together accounts for 96.13% of the total variance.

Appendix 2-4: Ifana 3, feature 17 – Set 1, 2 and 3

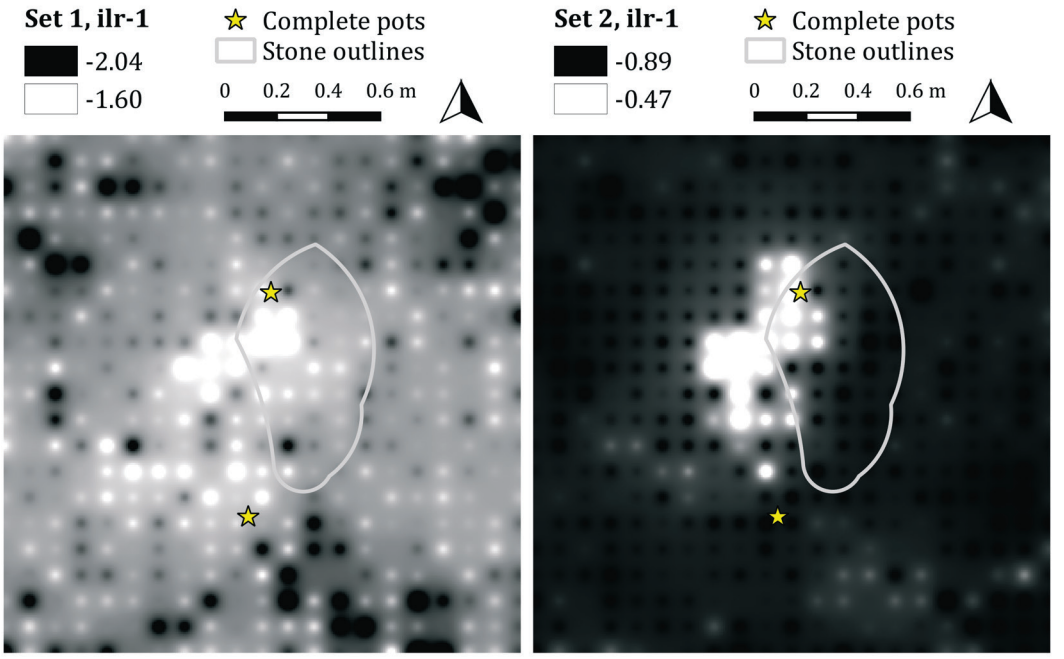

The interpolation pattern indicates an enrichment of grave soil elements within the stone-pot-arrangement. The increased values of ilr-1 between the two vessels suggest an enrichment of P in this area.

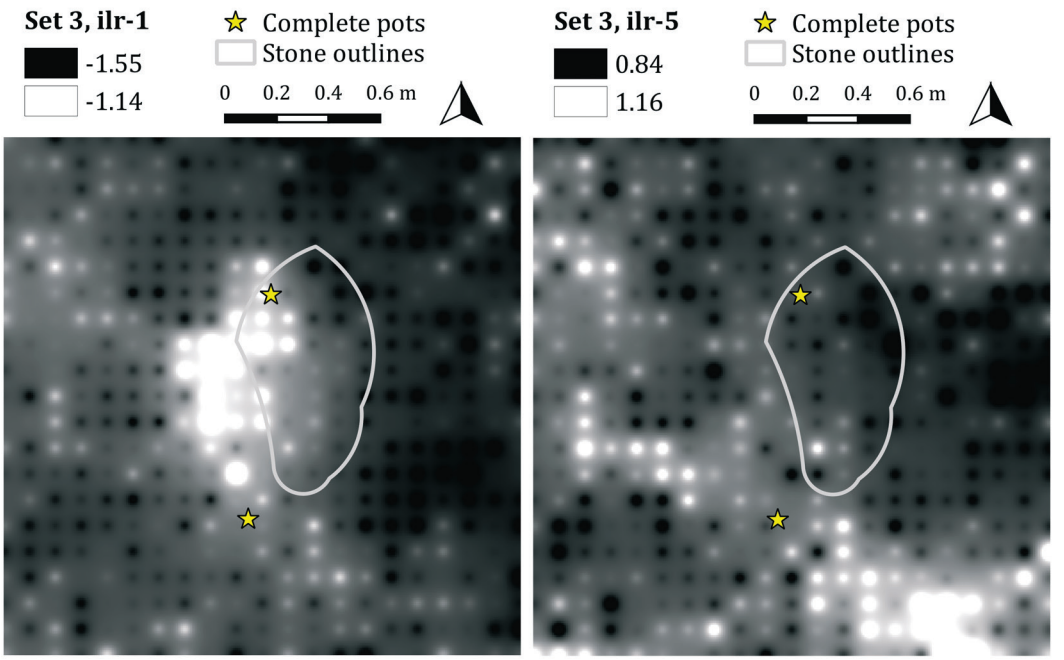

Based on the interpolation of coordinates ilr-1 and ilr-5, no geogenic interferences are visible within feature 17 at *Ifana 3*.

Appendix 2-4: Ifana 3, feature 17 – Clr-Biplot

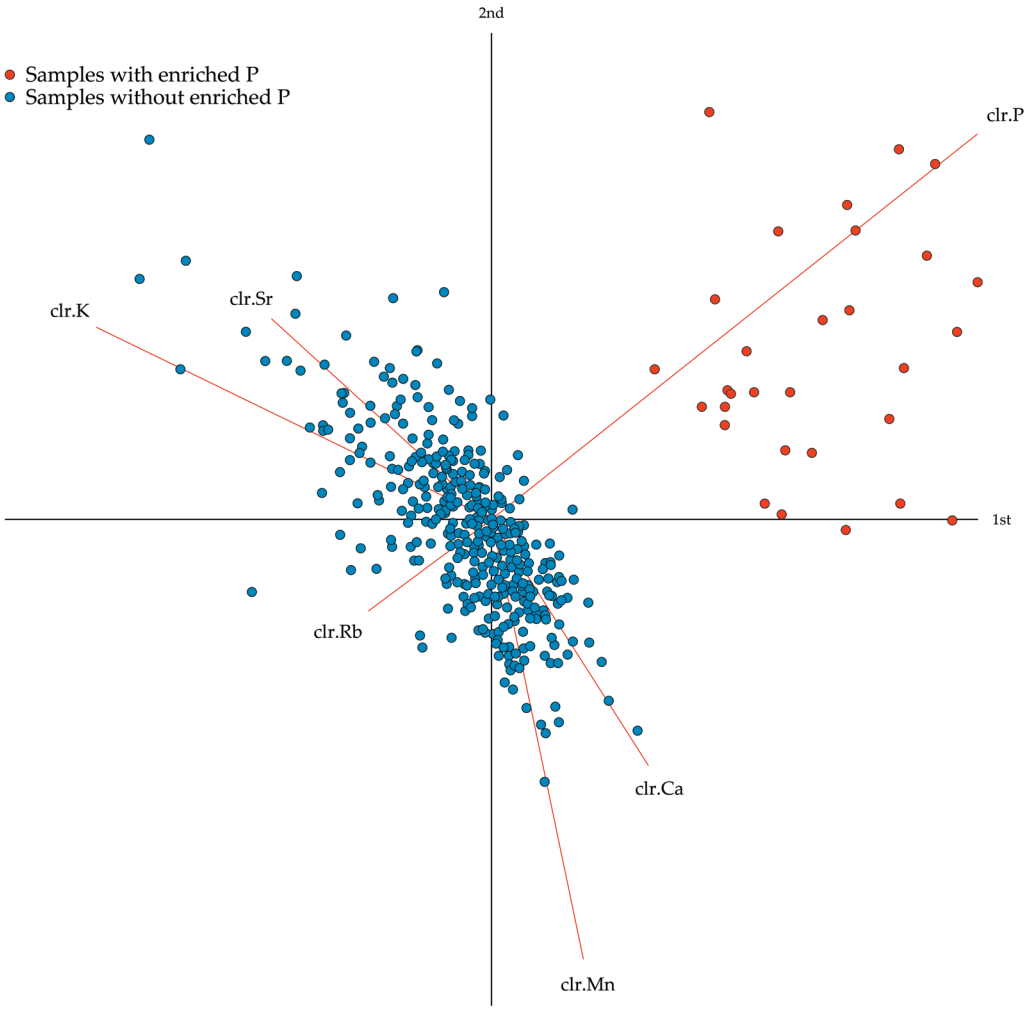

Form clr-biplot for the samples from feature 17 at *Ifana 3* with log-ratios of the elements P, Ca, Sr, Mn, K, and Rb. The samples with P enrichments (red) cluster together; no sample seems to have a different origin. The cumulative proportion explained is 0.6870, i.e. the first and second principal component together account for 68.70% of the total variance.

Appendix 2-5: Ifana 3, feature 8 – Set 2

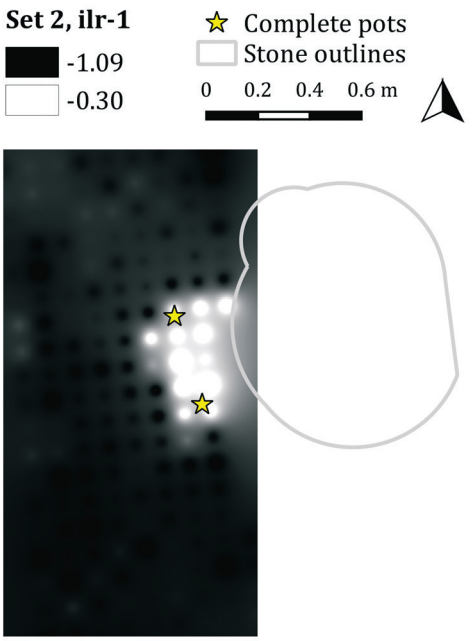

Visualisation of the P enrichments as indicated by the interpolation of coordinate ilr-1 of set 2, where P was set opposed to the remaining elements. The samples of feature 8 were measured with main and light filter only to focus on potential enrichments of P. Therefore, neither set 1 or 3, nor clr-biplots could be applied to the data.

Appendix 2-6: Kurmin Uwa 2D – Set 1, 2 and 3

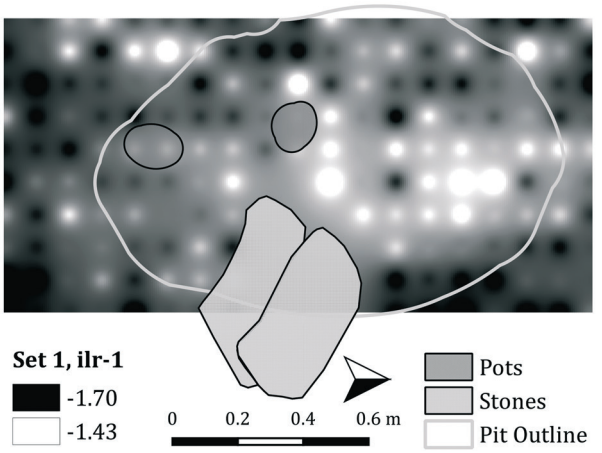

Interpolations indicate enrichments of grave soil elements within the pit.

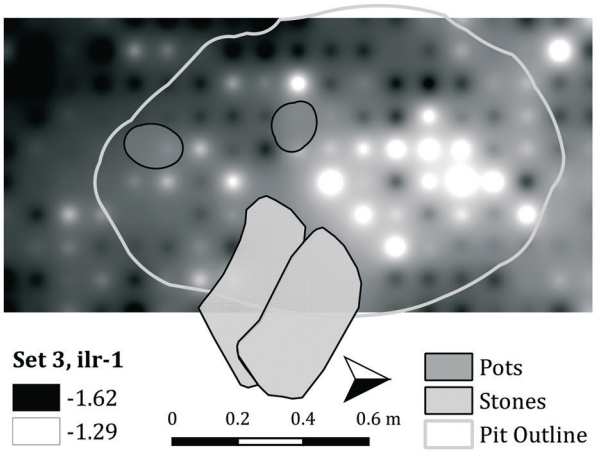

See text in the righthand panel.

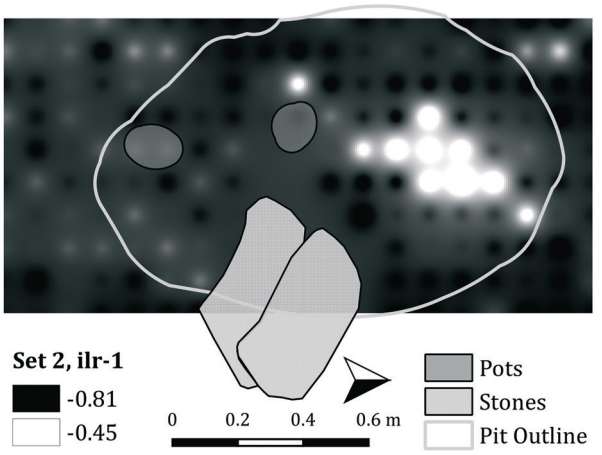

Enrichments of P occur concentrated within the pit associated with the stone-pot-arrangement.

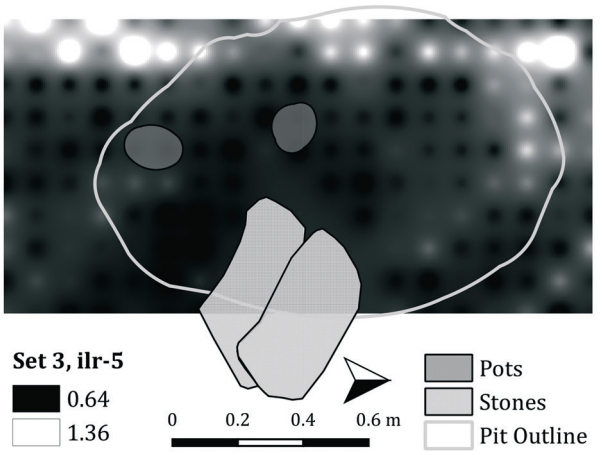

The interpolations of coordinate ilr-1 and ilr-5 reveal no geogenic interferences within the stone-pot-arrangement. Increased values of coordinate ilr-5 in the north of the trench correlate with changes in the soil – probably some sort of geogenic interference.

Appendix 2-6: Kurmin Uwa 2D – Clr-Biplot

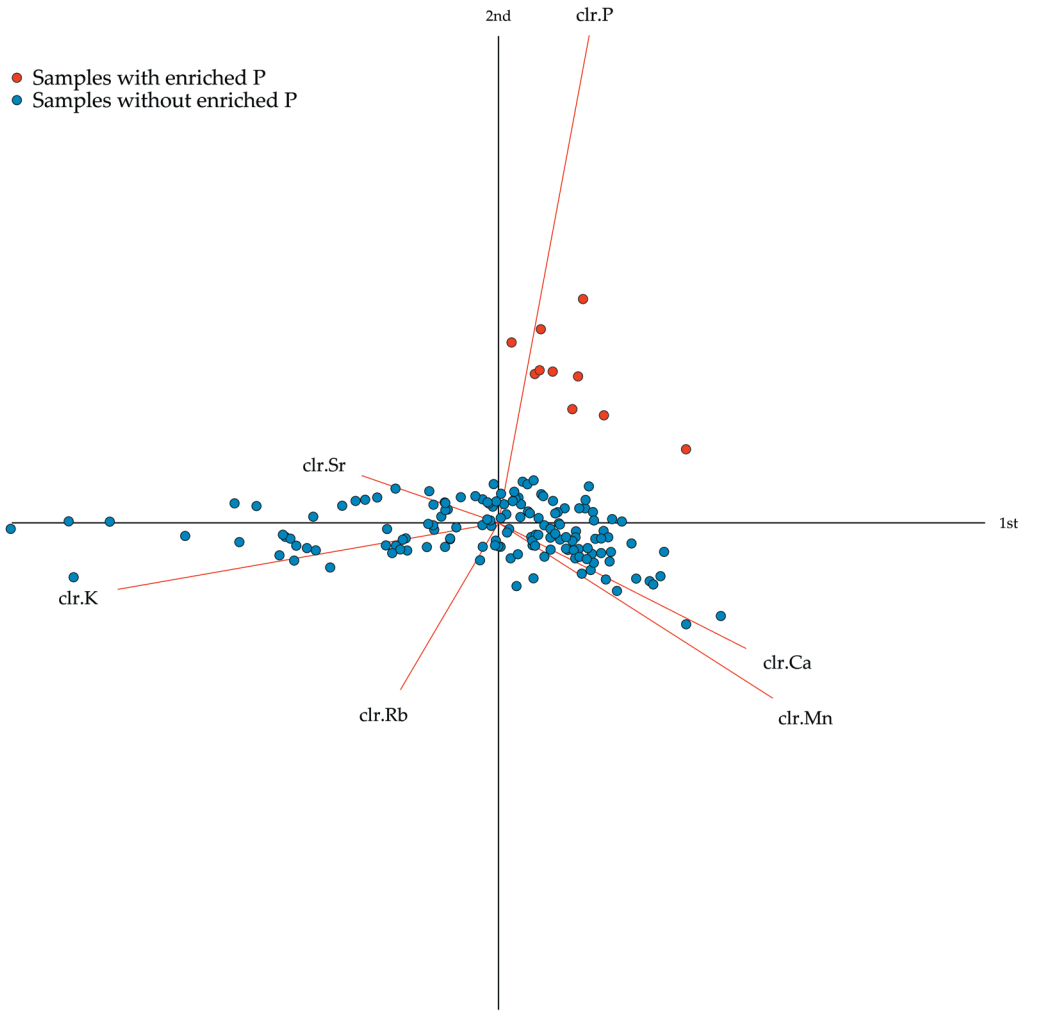

Form clr-biplot for the samples from *Kurmin Uwa 2D* with the log-ratios of the elements P, Ca, Sr, Mn, K, and Rb. The samples with enrichments of P (red) cluster together; no samples appear to have a different origin. The cumulative proportion explained is 0.8342, i.e. the first and second principal component together account for 83.42% of the total variance.

Appendix 2-7: Pangwari I – Set 1, 2 and 3

Interpolation of coordinate ilr-1. Aside from a few enrichments in the southwest corner, no other significant patterns are visible.

Seven spots of increased values indicate enrichments of P. The rectangular area of enrichment in the northern part of the trench is biased by a depletion of Si, which caused apparent enrichments of P.

The interpolated data suggest geogenic interferences for the areas encircled in red, since the interpolation patterns occur concurrently – enriched as ilr-1 and depleted as ilr-5. The sample in the southwest corner, however, has a different pattern. Since its pXRF values for Ti and Mn were below the limit of detection, a mismeasurement of this sample cannot be ruled out.

Appendix 2-8: Kurmin Uwa 2B – Set 1, 2 and 3

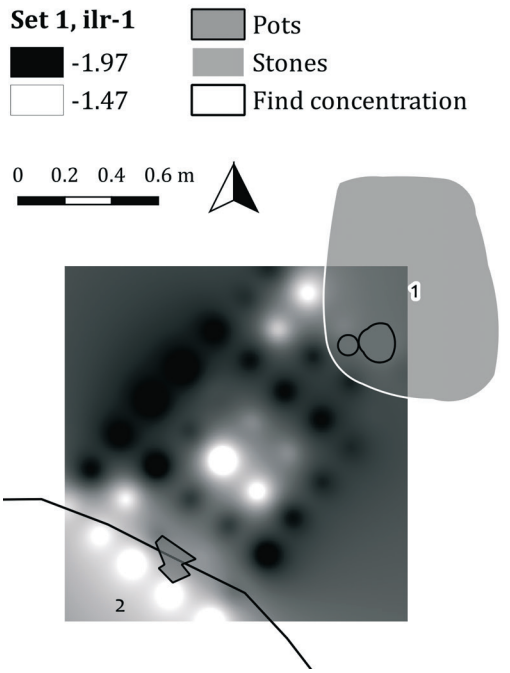

The interpolation of coordinate ilr-1 reveals enrichments of grave soil elements at several spots.

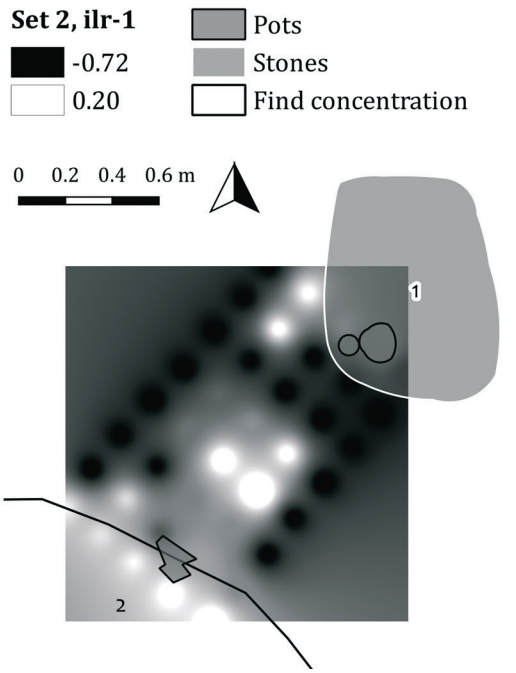

Enrichments of P are found at several spots as indicated by the interpolated coordinate ilr-1.

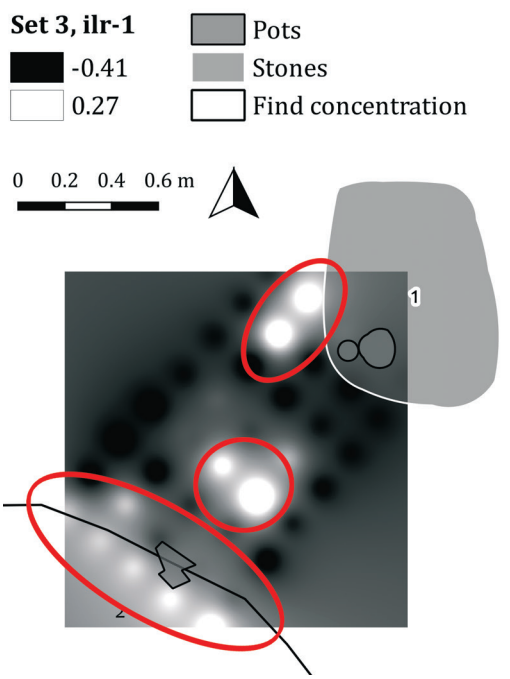

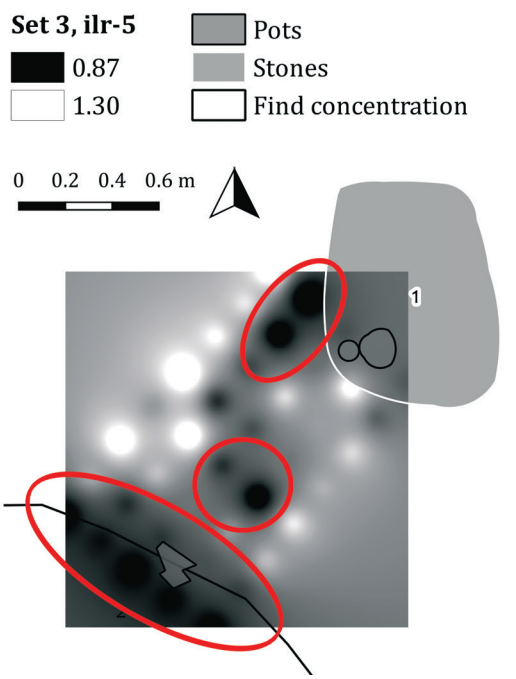

The interpolations of set 3 show a concurrent pattern in ilr-1 and ilr-5 for the areas circled in red and suggest a geogenic source.

Appendix 2-8: Kurmin Uwa 2B – Clr-Biplot

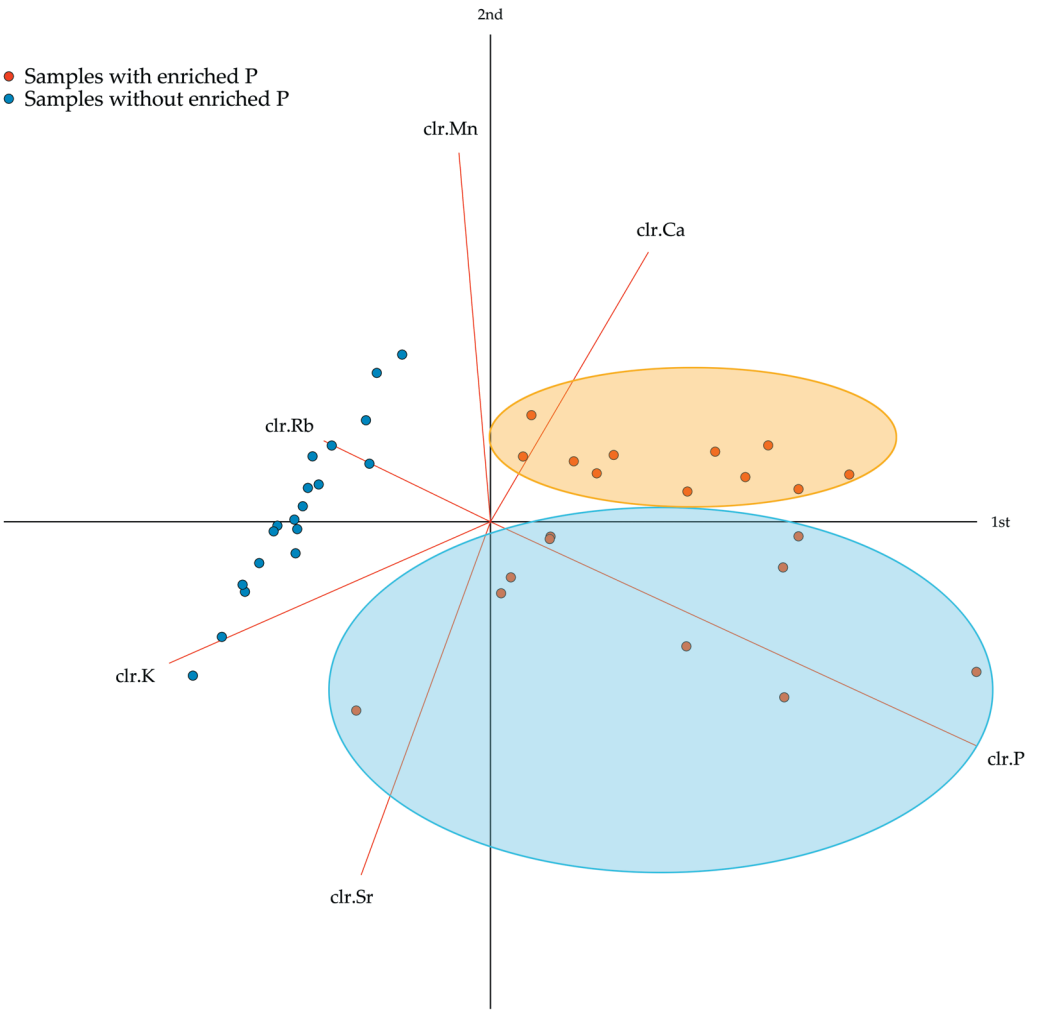

Form clr-biplot for the samples from *Kurmin Uwa 2B* with log-ratios of the elements P, Ca, Sr, Mn, K, and Rb. The samples with enrichments of P form neither a homogeous cluster nor do they separate clearly. Two distinct clusters (orange and blue) are suggested relating to the log-ratio of Ca. The cumulative proportion explained is 0.9428, i.e. the first and second principal component together account for 94.28% of the total variance.

Appendix 2-8: Kurmin Uwa 2B – Visualisation of Sample Cluster

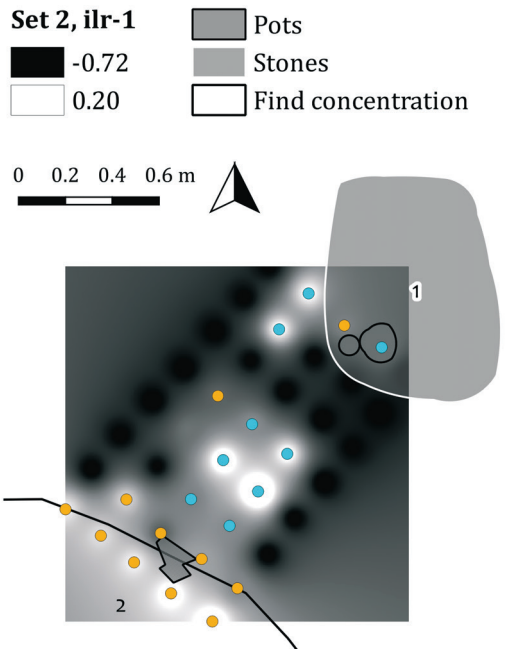

Visualisation of the samples enriched with P with higher Ca content (orange) and lower Ca content (blue). The majority of samples containing more Ca seem to concentrate adjacent to the find concentration, whereas the samples containing less Ca are next to the vessels and in the middle of the sampled area.

Appendix 2-9: Ido 2016 Layer A – Set 1, 2 and 3

Appendix 2-10: Ido 2016 Layer B – Set 1, 2 and 3

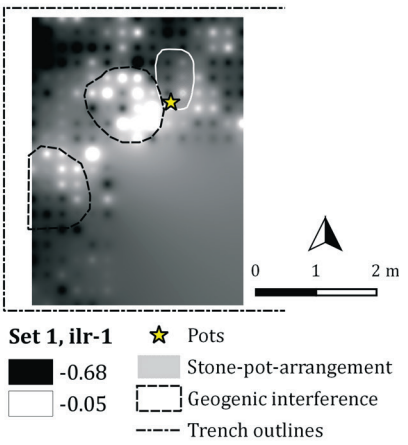

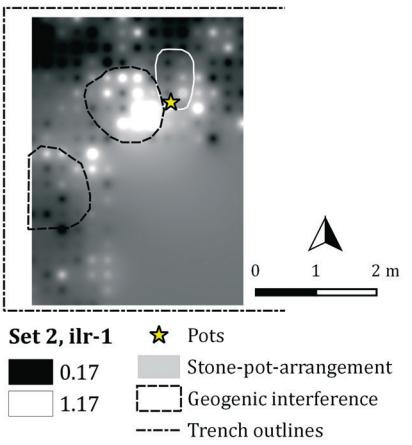

As for layer A, the interpolation patterns of set 1 and 2 suggest enrichments within the geogenic interference. Due to these interferences concealing any other signature, the remaining samples were not measured.

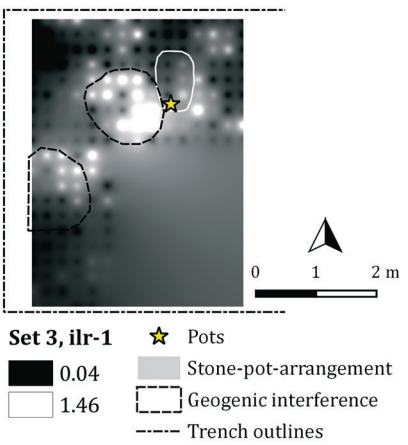

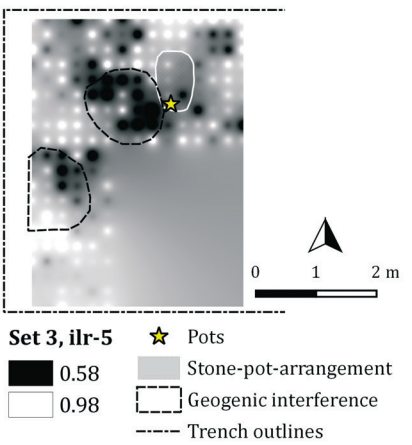

Set 3 shows, like layer A, enrichments of ilr-1 and depletions of ilr-5 within the geogenic interference, although with smaller dimensions at this depth.

Appendix 2-11: Ido 2016 Layer G – Set 1, 2 and 3

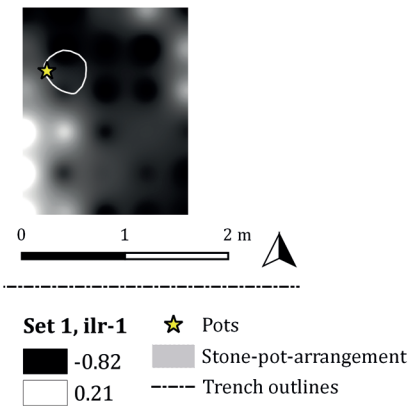

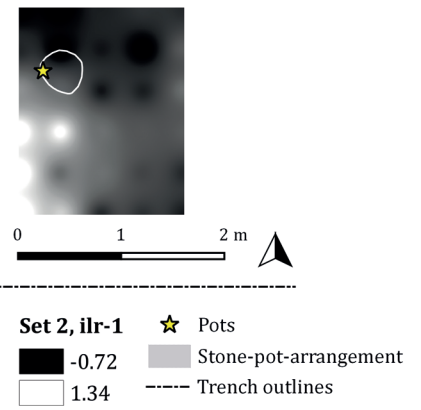

Set 1 and 2 show enrichments of the grave soil elements, among them P, adjacent to the stone-pot-arrangement of feature 9. Set 3, however, reveals that this is due to geogenic interferences.

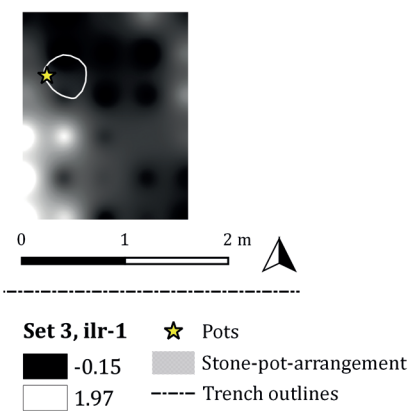

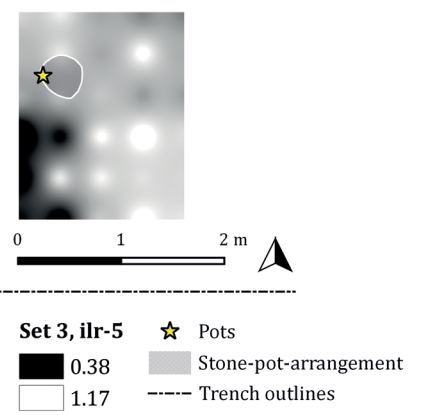

The interpolations of set 3 reveal that the assumed enrichment of grave soil elements is in fact due to geogenic interferences, since both interpolation patterns occur concurrently.

Appendix 3 – Pit Features

Balance Settings, Interpolations and Biplots

Appendix 3-1

- Balance Settings of Set 4 and 5

Appendix 3-2

- Kusuma 1 – Set 4 and 5

Appendix 3-3

- Kurmin Uwa 1 – Set 4 and Clr-Biplot

Appendix 3-4

- Ido 2016 (layer A and B) – Set 5
- Ido 2016 (layer A) – Clr-Biplot

Appendix 3-5

- Ifana 1 – Set 4 and Clr-Biplot
- Ifana 1 – Set 5

Appendix 3-6

- Pangwari E – Set 4 and 5
- Pangwari E – Clr-Biplot

Appendix 3-7

- Ifana 2 – Set 5 and Visualisation of Sample Cluster
- Ifana 2 – Clr-Biplot

Appendix 3-8

- Pangwari D and I – Clr-Biplot

Appendix 3-1: Balance Settings of Set 4 and 5

P	K	Ca	Sr	Mn	Fe	Zn	Ba	Rb	Si	Ti	Al	V	Cr	Y	Zr	Nb	Ce	La	Pb	Cl	ilr
+	-	-	-	-	-	-	-	-	-	-	-	-	-	-	-	-	-	-	-	-	1
	+	-	-	-	-	-	-	-	-	-	-	-	-	-	-	-	-	-	-	-	2
		+	-	-	-	-	-	-	-	-	-	-	-	-	-	-	-	-	-	-	3
			+	-	-	-	-	-	-	-	-	-	-	-	-	-	-	-	-	-	4
				+	-	-	-	-	-	-	-	-	-	-	-	-	-	-	-	-	5
					+	-	-	-	-	-	-	-	-	-	-	-	-	-	-	-	6
						+	-	-	-	-	-	-	-	-	-	-	-	-	-	-	7
							+	-	-	-	-	-	-	-	-	-	-	-	-	-	8
								+	-	-	-	-	-	-	-	-	-	-	-	-	9
									+	-	-	-	-	-	-	-	-	-	-	-	10
										+	-	-	-	-	-	-	-	-	-	-	11
											+	-	-	-	-	-	-	-	-	-	12
												+	-	-	-	-	-	-	-	-	13
													+	-	-	-	-	-	-	-	14
														+	-	-	-	-	-	-	15
															+	-	-	-	-	-	16
																+	-	-	-	-	17
																	+	-	-	-	18
																		+	-	-	19
																			+	-	20

Set 4: Each element is set individually (+) opposed to the remaining elements (-). Coordinate ilr-1 and ilr-6 (grey rows) are shown as an interpolation at *Kusuma 1* to illustrate significant patterns (see App. 3-2). Cu and Ni were included in the balance settings, if present (ilr-21 and ilr-22). For methodological approach see Egozcue & Pawlowsky-Glahn 2005.

P	Y	Zn	Fe	Al	V	Cr	ilr
+	+	+	-	-	-	-	1
+	-	-					2
	+	-					3
			+	-	-	-	4
				+	-	-	5
					+	-	6

Set 5: Balance setting of set 5 according to the outcome at *Kusuma 1*. The elements P, Y and Zn (+) are set opposed to Fe, Al, V, and Cr (-) in coordinate ilr-1 (grey row). For methodological approach see Egozcue & Pawlowsky-Glahn 2005.

Appendix 3-2: Kusuma 1 – Set 4 and 5

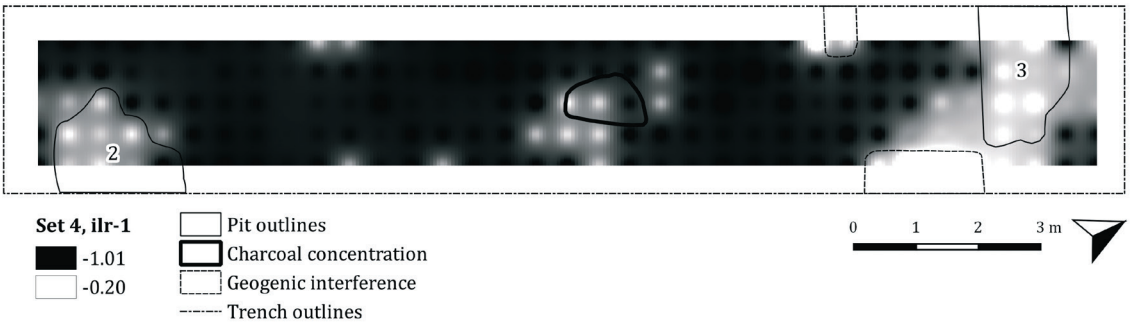

Interpolation of ilr-1, where P was set opposed to the remaining elements. Enrichments of P concentrate within the features, in the charcoal concentration in the middle of the trench as well as within geogenic patches.

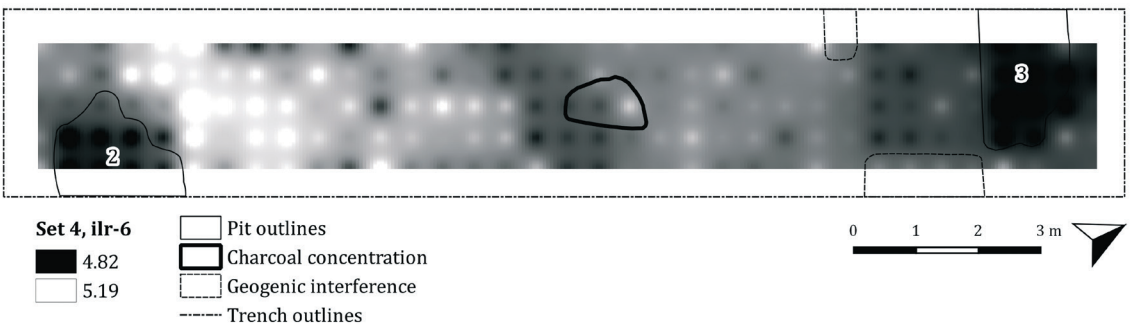

Interpolation of ilr-6, where Fe was set opposed to the remaining elements. Depletions of Fe occurred only within features 2 and 3.

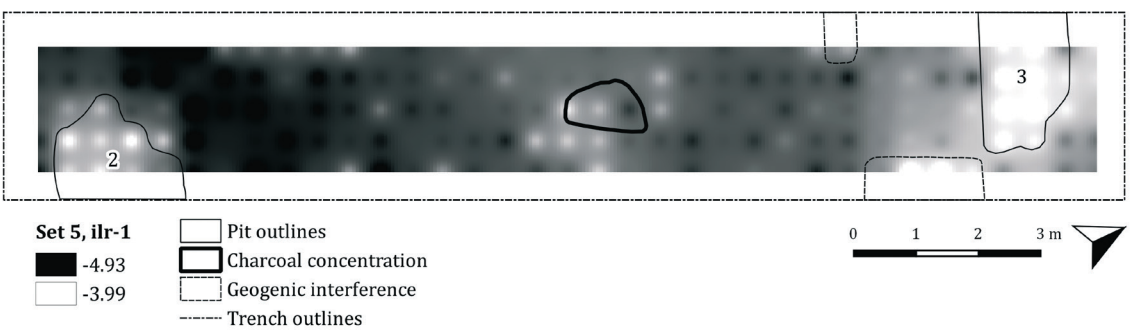

Interpolation of set 5 – both the enrichments of P, Y and Zn as well as the depletions of Fe, Al, V, and Cr are integrated in this balance setting.

Appendix 3-3: Kurmin Uwa 1 – Set 5 and Clr-Biplot

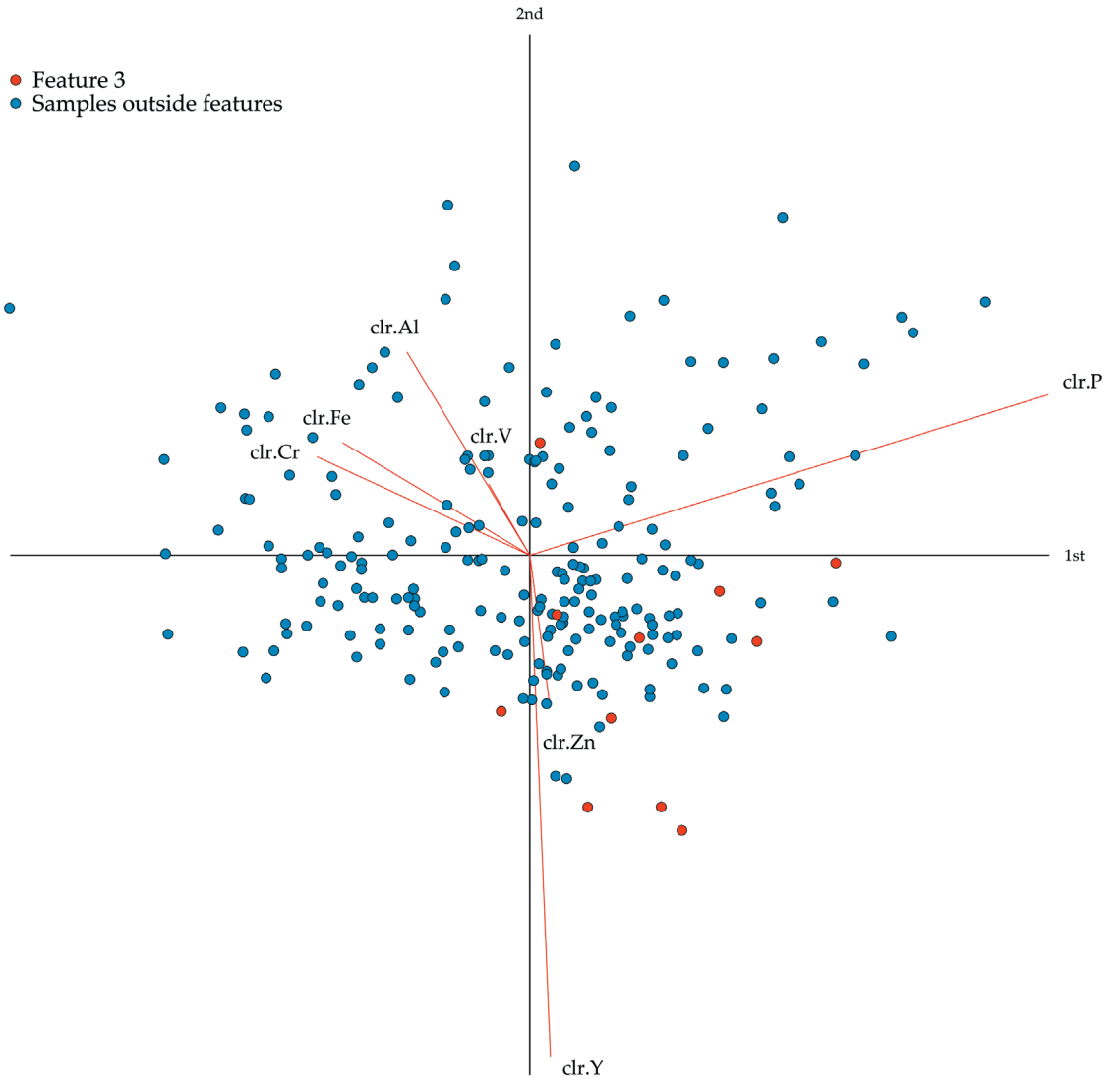

Form clr-biplot for the samples from *Kurmin Uwa 1*. Although the pit samples (red) do not form a cluster, their distribution is concordant with the pit signature – influenced by the log-ratios of Y and Zn as well as Al, Fe, V and Cr. The cumulative proportion explained is 0.8877, i.e. the first and second principal component together account for 88.77% of the total variance.

Appendix 3-3: Kurmin Uwa 1 – Clr-Biplot

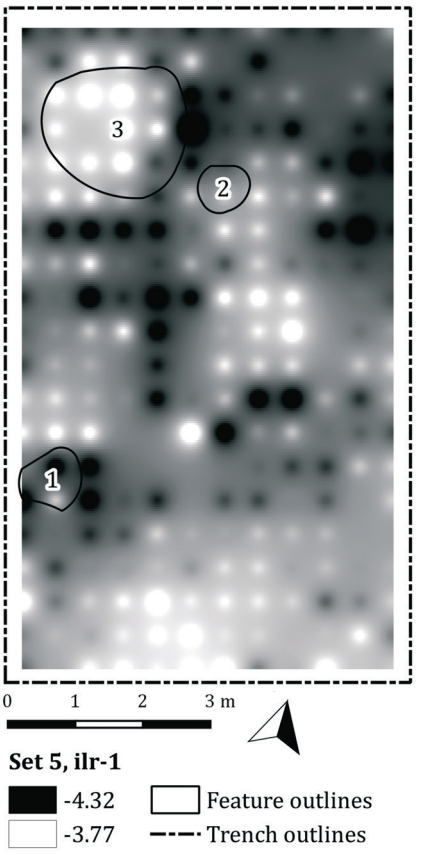

The interpolation at *Kurmin Uwa 1* represents the pit signature developed at *Kusuma 1*. The signature correlates with feature 3, a large pit with a dense find concentration. However, the signature is also present on other areas without features or find concentrations.

Appendix 3-4: Ido 2016 (layer A and B) – Set 5

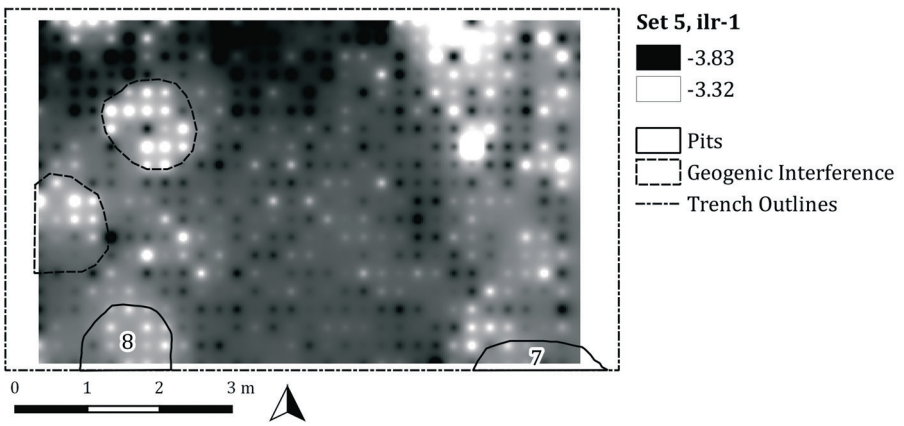

The pit signature, represented as interpolation of set 5, correlates in layer A both with areas of geogenic interferences and the pits, although less significantly.

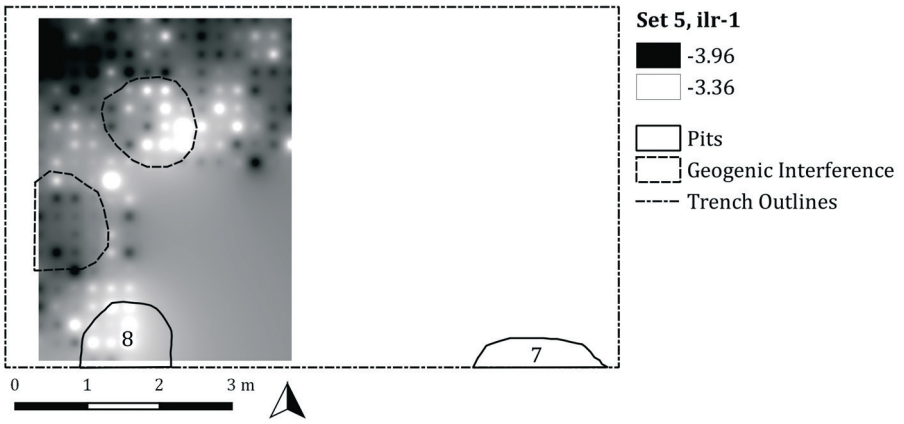

In layer B, the results are similar. The signature recurred within the pits and the geogenic interference. Not all samples of this layer were measured, since the focus was on the stone-pot-arrangements, which turned out to be concealed by geogenic signatures.

Appendix 3-4: Ido 2016 (layer A) – Clr-Biplot

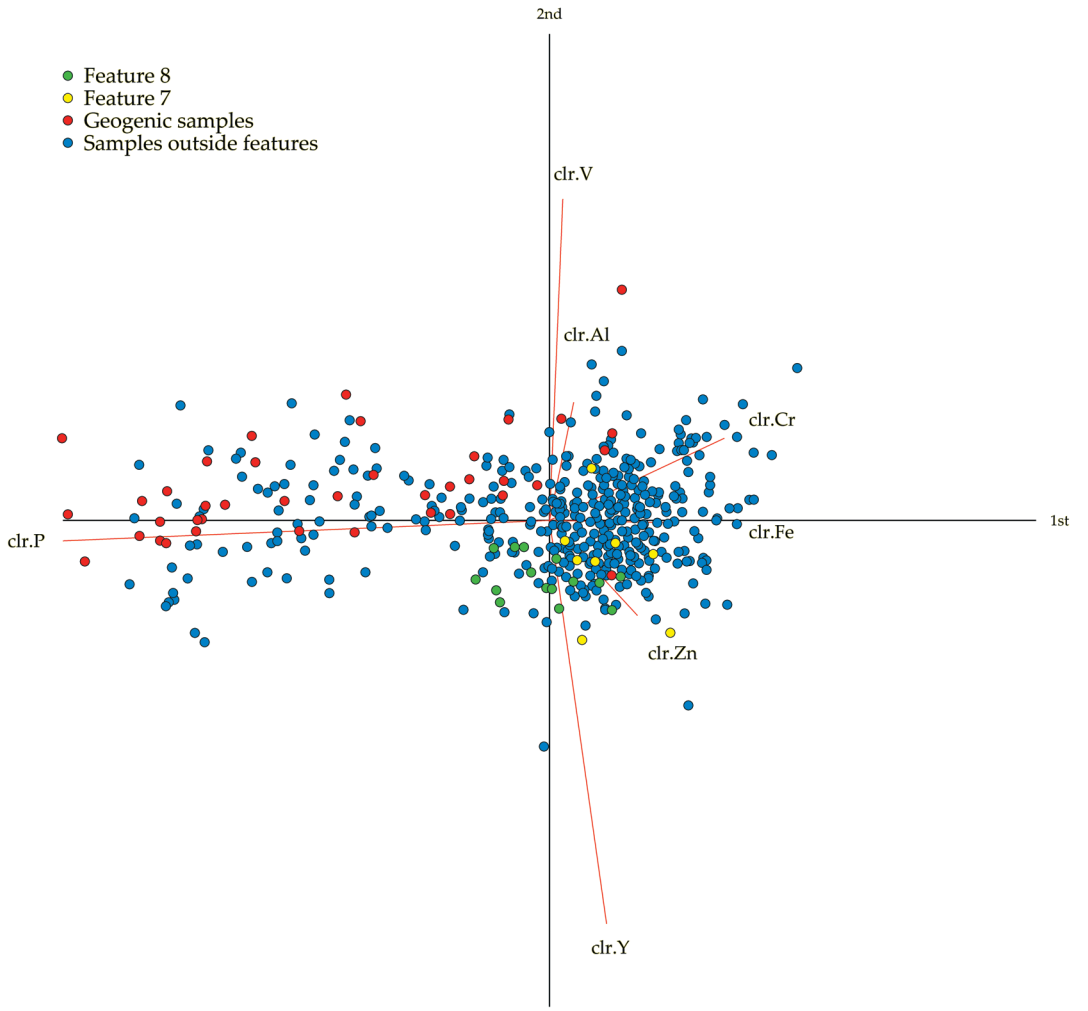

Form clr-biplot for the samples from *Ido 2016* (layer A) with log-ratios of the elements P, Y, and Zn as well as Fe, Al, V, and Cr. The pit samples form no cluster, whereas the samples from the geogenic interferences are dominated by the influence of the log-ratio values of P. The cumulative proportion explained is 0.8708, i.e. the first and second principal component together account for 87.08% of the total variance.

Appendix 3-5: Ifana 1 – Set 4 and Clr-Biplot

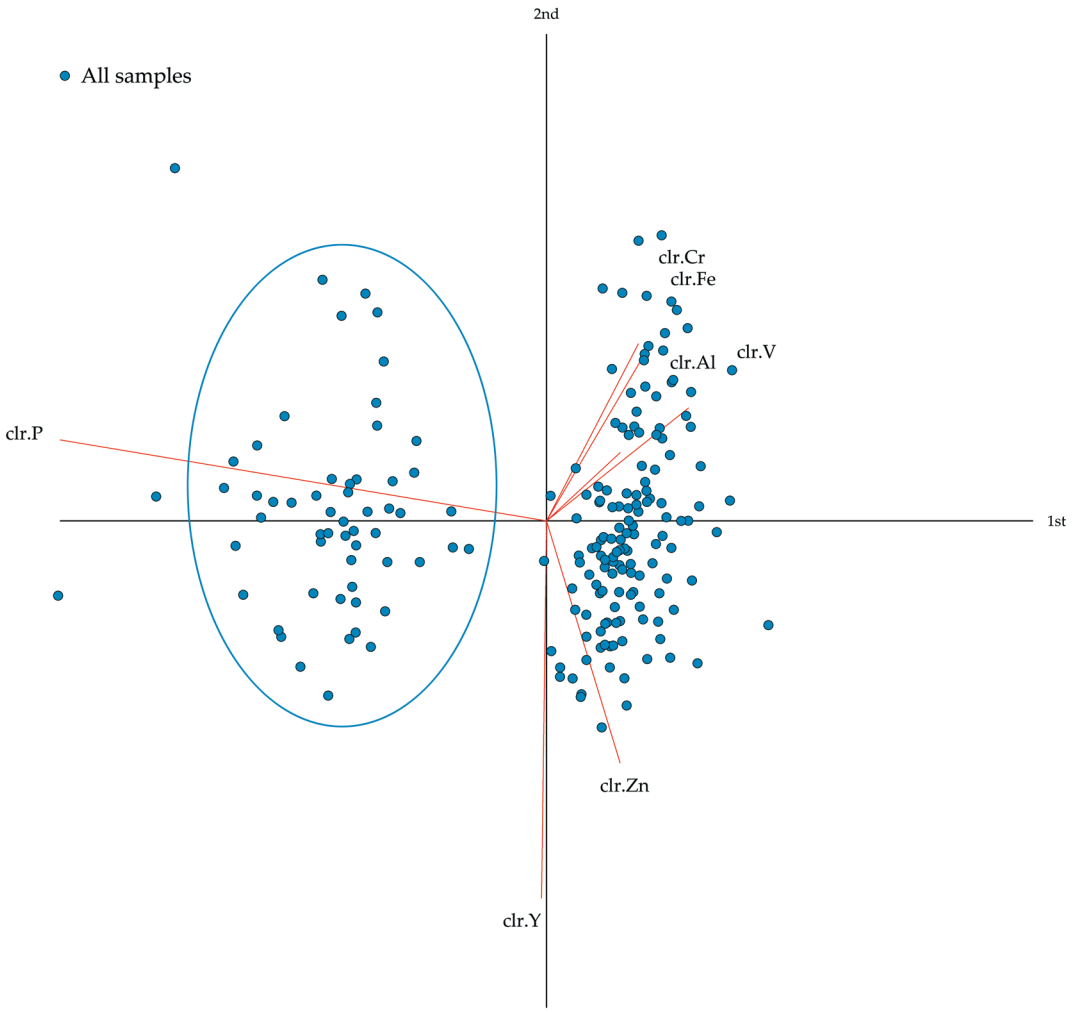

Form clr-biplot for the samples from *Ifana 1* with log-ratios of the elements P, Y and Zn as well as Fe, Al, V, and Cr. The encircled data separate by the log-ratio values of P and their position in the trench is shown on the right. The cumulative proportion explained is 0.7474, i.e. the first and second principal component together account for 74.74% of the total variance.

Appendix 3-5: Ifana 1 – Set 4 and Clr-Biplot

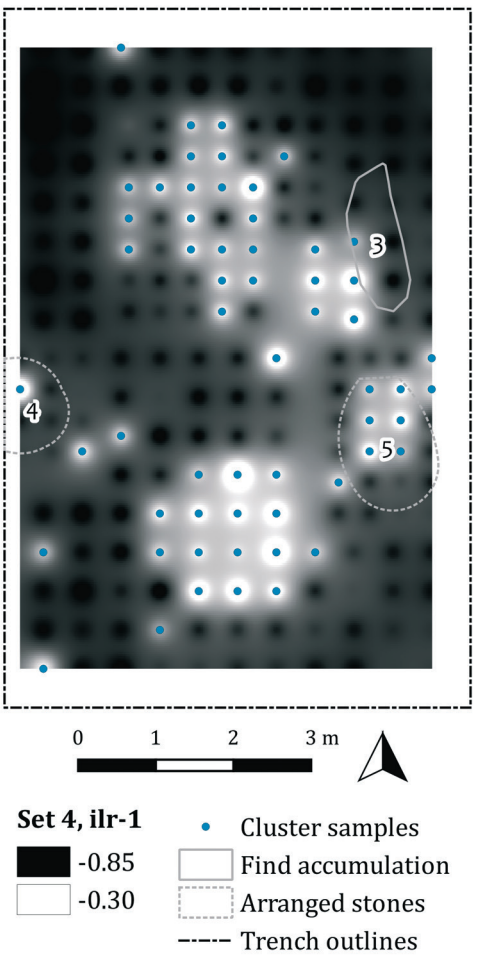

Enrichment pattern of P as indicated by coordinate ilr-1 of set 4. The samples with a higher P content also separate in the clr-biplot. However, the enrichments concentrate mainly outside the features.

Appendix 3-5: Ifana 1 – Set 5

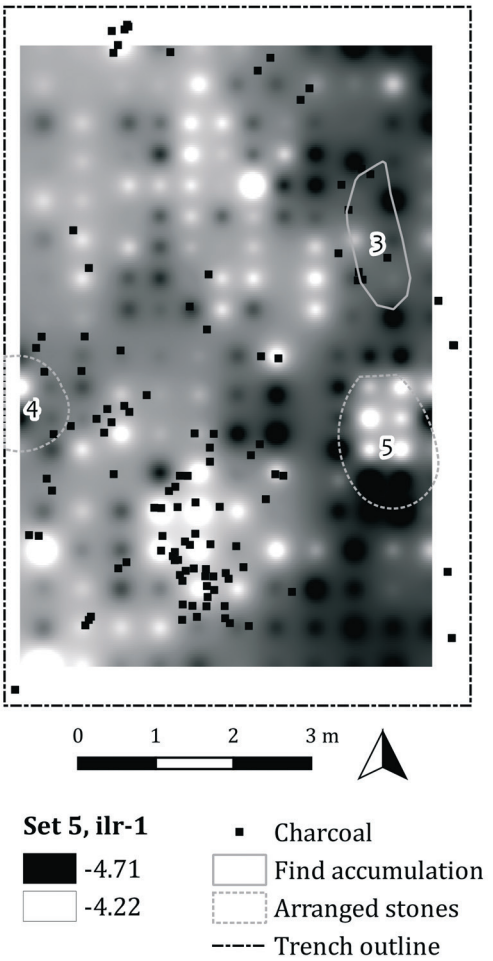

Interpolation of the pit signature showing a pattern partly concordant with the concentration of charcoal in the southern part of the trench. In general, however, the pattern appears rather blurry.

Appendix 3-6: Pangwari E – Set 4 and 5

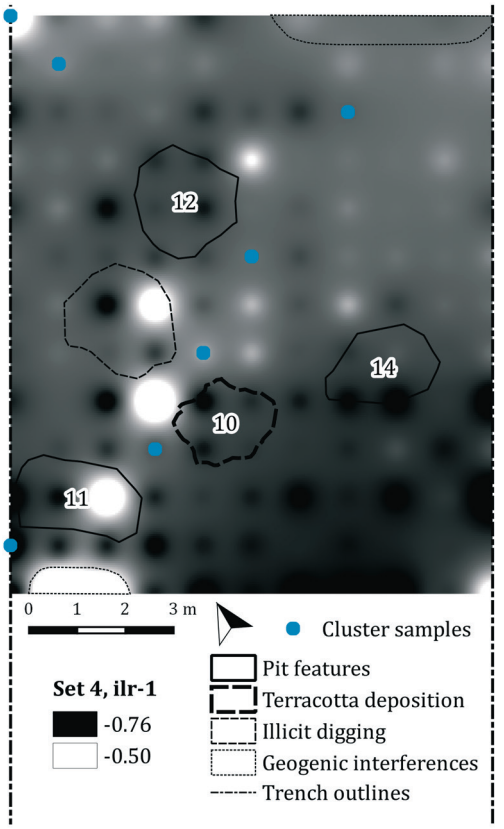

The enrichments of P concentrate in the western half of the sampled trench section. Some of the enrichments also correlate with geogenic interferences in the southwest corner. The samples from the cluster in the clr-biplot show no significant distribution.

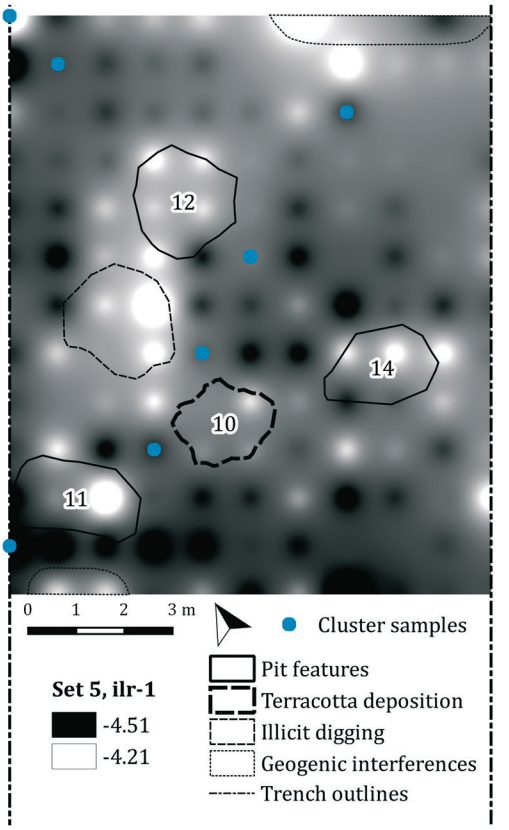

The pit signature correlates with features 10, 11, 12, and 14. However, since the trench is affected by illicit digging and accumulation of material, an affiliation of this signature to specific features is difficult. The sample points refer to the cluster in the clr-biplot but do not correlate with the distribution pattern of set 5.

Appendix 3-6: Pangwari E – Clr-Biplot

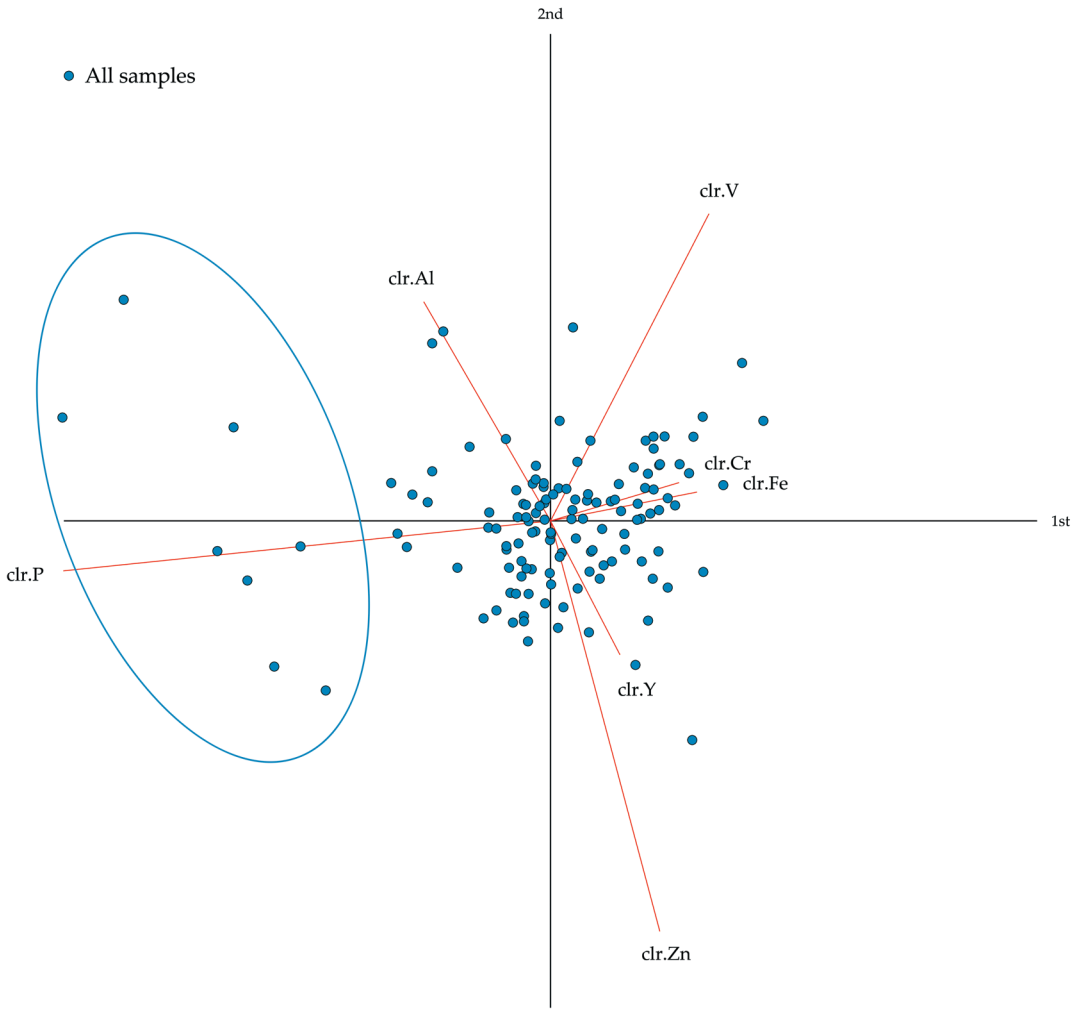

Form clr-biplot for the samples from *Pangwari E* with log-ratios of the elements P, Y, and Zn as well as Fe, Al, V, and Cr. The encircled samples differ by the log-ratio values of P. These samples are shown with their position in the trench in the interpolations of set 4 and 5 but do not correlate with them. The cumulative proportion explained is 0.6000, i.e. the first and second principal component together account for 60.00% of the total variance. The low value is concordant with the diffuse result.

Appendix 3-7: Ifana 2 – Set 5 and Visualisation of Sample Cluster

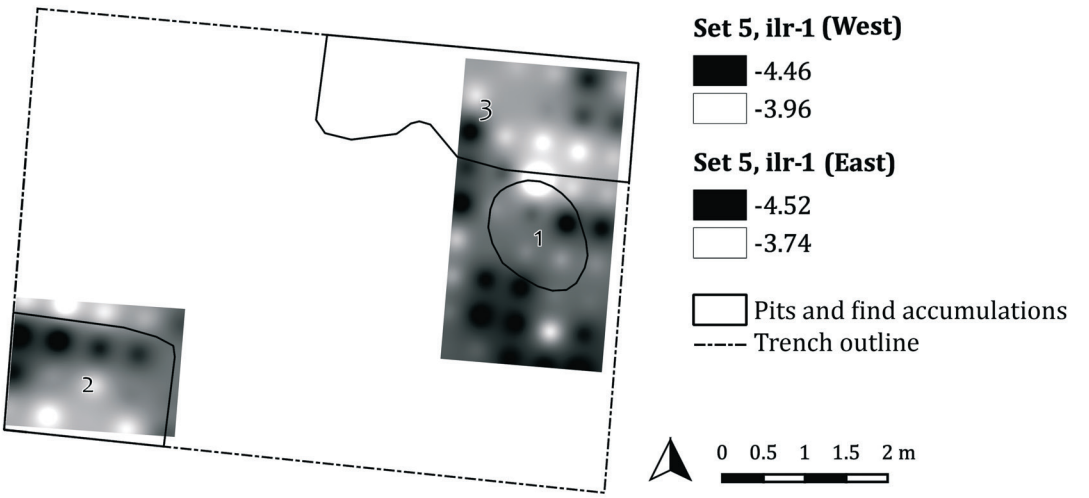

Interpolation of the pit signature. The pattern is not concordant with the features, especially not with the outlines of feature 2.

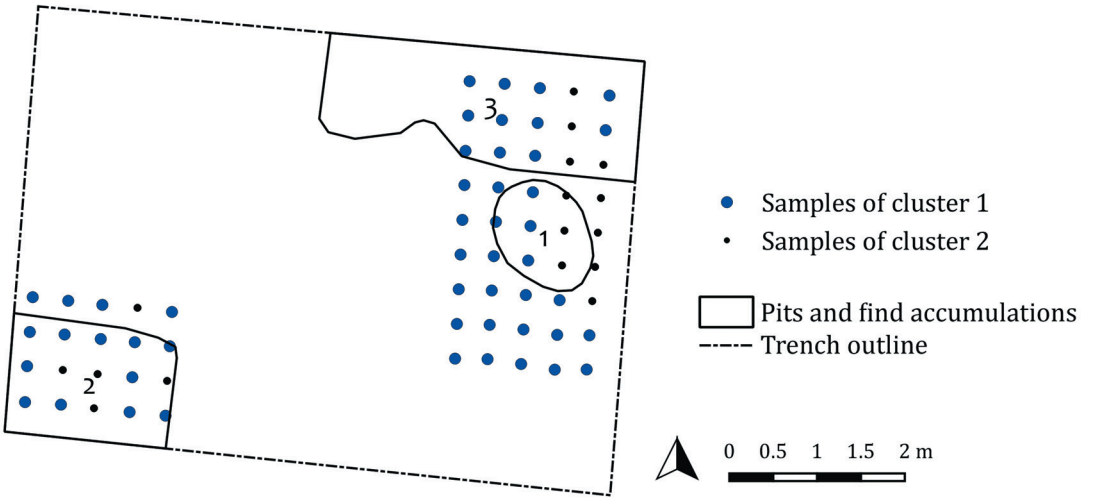

Visualisation of the sample cluster 1 and 2 identified in the clr-biplot. They neither comply with features nor reveal a significant pattern.

Appendix 3-7: Ifana 2 – Clr-Biplot

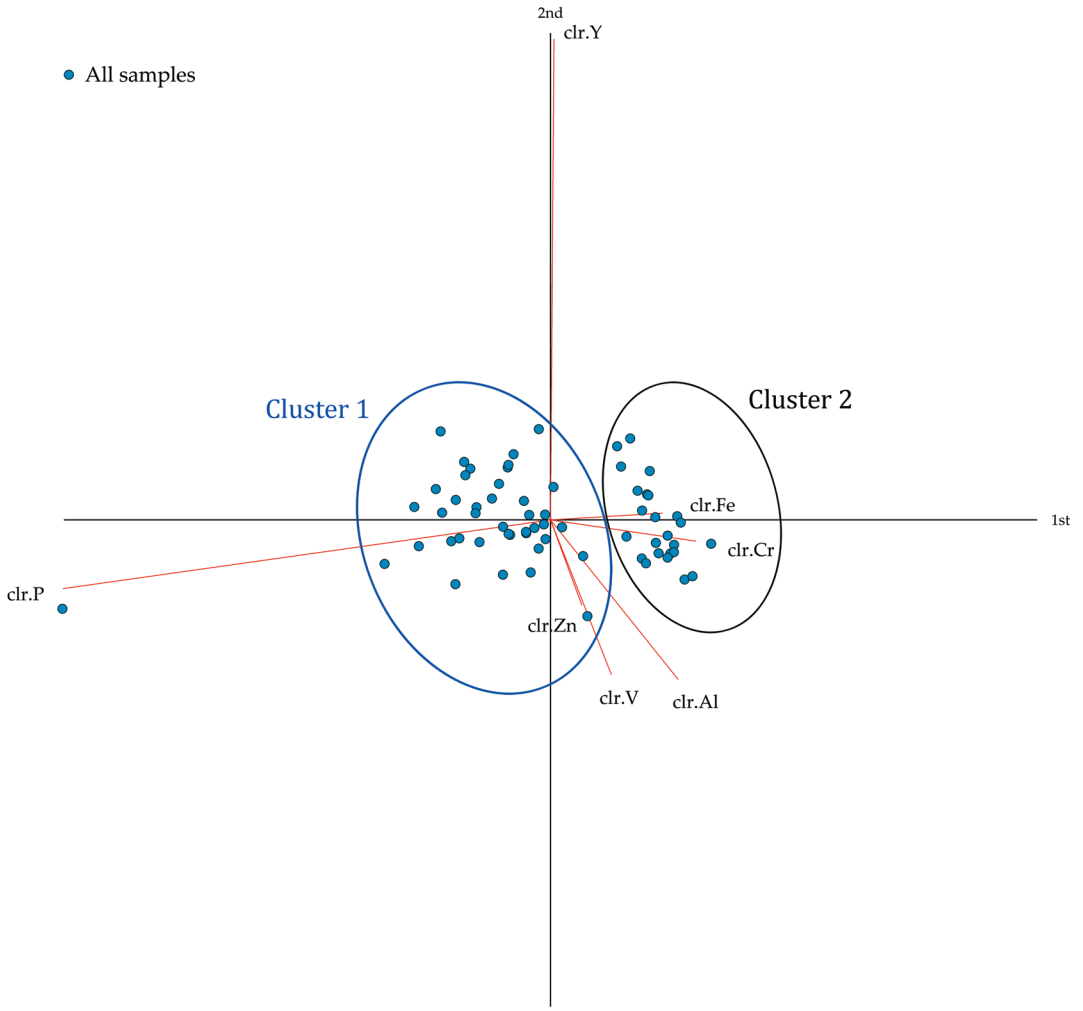

Form clr-biplot for the samples from *Ifana 2* with log-ratios of the elements P, Y and Zn as well as Fe, Al, V, and Cr. Although the samples form two clusters by the log-ratio values of P, Fe and Cr, their position in the trench does not reveal any pattern concordant with features or finds. The cumulative proportion explained is 0.8747, i.e. the first and second principal component together account for 87.47% of the total variance.

Appendix 3-8: Pangwari D and I – Clr-Biplot

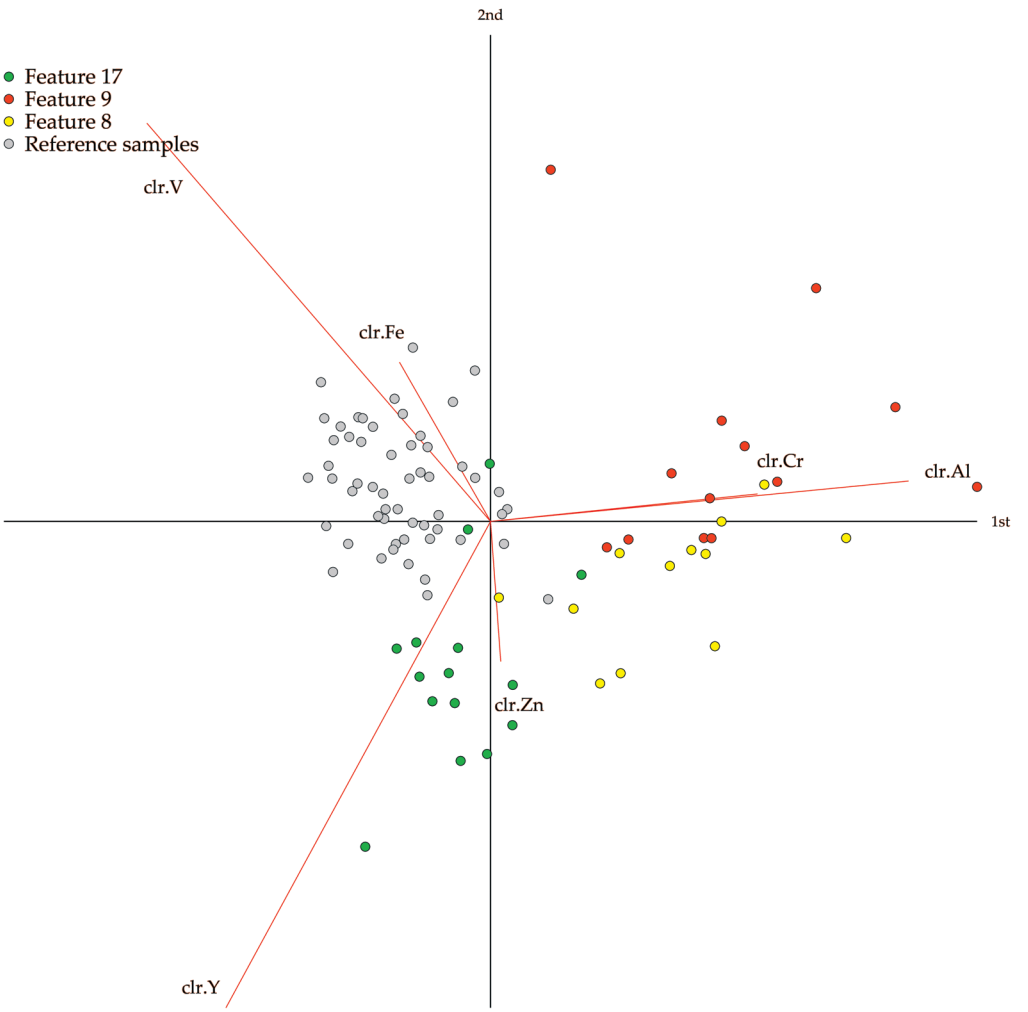

Form clr-biplot for the samples from features 8 and 9 (PGW D) together with feature 17 (PGW I) with log-ratios of the elements P, Y and Zn as well as Fe, Al, V, and Cr. Further samples from *trench I* were utilised as a replacement for absent reference samples. Although the samples form different clusters, it remains unknown whether this is biased by the replacement of reference samples from a different depth and area. The cumulative proportion explained is 0.7507, i.e. the first and second principal component together account for 75.07% of the total variance.

Appendix 4 – Fulani Village

Plan & Biplots

Appendix 4-1

- Plan of the Fulani Village

Appendix 4-2

- Sampling Scheme at the Fulani Village

Appendix 4-3

- Hearth and Ash

Appendix 4-4

- Cow Manure

Appendix 4-5

- Chicken Coop

Appendix 4-6

- Footpath

Appendix 4-7

- Sleeping Hut

Appendix 4-8

- Medicine Hut

Appendix 4-9

- Abandoned Village

Appendix 4-1: Plan of the Fulani Village

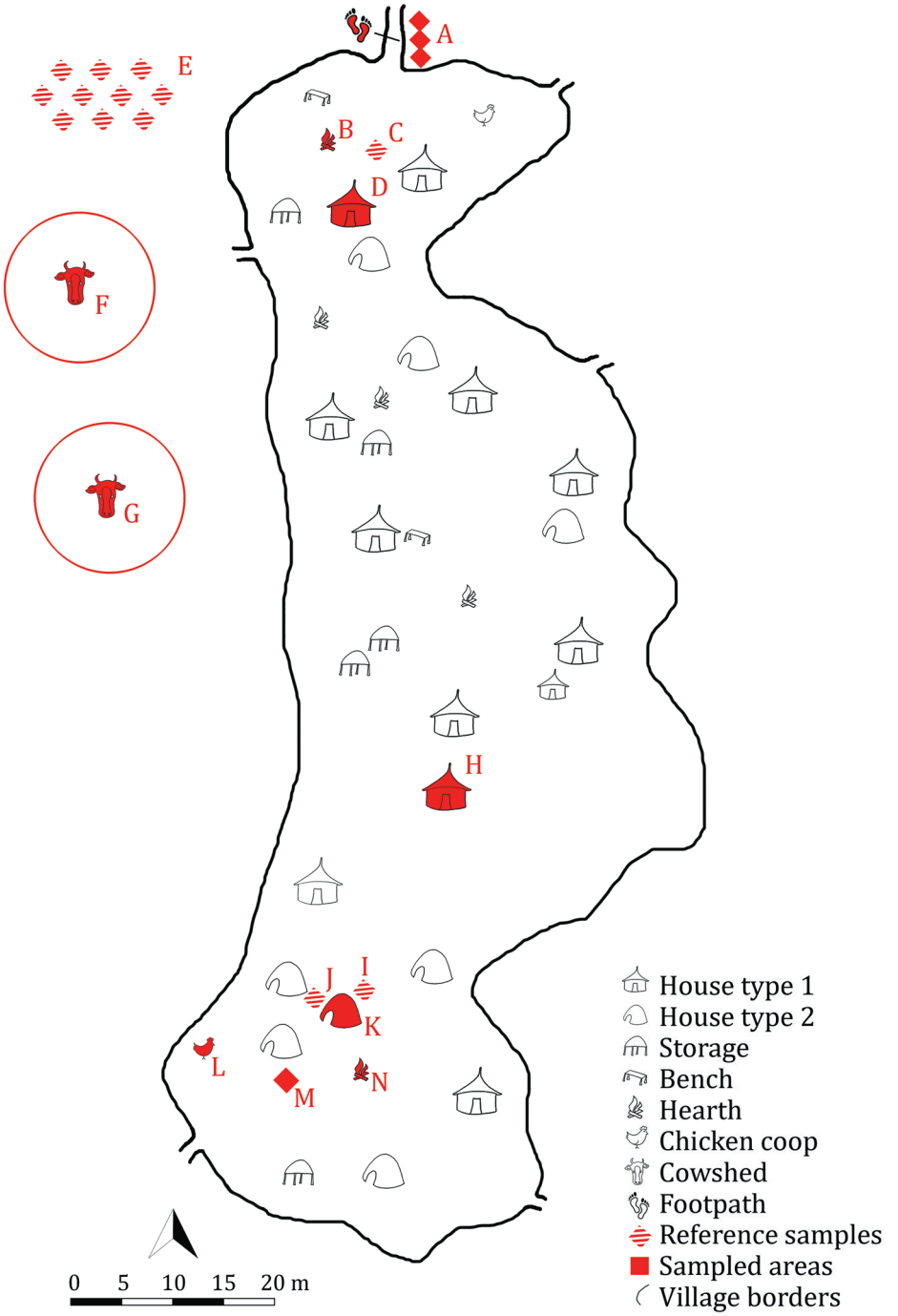

Schematic plan of the Fulani village. All houses are mapped but not all of the fireplaces, sheds and paths. The soil inside the village borders was compacted and mostly free of vegetation. The village borders were identified by aerial photographs. The letters refer to the sampling scheme in Appendix 4-2.

Appendix 4-2: Sampling Scheme at the Fulani Village

LETTER ON THE MAP	SUBJECT	SAMPLED AREA
A	Extensive usage High-traffic areas	Both on and beside a footpath.
B, N	Hearth	Ash, the soil within and adjacent to the hearth.
C, I, J	On-site samples Reference material	Reference material from the village, but without any specific function.
D	Human impact	Soil from a sleeping hut.
E	Off-site soil Reference material	Reference samples from outside the village.
F	Faeces and manure Animal penning	A currently used cowshed.
G	Faeces and manure Animal penning	Formerly used cowshed, also old manure.
H	Human impact	Soil of a 'medicine hut'.
K	Food processing	Soil of a 'kitchen hut'.
L	Faeces and manure Animal penning	A currently used chicken coop.
M	Food processing	The soil beneath a large mortar & pestle.

Appendix 4-3: Hearth and Ash – Clr-Biplot

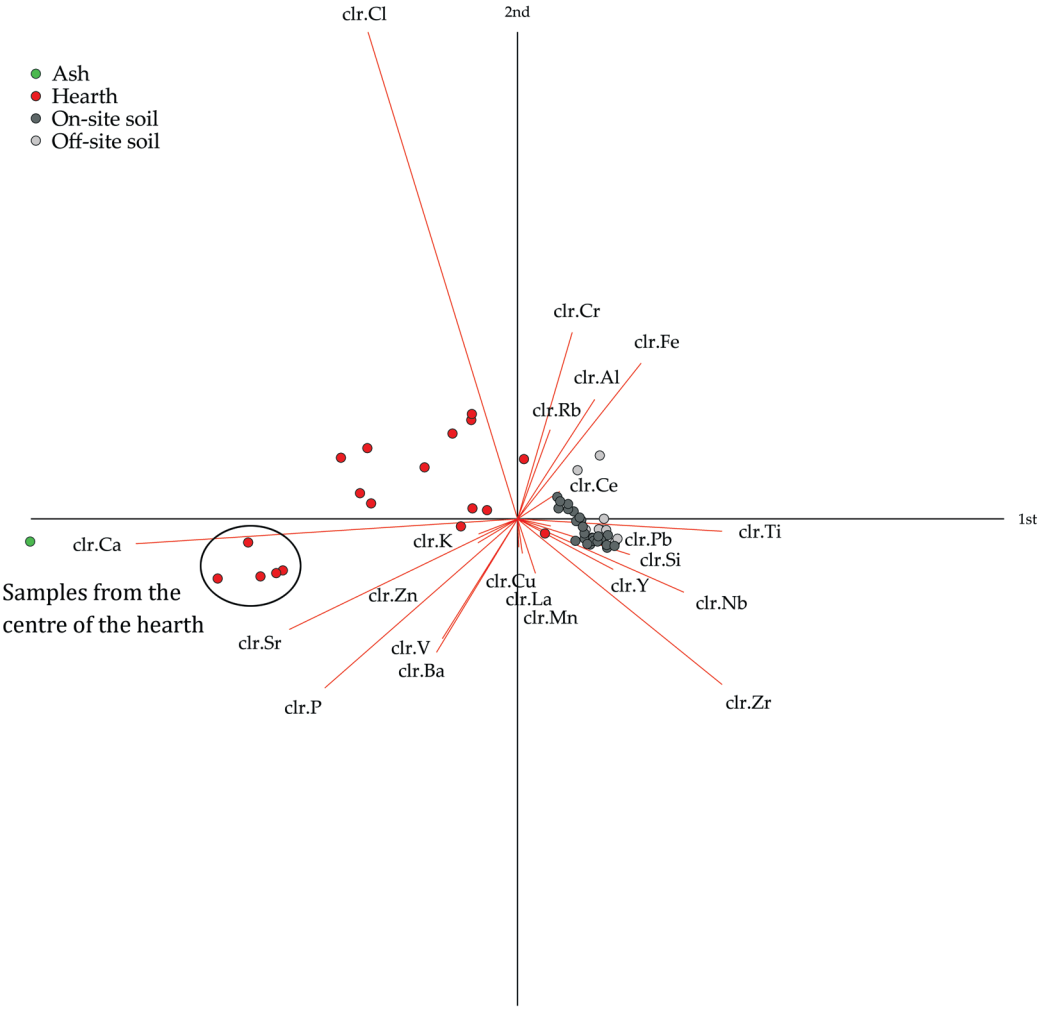

Hearth and ash samples taken from the Fulani village. Form clr-biplot with log-ratios of all elements. The ash and samples from the centre of the hearth were at greater distance from the reference samples compared to the samples from the rim of the hearth. The cumulative proportion explained is 0.8901, i.e. the first and second principal component together account for 89.01% of the total variance.

Appendix 4-4: Cow Manure – Clr-Biplot

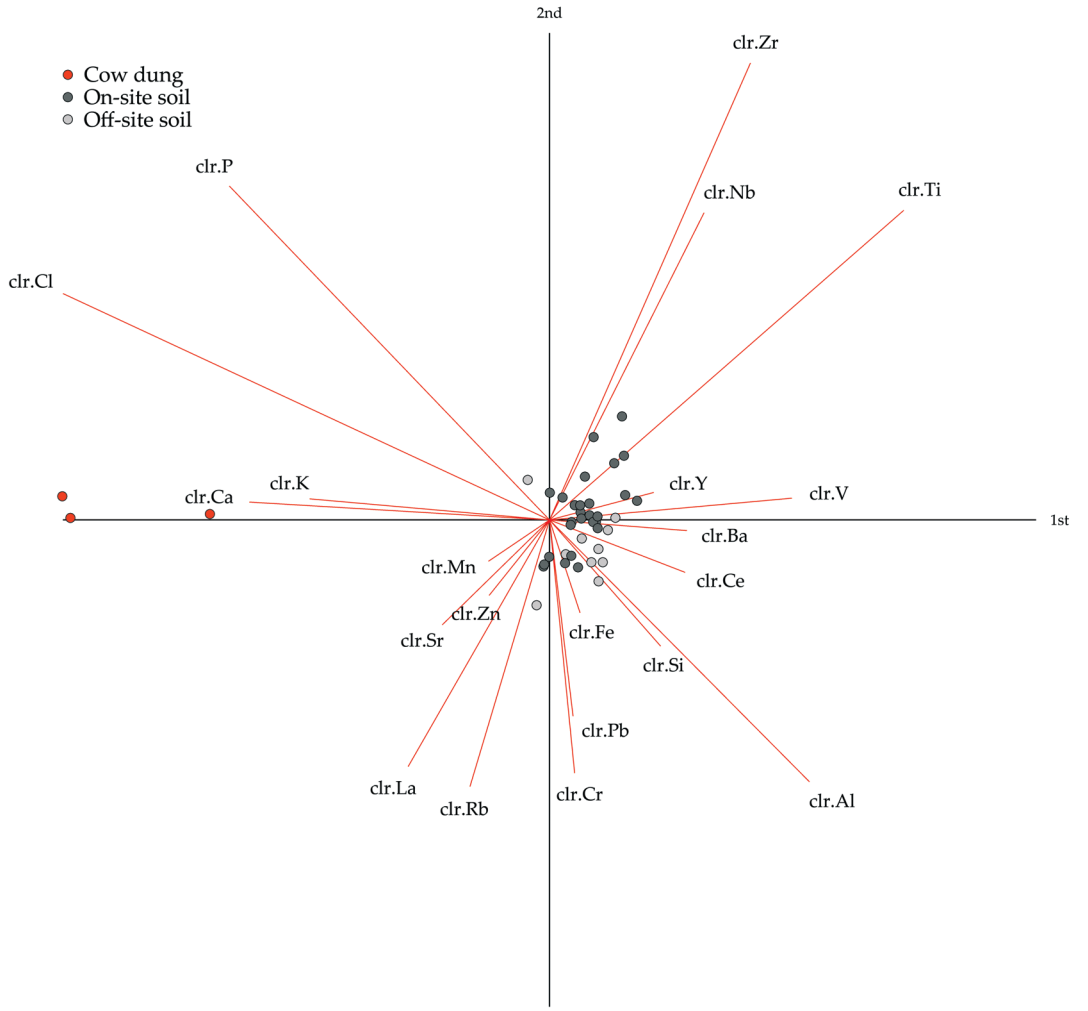

Mineralized cow manure samples taken from the Fulani village. Form clr-biplot with log-ratios of all elements. The soil mixed with mineralized manure differs by the log-ratios of Ca and K. The cumulative proportion explained is 0.8394, i.e. the first and second principal component together account for 83.94% of the total variance.

Appendix 4-5: Chicken Coop – Clr-Biplot

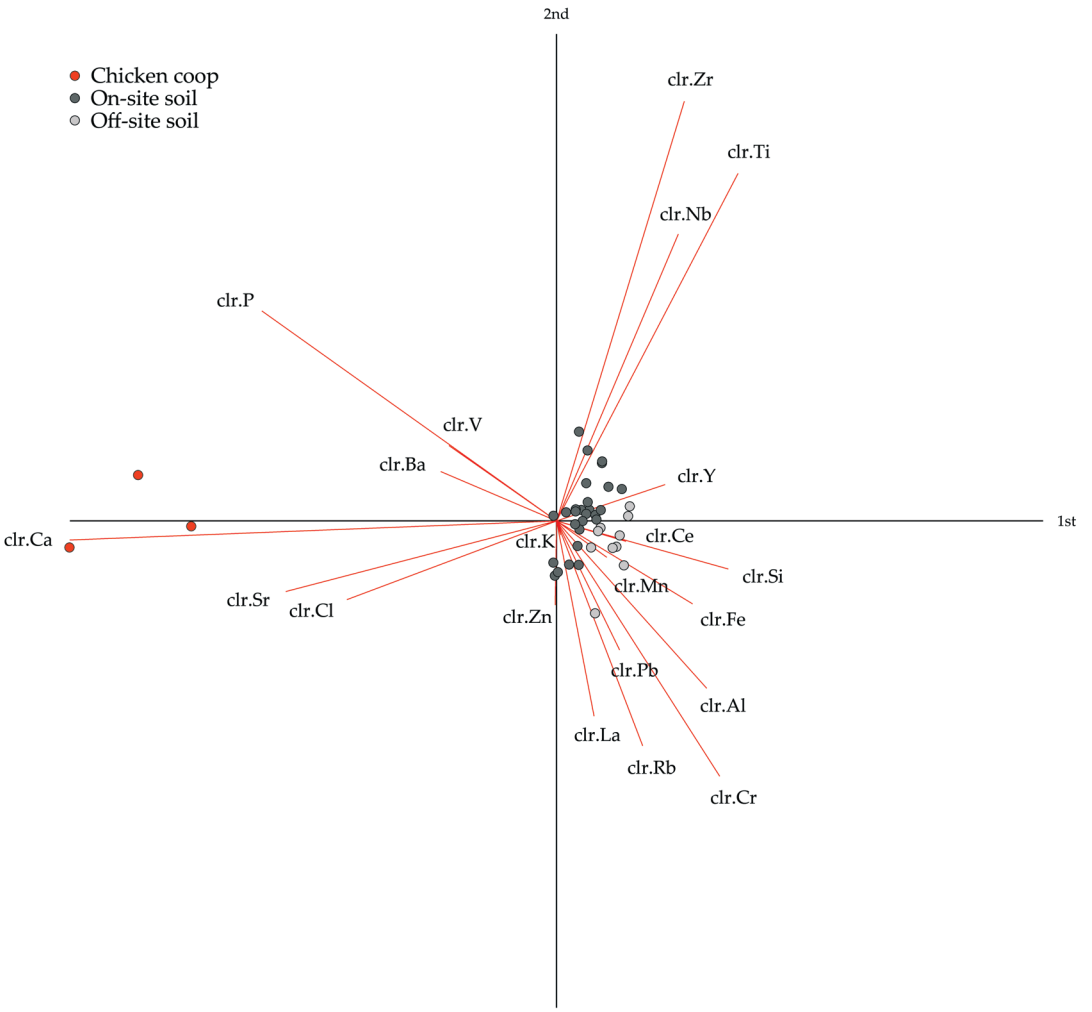

Samples taken from the chicken coop in the Fulani village. Form clr-biplot with log-ratios of all elements. The samples separate by the the log-ratio value of Ca. The cumulative proportion explained is 0.8673, i.e. the first and second principal component together account for 86.73% of the total variance.

Appendix 4-6: Footpath – Clr-Biplot

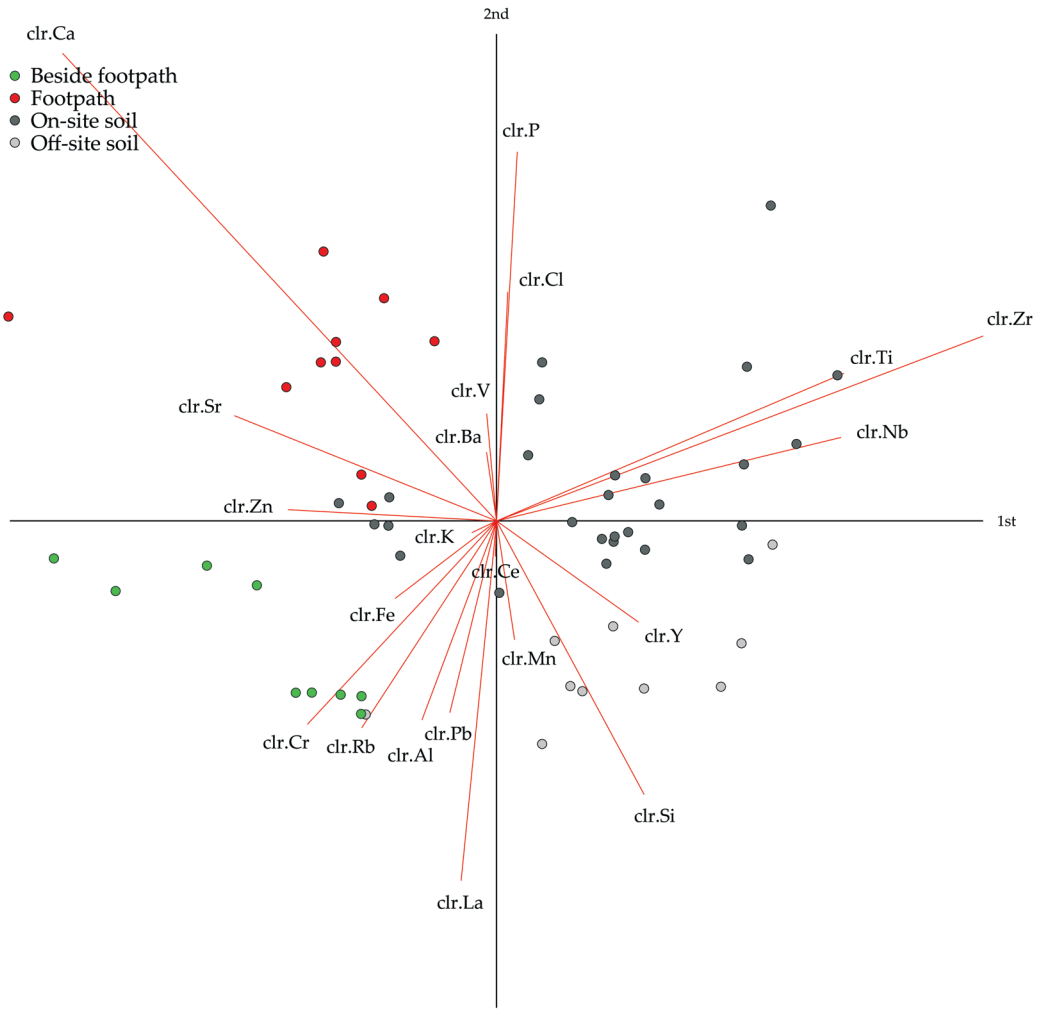

Samples taken from the footpath next to the Fulani village. Form clr-biplot with log-ratios of all elements. The samples from the footpath and the on-site samples differ from the samples beside the footpath and off-site samples by the log-ratio values of P, Cl, V, and Ba. The footpath itself is influenced by the log-ratios of Ca and Sr. The cumulative proportion explained is 0.6407, i.e. the first and second principal component together account for 64.07% of the total variance.

Appendix 4-7: Sleeping Hut – Clr-Biplot

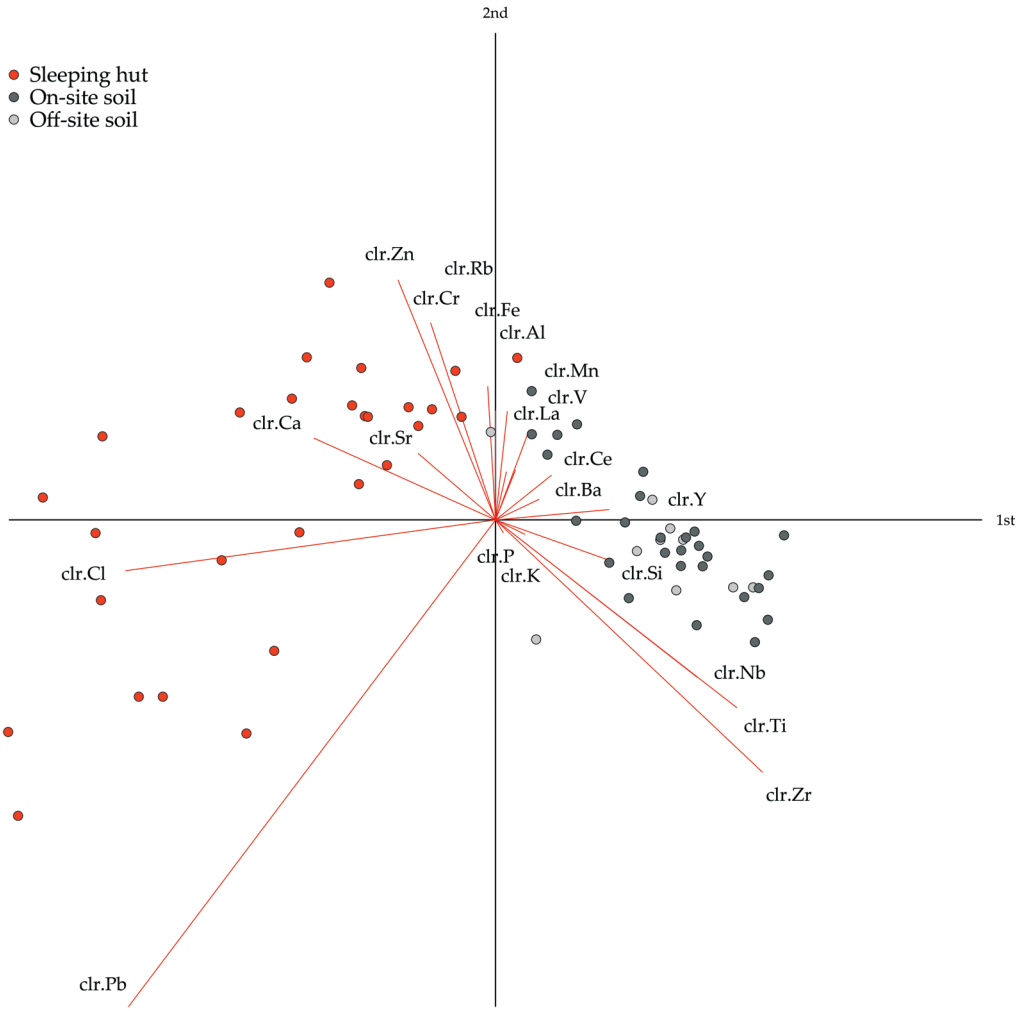

Samples obtained from a sleeping hut in the Fulani village. Form clr-biplot with log-ratios of all elements. The samples of the hut are influenced by the log-ratios of Cl, Ca, Sr, Zn, and Cr and differ among each other by the log-ratio values of Pb. The cumulative proportion explained is 0.7348, i.e. the first and second principal component together account for 73.48% of the total variance.

Appendix 4-8: Medicine Hut – Clr-Biplot

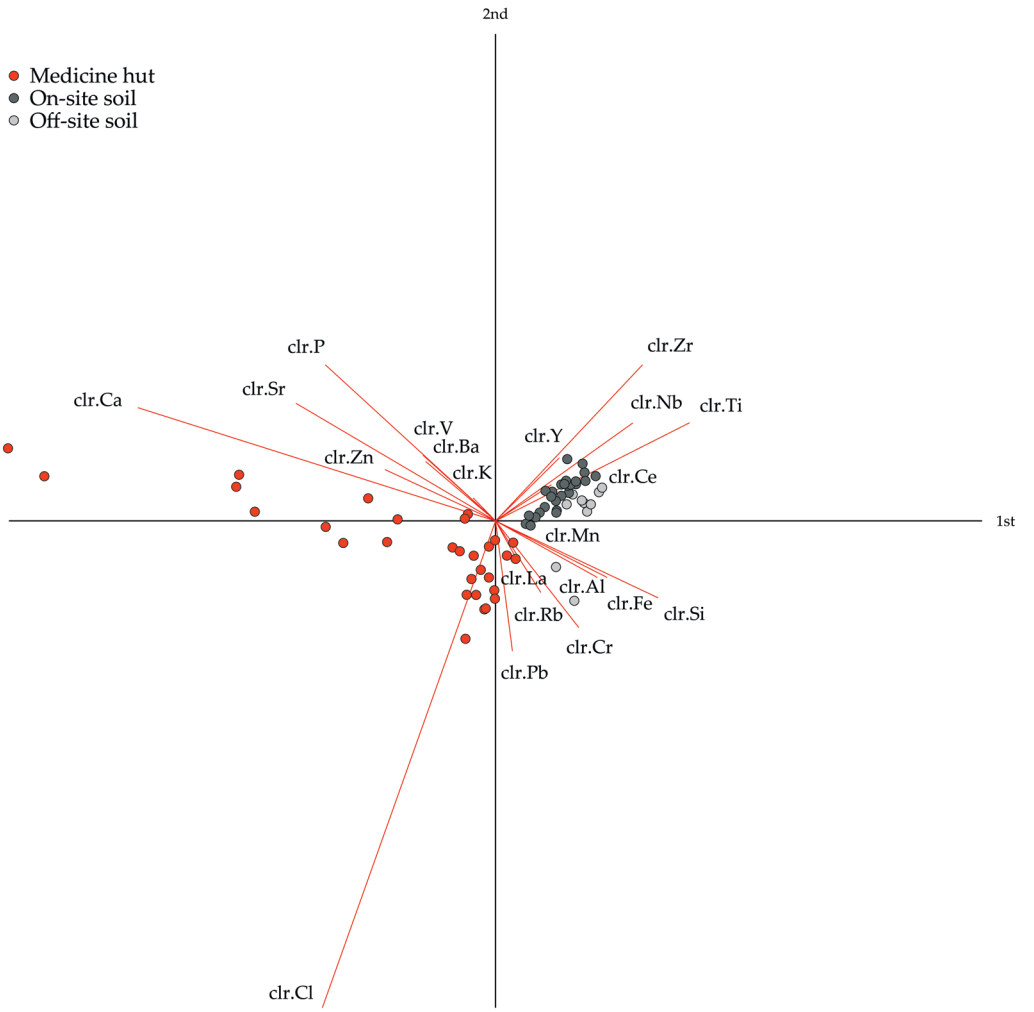

Samples obtained from the 'medicine hut' in the Fulani village. Form clr-biplot with log-ratios of all elements. Some of the samples obtained from the hut differ by the log-ratios of Ca, Sr and Zn as well as the log-ratios of Cl. The cumulative proportion explained is 0.8874, i.e. the first and second principal component together account for 88.74% of the total variance.

Appendix 4-9: Abandoned Village – Clr-Biplot

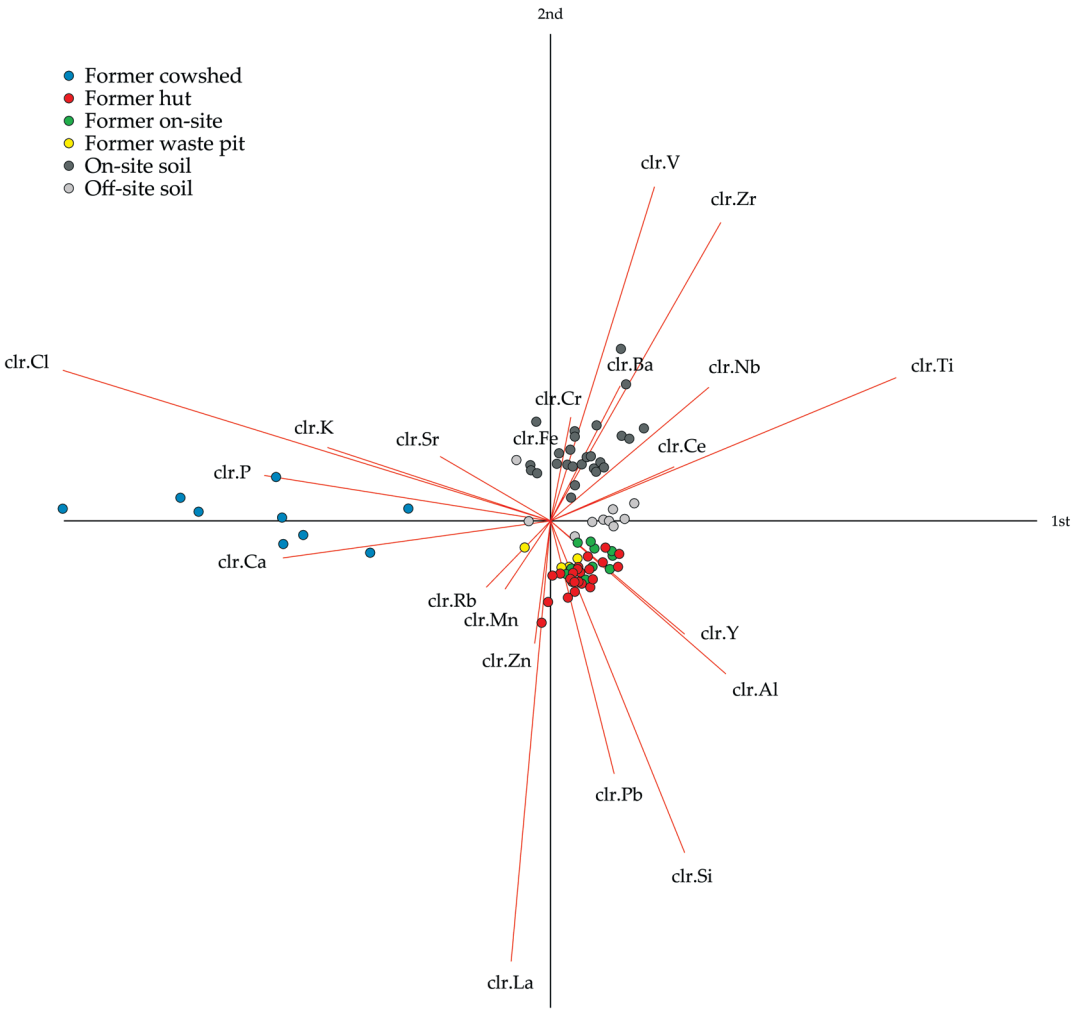

Samples obtained from an abandoned Fulani village. Form clr-biplot with log-ratios of all elements. The former cowshed is strongly influenced by the log-ratios of Ca, P and Cl. The samples taken from the abandoned village separate from the reference soil by the log-ratios of Y, Al, Si, Pb and La. The cumulative proportion explained is 0.7343, i.e. the first and second principal component together account for 73.43% of the total variance.